# Enhancing Triethylborane Initiation Through Mechanistic Understanding

**Ivan Ocaña**

Doctor of Philosophy

University of York

Chemistry

October 2024

**Abstract**

Triethylborane ($Et_3B$) in the presence of $O_2$ is one of the most widely used systems for radical chain initiation in organic synthesis. However, its initiation mechanism is poorly understood, and some reactions fail to initiate by this system. In this work we uncovered an obscure, previously unknown secondary mechanism of initiation using a novel radical trapping technique.

We utilised a new radical trap capable of capturing free radicals generated during initiation to allow their detection by mass spectrometry (MS) and quantification by nuclear magnetic resonance (NMR). This technique was applied to investigate the reactions involved in the initiation mechanism of $Et_3B/O_2$ system. We confirmed that the primary initiation mechanism generates ethyl radicals as the initiating radicals. However, as predicted by our kinetic simulations, the primary mechanism is very inefficient, and it is unlikely to account for the initiation alone. We hypothesized that diethyl(ethylperoxy)borane ($Et_2BOOEt$), the product of autoxidation, plays an important role in initiation.

We synthesised $Et_2BOOEt$ separately and reacted it with $Et_3B$ in the presence of the radical trap. It was found that this reaction generated 1 eq. of ethyl radicals, which were identified by MS and quantified by NMR. Our findings suggest that $Et_3B/Et_2BOOEt$ acts as a more efficient initiator than $Et_3B/O_2$ as the initiation proceeds.

When this mechanism was simulated computationally it was found the secondary initiation produces $7 \times 10^4$ times more initiating radicals than the primary initiation. We exploited this insight to overcome the challenges of initiation by using $Et_2BOOEt$ in combination with $Et_3B$ to initiate inefficient chains that could not be accessed using $Et_3B/O_2$ alone.

This work demonstrates the power of our novel radical trapping technique for studying complex radical mechanisms while further expanding our understanding of $Et_3B/O_2$ initiation, facilitating its application and opening new avenues for exploration in organic synthesis.

## Contents

**List of Schemes**

**List of Figures**

**List of Tables**

**Acknowledgments**

First and foremost, I would like to express my gratitude to my supervisors, Professor Victor Chechik and Dr. Andrew Rickard, for their invaluable guidance throughout my research and writing process. Their open and engaged approach created an environment where I felt supported and could rely on their expertise in moments of doubt. Our weekly meetings were helped shape the ideas presented in this thesis, and their professional values influenced my growth as both a professional and a scientist.

I would like to express my gratitude to Syngenta for their financial support, for the opportunities to present my research at their conferences and for the invitation to contribute to a publication in Chimia. Especial thanks go to my industry supervisors Dr. George Hodges and Neil Griffin who engaged in my work throughout my studies. I am very grateful for their insight as well as the approachability and support they offered.

I would also like to thank Dr. Michael James and Professor William Unsworth, the two IPMs who provided valuable feedback during my time at York. Their approachability was a source of great comfort and encouragement.

I would like to thank the academic support staff who provided training and guidance with experiments and measurements. Special thanks to Karl Heaton, Ed Bergstrom (MS), Heather Fish, and Mat Davy (NMR spectroscopy) for their assistance. I am also thankful to Professor Ed Anderson and Dr. Bethany Shire from the University of Oxford for their guidance in my work with TCP.

I would like to extend my appreciation to the entire Chechik group, both past and present members, for creating a supportive and friendly environment where I felt encouraged to express my ideas freely. Their support and kindness made my time in the lab much more enjoyable. Special thanks to Amy Wolstenholme-Hogg for always having a smile, even during challenging times; Mohammed Althuqbi for his good nature and ability to create a friendly atmosphere wherever he goes; Naeem Iqbal for his advice and engaging discussions that

boosted my confidence in my work; and Nik Vagkidis for being a true friend both inside and outside the lab.

A very special thanks goes to my family-my parents and my sister. All my achievements are and will always be thanks to their unconditional support. Their faith in my skills and values has been a constant source of strength, and I could not have made it this far without their patience and love.

I am also grateful to my friends in the UK and Spain for standing by me during tough times and making the good times even better.

Finally, I would like to extend my deepest thanks to my partner and best friend, Athina, for her love, care, and patience. I am profoundly grateful for the many ways she has supported me and for all the beautiful memories we have created together.

**Agraïments**

En primer lloc, m'agradaria expressar el meu agraïment als meus supervisors, el professor Victor Chechik i el doctor Andrew Rickard, per la seva inestimable orientació al llarg de la meva recerca i redacció. El seu enfocament obert i compromès ha creat un entorn on m'he sentit recolzat i on he pogut confiar en la seva experiència en els moments de dubte. Les nostres reunions setmanals han ajudat a donar forma a les idees presentades en aquesta tesi, i els seus valors professionals han influït el meu creixement tant com a professional com a científic.

M'agradaria expressar el meu agraïment a Syngenta per el seu suport econòmic, per les oportunitats de presentar la meva recerca a les seves conferències i per la invitació per contribuir a una publicació a Chimia. Un agraïment especial als meus supervisors de la indústria Dr George Hodges i Neil Griffin els quals s'han interessat per el meu treball durant dels meus estudis. Estic molt agraït per el seu coneixement i el suport que m'han ofert.

També m'agradaria donar les gràcies al Dr. Michael James i al professor William Unsworth, els dos IPM que han proporcionat observacions i comentaris valuosos durant la meva estada a York.

El meu sincer agraïment va al personal de suport acadèmic que han ofert formació i orientació amb experiments i mesures. Agraïment especial a Karl Heaton, Ed Bergstrom (MS), Heather Fish i Mat Davy (RMN) per la seva assistència. També estic agraït al professor Ed Anderson i a la doctora Bethany Shire de la Universitat d'Oxford per la seva orientació en el meu treball amb TCP.

M'agradaria estendre el meu agraïment a tot el grup Chechik, tant membres passats com actuals, per crear un entorn amable i de suport on em sentia animat a expressar les meves idees lliurement. El seu suport i amabilitat van fer que el meu temps al laboratori fos molt més agradable. Un agraïment especial a l'Amy Wolstenholme-Hogg per tenir sempre un somriure, fins i tot en moments difícils; el Mohammed Althuqbi pel seu bon caràcter i la seva capacitat per crear bon ambient allà on va; el Naeem Iqbal pels seus consells i discussions que

em van donar confiança en la meva feina; i el Nik Vagkidis per ser un veritable amic tant dins com fora del laboratori.

Un agraïment molt especial a la meva família: els meus pares i la meva germana. Tots els meus èxits són i seran sempre gràcies al seu suport incondicional. La seva fe en les meves habilitats i valors ha estat una font constant de força, i no hauria pogut arribar fins aquí sense la seva paciència i amor.

També estic agraït als meus amics del Regne Unit i Espanya per estar al meu costat durant els moments difícils i fer que els bons moments siguin encara millors.

Finalment, m'agradaria donar el meu més profund agraïment a la meva parella i millor amiga, Athina, pel seu amor, cura i paciència. Estic profundament agraït per les moltes maneres en què m'ha donat suport i per tots els records bonics que hem creat junts.

**Declaration**

I declare that this thesis is a presentation of original work, and I am the sole author. I also declare that in the event the work of others has been used, this has been fully acknowledged in the text and as references. This work has not previously been presented for a degree or other qualification at this University or elsewhere. All sources are acknowledged as references. Some of the research outlined in this thesis has been published in the following paper:

I. Ocaña, P. J. Williams, J. Donald, N. Griffin, G. Hodges, A. R. Rickard, and V. Chechik, *Chimia*, 2024, **78**, 123-128.

## 1. Introduction

Radicals are atoms, molecules, or ions that possess at least one unpaired valence electron, rendering them highly reactive.[1, 2] Their unique electronic configuration makes radicals valuable in various fields, including synthetic organic chemistry,[3-5] materials science,[6, 7] and biological chemistry.[7-9] Their reactivity often leads to spontaneous dimerization or polymerisation, and they are typically stable only at very low concentrations in inert media or a vacuum. There are examples of stable organic radicals like, nitroxides, phenalenyl, and triarylmethyl radicals, however, most organic radicals have very short lifetimes, which complicates their detection and characterisation.[1, 2]

The field of radical chemistry has evolved significantly since Moses Gomberg's discovery of the triphenylmethyl radical in 1900,[10] which marked the beginning of a new era in chemistry. Subsequent research demonstrated the existence of alkyl radicals and attributed radical mechanisms to various synthetic reactions.[11, 12] By the mid-1970s, physical organic chemists had gathered extensive structural and rate information about different types of organic radicals.[13]

Despite these advancements, radical chemistry did not become a central focus in conventional organic synthesis for much of the 20th century. While some radical reactions were known, they were often eclipsed by other transformations. However, the foundations for modern synthetic radical reactions were laid before 1980, with key developments in atom transfer reactions,[14] the introduction of tributyltin hydride, aromatic substitutions through Minisci reaction,[15] and allylations with allyltributylstannane.[16]

### 1.1. Radical Formation

Radicals are often formed through the homolytic cleavage of covalent bonds, a process that requires a significant amount of energy, known as bond dissociation energy (BDE) (ΔH°) (Scheme 1).[1, 2] Radicals that require more energy to form are normally less stable. Homolytic bond cleavage occurs with weak bonds such as the O-O bond in peroxide species or O-N bonds.

Radicals can also form through single electron oxidation or reduction of an atom or molecule.[1, 2]

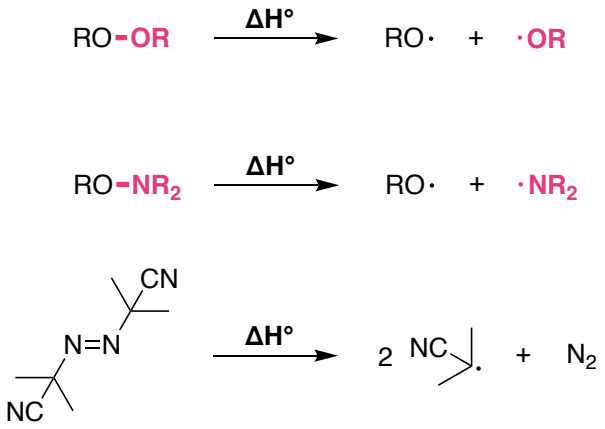


*Scheme 1. Radical formation via bond homolysis.*

The factors affecting the stability of radicals are important to understand, as they determine their behaviour and reactivity.

### 1.2. Radical Stability and Types

Radical stability is always dependent on the environment the radical is found; an isolated radical can only react by unimolecular decomposition. Therefore, when a radical is found in an environment its stability is related to its reactivity with other species.

However, it is useful to speak of intrinsic radical stability and the structural elements that can affect radical reactivity. It is often distinguished between thermodynamic stability and kinetic stability.

Thermodynamic stability is directly related to the BDE of the bond that breaks to form the two radicals.[1, 2] The thermodynamic stability is determined by the atom where the spin density is centred at and the delocalisation of this spin density:

1. **Electronegativity:** Increased electronegativity of the radical atom destabilizes the radical.
2. **Proximity to the nucleus:** Larger radical atoms with increased delocalisation opportunities are more stable.
3. **Neighbouring electron-donating groups:** Electron-donating groups adjacent to the radical stabilise it.
4. **Resonance:** Increased delocalisation through p orbital overlap stabilizes the radical.

Some radicals can be more stable than the BDE of reaction would suggest. In these cases, we speak of kinetic stability and it is largely controlled by steric factors around the radical centre. When there is steric crowding around the radical centre its reactivity with other compounds decreases.

Although many radicals are short-lived, some, such as the triphenylmethyl radical (trityl radical), have significantly longer lifetimes. Others, like the (2,2,6,6-tetramethylpiperidin-1-yl)oxyl radical (TEMPO) and molecular oxygen ($O_2$), are indefinitely stable. Understanding the different types of stability helps in categorizing radicals based on their lifetimes and reactivity. This classification helps in comprehending their behaviour and applications of different radicals.

### 1.2.1. Stable Radicals

Stable radicals are often referred to radicals that can be isolated in pure form in the presence of air and water and whose stability is usually due to delocalisation factors. A well-known example of a stable radical is molecular dioxygen ($O_2$).[17, 18] Dioxygen is the only molecule in abundance in our environment that is paramagnetic with a triplet ground state. According to molecular orbital (MO) theory, the MO diagram for $O_2$ reveals two unpaired electrons in two degenerate orbitals due to Hund's rule (Figure 1). Another example is nitric oxide (NO), which also has an unpaired electron in its molecular orbitals (Figure 1).

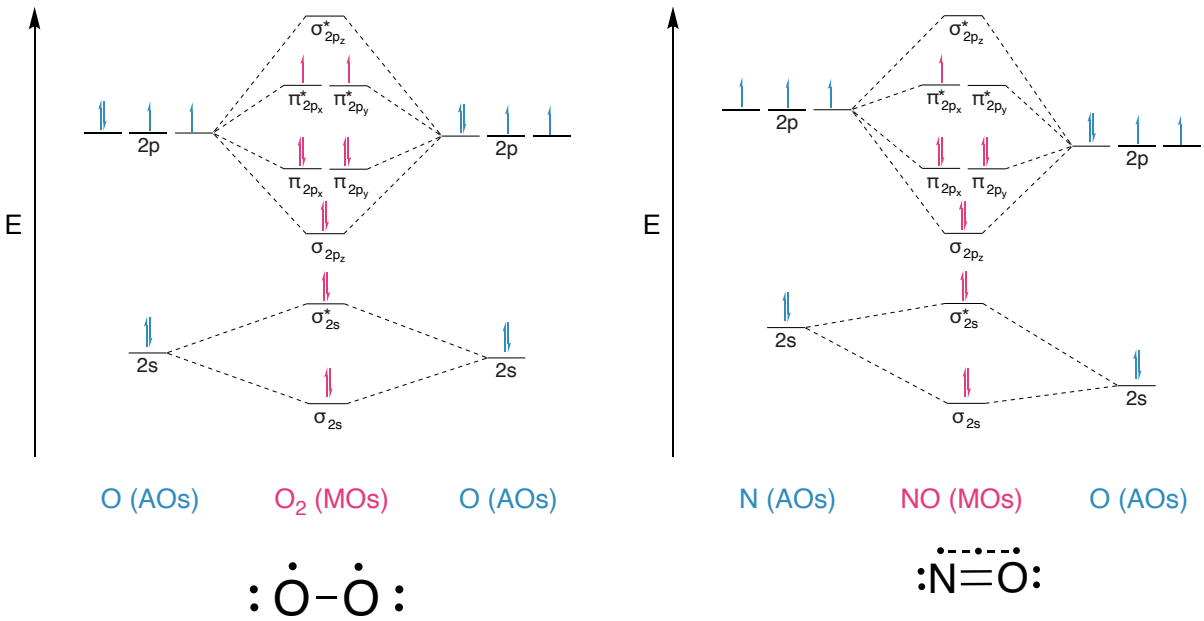


*Figure 1. Molecular orbitals of $O_2$ and NO.*

Aminoxyl radicals, such as TEMPO and TEMPOL, are further examples of stable radicals (Scheme 2). Sterically hindered aminoxyls without α-hydrogens are persistent, while those with α-hydrogens are unstable and rapidly disproportionate to nitrones and hydroxylamines.[19] Their stability is due to the delocalisation of the radical, forming a two-centre three-electron N–O bond, similar to NO and nitrogen dioxide ($NO_2$).

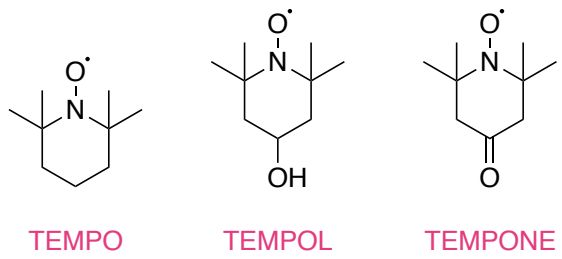


*Scheme 2. Structures of aminoxyl radicals TEMPO, TEMPOL and TEMPONE.*

### 1.2.2. Persistent Radicals

Persistent radicals refer to the species that can exist for a relatively short period of time, such as several hours or days.[18] They have sufficiently long lives to be detected and identified by instruments, such as absorption spectroscopy, electron paramagnetic resonance spectroscopy (EPR), and their stability is largely the result of steric hindrance.

A classic example of a persistent radical is Gomberg's triphenyl methyl radical (Scheme 3). In dilute solutions, the radical quickly reacts with oxygen to form peroxide. However, the triphenylmethyl radical remains highly persistent in an anaerobic atmosphere, showing stability among transient radicals. X-ray crystallography studies revealed that this stability is due to the steric protection from three bulky phenyl rings, resulting in a propeller conformation with a 30° twist. EPR spectroscopy confirmed that the unpaired electron is mainly localized on the central carbon and partially delocalized on the phenyl rings.

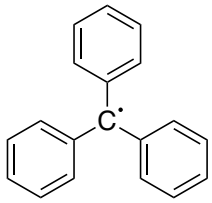


*Scheme 3. Gomberg's triphenyl methyl radical.*

## 1.3. Radical Chain Reactions

Radical chain reactions are very common mechanisms in radical chemistry. They are particularly common in the synthesis of polymers or complex molecules. Chain reactions involve three distinct steps: initiation, propagation, and termination (Scheme 4).[1]

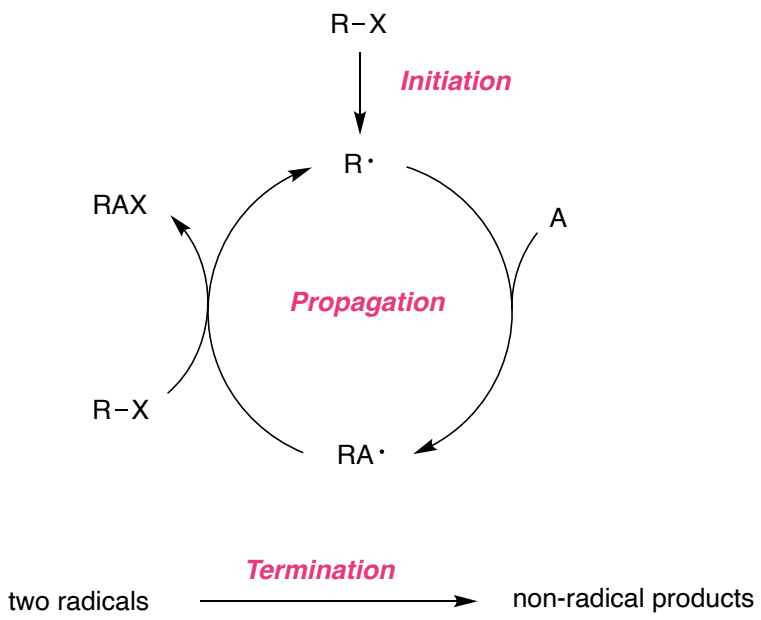


*Scheme 4. Mechanism of a hypothetical radical chain reaction.*

### 1.3.1. Initiation

The first step in a radical chain reaction will always be initiation. The initiation step consists of the formation of the first radical in the chain. Generation of a radical involves homolytically cleaving a covalent bond, resulting in two fragments each with an electron. This cleavage is typically achieved using heat, light, or a redox reaction.

#### 1.3.1.1. Radical Production by Thermolysis

Thermolysis involves the cleavage of covalent bonds at high temperatures, typically above 800 °C. However, certain weak bonds with dissociation energies below 30-40 kcal/mol can be cleaved at temperatures below 150 °C.[1, 3] Examples of compounds that undergo thermolysis include azo compounds, peroxides, nitrite esters, and esters of N-hydroxy-2-thiopyridone (Scheme 5).

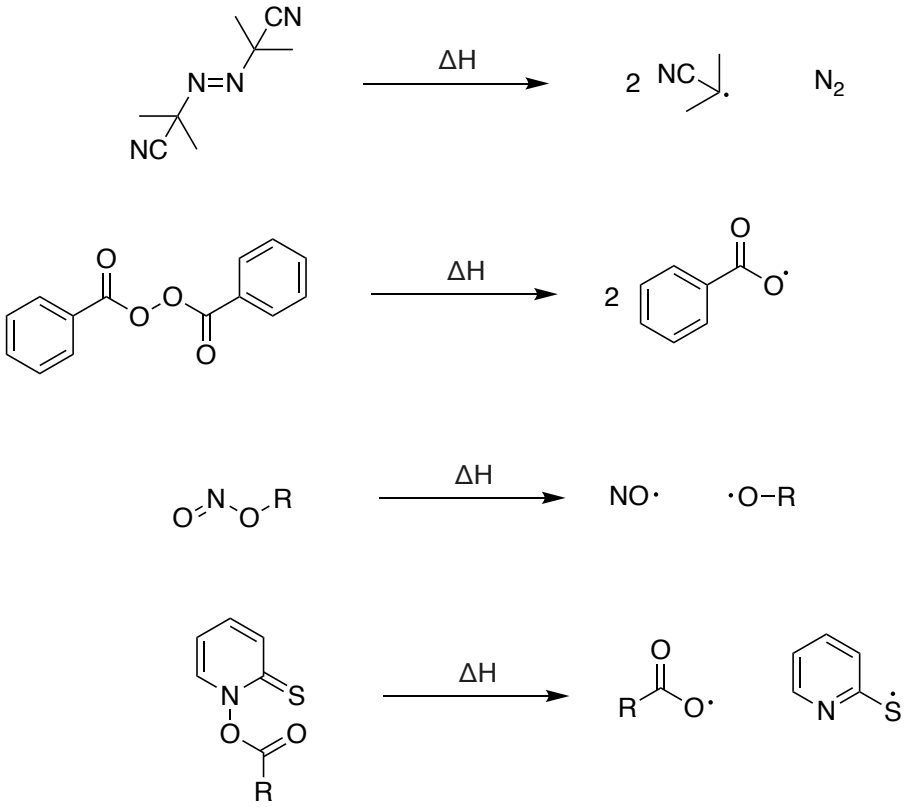


*Scheme 5. Thermolysis of azo compounds, peroxides, nitrile esters and esters of N-hydroxy-2-thiopyridone.*

#### 1.3.1.2. Radical Production by Photolysis

Photolysis utilises light energy to achieve homolytic fission of covalent bonds. For instance, azo compounds can produce radicals through the absorption of light, leading to the formation of unstable cis isomers (Scheme 6).[1, 3] Similarly, peroxides can generate alkoxy and acyloxy radicals upon exposure to light. High-energy radiation, such as X-rays or gamma rays, can also induce the formation of radicals.

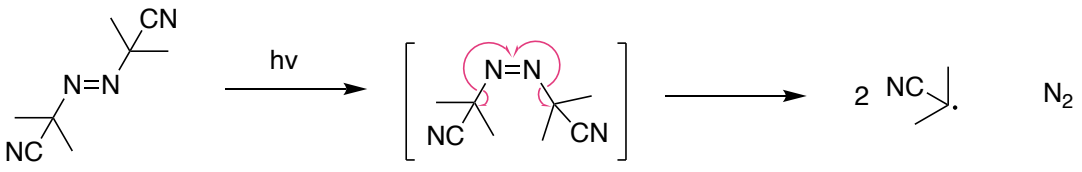


*Scheme 6. Photolysis of azoalkanes.*

### 1.3.1.3. Radical Production by Redox Systems

Redox reactions, involving oxidation or reduction, can generate radicals through intermolecular electron transfer (Scheme 7).[1, 3]

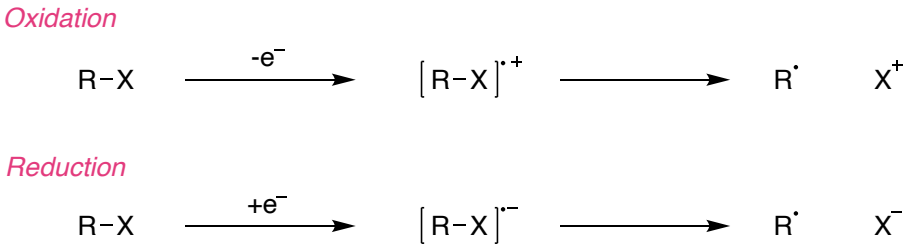


*Scheme 7. Radical formation by redox.*

### 1.3.1.4. Radical Initiators in Organic Synthesis

The most common way to initiate a radical chain reaction in practical organic synthesis is via radical initiators. Radical initiators facilitate the formation of radicals under controlled conditions. Among the various types of radical initiators, azo compounds, peroxides, and organometallic compounds are widely used.

**Azo Compounds**

Azo compounds are common radical initiators in organic synthesis. One of the most commonly used azo compounds is 2,2'-azobisisobutyronitrile (AIBN), known for its high decomposition ability and stability. AIBN decomposes upon heating to produce alkyl radicals

and nitrogen. It is commercially available and has a half-life of 10 h at 65 °C in toluene. In organic synthesis it is often used in combination with trialkyltin hydride (Scheme 8).[20]

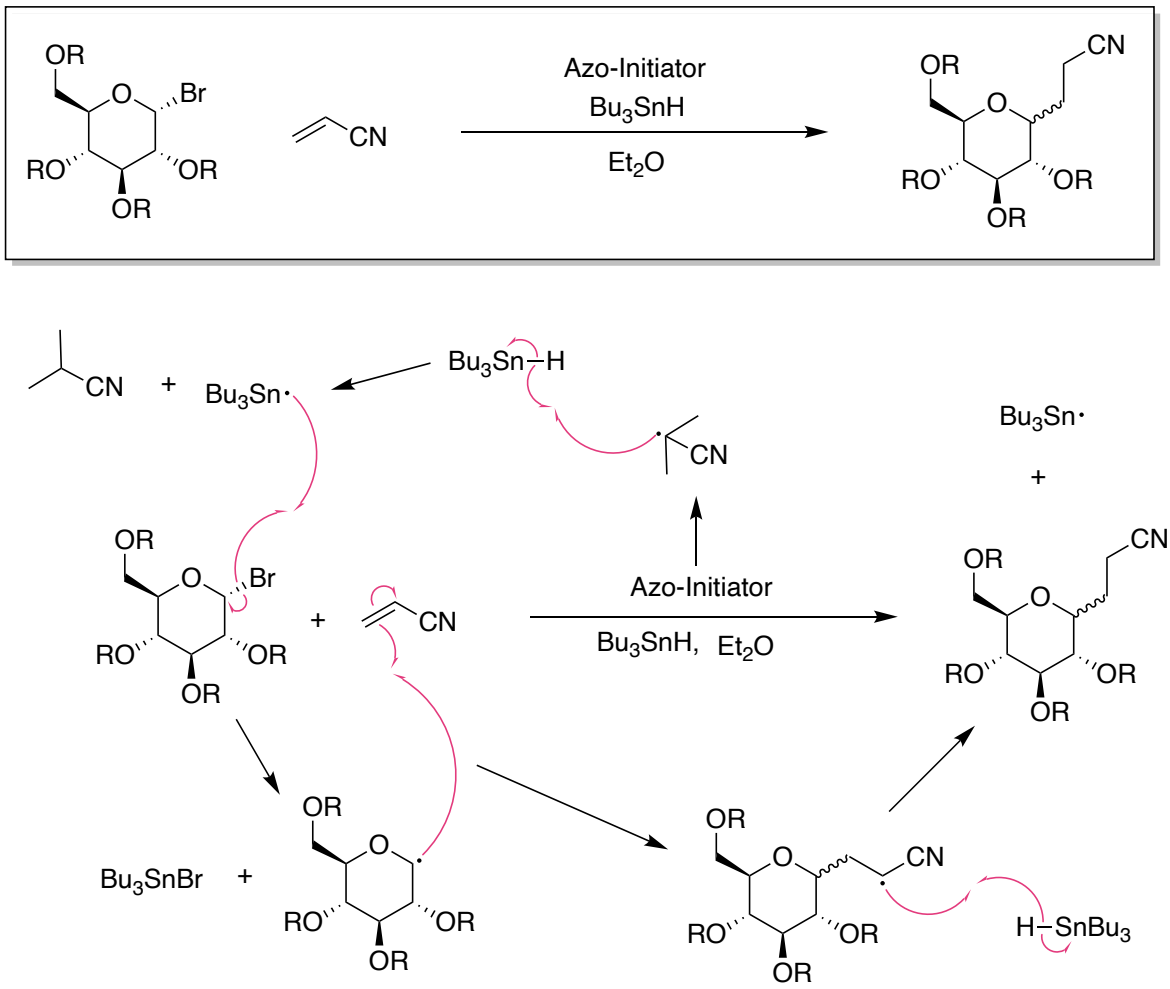


*Scheme 8. Synthesis of C-glycopyranoside.*

**Peroxides**

Upon heating, peroxides decompose to produce alkoxy or acyloxy radicals. The nature of the radicals generated depends on the structure of the peroxide. Benzoyl peroxide, a commonly used peroxide initiator, decomposes to form phenyl radicals and carbon dioxide (Scheme 9). Other more reactive peroxides such as acetyl peroxide decompose at lower temperatures allowing for heat-sensitive chain reactions, however, they require careful handling as these are sensitive to shock, light and heat.

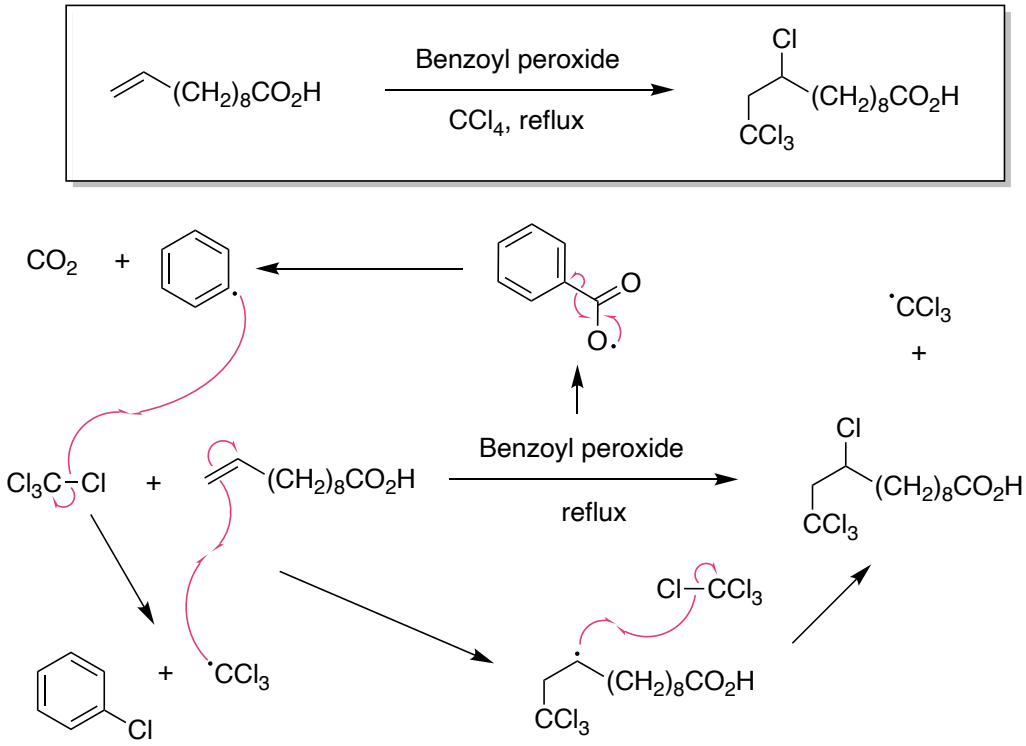


*Scheme 9. Benzoyl peroxide initiated radical addition to a double bond.*

**Organometallic Compounds**

Certain organometallic compounds, such as trialkylboranes, act as radical initiators. These compounds are highly sensitive to oxidation and are typically handled under inert conditions. Triethylborane ($Et_3B$) is a notable example, capable of initiating radical reactions in the presence of oxygen even at low temperatures, such as –78 °C (Scheme 10). This allows for greater control over stereoselectivity and the use of thermally unstable substrates.[3]

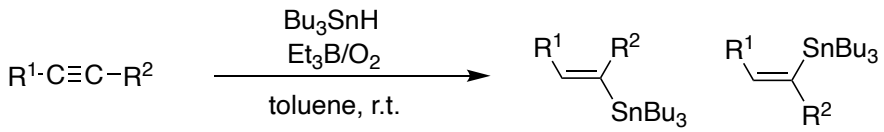


*Scheme 10. $Et_3B$ initiated hydrostannylation of alkynes.*

## 1.4. Radicals in Organic Synthesis

The application of radical chemistry in synthesis has resulted in the development of a multitude of innovative methodologies. Radicals can facilitate the formation of carbon-carbon (C–C) and carbon-heteroatom (C–X) bonds, which are fundamental to the construction of complex organic molecules. These transformations are not only efficient but also offer high selectivity, which makes them valuable for late-stage functionalisation of complex molecules.

Key advancements in modern synthetic radical chemistry began in the early to mid-1980s with Giese and coworkers' reductive additions of nucleophilic radicals to alkenes (Scheme 11).[21] This demonstrated that radical additions to alkenes do not necessarily result in polymerisation. Barton and coworkers' thiohydroxamates emerged as new sources of carbon and heteroatom radicals (Scheme 11).[22] Hart and coworkers' work on radical reactions in natural products synthesis,[23] Keck and coworkers' recognition of the preparative importance of radical allylations (Scheme 11),[24] Stork and coworkers' strategic use of radicals in regio- and stereoselective carbon-carbon bond-forming reactions,[25] and Porter and coworkers' pioneering work on radical macrocyclisations further highlighted the potential of radical chemistry for synthetic transformations.[26] Curran and coworkers' syntheses of hirsutene and related natural products by tandem radical cyclisation showcased the unique power of radical reactions conducted in sequence.[27]

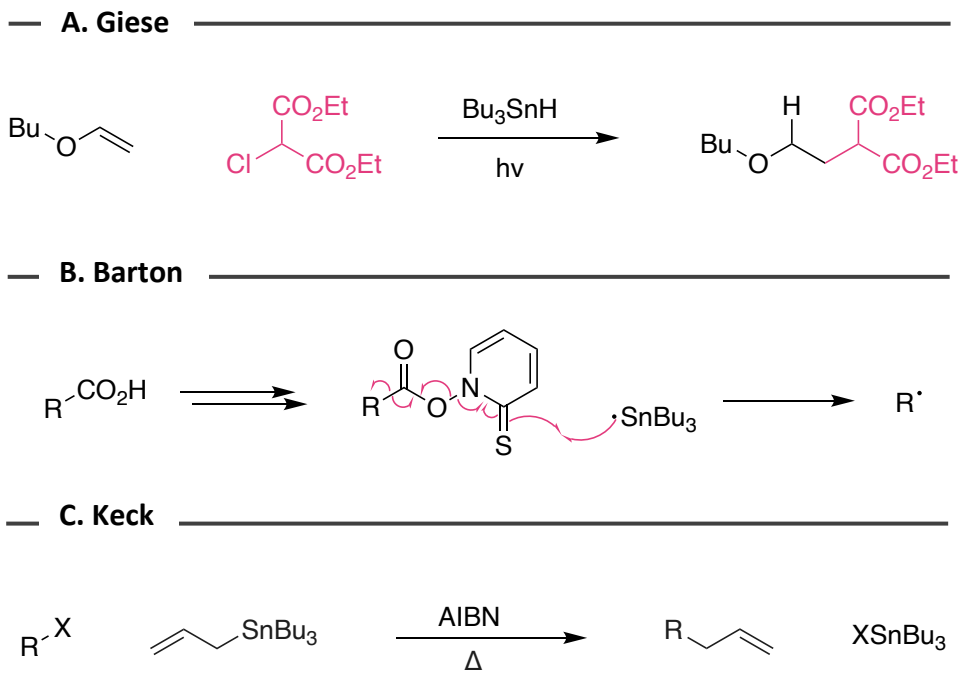


*Scheme 11. Key synthetic radical reactions: (A) Giese and coworkers' reductive addition to alkenes. (B) Barton and coworkers' decarboxylation. (C) Keck and coworkers' radical allylations.*

These early contributions revealed the potential of radical reactions. Over time, the favourable features of radical chemistry-mild conditions, orthogonality to many ionic reactions, predictability, reactivity, selectivity, and generality-have become more widely recognised and have been used to solve difficult synthetic problems. The resurgence of radical chemistry in organic synthesis over the past decade has sparked renewed interest in photochemistry, particularly photoredox catalysis, for its mild and unique reactivity (Scheme 12).[28]

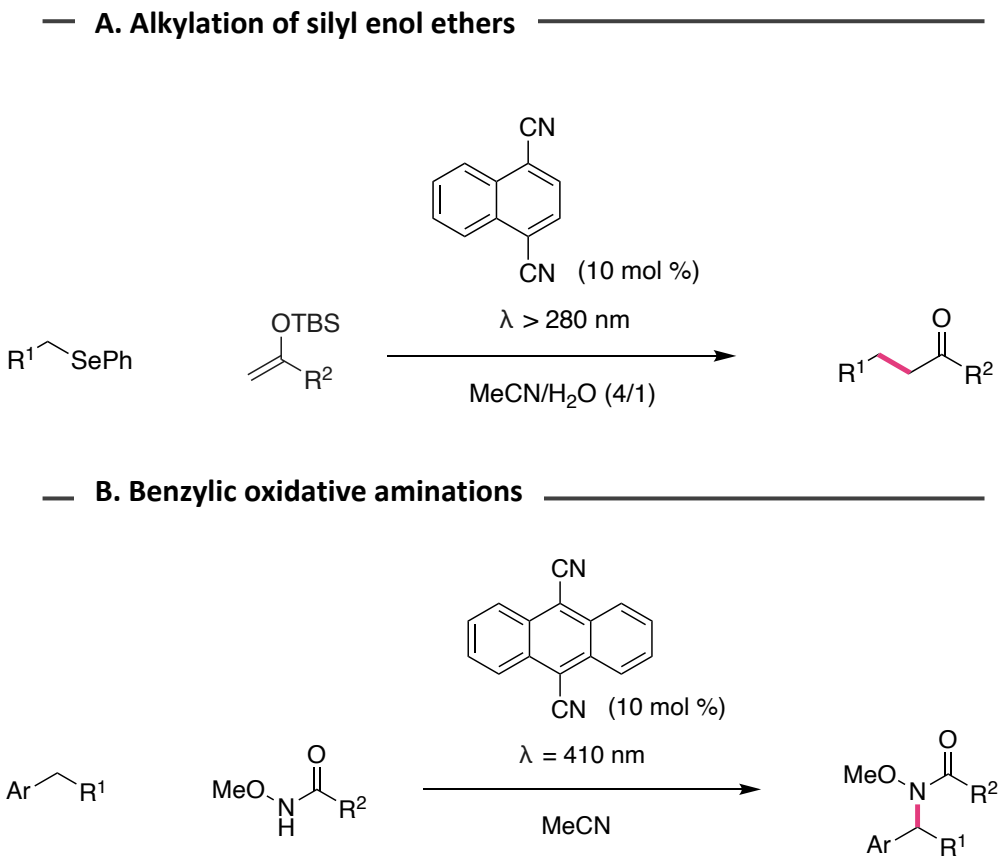


*Scheme 12. Example of photoredox catalysis: (A) Oxidative alkylation of silyl enol ethers with alkyl phenyl selenides. (B) Benzylic oxidative aminations via cyanoarene photoredox catalysis.*

In addition to their synthetic utility, radicals and radical transformations align with the principles of green chemistry.[29] The use of non-toxic reagents, atom economy, and the generation of eco-friendly byproducts are important factors in modern synthetic chemistry. With its ability to activate strong bonds under mild conditions, radical chemistry offers a route to more sustainable synthetic processes.

Understanding the underlying mechanisms of these radical reactions is essential to harness their full potential in synthesis. By comprehending the step-by-step processes by which radicals interact with other molecules, we can predict the products that will be formed and design new synthetic pathways through rational design. This involves selecting appropriate reagents, solvents, and conditions to achieve the desired transformation. Rational design is

particularly important in complex syntheses, where multiple steps must be carefully arranged to achieve the desired product. Additionally, mechanistic insight often leads to the discovery of new reactions. By understanding how existing reactions work, chemists can identify opportunities for innovation.

Mechanistic understanding is not only beneficial for the design of new transformations, but also for optimising existing ones. It allows chemists to identify reactive intermediates, anticipate side reactions, and control the selectivity of reactions ensuring that the desired product is primarily formed. By understanding the steps involved in a reaction, chemists can identify the rate-determining step and address any issues, thereby improving the overall efficiency of the reaction. This can lead to in higher yields, faster reaction times, and reduced costs.

A thorough understanding of reaction mechanisms is also important for safety and environmental reasons. Knowing how reactions proceeds can help chemists identify potentially hazardous intermediates and develop strategies to mitigate risks. It is also beneficial for designing new reactions that minimize the generation of toxic byproducts and waste.[29]

Mechanistic understanding of radical reactions provides valuable insights for designing and optimising chemical syntheses, however, gathering mechanistic information from these reactions is often challenging due to the transient nature of organic radicals. Most organic radicals have short lifetimes, with half-lives often much less than a second. This makes them difficult to detect, characterise and quantify, since most characterisation techniques require longer acquisition times than a short-lived radical lifetime. Many direct and indirect radical characterisation techniques exist, however, all have significant drawbacks. Development of better methods for short-lived radical detection, characterisation and quantification could significantly develop the areas of chemistry described above.

## 1.5. Characterisation of Radicals

### 1.5.1. Electron Spin Resonance (ESR) and Electron Paramagnetic Resonance (EPR) Spectroscopy

Electron spin resonance (ESR) spectroscopy, also known as electron paramagnetic resonance (EPR) spectroscopy, is one of the most important techniques for studying free radicals. This method is analogous to nuclear magnetic resonance (NMR), but it focuses on electron spins rather than nuclear spins. EPR spectroscopy detects the absorption of monochromatic microwaves by unpaired electrons in singly occupied molecular orbitals (SOMOs) when they transition from a magnetically aligned state to an anti-aligned state under a changing magnetic field (Figure 2).[30] Variations in the environment of the unpaired electrons change the external magnetic field at which electron excitation occurs, which helps in the characterisation of the radical species.[31-34] This technique is quantitative and non-invasive, which makes it suitable for in situ measurements. However, it has moderate sensitivity for liquid phase radical detection and provides limited structural information for atoms distant from the unpaired electron.[33, 35]

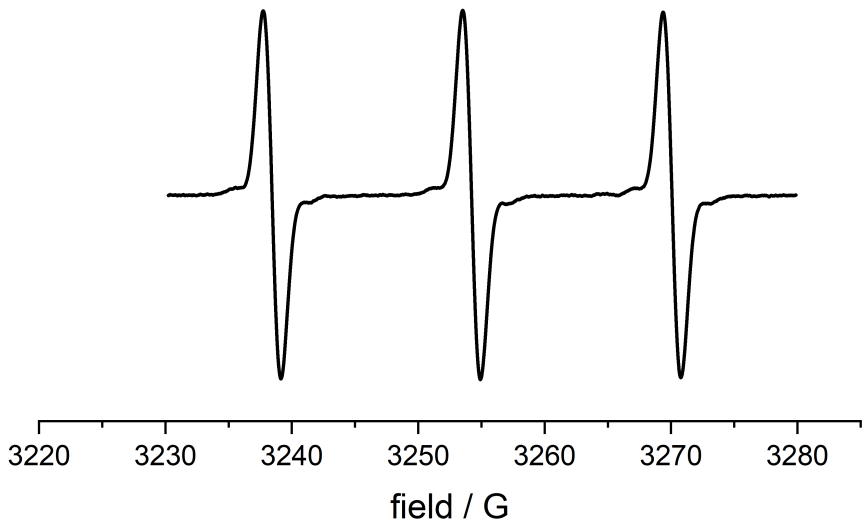


*Figure 2. EPR spectrum of 10 µM TEMPO in DCM at 25 °C.*

The exclusive detection of radicals by EPR spectroscopy makes it a useful tool for studying long-lived radicals such as TEMPO. An example of this is the use of EPR spectroscopy to monitor the photolysis of a TEMPO-functionalized benzofuran (an anticancer agent) to measure the formation of TEMPO and determining kinetics of photolysis and chemical stability.[34] However, direct characterisation of short-lived radicals is challenging due to their low steady-state concentration.

### 1.5.2. Chemically Induced Dynamic Nuclear Polarisation (CIDNP) NMR Spectroscopy

Chemically induced dynamic nuclear polarisation (CIDNP) NMR spectroscopy is another technique used in radical detection. A radical reaction monitored by NMR can display anomalies, such as enhanced absorption or emission, in the recorded spectrum. These anomalies are caused by the CIDNP effect and it is caused by the formation of spin-polarized radical pairs.[36]

When a radical pair is formed, either in cage formation or through the encounter of two radicals, the pair can only recombine in the singlet state. The orientation of some nuclear spins can influence the orientation of the electron spins in what is known as spin-orbit coupling. This results in some nuclear spins favouring singlet over triplet state, consequently the products of recombination will have an abnormal population of nuclear spins. This abnormal population is what CIDNP NMR spectroscopy detects and displays in the form of anomalous signal intensities (Figure 3).[37-39]

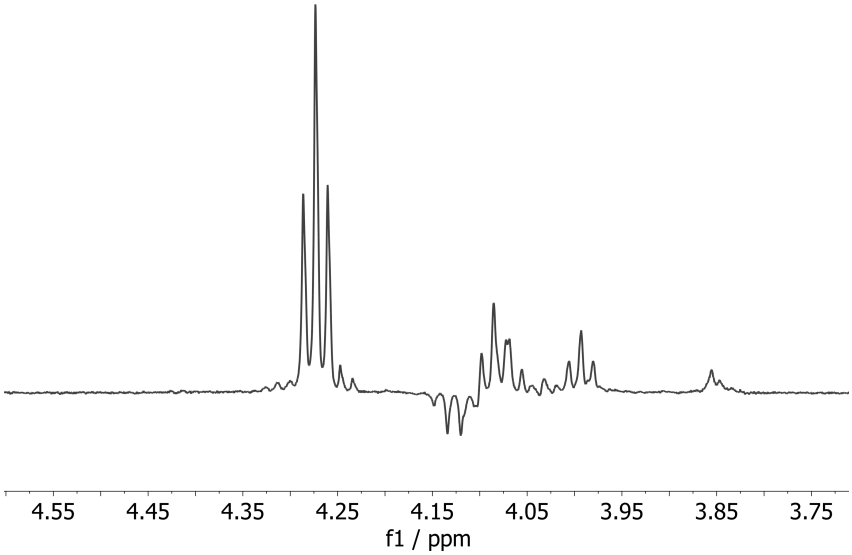


*Figure 3. $^{1}H$ NMR of a solution of $Et_3B$ (50 mM) and oxidised $Bu_3B$ (50 mM) in hexane at 25 °C, showing CIDNP effect in the form of an inverted quartet at 4.12 ppm.*

CIDNP NMR spectroscopy provides highly characteristic data, making it valuable for studying radical reactions. One example of the use of CIDNP NMR spectroscopy was the use of the technique in the study of UV-irradiated 2-phenylacetophenone. This revealed the formation of benzoyl and benzyl radicals, which offered mechanistic insights into UV-initiated degradation.[40]

However, CIDNP NMR spectroscopy is not without its challenges. The technique must be performed in situ, complicating reaction setup or field measurements. It also has poor sensitivity which makes it unsuitable for reactions with low radical concentrations like in the gas phase. Analysing CIDNP NMR spectra is challenging due to overlapping spectra in complex mixtures, requiring time-consuming deconvolution. The main limitation of the technique is that it requires the species to be formed though a recombination of a radical pair. Thus, it's best for studying simple radical reactions with high radical concentrations.

### 1.5.3. Mass Spectrometry (MS)

Mass spectrometry (MS) is employed for the direct characterisation of persistent radicals. MS measures the mass-to-charge ratio (m/z) of charged adducts or fragments formed through ionisation of neutral species.[41-46] The technique can detect both radicals and non-radical species simultaneously. One example is the use of electrospray ionisation MS (ESI-MS) to detect stable radicals like TEMPO.[47] MS is highly sensitive and can detect even gaseous radicals with detection limits of $<10^6$ molecules $cm^{-3}$.[48-50]

MS is suitable for characterising complex mixtures, as MS peaks can be attributed to specific molecular formulas. However, the detection intensity of a species depends on its ionisation efficiency, which is dependent on the structure and the composition of the reaction mixture, complicating quantification. Furthermore, this technique is not suitable for detecting short lived radicals and MS techniques are invasive and can cause the destruction of unstable species or alter their nature. Despite these limitations, MS can provide valuable mechanistic into radical reactions.

### 1.5.4. Ultraviolet-Visible (UV-Vis) and Fluorescence Spectroscopy

Ultraviolet-visible (UV-Vis) spectroscopy and fluorescence spectroscopy are techniques used for direct radical characterisation. UV-Vis spectroscopy measures the light absorbed when electrons are excited by specific wavelengths of ultraviolet-visible light, while fluorescence spectroscopy measures the light spectrum emitted when electrons relax after excitation.[51, 52] These techniques have been employed for studying long-lived radical chromophores and fluorophores. UV-Vis spectroscopy has been used to monitor the consumption of DPPH in the presence of Vitamin E,[53] and fluorescence spectroscopy has been employed to determine the emission wavelengths of highly conjugated dithiadiazolyl radicals.[54]

However, both UV-Vis and fluorescence spectroscopy produce broad peaks that might require deconvolution to obtain quantitative data. Furthermore, these techniques provide little structural information of the radical species, complicating the characterisation of unknown radicals.

Direct radical characterisation techniques provide the most definitive proof of radical identity. However, they suffer from several drawbacks such as limited applicability to specific radicals or reactions, poor sensitivity for detecting radicals with low concentrations, and challenges in characterising complex mixtures. These limitations necessitate the development of indirect radical characterisation techniques.

## 1.6. Indirect Radical Characterisation Techniques

Indirect radical characterisation techniques address some of the limitations of direct methods by chemically converting short-lived radicals to longer-lived species through reaction with trapping agents. These techniques broaden the scope for studying radicals and provide valuable insights into radical reactions.

### 1.6.1. Spin Traps

Spin trapping is a method where transient radicals are chemically transformed into more stable radicals using spin traps. Examples of spin traps are nitroso or nitrone compounds, which react with short-lived radicals to form longer-lived radical spin adducts (nitroxides) (Figure 4).[1, 2] The longer-lived radicals can be studied by EPR spectroscopy. The primary advantage of spin trapping is that it allows for the accumulation of sufficient spin adduct concentration for characterisation, thus, overcoming the sensitivity issues associated with direct radical characterisation techniques.[33-35]

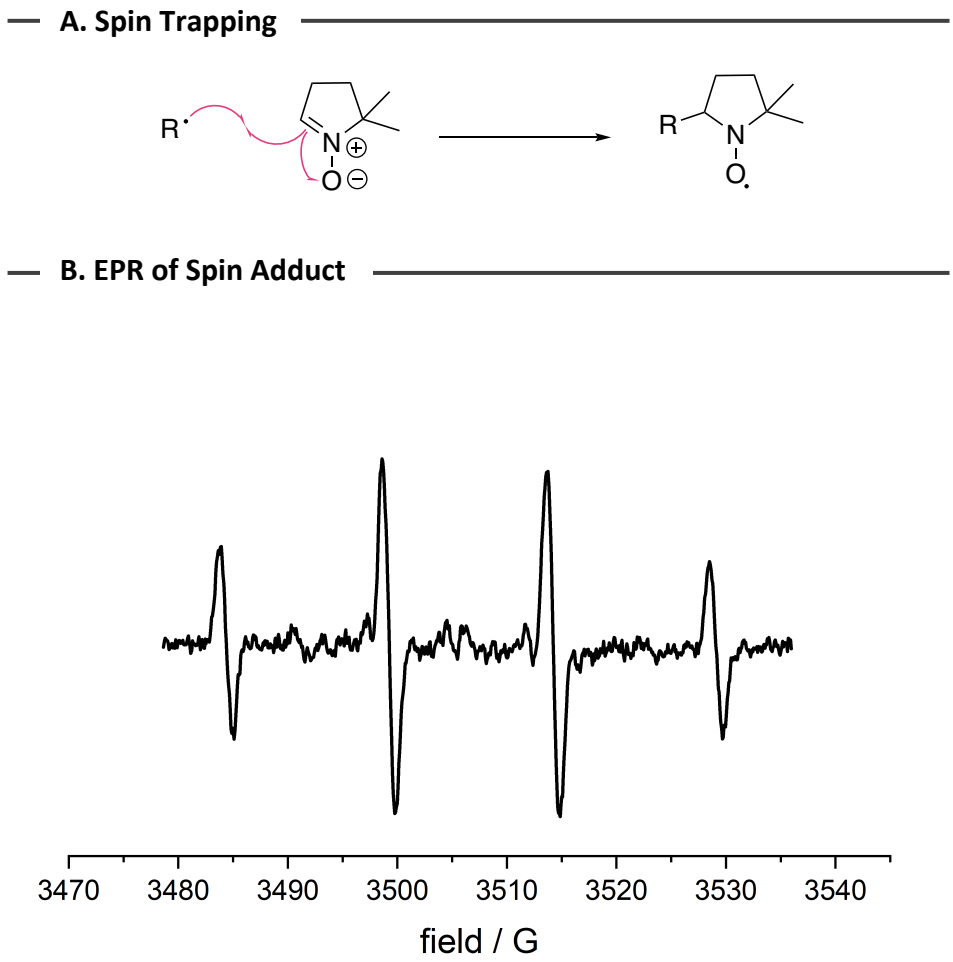


*Figure 4. (A) DMPO trapping of a radical to form a radical spin adduct. (B) EPR spectrum of a DMPO-OH adduct formed in a solution of DMPO (90 µM), $H_2O_2$ (50 µM), and $FeSO_4$ (0.04 µM) in $H_2O$.*

For instance, 5,5-dimethyl-1-pyrroline N-oxide (DMPO) nitrone spin trap and EPR spectroscopy have been utilised to detect sulphur oxide radical anions like $SO_3^{\cdot-}$ and $SO_4^{\cdot-}$.[55] These radicals are environmentally pervasive and highly toxic, with their radical forms speculated to be primarily responsible for their toxicity.[56] $SO_3^{\cdot-}$ and $SO_4^{\cdot-}$ have been trapped using DMPO, and the resulting spin adducts analysed using EPR spectroscopy.[55]

However, a significant limitation of this method is that EPR spectra of spin adducts are relatively insensitive to changes in the reactant radical. The further an atom is from the unpaired electron, the less impact it has on the EPR spectra.[32, 33] Therefore, while this method is useful for quantifying short-lived radicals, it is less effective for their characterisation.

However, MS can be employed to overcome this problem, providing further characterisation of reactant radicals.[57-63]

Despite its advantages, spin trapping has several drawbacks. Side reactions of non-radical species can lead to artifacts, resulting in false positives. For instance, nucleophilic addition of non-radical substrate to a spin trap yields a hydroxylamine, which can be oxidised to form the same species produced from radical reaction with a spin trap (Scheme 13).[64] Furthermore, nitrone and nitroso spin traps are not particularly stable and can be degraded by trace metals.[65] Spin adducts often have poor stability and short lifetimes, which complicates experimental setup and field measurements.[66-69]

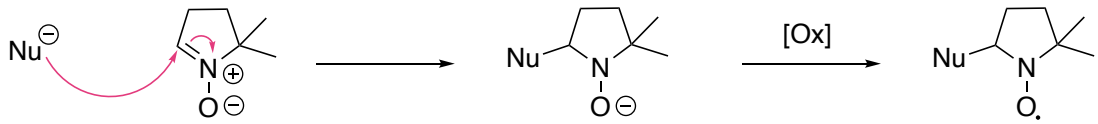


*Scheme 13. Nucleophilic addition of non-radical substrate to DMPO followed by oxidation of the resulting hydroxylamine to yield the same species produced from radical addition to DMPO.*

### 1.6.2. Recombination Traps

Recombination trapping is another technique where short-lived radicals are chemically converted into longer-lived non-radical products using stable radical trapping agents (Scheme 14).[70] This results in a longer-lived non-radical adduct, which can be characterised using conventional techniques such as MS, NMR, and UV-Vis.[70-72] This method addresses many problems associated with the instability of short-lived reactant radicals, similar to spin trapping.

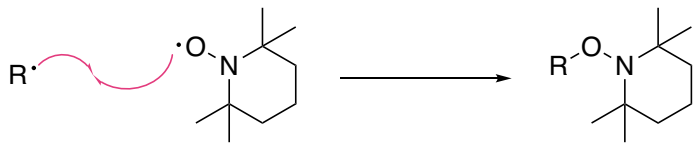


*Scheme 14. TEMPO trapping of a radical to form a non-radical stable adduct.*

The most commonly used recombination traps are nitroxyl radicals, such as TEMPO (Scheme 14). These radicals react rapidly with carbon-centred radicals and are relatively robust under a range of conditions, simplifying experimental setup and field measurements. For example, TEMPO has been used to capture radicals formed in the one-electron oxidation of N-acetyl-L-tyrosinamide, catalysed by horseradish peroxidase (HRP). The resulting non-radical recombination adduct was characterised using MS, indicating the presence and structure of the intermediate radical.[73]

However, persistent nitroxyl radicals do not trap heteroatom-centred radicals, which form weak bonds with nitroxyl radical recombination traps.[74] This limits their applicability. For instance, no recombination adducts were detected for recombination trapping of tert-butyl peroxyl radicals using TEMPO. Instead, tert-butyl oxyl radicals and molecular oxygen were formed, and TEMPO acted as a catalyst rather than a trapping agent.[75] This highlights a separate issue which is that nitroxyl radicals can initiate some radical reactions, leading to false positives.

Other recombination traps, such as 2,2-diphenyl-1-picrylhydrazyl (DPPH) and 2,4,6-tri-tert-butylphenol, have also been used for indirect radical characterisation. DPPH is frequently used as a chemical label, as its recombination adducts can be quantified using UV-Vis spectroscopy.[53] However, DPPH suffers similar issues to nitroxyl radicals, including ineffective reaction with heteroatom-centred radicals and potential false positives. 2,4,6-Tri-tert-butylphenol can be oxidised to long-lived 2,4,6-tri-tert-butylphenoxyl radicals, which can trap heteroatom-centred radicals through radical-radical recombination. These radicals react more effectively with heteroatom-centred radicals than nitroxyl radicals and DPPH, but they can also initiate radical reactions, leading to false positives.[76-78] Additionally, 2,4,6-tri-tert-butylphenol is not easily tuneable and has poor water solubility, which limits its applicability.

To address the limitations of both spin traps and recombination traps, a novel class of radical traps has been developed. The new traps, known as allyl-TEMPO traps, combine the advantages of both techniques, offering enhanced stability and sensitivity for radical characterisation.[79]

### 1.6.3. Allyl-TEMPO Traps

Allyl-TEMPO traps constitute novel type of radical traps that combine features from both spin traps and recombination traps.[79-81] These traps are characterised by a leaving group attached to a terminal allyl group, which generates a persistent radical upon bond cleavage (Scheme 15). When radicals react with these traps, they yield a non-radical product and a stable radical. The proximity of the radical leaving group to the allyl double bond facilitates allylic rearrangement and rapid and selective radical addition, which is analogous to spin trapping. The resultant non-radical product can be analysed using highly sensitive techniques such as MS and NMR spectroscopy, similar to recombination trapping. These traps can be functionalized at the allyl or non-terminal alkene position to accommodate the specific radical system under investigation, including the incorporation of water-soluble groups for biochemical studies.

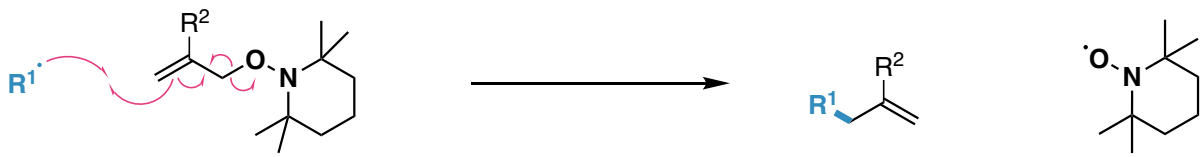


*Scheme 15. Allyl-TEMPO trapping of a radical to form a non-radical stable adduct and persistent radical TEMPO.*

These novel radical traps offer several advantages over existing techniques for radical characterisation. The non-radical products exhibit greater stability compared to spin-trapped products which often have limited lifetimes. Allyl-TEMPO traps also exhibit reactivity towards a wider variety of radicals, unlike recombination traps which show limited reactivity with heteroatomic-centred radicals. This makes allyl-TEMPO traps more suitable for studying a diverse range of radicals in different systems.[79] Moreover, allyl-TEMPO trapping is less prone to producing false positives, unlike recombination traps which are highly reactive and non-innocent components of reaction mixtures, and spin traps which are susceptible to side reactions.

When coupled with MS analysis, this radical trapping approach combines the best features of the two most common alternatives: spin trapping with EPR detection (applicability to most short-lived radicals) and TEMPO cross-coupling with MS detection (high sensitivity, detailed structural information). The new traps can be applied to both gas and liquid-phase reactions.[79-81] This method is a valuable mechanistic tool for studying radical reactions in highly complex systems, thanks to the ability to detect trapped radicals, intermediates, and by-products simultaneously. As with any trapping technique, the kinetics of the trapping reaction must be considered, and for some relatively longer-lived radicals (e.g., $RO_2\cdot$), the trapping reaction may be outcompeted by other reactions such as self-reaction.

### 1.7. Project Outline and Aims

The new Allyl-TEMPO traps offer solutions to many of the limitations faced by previous radical traps. By leveraging these advanced tools, we wondered if we could utilise this new tool to tackle a longstanding mechanistic question.

One such question is the mechanism of action of triethylborane ($Et_3B$). $Et_3B$ in air is a widely used radical initiator in organic synthesis,[82, 83] offering unique advantages over traditional initiators such as AIBN and benzoyl peroxide.[83-85] The journey of $Et_3B$ as a radical initiator began with its discovery in the mid-19th century by Frankland, who noted its spontaneous inflammability in air.[86] However, it wasn't until the growing of organometallic chemistry in the 1950s that the full potential of $Et_3B$ was realised.[87-90]

The initial breakthrough came in the 1970s when Brown's group demonstrated that the conjugate addition of trialkylborane to α,β-unsaturated carbonyl compounds was a radical reaction.[91, 92] This laid the foundation for the use of $Et_3B$ in radical processes. In 1987, the $Et_3B$-induced hydrostannylation of alkynes opened new avenues for using $Et_3B$ as a radical initiator, particularly in reactions conducted at low temperatures.[84] Unlike AIBN and benzoyl peroxide, $Et_3B$ can initiate radical reactions even at −78 °C, providing greater control over stereoselectivity and enabling the use of thermally unstable substrates.

$Et_3B$'s ability to generate radicals in the presence of a trace amount of oxygen has made it a versatile tool in organic synthesis. The ethyl radical produced by $Et_3B$ is reactive enough to abstract iodine atoms from alkyl iodides, facilitating radical addition reactions.[3, 83, 93, 94] In organic synthesis it is commonly used in combination with trialkyltin hydride, this has been exploited in the synthesis of complex molecules, including dehydroiridodiol and α-methylene-γ-butyrolactone, as well as in the stereoselective olefination of alkenes (Scheme 16).[82, 95]

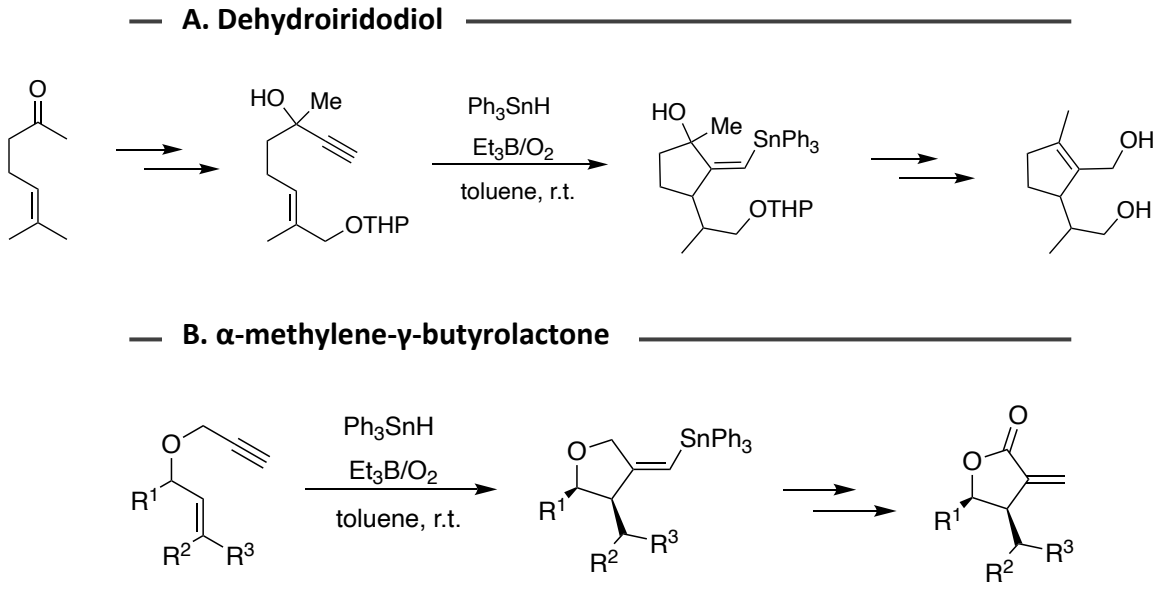


*Scheme 16. $Et_3B$ initiated hydrostannylation of alkynes in the synthesis of (A) dehydroiridodiol and (B) α-methylene-γ-butyrolactone.*

Despite its numerous advantages, the application of $Et_3B/O_2$ as a radical initiator is not without challenges, particularly concerning the reproducibility of results. Synthetic chemists often experience difficulties in replicating reactions, likely due to variations in the method of oxygen provision.[83] The bimolecular nature of the $Et_3B/O_2$ initiation mechanism introduces sensitivity to the concentrations of both reactants, complicating control compared to unimolecular initiators like AIBN (Scheme 17).[85]

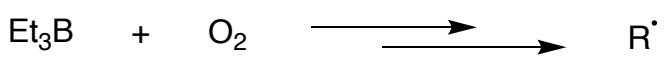


*Scheme 17. Reaction of $Et_3B$ with $O_2$.*

Moreover, the initiation with $Et_3B/O_2$ is known for its experimental inconsistencies. While some reactions initiate reliably with minimal amounts of $Et_3B/O_2$, others are challenging to start or sustain.[85] There is no consensus on the optimal conditions for oxygen provision, with varying opinions ranging from trace amounts of $O_2$ to direct bubbling of $O_2$ into the solution.[85]

The underlying complexity of $Et_3B$ initiation worsens these issues. Although AIBN and $Et_3B/O_2$ are often considered interchangeable, their initiation chemistries are very different. AIBN undergoes unimolecular homolysis to form radicals, whereas $Et_3B$ and $O_2$ react bimolecularly, making the rate dependent on the concentrations of both reactants. Additionally, the fate of the initiating radicals differs; AIBN radicals terminate through standard radical-radical reactions, while $Et_3B/O_2$ radicals initiate a radical chain autoxidation of $Et_3B$. Additionally, the products of autoxidation are not inert in and can act as secondary initiators.[87, 90]

Despite extensive studies, the initiation mechanism of $Et_3B$ is so complex that some parts of the mechanism remain elusive.[96] The primary reaction between $Et_3B$ and $O_2$ is slow, yet $Et_3B$ is rapidly consumed upon contact with $O_2$, potentially leading to runaway reactions. This rapid consumption is due to the efficient autoxidation chain that follows the primary reaction of initiation, which recycles radicals without generating new ones (Scheme 18).[90] Consequently, the initiation reaction appears inefficient, producing few radicals, while the autoxidation chain consumes both reactants without contributing to radical generation. Despite these issues, $Et_3B$ remains a staple radical initiator in organic chemistry due to its efficiency when it functions correctly.[3, 83]

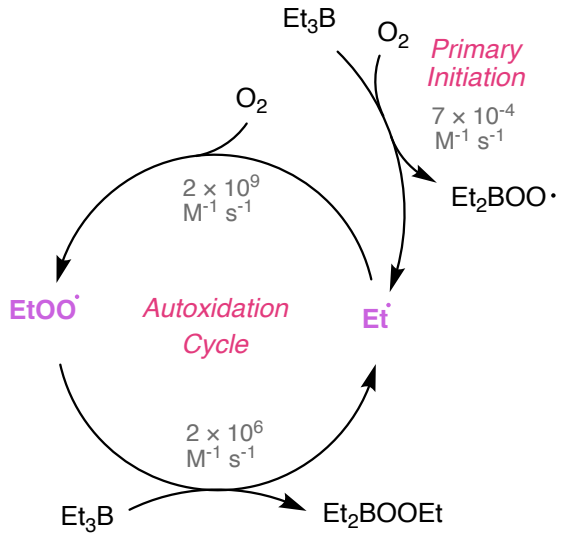


*Scheme 18. Mechanism of autoxidation of $Et_3B$.*

The question then arises: what conditions of $Et_3B$, $O_2$, and solvent optimise $Et_3B$ as a radical initiator? Should the autoxidation chain be promoted, or should $O_2$ provision be limited to prevent inefficient consumption of $Et_3B$?

Some studies suggest that autoxidation is beneficial due to the formation of $Et_2BOOEt$, which may also contribute to the radical initiation.[97, 98] However, there is no consensus on its efficiency, and the mechanism by which this peroxide produces radicals remains unclear.[85, 99] The literature lacks quantitative data and direct experimental proof of the peroxide's relevance in overall radical production within the $Et_3B$ system.

Even if $Et_2BOOEt$ was an effective initiator, the optimal conditions for $Et_3B$ initiation remain unclear. Should autoxidation be promoted to form the desired peroxide, or is it more efficient to maintain low $O_2$ concentrations and avoid inefficient autoxidation?[85]

The complexity of the system and the numerous unknowns complicate the development of predictive models.[85, 99] This is where our research comes in. We wondered if we could use the newly developed radical traps to elucidate the unknowns of the mechanism of $Et_3B$ initiation.

**Aim**

To use the newly developed allyl-TEMPO radical traps to study the mechanism of initiation of $Et_3B$. By addressing the unknowns in the mechanism, we hope to establish a model that identifies the most efficient conditions for radical generation with $Et_3B$.

Our goal is to leverage this new information to initiate challenging reactions that have historically struggled with $Et_3B/O_2$. By efficiently generating radicals from $Et_3B$, we aim to overcome the limitations of inefficient reactions that require constant initiation.

## 2. Mechanistic Study on the Autoxidation of Triethylborane

### 2.1. Introduction

#### 2.1.1. Historical Background

The exploration of borane chemistry dates back to the mid-19th century, with significant discoveries that have shaped our understanding and utilisation of these compounds. The reaction of boranes with oxygen has been known for about 150 years,[86] but it wasn't until the mid-20th century that intensive studies began to reveal the mechanistic complexities of these reactions.

Early attempts to inhibit the autoxidation of organoboranes using chain inhibitors like quinol, iodine, or methyl methacrylate were unsuccessful.[100-102] This led to the hypothesis of a nucleophilic 1,3-rearrangement mechanism (Scheme 19). However, this hypothesis was later disproven by the complete racemisation observed in chiral organoboranes during autoxidation.[103]

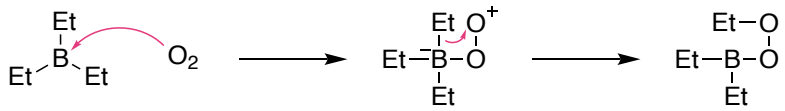


*Scheme 19. Proposed heterolytic mechanism of $Et_3B$ autoxidation before the determination that the mechanism is homolytic.*

The inhibition of autoxidation by galvinoxyl, a strong antioxidant, provided strong evidence for a radical chain mechanism.[104, 105]

In the 1960s, significant progress was made in understanding the radical chain reactions involving boranes and oxygen. In 1969, Contreras initiated polymerisations using $Et_3B$ and hydrogen peroxide.[106] This marked an important moment in the study of borane chemistry, as it opened up new avenues for exploring the reactivity of $Et_3B$.

Around the same time, researchers like Davies and Roberts were working to elucidate the mechanism of radical chain reactions involving various boranes and oxygen.[88-90, 107] Their work laid the foundation for a detailed understanding of how these reactions proceed, highlighting the role of radical intermediates.

### 2.1.2. Mechanism of Triethylborane Autoxidation

The autoxidation of $Et_3B$ is a complex process that involves radical chain mechanisms. Understanding this mechanism is important for using $Et_3B$ in chemical reactions, particularly in radical initiations and polymerisations.

**Initiation:**

The initiation step consists of a bimolecular homolytic substitution ($S_H2$) which involves the homolytic cleavage of the B-C bond in $Et_3B$ by triplet oxygen. This reaction generates an ethyl radical (Et·) and a boron peroxyl radical ($Et_2BOO$·) (Scheme 20).

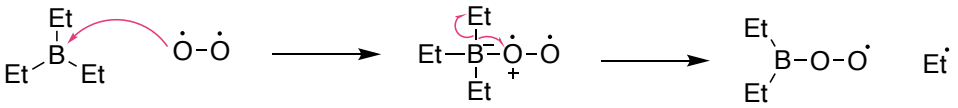


*Scheme 20. Primary initiation step in $Et_3B$ autoxidation involving an $S_H2$ reaction of $O_2$ at the boron.*

**Propagation:**

In the propagation steps, the ethyl radical reacts with molecular oxygen to form an ethyl peroxyl radical (EtOO·). This peroxyl radical can then react with another molecule of triethylborane to produce diethyl(ethylperoxy)borane ($Et_2BOOEt$) and another ethyl radical, continuing the chain reaction (Scheme 21).

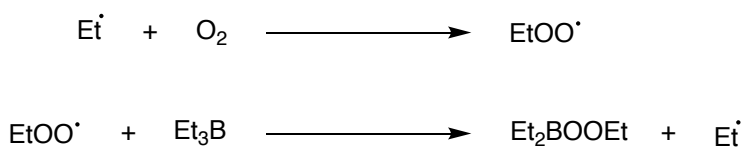


*Scheme 21. Chain propagation steps of the autoxidation of $Et_3B$.*

**Termination:**

Termination involves the combination of radicals to form stable products, thus, ending the chain reaction. Possible termination reactions include the combination of two ethyl radicals, the combination of an ethyl radical with an ethyl peroxyl radical, and the combination of two ethyl peroxyl radicals (Scheme 22).

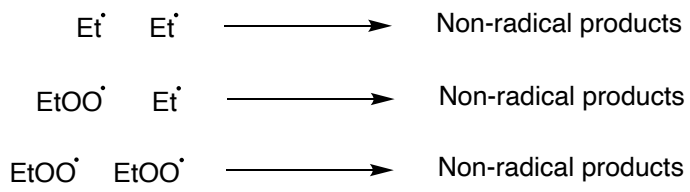


*Scheme 22. Possible termination reactions in the autoxidation of $Et_3B$.*

### 2.1.3. Kinetic Analysis and Rate Constants

The kinetics of triethylborane autoxidation have been extensively studied. The rate constant for the primary initiation process (Scheme 20) has been estimated to be $7 \times 10^{-4}$ $M^{-1}$ $s^{-1}$ at 25 °C.[87] This is a very slow process, however $Et_3B$ reacts with $O_2$ very rapidly. This is because the propagation steps are very fast. The reaction of ethyl radical with $O_2$ to give ethyl peroxyl radicals is near diffusion limit, with a rate constant estimated to be $2 \times 10^9$ $M^{-1}$ $s^{-1}$. The rate constant for the homolytic substitution at the boron centre of tributylborane by a butylperoxyl radical has been measured to be $2 \times 10^6$ $M^{-1}$ $s^{-1}$ at 30 °C.[88, 90] This high-rate constant explains why conventional inhibitors, such as quinol or iodine, are ineffective in preventing the autoxidation of organoboranes.[100, 102, 108]

These reaction kinetics show that $Et_3B$ autoxidation is an efficient chain reaction which has a very slow initiation step (Scheme 23).

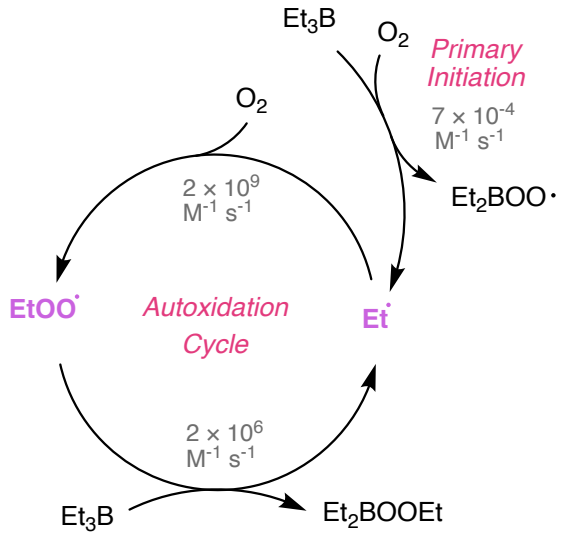


*Scheme 23. Mechanism of autoxidation of triethylborane.*

Despite extensive research, there are still gaps in our understanding of the mechanisms underlying the autoxidation and initiation processes of triethylborane. Some of the key areas that require further investigation include:

**Radical Intermediates:**

The identification and characterisation of the radical intermediates formed during the autoxidation of triethylborane are crucial for a comprehensive understanding of the reaction mechanism. While some intermediates, such as ethyl radicals and peroxyl radicals, have been identified, the full spectrum of radical species and their roles in the propagation and termination steps remain to be fully elucidated.

**Reaction Kinetics:**

Although the rate constants for certain steps in the autoxidation mechanism have been measured, a complete kinetic model that accounts for all the elementary steps and intermediates is still lacking.[85] Such a model would provide a more accurate prediction of

reaction rates and would help identifying potential bottlenecks or side reactions that could affect the overall efficiency of the process.

**Initiation Process:**

The mechanism by which $Et_3B$ initiates radical reactions remains incompletely understood. While it is generally accepted that the initiation involves the reaction between triplet oxygen and $Et_3B$, other mechanisms of initiation have been proposed such as the homolysis of the peroxide $Et_2BOOEt$.[99] The reactivity of this intermediate and its role in the autoxidation of $Et_3B$ remains one of the most obscure parts of the mechanism.

**Reproducibility and Consistency:**

Another issue with $Et_3B$ is the reproducibility and consistency of its reactions. The effectiveness of $Et_3B$ as a radical initiator is greatly influenced by the specific conditions under which the reactions are conducted. Researchers often experience issues when reproducing a method from the literature, these issues often stem from the heterogeneity of the system and the purity of $Et_3B$.[83]

## 2.2. Chapter 2 Aims

1. Use the allyl-TEMPO radical trap to detect and characterise the radical intermediates formed in the mechanism of $Et_3B$ autoxidation.
2. Perform a kinetic analysis of the reaction to understand the individual processes taking place.
3. Study the formation and reactivity of intermediate $Et_2BOOEt$ in the autoxidation of $Et_3B$

## 2.3. Radical Trapping

It is well known that $Et_3B$ autoxidation involves formation of ethyl and ethyl peroxyl radicals, however, the full spectrum of radical species and their roles in the propagation and termination steps remain to be fully characterised. We decided to implement the new allyl-TEMPO radical traps to shine some light onto the formation of other radical species.

Additionally, the allyl-TEMPO trapping would allow us to measure the trapped radicals individually, providing semi-quantitative data that can inform us on which radicals are formed in higher concentrations and which radicals are more reactive.

Radical trapping was performed in a solution of $Et_3B$ in THF in the presence of $O_2$ using radical trap CHANT, followed by MS analysis to identify the trapped species (Table 1) (50 mM $Et_3B$, 5mM CHANT, 1 mL THF. Experiment detailed in section 6.3.1). The table shows the different types of trapped radicals (first column), the MS species that is detected, e.g. trapped ethyl radical can appear as a CHANT adduct sodiated $[CHANT+Et\cdot+Na]^+$ (second column), the m/z of said species (third column), and the intensity of the peak that appears at that m/z (fourth column).

*Table 1. Trapped radicals using CHANT in the oxidation of $Et_3B$ under air, in THF, and at 25 °C. Experiment detailed in section 6.3.1.*

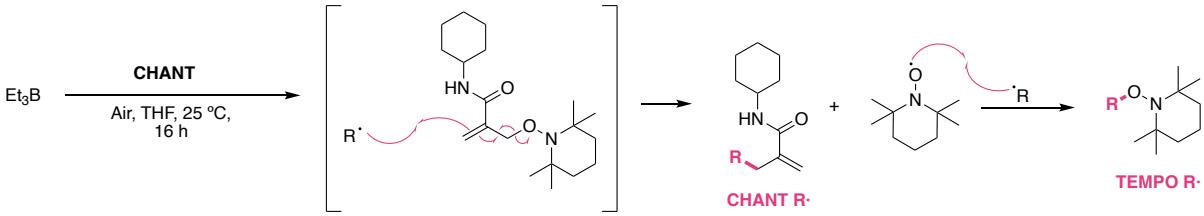


| Species | | m/z | MS peak Intensity |
|---|---|---|---|
| Unreacted Trap | $[CHANT+H]^+$ | 323.2699 | 9946 |
| Trapped Et· | $[CHANT+Et\cdot+H]^+$ | 196.1698 | 68 |
| | $[CHANT+Et\cdot+Na]^+$ | 218.1518 | 1219 |
| | $[TEMPO+Et\cdot+H]^+$ | 186.1855 | 633 |
| Trapped $Et_2BOO\cdot$ | $[CHANT+Et_2BOO\cdot+H]^+$ | 268.2084 | - |
| | $[CHANT+Et_2BOO\cdot+Na]^+$ | 290.1903 | - |
| Trapped $Et_2BO\cdot$ | $[CHANT+Et_2BO\cdot+H]^+$ | 252.2135 | - |
| | $[CHANT+Et_2BO\cdot+Na]^+$ | 274.1954 | - |
| Trapped EtO· | $[CHANT+EtO\cdot+H]^+$ | 212.1650 | 23 |
| | $[CHANT+EtO\cdot+Na]^+$ | 234.1470 | 6 |
| Trapped EtOO· | $[CHANT+EtOO\cdot+H]^+$ | 228.1600 | - |
| | $[CHANT+EtOO\cdot+Na]^+$ | 250.1419 | - |

Trapped ethyl radicals were successfully observed in both protonated and sodiated forms, as expected due to their high reactivity and expected abundance.

Ethylperoxyl radicals (EtOO·) are formed in the autoxidation cycle of $Et_3B$, however, these were not detected. The reason we don't see ROO· is that their trapping rates are slow ($k \approx 10^{-1}$ $M^{-1}$ $s^{-1}$),[109] and the rates of their reaction with $Et_3B$ are very fast ($k \approx 10^6$ $M^1$ $s^{-1}$).[88]

In addition to ethyl radicals, trapped ethoxyl radicals (EtO·) were detected. The formation of these radicals provides an interesting insight into the underlying mechanism as ethoxyl

radicals are not formed during autoxidation but via auto-initiation processes, specifically the homolysis of $Et_2BOOEt$ (Scheme 24). EtO· can also form through recombination of two EtOO· radicals, however this is a very minor pathway as most recombinations proceed via a non-radical route.[1] This might suggests the formation and of intermediate $Et_2BOOEt$ in $Et_3B$ autoxidation.[99]

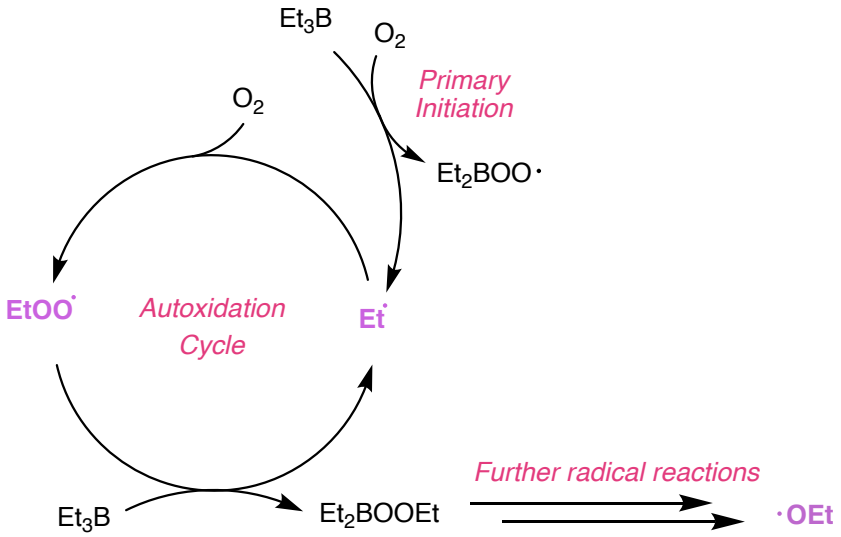


*Scheme 24. Radicals formed in the autoxidation of $Et_3B$.*

No boron-containing products were observed, likely due to very poor ionisation efficiency in positive mode ESI, possibly because of the acidic nature of boron compounds. ESI typically ionizes molecules using small amounts of acid, effective for organic molecules with basic functional groups. For acidic compounds like carboxylic acids, negative mode ionisation in MS is preferable. This may apply to our boron compounds, given the empty p orbital in boron. Further discussion and optimisation of MS conditions for boron compounds will be addressed in Section 3.4.1.

Additionally, strong signals were identified for trapped solvent radicals (Table 2). The peak for the protonated trapped THF radical was 30 times more intense than that for captured ethyl radicals and 4 times stronger than the unreacted trap.

*Table 2. Trapped radicals using CHANT in the oxidation of $Et_3B$ under air, in THF, and at 25 °C. Experiment detailed in section 6.3.1.*

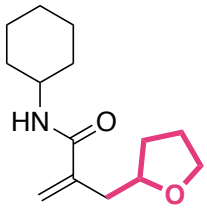


Trapped THF·

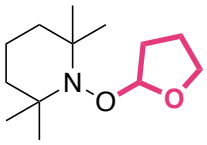


TEMPO THF·

| Species | | m/z | MS peak Intensity |
|---|---|---|---|
| Unreacted Trap | $[CHANT+H]^+$ | 323.2699 | 9946 |
| Trapped Et· | $[CHANT+Et\cdot+H]^+$ | 196.1698 | 68 |
| | $[CHANT+Et\cdot+Na]^+$ | 218.1518 | 1219 |
| | $[TEMPO+Et\cdot+H]^+$ | 186.1855 | 633 |
| Trapped THF· | $[CHANT+THF\cdot+H]^+$ | 238.1803 | 38110 |
| | $[CHANT+THF\cdot+Na]^+$ | 260.1622 | 5264 |
| | $[TEMPO+THF\cdot+H]^+$ | 228.1960 | 49028 |
| | $[TEMPO+THF\cdot+Na]^+$ | 250.1780 | 106 |

THF molecules contain labile H atoms in the α-carbon susceptible to H-abstraction by Et· or EtOO· radicals (Scheme 25).[110, 111] Despite it being likely that there is a faster rate of trapping than H-abstraction, the much higher concentration of solvent molecules than CHANT may result in more H-abstraction.

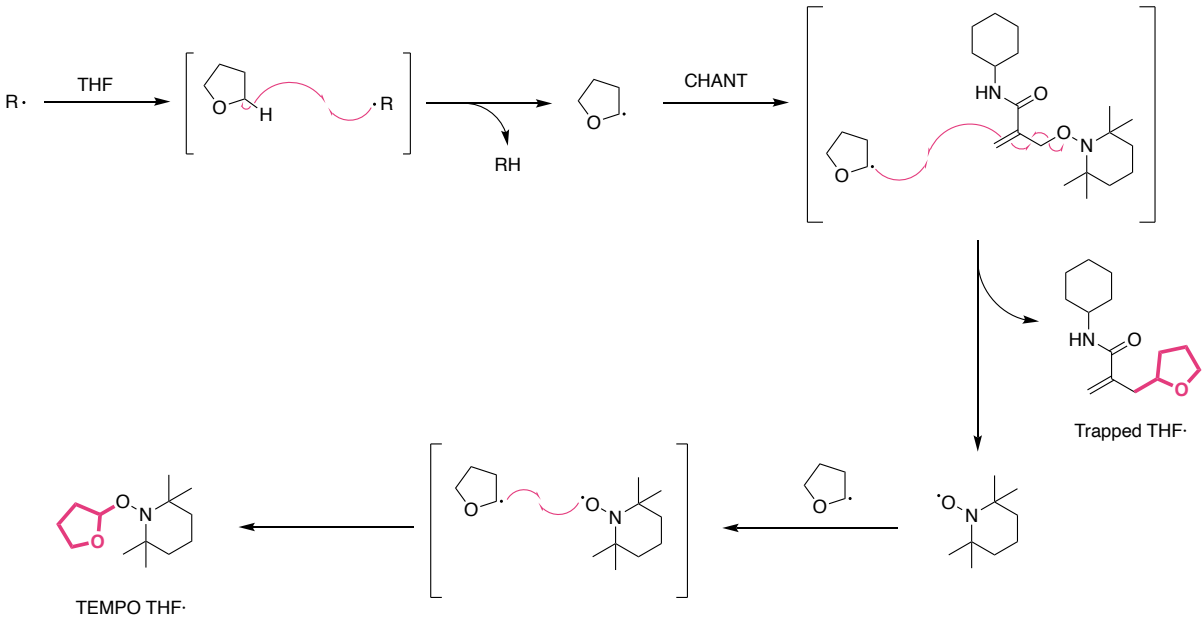


*Scheme 25. Mechanism of formation of trapped THF· and TEMPO THF·.*

H-abstraction from THF competes with radical trapping and chain initiation. When $Et_3B$ is used as a radical chain initiator in THF it is likely that a similar process occurs where ethyl radicals predominantly abstract H from THF rather than initiate chains. It is possible that the resulting THF radical is able to initiate the target chain. However, in the present study, the reaction of Et· with THF interferes with the detection of these and perhaps other radicals.

To mitigate this, DCM was chosen as the solvent for future experiments, as its protons are less prone to hydrogen abstraction.[112] However, since $Et_3B$ was used as a THF solution, some THF will still be present, though its impact will be reduced, resulting in weaker MS signals for captured THF.

This was confirmed by using DCM as the solvent (Table 3). Peaks for trapped THF appeared with an intensity of 472 S/N, about 80 times weaker than previously reported, with minimal peaks for trapped DCM radicals (50 mM $Et_3B$, 5 mM CHANT, 1 mL DCM. Experiment detailed in section 6.3.2.). The sodiated ion of the captured ethyl radical was the most intense peak, followed by the unreacted trap.

*Table 3. Trapped radicals using CHANT in the oxidation of $Et_3B$ under air, in DCM, and at 25 °C. Experiment detailed in section 6.3.2.*

| Species | | m/z | MS peak Intensity |
|---|---|---|---|
| Unreacted Trap | $[CHANT+H]^+$ | 323.2699 | 572 |
| Trapped Et· | $[CHANT+Et\cdot+H]^+$ | 196.1698 | 21 |
| | $[CHANT+Et\cdot+Na]^+$ | 218.1518 | 1072 |
| | $[TEMPO+Et\cdot+H]^+$ | 186.1855 | 610 |
| Trapped $Et_2BOO\cdot$ | $[CHANT+Et_2BOO\cdot+H]^+$ | 268.2084 | - |
| | $[CHANT+Et_2BOO\cdot+Na]^+$ | 290.1903 | - |
| Trapped $Et_2BO\cdot$ | $[CHANT+Et_2BO\cdot+H]^+$ | 252.2135 | - |
| | $[CHANT+Et_2BO\cdot+Na]^+$ | 274.1954 | - |
| Trapped EtO· | $[CHANT+EtO\cdot+H]^+$ | 212.165 | 6 |
| | $[CHANT+EtO\cdot+Na]^+$ | 234.147 | 5 |
| Trapped EtOO· | $[CHANT+EtOO\cdot+H]^+$ | 228.16 | - |
| | $[CHANT+EtOO\cdot+Na]^+$ | 250.1419 | - |
| Trapped THF· | $[CHANT+THF\cdot+H]^+$ | 238.1803 | 473 |
| | $[CHANT+THF\cdot+Na]^+$ | 260.1622 | 344 |
| | $[TEMPO+THF\cdot+H]^+$ | 228.1960 | 572 |
| | $[TEMPO+THF\cdot+Na]^+$ | 250.1780 | 3 |
| Trapped DCM· | $[CHANT+CHCl_2\cdot+H]^+$ | 250.0760 | 15 |
| | $[CHANT+CHCl_2\cdot+Na]^+$ | 272.0578 | 18 |

A detailed analysis of the MS peaks revealed that several previously unidentified peaks corresponded to multiple additions of radicals to the trap. This raised concerns as several of these peaks were among the most intense in the spectrum. Notably, from the twenty most intense peaks, ten were identified as products of these reactions (Table 4).

*Table 4. Products of multiple radical addition to CHANT in the oxidation of $Et_3B$ under air, in DCM, and at 25 °C. Experiment detailed in section 6.3.2.*

| Species | | | m/z | MS peak Intensity |
|---|---|---|---|---|
| 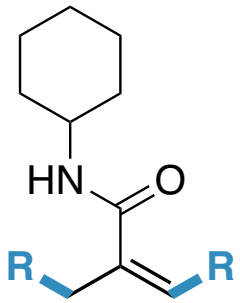 | Et· + Et· | $H^+$ | 224.2009 | 203 |
| | | $Na^+$ | 246.1828 | 139 |
| | Et· + EtO· | $H^+$ | 240.1958 | 6 |
| | | $Na^+$ | 262.1777 | 4 |
| | Et· + THF· | $H^+$ | 266.2114 | 175 |
| | | $Na^+$ | 288.1933 | 74 |
| | Et· + $CHCl_2$· | $H^+$ | 278.1072 | 24 |
| | | $Na^+$ | 300.0891 | 26 |
| | THF· + THF· | $H^+$ | 308.2219 | 20 |
| | | $Na^+$ | 330.2038 | 16 |
| | THF· + $CHCl_2$· | $H^+$ | 320.1177 | 12 |
| 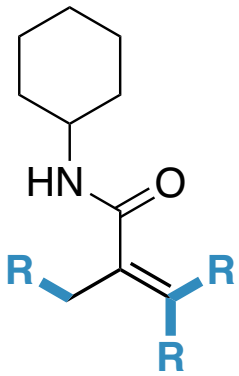 | Et· + Et· + Et· | $H^+$ | 252.2321 | 9 |
| | | $Na^+$ | 274.214 | 4 |
| | Et· + Et· + EtO· | $H^+$ | 268.227 | 90 |
| | | $Na^+$ | 290.209 | 38 |
| | Et· + Et· + THF· | $H^+$ | 294.2426 | 7 |
| | | $Na^+$ | 316.2246 | 4 |
| | Et· + EtO· + EtO· | $H^+$ | 284.2219 | 4 |
| | | $Na^+$ | 306.204 | 4 |
| | Et· + EtO· + THF· | $H^+$ | 310.2375 | 15 |
| | | $Na^+$ | 332.2194 | 11 |
| | Et· + EtO· + $CHCl_2$· | $H^+$ | 322.1334 | 6 |
| | | $Na^+$ | 344.1152 | 6 |

| Species | | | m/z | MS peak intensity |
|---|---|---|---|---|
| 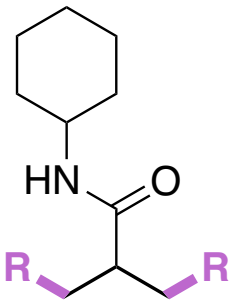 | Et· + Et· | $H^+$ | 226.2165 | 100 |
| | | $Na^+$ | 248.1984 | 45 |
| | Et· + EtO· | $H^+$ | 242.2114 | 32 |
| | | $Na^+$ | 264.1933 | 8 |
| | Et· + THF· | $H^+$ | 268.227 | 90 |
| | | $Na^+$ | 290.209 | 38 |
| | Et· + $CHCl_2$· | $H^+$ | 280.1229 | 8 |
| | | $Na^+$ | 302.1047 | 8 |
| | EtO· + EtO· | $H^+$ | 258.2064 | 4 |
| | | $Na^+$ | 280.1882 | 7 |
| | EtO· + THF· | $H^+$ | 284.2219 | 4 |
| | | $Na^+$ | 306.204 | 4 |
| | THF· + THF· | $H^+$ | 310.2375 | 15 |
| | | $Na^+$ | 332.2194 | 11 |
| | THF· + $CHCl_2$· | $H^+$ | 322.1334 | 6 |
| | | $Na^+$ | 344.1152 | 6 |
| 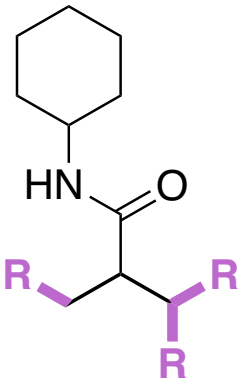 | Et· + Et· + Et· | $H^+$ | 254.2478 | 111 |
| | | $Na^+$ | 276.2297 | 90 |
| | Et· + Et· + EtO· | $H^+$ | 270.2427 | 9 |
| | | $Na^+$ | 292.2247 | 3 |
| | Et· + Et· + THF· | $H^+$ | 296.2583 | 178 |
| | | $Na^+$ | 318.2402 | 89 |
| | Et· + Et· + $CHCl_2$· | $H^+$ | 308.1541 | 13 |
| | | $Na^+$ | 330.136 | 19 |
| | Et· + EtO· + THF· | $H^+$ | 312.2531 | 5 |
| | | $Na^+$ | 334.2352 | 4 |
| | Et· + EtO· + THF· | $H^+$ | 338.2688 | 37 |
| | | $Na^+$ | 360.2507 | 28 |
| | Et· + THF· + $CHCl_2$· | $H^+$ | 350.1646 | 15 |

| | | | |
|---|---|---|---|
| | $Na^+$ | 372.1465 | 16 |
| EtO· + EtO· + THF· | $Na^+$ | 350.2302 | 3 |
| THF· + THF· + THF· | $Na^+$ | 402.2612 | 3 |
| THF· + THF· + $CHCl_2$· | $H^+$ | 392.1749 | 3 |

Products of multiple addition form when a free radical reacts with a trapped radical adduct. As most of CHANT is gone at the end of the reaction and its concentration is lower than the concentration of radical adducts, multiple additions become important. There are various possible reactions for the formation of these side products, some of these are shown in Scheme 26. The trapped adducts have a terminal olefin to which a free radical can add, forming a tertiary radical. One possibility is that this radical terminates with another free radical, resulting in the product of triple addition (blue). It can also undergo hydrogen abstraction by a second radical, reforming the double bond (red). Another possibility is that the radical formed abstracts a labile hydrogen from another molecule, yielding the reduced product of double addition to the trap (purple).

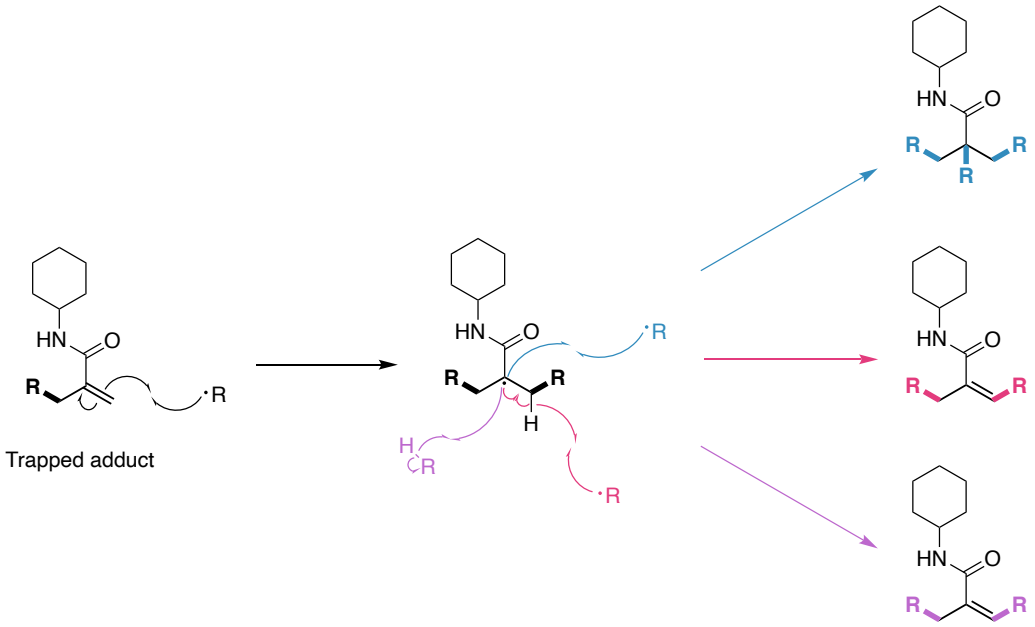


*Scheme 26. Possible mechanism of formation of products of multiple additions.*

These are examples of possible reactions involved in the formation of multiple addition products. There may be more processes, such as radical addition to the olefin formed in the red and purple products. The variety of reactions is evidenced by the variety of products observed in Table 4. However, they all involve a reaction of a free radical with the radical adduct. Therefore, an effective way to prevent the addition of radicals to the trapped adducts would be to increase the concentration of the trap (50 mM $Et_3B$, 16 mM CHANT, 1 mL DCM. Experiment detailed in section 6.3.3.). Under these conditions, trapping will be favoured over multiple additions (Table 5).

*Table 5. Trapped radicals using CHANT in the oxidation of $Et_3B$ under air, in DCM, and at 25 °C. Experiment detailed in section 6.3.3.*

| | Species | m/z | MS peak Intensity | |
|---|---|---|---|---|
| | | | **0.1 eq. CHANT** | **0.3 eq. CHANT** |
| Unreacted Trap | $[CHANT+H]^+$ | 323.2699 | 572 | 62038 |
| Trapped Et· | $[CHANT+Et\cdot+H]^+$ | 196.1698 | 21 | 106 |
| | $[CHANT+Et\cdot+Na]^+$ | 218.1518 | 1072 | 2295 |
| | $[TEMPO+Et\cdot+H]^+$ | 186.1855 | 610 | 594 |
| Trapped $Et_2BOO\cdot$ | $[CHANT+Et_2BOO\cdot+H]^+$ | 268.2084 | - | - |
| | $[CHANT+Et_2BOO\cdot+Na]^+$ | 290.1903 | - | - |
| Trapped $Et_2BO\cdot$ | $[CHANT+Et_2BO\cdot+H]^+$ | 252.2135 | - | - |
| | $[CHANT+Et_2BO\cdot+Na]^+$ | 274.1954 | - | - |
| Trapped EtO· | $[CHANT+EtO\cdot+H]^+$ | 212.165 | 6 | 41 |
| | $[CHANT+EtO\cdot+Na]^+$ | 234.147 | 5 | 14 |
| Trapped EtOO· | $[CHANT+EtOO\cdot+H]^+$ | 228.16 | - | 3 |
| | $[CHANT+EtOO\cdot+Na]^+$ | 250.1419 | - | 2 |
| Trapped THF· | $[CHANT+THF\cdot+H]^+$ | 238.1803 | 473 | 1450 |
| | $[CHANT+THF\cdot+Na]^+$ | 260.1622 | 344 | 332 |
| | $[TEMPO+THF\cdot+H]^+$ | 228.196 | 572 | 410 |
| | $[TEMPO+THF\cdot+Na]^+$ | 250.178 | 3 | 8 |
| Trapped DCM· | $[CHANT+DCM\cdot+H]^+$ | 250.076 | 15 | 239 |
| | $[CHANT+DCM\cdot+Na]^+$ | 272.0578 | 18 | 97 |

A significant improvement was observed when these conditions were implemented. As expected, there was a notable increase in the intensity of trapped radicals. Importantly, for the first time, the presence of trapped ethyl peroxyl radicals (EtOO·) was observed, albeit with low intensity. This is the first evidence of EtOO· in the system. Unfortunately, no other boron containing radicals were observed.

Additionally, the number of multiple additions decreased, with 17 fewer peaks of multiple additions, and the intensity of the remaining peaks decreased by a factor of 5 on average.

With the trapping method optimised, we compared the results of trapping the radicals from $Et_3B$ autoxidation to those trapped in tributylborane ($Bu_3B$) autoxidation.

The chemistry of $Bu_3B$ is similar to that of $Et_3B$. In the presence of oxygen, $Bu_3B$ oxidises, forming butyl radicals (Bu·) and peroxyl radicals ($Bu_2BOO$·). The mechanism of autoxidation is the same as for $Et_3B$.[90] It was theorized that studying this analogous organoboron compound in parallel would shed light on the $Et_3B/O_2$ system. As molecular weight of $Bu_3B$ is higher than that of $Et_3B$, the peaks for the observed captured radicals would be shifted to higher m/z. This approach offers two primary benefits. First, it corroborates the assignment of peaks. If a peak corresponding to a trapped ethyl radical was previously identified, it should be absent, and instead, a peak corresponding to a trapped butyl radical at a higher m/z should be observed. This applies to other trapped radicals as well; for instance, BuO· should replace EtO·, and BuOO· should replace BuO·. This would confirm that the peaks assigned to these species indeed correspond to them.

Second, shifting the masses to higher m/z allows the detection of products that would otherwise fall below the detection limit of the MS instrument (100 m/z). For example, products such as $Et_2BOH$ (86.09 m/z) would now be $Bu_2BOH$ (142.15 m/z), making them detectable by the MS instrument.

Under the trapping conditions previously optimised for the $Et_3B/O_2$ system the same types of radicals were detected, further supporting the assignment (50 mM $Bu_3B$, 16 mM CHANT, 1 mL DCM. Experiment detailed in section 6.3.6.) (Table 6).

*Table 6. Trapped radicals using CHANT in the oxidation of $Bu_3B$ under air, in DCM, and at 25 °C. Experiment detailed in section 6.3.6.*

| | Species | m/z | MS peak Intensity |
|---|---|---|---|
| Unreacted Trap | $[CHANT+H]^+$ | 323.2699 | 63452 |
| Trapped Bu· | $[CHANT+Bu\cdot+H]^+$ | 224.201 | 8792 |
| | $[CHANT+Bu\cdot+Na]^+$ | 246.183 | 3258 |
| | $[TEMPO+Bu\cdot+H]^+$ | 214.2166 | 15441 |
| | $[TEMPO+Bu\cdot+Na]^+$ | 236.1986 | 2 |
| Trapped $Bu_2BOO\cdot$ | $[CHANT+Bu_2BOO\cdot+H]^+$ | 324.271 | - |
| | $[CHANT+Bu_2BOO\cdot+Na]^+$ | 346.253 | - |
| Trapped $Bu_2BO\cdot$ | $[CHANT+Bu_2BO\cdot+H]^+$ | 308.2761 | - |
| | $[CHANT+Bu_2BO\cdot+Na]^+$ | 330.258 | - |
| Trapped BuO· | $[CHANT+BuO\cdot+H]^+$ | 240.1959 | 217 |
| | $[CHANT+BuO\cdot+Na]^+$ | 262.1779 | 136 |
| | $[TEMPO+BuO\cdot+H]^+$ | 230.2116 | 505 |
| Trapped BuOO· | $[CHANT+BuOO\cdot+H]^+$ | 256.1909 | 15 |
| | $[CHANT+BuOO\cdot+Na]^+$ | 278.173 | 5 |
| Trapped THF· | $[CHANT+THF\cdot+H]^+$ | 238.1803 | 1565 |
| | $[CHANT+THF\cdot+Na]^+$ | 260.1622 | 574 |
| | $[TEMPO+THF\cdot+H]^+$ | 228.1960 | 480 |
| | $[TEMPO+THF\cdot+Na]^+$ | 250.1780 | 5 |
| Trapped DCM· | $[CHANT+DCM\cdot+H]^+$ | 250.0760 | 242 |
| | $[CHANT+DCM\cdot+Na]^+$ | 272.0578 | 161 |

As mentioned in the previous section, one persistent issue encountered in the trapping experiments was the absence of trapped boron-containing radicals. Moreover, the analysis of the samples never detected the presence of any boron-containing products present during $Et_3B$ autoxidation ($Et_3B$, $Et_2BOOEt$, $Et_2BOEt$, $Et_2BOBEt_2$). A possible explanation, apart from the suggestion that boron derivatives simply don't fly well in positive mode ESI, was that the boron products and boron adducts were not stable in the solvent used for MS. The solvent

used for the analysis of the samples was 0.1% formic acid in $H_2O$/MeCN 1:1. It was thought that the boron-containing species formed during the experiments could hydrolyse when the aliquot of the sample was diluted in the $H_2O$-containing solvent. The product of hydrolysis would be boric acid, which would be undetectable by MS since it has a molecular weight of 61.84, below the m/z limit of 100 in the spectrometer used.

The hypothesis was tested by switching the solvent used for sample injection to 0.1% formic acid in anhydrous acetonitrile (50 mM $Et_3B$, 16 mM CHANT, 1 mL DCM. Experiment detailed in section 6.3.4.). An additional injection was performed using non-acidic anhydrous MeCN. Both injections yielded the same results: none of the desired species were detected, while previously observed radicals (Et·, EtO·, and EtOO·) were again identified. This outcome invalidated the hypothesis that hydrolysis was responsible for these observations. Nevertheless, anhydrous solvent was used in subsequent experiments to prevent potential hydrolysis.

A detailed analysis of the MS spectrum from the experiment detailed in Table 6 (Experiment detailed in section 6.3.6), revealed, for the first time, peaks corresponding to boron-related compounds. The observed m/z values matched the species listed in Table 7.

*Table 7. MS peaks of B-containing species in $Et_3B$ autoxidation under air, in DCM, and at 25 °C. Experiment detailed in section 6.3.6.*

| Entry | Molecular formula | m/z | Peak Intensity | Number of unsaturations |
|---|---|---|---|---|
| 1 | $C_{12}H_{25}O_2BNa$ | 235.1845 | 402 | 1 |
| | $C_{12}H_{26}O_2B$ | 213.2026 | 125 | 1 |
| 2 | $C_{12}H_{25}O_3BNa$ | 251.1794 | 39 | 1 |

Since these compounds were not among the predicted species and mass spectrometry does not provide structural information, assigning possible structures to the observed peaks is challenging. However, the number of unsaturations in the detected species offers some insight.

Both detected compounds exhibited one unsaturation, likely originating from the THF solvent. Previous experiments had trapped and observed THF radicals by MS. The formation of boron adducts with THF with m/z matching entries 1 and 2 from the above table remains unclear, with several possibilities suggested (Scheme 27).

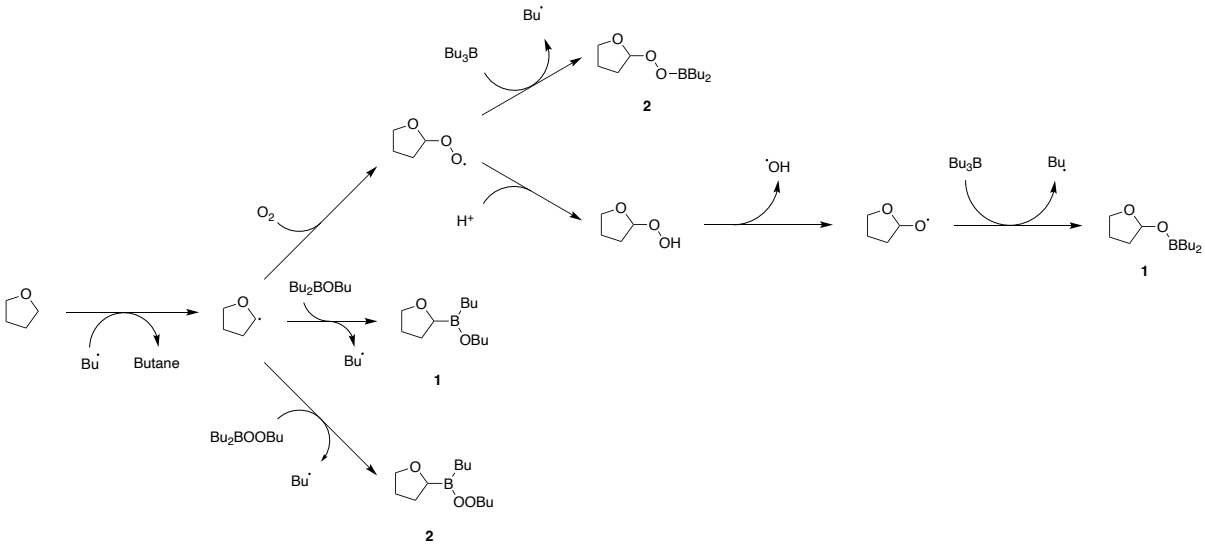


*Scheme 27. Possible mechanisms of formation of products in Table 7.*

Although the formation and structures of the detected products are not fully understood with the available data and are not directly relevant to the studied reaction, the observation of these adducts provides valuable information about the problem with ionising boron compounds.

The detection of these adducts indicates that boron-containing products can be stable and observable by MS. A notable difference between the observed compounds and the predicted boron products ($Et_3B$, $Et_2BOOEt$, $Et_2BOEt$, $Et_2BOBEt_2$) is that the observed compounds are THF adducts. This suggests that alkyl and alkoxyboranes alone do not ionize in MS under the current conditions, but the presence of other ionizable groups (e.g., the ether group in THF) makes these compounds detectable by ESI-MS. The high intensity of other THF adducts confirms high ionisation efficiency of these derivatives.

This premise also suggests that no or very little boron-containing radicals are being trapped in the experiments. If they were trapped, the formed adducts would presumably be stable and detectable in the same way as the THF adducts, due to the ionizable groups from the trap segment.

To test this, a sample of commercially available triethylborate ($B(OEt)_3$) was analysed by MS using the same MS method as the experiments above (50 mM $B(OEt)_3$, 1 mL DCM. MS method detailed in section 6.10.1). As expected, there was no peak corresponding to the injected compound. This confirmed the hypothesis that under the current conditions, the ionisation efficiency of boron derivatives in positive mode ESI is low, below the detection limit.

### 2.4. Reaction Kinetics

With some information of the radicals formed during $Et_3B$ autoxidation, we proceeded to monitor the progression of the reaction over time, this would provide useful mechanistic information such as reaction rate, presence of secondary processes, formation of products and intermediates, etc.

EPR spectroscopy was employed to measure oxygen concentration in solution. Backer et al. (1977) reported the effect of oxygen concentration on the superhyperfine structure of EPR spectra of a soluble spin probe.[113] As oxygen is a radical, its collisions with other radicals lead to faster relaxation (Heisenberg exchange). This effect causes a broadening of the EPR signal, which can be measured and quantified (Figure 5).

The consumption of oxygen by $Et_3B$ was monitored using EPR oximetry, with TEMPO radicals serving as stable radicals to generate the EPR signal.

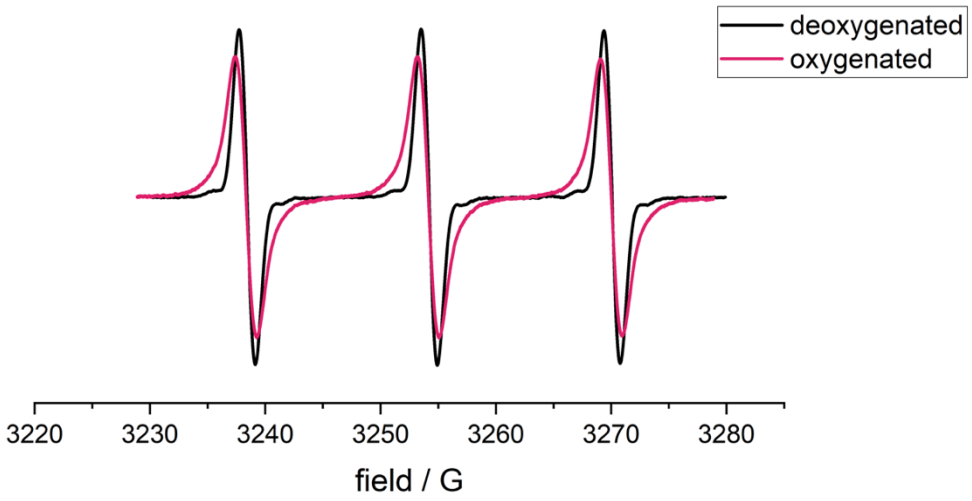


*Figure 5. Broadening effect of dissolved oxygen in the EPR signal of a TEMPO solution.*

It was quickly observed that the samples were rapidly deoxygenated, appearing completely deoxygenated within 1-2 minutes of reaction (the time required to tune the instrument between bubbling air through the solution and the first measurement) (Experiment detailed in section 6.6.1, Entry 1). This rapid deoxygenation was expected, as the propagation of $Et_3B$ autoxidation is known to be very fast. Many kinetic studies in the literature use inhibitors to slow down the reaction.[92] Amines, which react as Lewis bases to reversibly form an adduct with trialkylboranes, are commonly used inhibitors.[114] Here we can take a different approach using TEMPO radicals not just as an EPR probe but also as a radical scavenger. This is similar to using a Lewis base to slow down $Et_3B$ autoxidation, however the mechanism of action is different. In this case TEMPO radicals act as chain terminators, capturing radicals in the propagation chain, thus, slowing down the reaction to monitor oxygen consumption over time.

EPR measurements take approximately 30 seconds, allowing for one measurement per minute. To measure the consumption of oxygen over time, complete deoxygenation of the reaction mixture should take between 10 to 90 minutes. The reaction conditions were optimised to meet these criteria (Experiment detailed in section 6.6.1, Entry 2).

At a concentration of 0.1 mM TEMPO and 5 mM $Et_3B$, complete consumption of $O_2$ in solution was achieved after 1 hour of reaction. These conditions were ideal for observing and quantifying the rate of $O_2$ consumption (Figure 6).

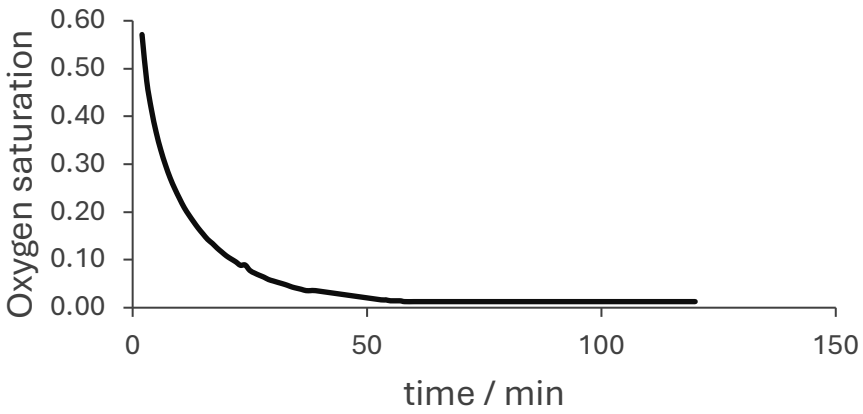


*Figure 6. Consumption of $O_2$ over time in a solution of $Et_3B$ and TEMPO in DCM. Experiment detailed in section 6.6.1, Entry 2.*

In addition to the consumption of $O_2$, EPR experiments also allow for monitoring the consumption of TEMPO as these radicals react with those generated from the oxidation of $Et_3B$. Analysing the results from this experiment revealed an interesting finding: the consumption of TEMPO continued even after all the $O_2$ was consumed (Figure 7).

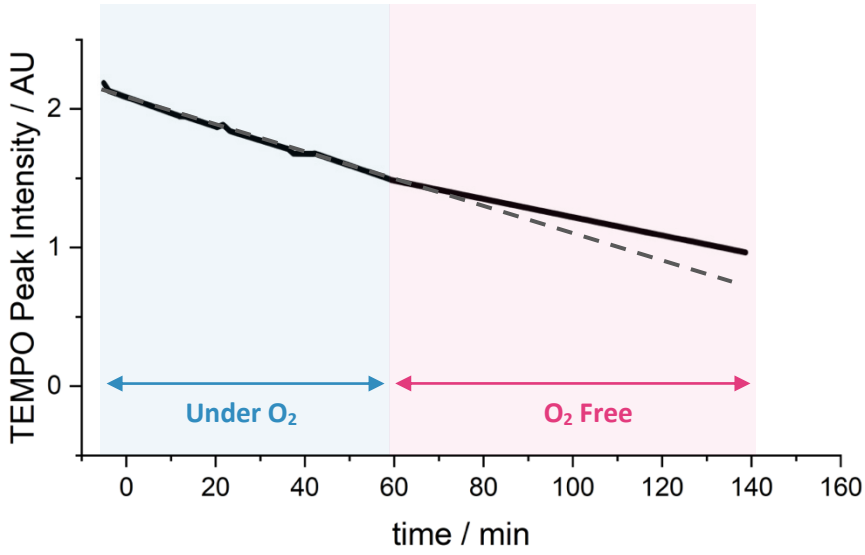


*Figure 7. Consumption of TEMPO over time. Experiment detailed in section 6.6.1, Entry 2. The dashed lines in the plot highlight a difference in the rate of TEMPO consumption after the reaction has been completely deoxygenated.*

There are two possible reasons why TEMPO continued being consumed:

1. After $O_2$ consumption, there is still supply of $O_2$ by diffusion from the headspace.
2. After $O_2$ consumption, there is another radical-generating process consuming TEMPO.

Diffusion of $O_2$ was initially thought to be slow due to the small surface area of the EPR cell. However, an experiment was designed to distinguish between the two possibilities.

Air was bubbled in a solution of $Et_3B$ and TMEPO in DMC, and when the $O_2$ was completely consumed by the reaction, $N_2$ was bubbled through it to remove the $O_2$ from the headspace of the cell (25 mM $Et_3B$, 0.25 mM TEMPO, 2 mL DCM. Experiment detailed in section 6.6.2). The same phenomenon was observed: after the $O_2$ was completely consumed, the TEMPO concentration continued decreasing, and when $N_2$ was bubbled through the solution, the decline continued at the same rate (Figure 8). This indicated that the consumption of TEMPO radicals was not related to the diffusion of $O_2$ into the solution. There must be another radical-generated process which operates in the absence of oxygen.

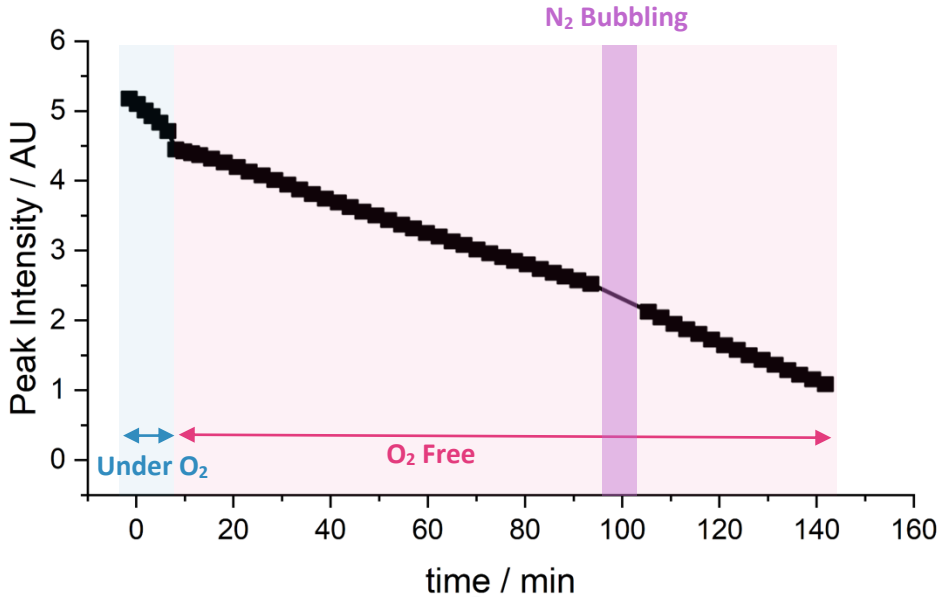


*Figure 8. Peak intensity of the TEMPO signal in EPR in a solution of $Et_3B$ in DCM. Experiment detailed in section 6.6.2.*

A possible explanation for this phenomenon is the decomposition by homolytic O-O bond cleavage of $Et_2BOOEt$. These peroxides are generated during the propagation steps of the autooxidation mechanism and can decompose to generate ethoxy (EtO·) and diethylboryloxy ($Et_2BO$·) radicals. It has also been suggested that the decomposition of the peroxides is a bimolecular step involving molecule-induced homolysis (Scheme 28).[85]

***Homolysis***

$$EtOOBEt_2 \longrightarrow Et_2BO^{\cdot} + {}^{\cdot}OEt$$

***Molecule-Assisted Homolysis***

$$EtOOBEt_2 + Et_3B \longrightarrow EtOBEt_2 + Et_2BO^{\cdot} + Et^{\cdot}$$

*Scheme 28. Proposed mechanisms for $Et_2BOOEt$ homolysis.*

There is some debate over the importance of this secondary initiation mechanism. A recent review by Curran et al. suggests that this secondary mechanism is "only accountable for occasional chain initiation, not product formation".[85] It is argued that the majority of $Et_2BOEt$ is formed by ionic oxidation of $Et_3B$ with $Et_2BOOEt$. However, in a more recent publication, Uematsu et al. use DFT calculations to argue that this secondary initiation mechanisms might play a key role in the generation of ethyl radicals.[99]

If the secondary mechanism is responsible for the continued decrease in the intensity of the EPR signal of TEMPO once the reaction is deoxygenated, this opens the possibility to study the role of the secondary mechanism in the total production of radical initiators.

As previously mentioned, even at low concentrations, the reaction between $Et_3B$ and $O_2$ is too rapid to monitor without inhibitors. We used TEMPO as both a radical scavenger and a monitorable probe via EPR. The use of TEMPO is also compatible with $^{11}B$ NMR, thus allowing us to monitor the reaction via both techniques simultaneously. We employed both techniques to monitor a solution of partially oxidised $Et_3B$ in the absence of $O_2$. This allows us to monitor not only the consumption of $O_2$ via EPR but also the consumption of $Et_3B$ and the formation of products of oxidation by $^{11}B$ NMR simultaneously.

$Et_3B$ was dissolved in a solution of TEMPO in DCM, and $O_2$ was bubbled through for 20 seconds. $N_2$ was immediately bubbled through for another 20 seconds, and the solution was monitored by $^{11}B$ NMR and EPR (5 mM $Et_3B$, 0.1 mM TEMPO, 2 mL DCM. Experiment detailed in section 6.5.1.) (Figure 9).

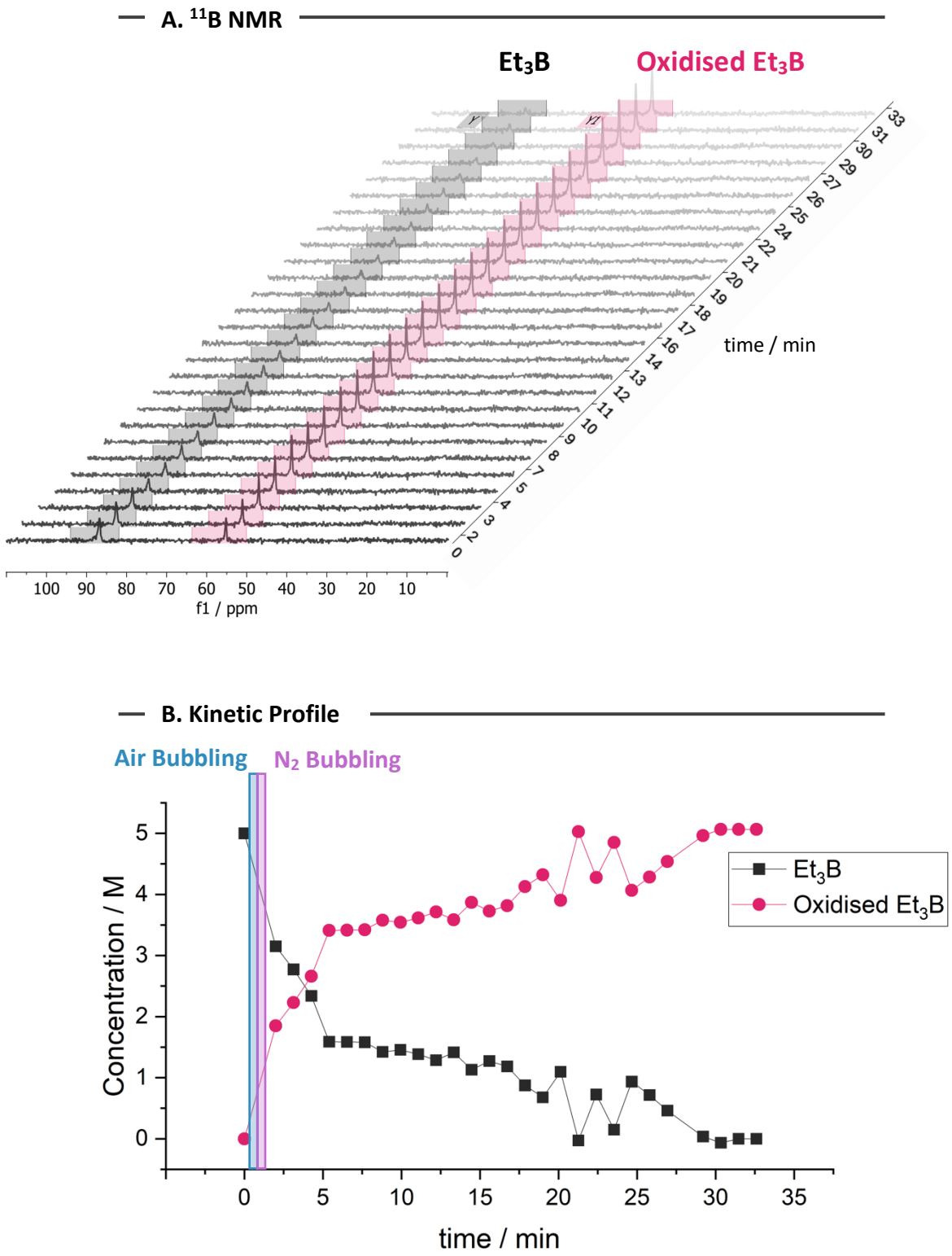


*Figure 9. (A) $^{11}B$ NMR monitoring of the reaction between $Et_3B$ and $O_2$ in DCM in the presence of TEMPO. The reaction was run at 25 °C, and under $N_2$. (B) Kinetic profile the reaction followed by $^{11}B$ NMR using the initial concentration as reference. Measurements were taken at the indicated timestamps. Experiment detailed in section 6.5.1.*

Both techniques provide insight into the reaction's progress. Initially, when air is bubbled through the solution, $Et_3B$ is partially oxidised into an unassigned oxidation product. This results in similar concentrations of $Et_3B$ and the oxidation product, as observed by $^{11}B$ NMR. Subsequently, $N_2$ is bubbled through the solution, removing all the $O_2$ present. This is confirmed by EPR, where the first measurement shows a completely deoxygenated reaction that remains so throughout the reaction time.

However, after this point, $Et_3B$ continues to be consumed even under anaerobic conditions. This phenomenon is likely due to the reaction between $Et_3B$ and the oxidation product, $Et_2BOOEt$. The oxidation product formed at the beginning of the kinetic run (56 ppm) is likely $Et_2BOOEt$ for the following reasons:

1. This product is the main one formed through the autoxidation cycle, so it is logical that it accumulates during oxidation.
2. It appears at the expected chemical shift for boron molecules with the structure $R_2BOR$.[115]
3. Since it is suspected that $Et_2BOOEt$ reacts with $Et_3B$, formation of $Et_2BOOEt$ would explain the reactivity observed for $Et_3B$.

The reaction between $Et_3B$ and $Et_2BOOEt$ has been discussed in the literature, with two proposed mechanisms.[96, 97] In one mechanism, $Et_3B$ reacts with $Et_2BOOEt$ via a heterolytic pathway, leading to the formation of 2 equivalents of $Et_2BOEt$. In the other mechanism, $Et_3B$ and $Et_2BOOEt$ react homolytically via molecule-assisted homolysis of the peroxide, resulting in the formation of $Et_2BOEt$, Et·, and Et2BO· (Scheme 29).[97, 116]

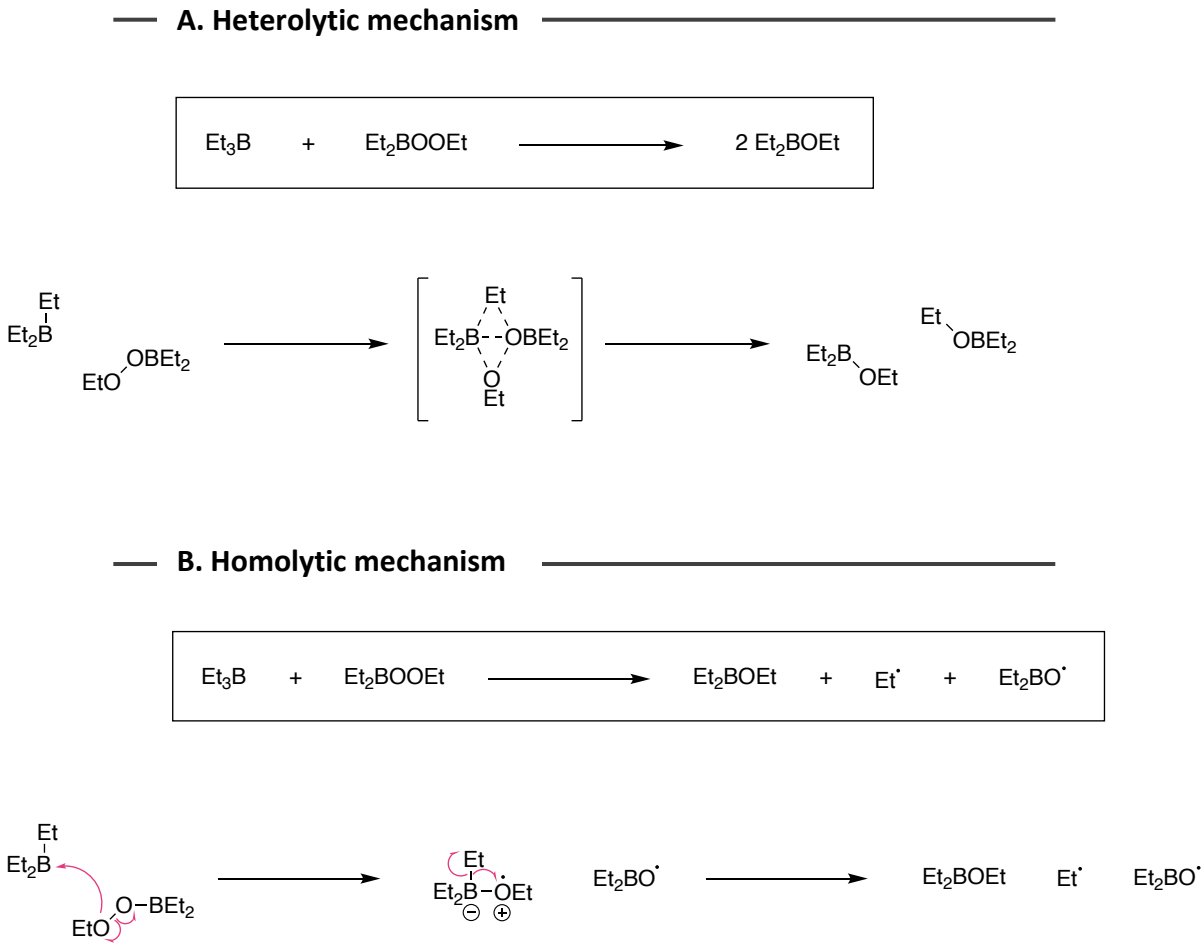


*Scheme 29. Proposed mechanism for the reaction between $Et_3B/Et_2BOOEt$. (A) heterolytic reaction, (B) homolytic reaction.*

There is limited knowledge in the literature about this reaction. There is disagreement regarding whether the homolytic or heterolytic mechanisms prevail and the relevance of this process within the overall production of radicals by the $Et_3B/O_2$ system.

We decided to test whether we could trap radicals generated from this reaction. The idea was to generate a partially oxidised solution of $Et_3B$, where presumably $Et_2BOOEt$ would be present. As before, we purged the solution with $N_2$ to ensure no $O_2$ was present, and then we added our radical trap. Under these conditions, we expected the reaction $Et_3B$ + $Et_2BOOEt$ to occur under $N_2$, with the trap capturing only radicals formed after all $O_2$ had been removed

from the system. Therefore, the trapped radicals would be formed under anaerobic conditions (25 mM $Et_3B$, 8 mM CHANT, 2 mL DCM. Experiment detailed in section 6.3.5.).

We carried out the trapping experiment and observed high peak intensities for trapped ethyl radicals as well as ethoxyl radicals (Table 8).

*Table 8. Trapped radicals using CHANT in a partially oxidised sample of $Et_3B$ under $N_2$ in DCM, and at 25 °C. Experiment detailed in section 6.3.5.*

| | Species | m/z | MS peak Intensity/Noise | |
|---|---|---|---|---|
| | | | Control[a] | Sample |
| Unreacted Trap | $[CHANT+H]^+$ | 323.2699 | 32489 | 3111 |
| Trapped Et· | $[CHANT+Et\cdot+H]^+$ | 196.1698 | 65 | 990 |
| | $[CHANT+Et\cdot+Na]^+$ | 218.1518 | 35 | 443 |
| | $[TEMPO+Et\cdot+H]^+$ | 186.1855 | 29 | 49 |
| Trapped $Et_2BOO\cdot$ | $[CHANT+Et_2BOO\cdot+H]^+$ | 268.2084 | - | - |
| | $[CHANT+Et_2BOO\cdot+Na]^+$ | 290.1903 | - | - |
| Trapped $Et_2BO\cdot$ | $[CHANT+Et_2BO\cdot+H]^+$ | 252.2135 | - | - |
| | $[CHANT+Et_2BO\cdot+Na]^+$ | 274.1954 | - | - |
| Trapped EtO· | $[CHANT+EtO\cdot+H]^+$ | 212.165 | - | 11 |
| | $[CHANT+EtO\cdot+Na]^+$ | 234.147 | - | - |
| Trapped EtOO· | $[CHANT+EtOO\cdot+H]^+$ | 228.16 | - | - |
| | $[CHANT+EtOO\cdot+Na]^+$ | 250.1419 | - | - |

[a]*Control received the same treatment as the sample except the solution of $Et_3B$ was not pre-oxidised.*

A control experiment was conducted to confirm that the radicals trapped in this study originated from the reaction between $Et_3B$ and its oxidation products, rather than from any adventitious oxygen introduced into the reaction mixture during analysis. The control experiment consisted of a solution of $Et_3B$ in DCM the same as the sample, except that the solution was not pre oxidised, thus, it was kept from any contact with oxygen (Experiment detailed in section 6.3.5). CHANT was added, and the solution was analysed by MS under $N_2$.

The results displayed in Table 8 show that while some radicals were indeed trapped during analysis, the intensity of these trapped radicals is significantly lower in the control compared to the partially oxidised sample. Furthermore, the peak intensity corresponding to the unreacted trap is much higher in the control than in the partially oxidised sample, indicating substantial consumption of the trap in the sample.

These findings demonstrate that the reaction between $Et_3B$ and its oxidation products generates radicals. The radicals were identified as ethyl radicals and a small amount of ethoxyl radicals. Previous reports have indicated that a partially oxidised solution of $Me_3B$ generates radicals under $O_2$-free conditions.[97] However, a quantitative analysis for this reaction has not been undertaken. It is plausible that while some radicals are generated, the majority of the reaction between $Et_3B$ and $Et_2BOOEt$ proceeds via a heterolytic mechanism, with the homolytic component being relatively minor. Without a quantitative analysis of this reaction, we cannot definitively determine the relevance of $Et_3B$ + $Et_2BOOEt$ (secondary mechanism of initiation) within the $Et_3B/O_2$ initiation process.

There are numerous questions and possibilities regarding this secondary initiation, none of which can be answered without a quantitative analysis of the reaction. Conducting a quantitative study with a partially oxidised solution of $Et_3B$ introduces significant variability due to the use of air as a reagent. The concentrations of reagents and products are uncertain, and multiple oxidation products may form, whose reactivities are unknown. The ideal scenario would be to work directly with pure $Et_3B$ and pure $Et_2BOOEt$.

### 2.5. Synthesis of $Et_2BOOEt$

To study the secondary mechanism, pure $Et_2BOOEt$ and $Et_3B$ were used. While triethylborane is commercially available, $Et_2BOOEt$ is not. Contrary to reports suggesting peroxides as the major product of autoxidation, our observations did not align with this. When $Et_3B$ reacted with $O_2$ (Experiment detailed in section 6.3.5), multiple peaks were detected by $^{11}B$ NMR, indicating the formation of various products (Figure 10).

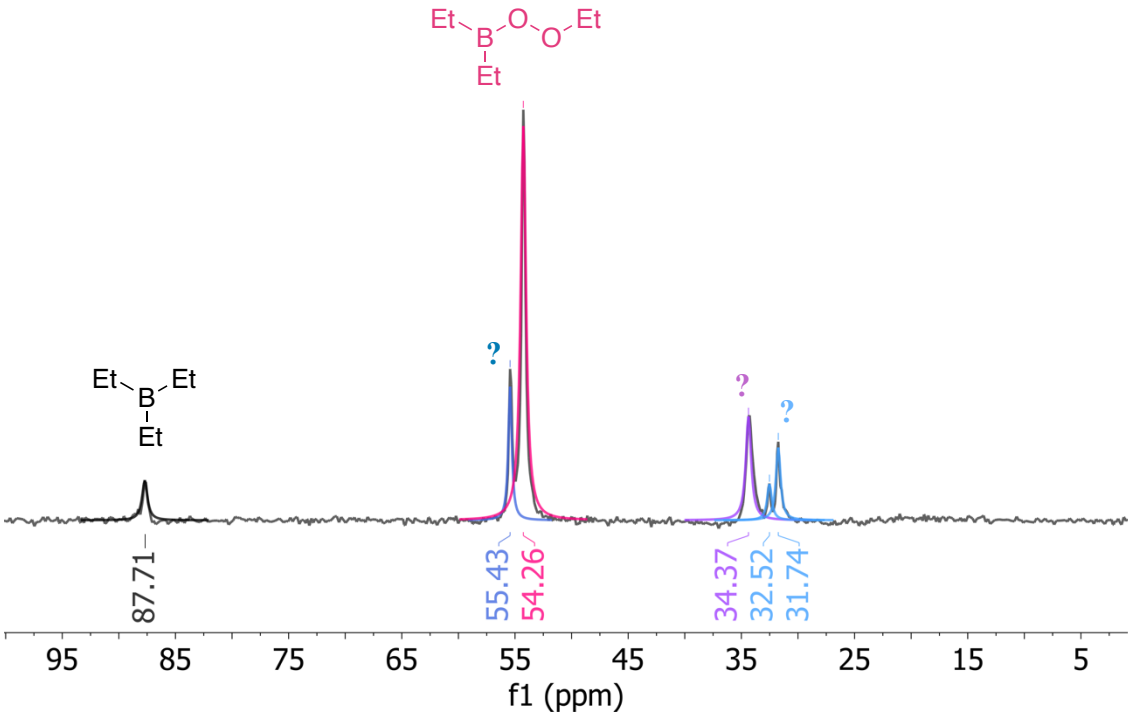


*Figure 10. $^{11}B$ NMR of a solution of $Et_3B$ in DCM exposed to ambient air for 2 minutes. Experiment detailed in section 6.3.5.*

This discrepancy can be elucidated by examining the mechanism of $Et_3B$ autoxidation (Scheme 30). The rapid chain propagation results in peroxides as the sole closed-shell product [steps (2) and (3)], leading to the accumulation of $Et_2BOOEt$ in the reaction mixture during autoxidation.

*Initiation reactions*

$$Et_3B + O_2 \longrightarrow Et_2BOO^{\bullet} + Et^{\bullet} \quad (1)$$

$$Et_2BOO^{\bullet} + Et_3B \longrightarrow Et_2BOOBEt_2 + Et^{\bullet} \quad (6)$$

$$EtOOBEt_2 \longrightarrow Et_2BO^{\bullet} + \dot{O}Et \quad (5)$$

$$EtOOBEt_2 + Et_3B \longrightarrow EtOBEt_2 + Et_2BO^{\bullet} + Et^{\bullet} \quad (4)$$

$$\dot{O}Et + Et_3B \longrightarrow EtOBEt_2 + Et^{\bullet} \quad (7)$$

$$Et_2BO^{\bullet} + Et_3B \longrightarrow Et_2BOBEt_2 + Et^{\bullet} \quad (8)$$

*Propagation reactions*

$$Et^{\bullet} + O_2 \longrightarrow EtOO^{\bullet} \quad (2)$$

$$EtOO^{\bullet} + Et_3B \longrightarrow EtOOBEt_2 + Et^{\bullet} \quad (3)$$

*Ionic reaction*

$$EtOOBEt_2 + Et_3B \longrightarrow 2\ EtOBEt_2 \quad (9)$$

*Scheme 30. Reactions involved in the autoxidation of $Et_3B$.*

However, the peroxide is reactive and reacts with triethylborane through various mechanisms [steps (4) and (9)]. If $O_2$ is limited, reactions (4) and (9) will consume $Et_2BOOEt$ as the oxygen concentration decreases.

Maintaining a high $O_2$ concentration favours the rapid consumption of triethylborane by the propagation chain over its reaction with $Et_2BOOEt$. Friebolin demonstrated a similar approach to selectively form $Me_2BOOMe$ by slowly bubbling trimethylborane ($Me_3B$) through an oxygen-saturated solution.[97] By keeping $Me_3B$ concentration low in an $O_2$-saturated solution, the propagation chain is favoured over the reaction of $Me_3B$ with $Me_2BOOMe$.

However, our attempts to replicate this methodology with $Et_3B$ revealed issues with overoxidation. By slowly adding $Et_3B$ to hexane and maintaining a high $O_2$ concentration through constant air bubbling at room temperature, we observed the formation of diperoxyborane ($EtB(OOEt)_2$) (Figure 11). Friebolin's studies with $Me_3B$ showed that $Me_3B$ primarily forms the monoperoxide,[117] whereas higher alkylboranes typically form the diperoxide.[100, 118]

Slow addition suppresses the reaction between $Et_3B$ and $Et_2BOOEt$, but if the addition is too slow, $Et_2BOOEt$ accumulates and absorbs a second equivalent of $O_2$ to form diperoxyborane ($EtB(OOEt)_2$) (). This means that under the current conditions we have two undesired side-reactions, and impeding one favours the other.


*Scheme 31. Reaction of $Et_3B$ with two moles of $O_2$ to give the diperoxide $EtB(OOEt)_2$.*

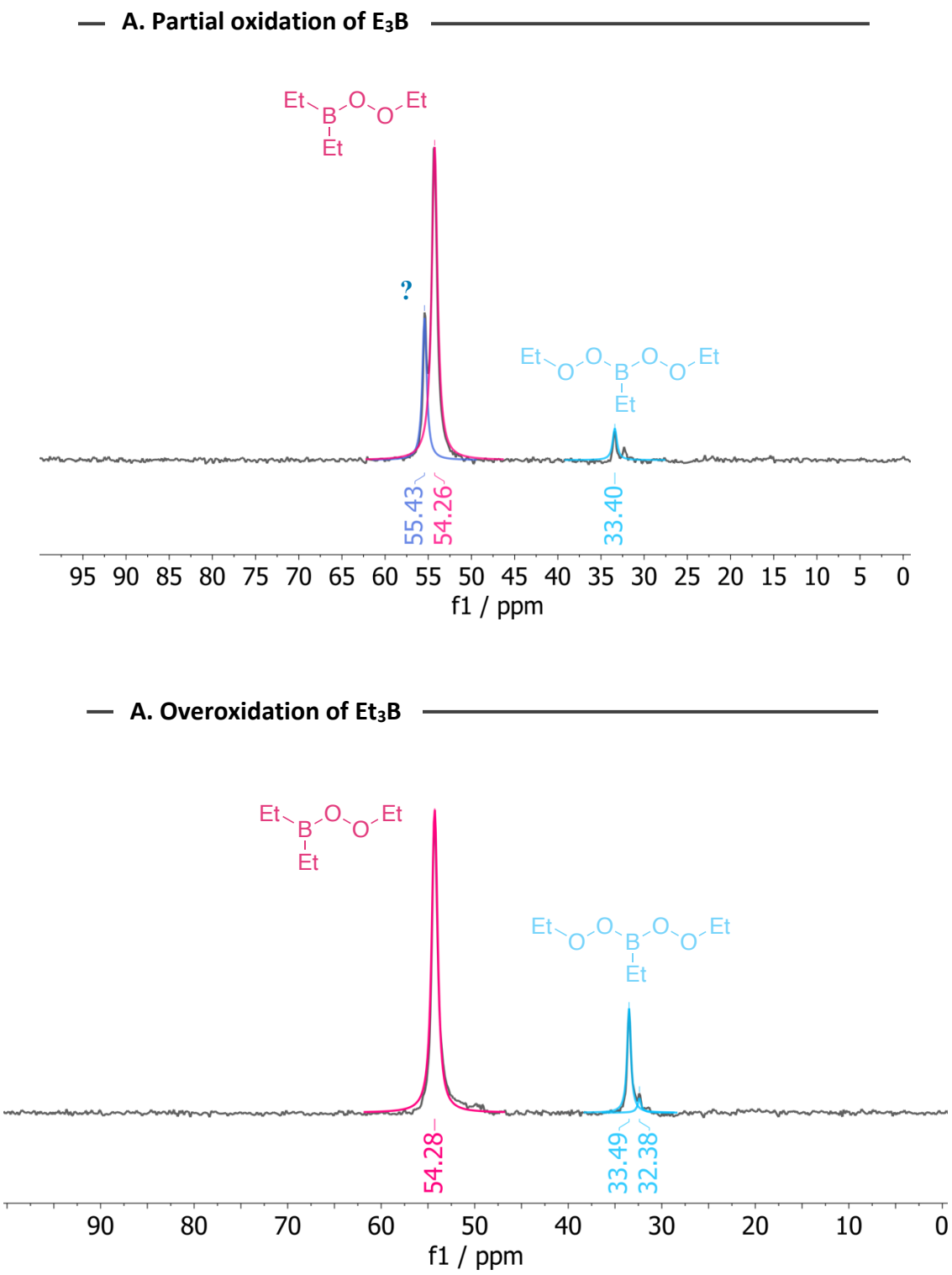


*Figure 11. $^{11}B$ NMRs of $Et_3B$ oxidation in hexane (A) Fast addition of $Et_3B$ (100 µL/min) into $O_2$ saturated hexane results in $Et_3B$ reacting with $Et_2BOOEt$. Experiment detailed in section 6.8.1, Entry 3. (B) Slow addition of $Et_3B$ (20 µL/min) into $O_2$ saturated hexane causes overoxidation of peroxides forming the diperoxide at 33 ppm. Experiment detailed in section 6.8.1, Entry 1.*

We aimed to optimise the conditions for the selective formation of $Et_2BOOEt$, avoiding both overoxidation and the reaction of $Et_3B$ with $Et_2BOOEt$ (Table 9). Experiment detailed in section 6.8.1.

*Table 9. Optimisation of $Et_2BOOEt$ formation via slow oxidation of $Et_3B$. Experiment detailed in section 6.8.1.*

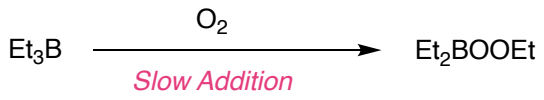


| Entry | $Et_3B$ / µmol | Injection time / min | $Et_2BOOEt$ selectivity / % |
|---|---|---|---|
| 1 | 100 | 1 | 72 |
| 2 | 25 | 1 | 73 |
| 3 | 100 | 2 | 71 |
| 4 | 75 | 1.5 | 70 |

Initially, injecting 100 µmol of $Et_3B$ over 1 minute in 2 mL of hexane yielded only 72% of $Et_2BOOEt$, indicating the presence of both $EtB(OOEt)_2$ and products of the $Et_3B/Et_2BOOEt$ reaction (Entry 1). To minimize the $Et_3B/Et_2BOOEt$ reaction, we decreased the amount of $Et_3B$ injected over the same period. However, this resulted in only 73% selectivity for the peroxide, with the remaining 27% being the diperoxide $EtB(OOEt)_2$, indicating overoxidation of $Et_2BOOEt$ (Entry 2). Returning to the conditions in Entry 1, we injected the same amount of $Et_3B$ over a longer period to lower the $Et_3B$ concentration (Entry 3). Similar to previous conditions, extending the injection time led to overoxidation of $Et_2BOOEt$, yielding the desired peroxide with only 71% selectivity. Combining both strategies-decreasing the amount of $Et_3B$ injected and extending the injection time-did not improve selectivity, yielding 70% $Et_2BOOEt$ (Entry 4).

We could not optimise the selective formation of $Et_2BOOEt$ beyond 73% selectivity. Under these conditions, either overoxidation or the $Et_3B/Et_2BOOEt$ reaction significantly reduced the amount of $Et_2BOOEt$ formed. Synthesizing $Et_2BOOEt$ under these conditions followed by purification was not an attractive option, considering that (a) purification would need to be carried out under $O_2$-free conditions due to the $O_2$ sensitivity of $Et_2BOOEt$, and (b) purification would need to be performed quickly or at very low temperatures, as $Et_2BOOEt$ degrades at room temperature. While both of these can be done, it would be preferable to optimise conditions for the selective formation of $Et_2BOOEt$.

Brown reported that the absorption of two equivalents of $O_2$ is strongly influenced by temperature.[119] They noted that trialkylboranes rapidly absorb one equivalent of oxygen even at –78 °C, but the absorption of a second equivalent is very slow at that temperature and increases significantly above –45 °C. Considering this, the slow addition of triethylborane at –78 °C over a longer period could avoid significant formation of diperoxides. Indeed, after optimising the injection rate at –78 °C, the target peroxide ($Et_2BOOEt$) was selectively formed with 96% selectivity (Figure 12). Experiment detailed in section 6.8.2.

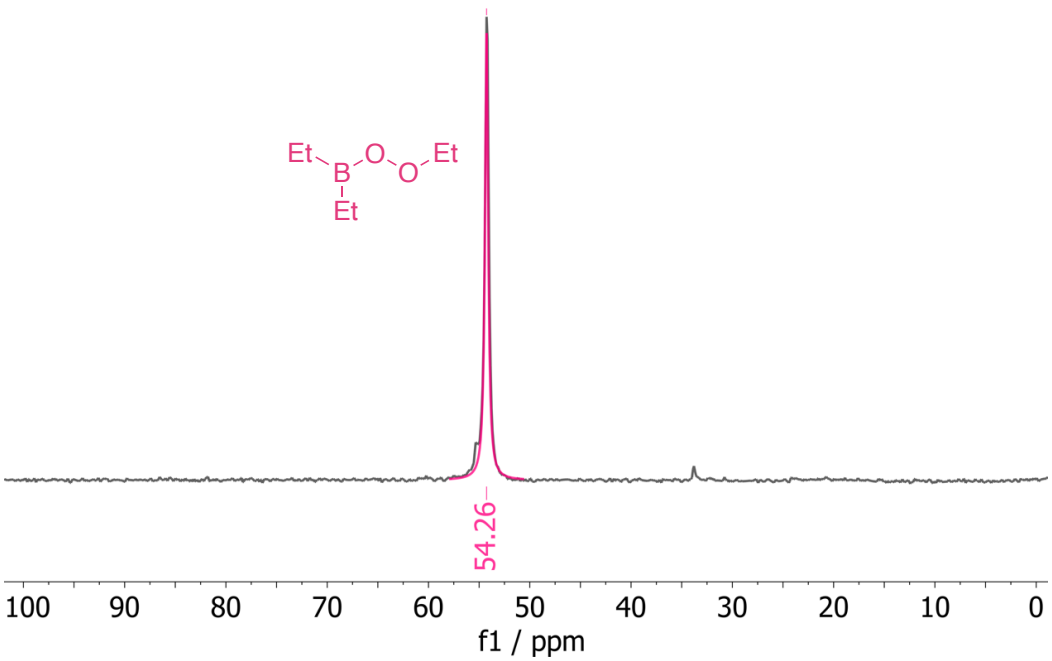


*Figure 12. $^{11}B$ NMR of $Et_2BOOEt$ synthesised in hexane at –78 °C (50 mM). Experiment detailed in section 6.8.2.*

Ethylperoxyborane ($Et_2BOOEt$) is a crucial intermediate in the auto-initiation process. The selective formation of $Et_2BOOEt$ allows for the investigation of its reactivity both in isolation and in combination with $Et_3B$.

### 2.6. Conclusions Chapter 2

The reaction between $Et_3B$ and air generates ethyl, ethoxyl, and ethylperoxyl radicals (Et·, EtO·, and EtOO·). The majority of the reactive radicals are Et·, which are likely responsible for target chain initiation when $Et_3B/O_2$ is used as a radical initiator. The presence of EtO· suggests a secondary initiation mechanism, as there are limited pathways for its formation, with peroxide homolysis being the most probable.

Our observations indicate that the reaction between $Et_3B$ and $O_2$ is rapid, quickly depleting oxygen from the reaction environment. Despite the deoxygenation, oxidation products continue to react under $O_2$-free conditions. This unknown reaction generates Et· and EtO·, as demonstrated by our trapping experiments, this suggests that apart from $Et_3B+O_2$, there is another radical-generating reaction which proceeds in the absence of $O_2$.

To gain a deeper understanding and obtain quantitative data on this reaction, we synthesized $Et_2BOOEt$, the intermediate suspected to be responsible for the observed reactivity. By varying reagent concentrations, rate of addition and reaction temperature, the synthesis was optimised to yield pure $Et_2BOOEt$. We can now conduct a quantitative mechanistic study on the reactivity of $Et_2BOOEt$ in isolation and in reaction with $Et_3B$.

We aim to investigate the significance of the secondary initiation mechanism in the overall radical production of $Et_3B/O_2$.

## 3. Elucidating the Role of $Et_2BOOEt$ in $Et_3B$ Autoxidation

### 3.1. Introduction

The primary product of the autoxidation of $Et_3B$ is $Et_2BOOEt$. Despite its significance, the reactivity of $Et_2BOOEt$ remains one of the least understood aspects of the autoxidation mechanism.[96] The behaviour of this peroxide is influenced by the concentrations of both $Et_3B$ and oxygen, leading to several possible reaction pathways.

At high oxygen concentrations, $Et_2BOOEt$ can absorb an additional mole of $O_2$, resulting in the formation of diethylperoxy(ethyl)borane ($EtB(OOEt)_2$) (Section 2.5, Scheme 31).[100, 117, 118, 120, 121] Conversely, when the concentration of $O_2$ is low, $Et_2BOOEt$ can undergo unimolecular homolysis (Section 2.4, Scheme 28). A recent publication used DFT calculations and kinetic simulations to argue that in the autoxidation of $Et_3B$, the peroxide species play a crucial role in the radical propagation mechanism.[99] The efficiency of this reaction was never measured experimentally and therefore it remains a matter of speculation.

When the concentration of $O_2$ is low and the concentration of $Et_3B$ is high, $Et_2BOOEt$ can react with $Et_3B$. This reaction is thought to be primarily heterolytic,[85] but there is evidence from CIDNP studies suggesting a competing homolytic pathway (Section 2.4, Scheme 29).[97, 98, 116]

Overall, there is substantial evidence supporting the existence of secondary initiation mechanisms in the autoxidation of triethylborane.[96] However, quantitative studies are lacking, and the importance of these secondary initiation pathways is not fully understood. Given that these reactions are dependent on the concentrations of $O_2$ and triethylborane, a deeper understanding of secondary initiation could be key to optimising triethylborane as a radical initiator.

## 3.2. Chapter 3 Aims

1. Implement the allyl-TEMPO radical traps to determine if there are any radicals formed in both the homolysis of $Et_2BOOEt$ and the reaction of $Et_2BOOEt$ with $Et_3B$.
2. Provide quantitative data for the reactions involved in the secondary mechanism to assess their relevance in the overall radical production in $Et_3B/O_2$ system.
3. Build a comprehensive understanding of the initiation process of $Et_3B/O_2$ system.

## 3.3. $Et_2BOOEt$ Decomposition

Given the high reactivity of alkyl and alkoxy boranes with $O_2$, all experiments in this chapter were conducted under an inert atmosphere, either $N_2$ or argon unless otherwise specified. Procedures were carried out inside the glovebox and solvents and solutions were purged with $N_2$ or argon followed by degassing by freeze-pump-thaw.

Once the procedure for synthesising pure $Et_2BOOEt$ has been optimised, we can explore the reactions involved in the autoinitiation of $Et_3B$ autoxidation. One such process is the homolysis of the peroxide bond in $Et_2BOOEt$ (Scheme 32).

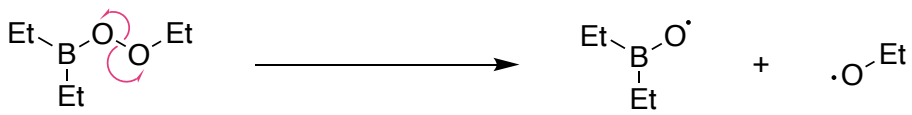


*Scheme 32. Mechanism of homolysis of $Et_2BOOEt$.*

### 3.3.1. Reaction Kinetics and Products

We followed the kinetics of decomposition of a 50 mM solution of $Et_2BOOEt$ in hexane, at room temperature and under $N_2$ (Experiment detailed in section 6.5.3) (Figure 13).

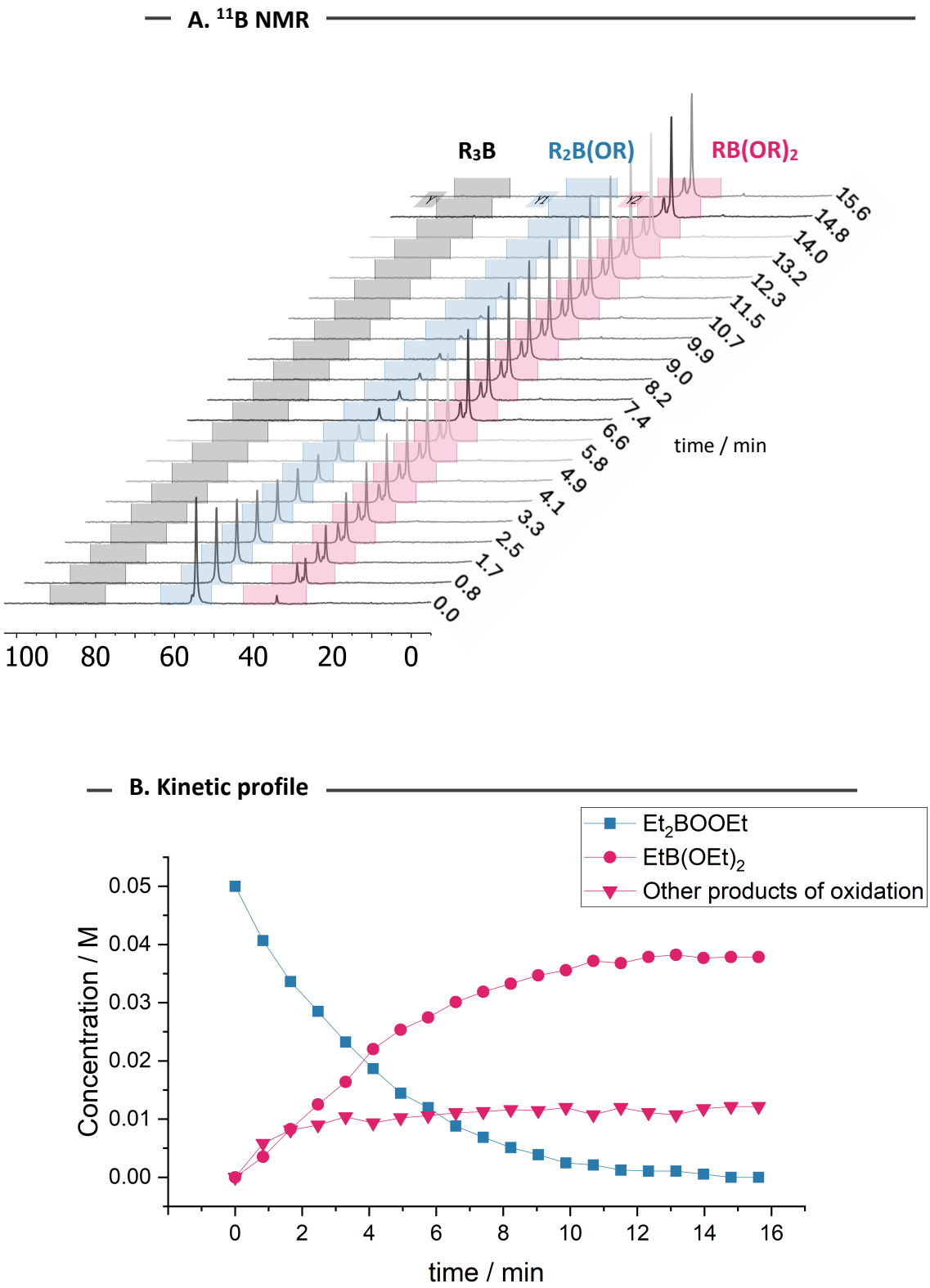


*Figure 13. (A) $^{11}B$ NMR monitoring of a solution of $Et_2BOOEt$ in hexane, at 25 °C, under $N_2$ over 16 h. (B) Kinetic profile for the reaction followed by $^{11}B$ NMR using the initial concentration as reference. Experiment detailed in section 6.5.3. Measurements were taken at the indicated timestamps.*

The peroxide decomposes in solution at room temperature with a half-life of 2h 45 min, forming 0.8 eq. of $EtB(OEt)_2$ as the primary product, while the remaining 0.2 eq. form other oxidised products.

The formation of $EtB(OEt)_2$ is likely the result of a nucleophilic 1,2-rearrangement, a well-known reaction in organoborane chemistry (Scheme 33).[117]

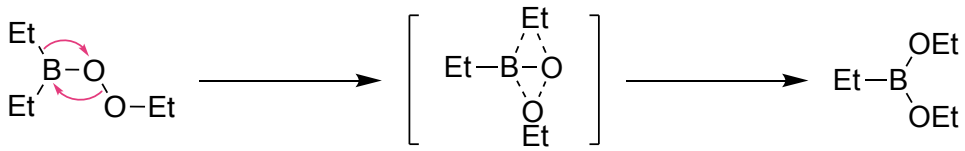


*Scheme 33. Mechanism of nucleophilic 1,2-rearrangement of $Et_2BOOEt$ to give $EtB(OEt)_2$.*

As anticipated, the decomposition of the peroxide follows a first-order reaction (Figure 14).

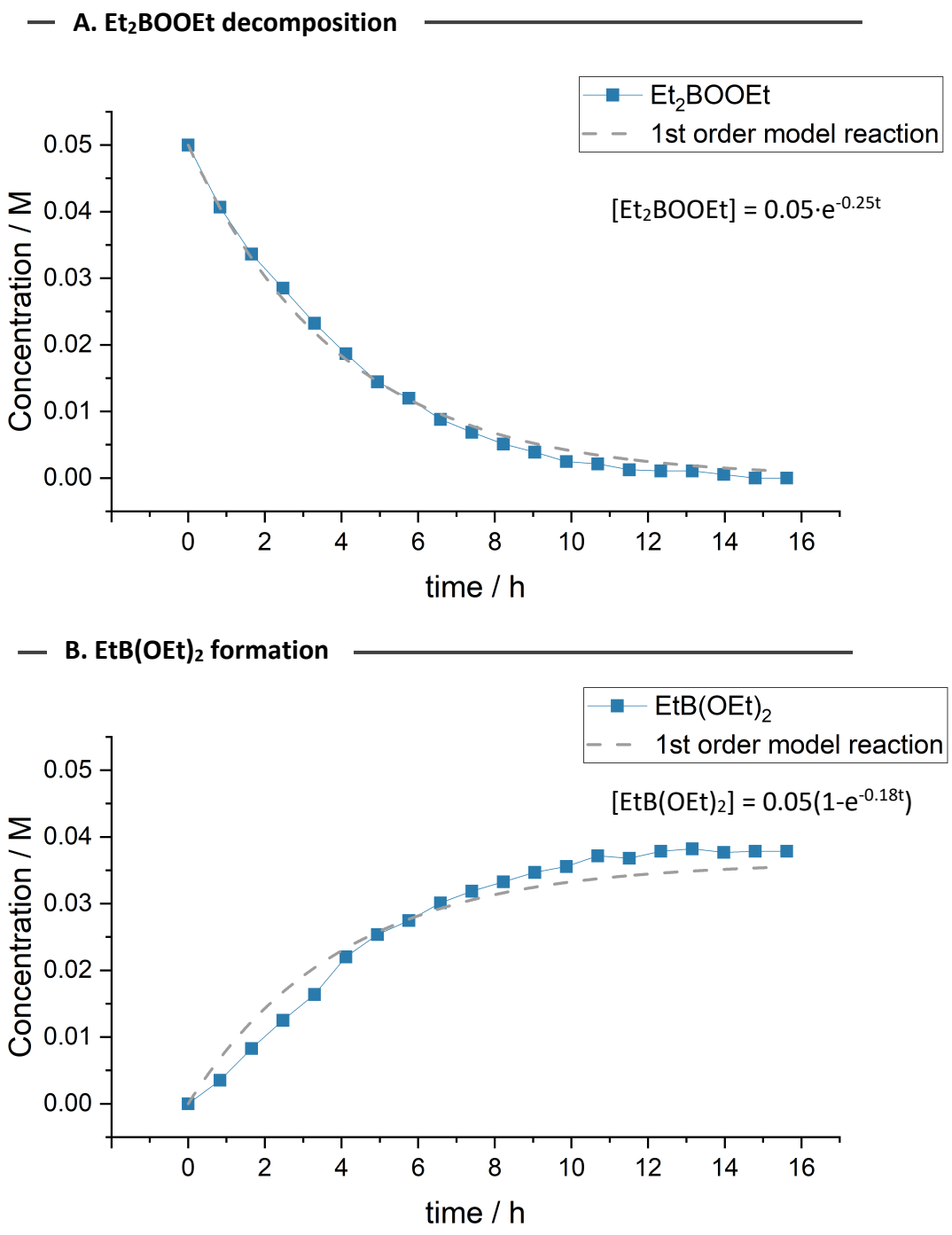


*Figure 14. Kinetic profile for the decomposition of $Et_2BOOEt$ (A) and formation of $EtB(OEt)_2$ (B) in hexane, at 25 °C, under $N_2$ over 16 h fitted to a first order model reaction. The reaction was followed by $^{11}B$ NMR using the initial concentration as reference. Experiment detailed in section 6.5.3. Measurements were taken at the indicated timestamps.*

The formation of the rearranged product, $EtB(OEt)_2$, also appears to follow first-order kinetics, but the fit is not as precise. This discrepancy can be elucidated by examining the $^{11}B$ NMR of the decomposition products (Figure 13 (A)). While the rearrangement seems to be the dominant reaction, there must be one or more secondary processes occurring, as 0.2 eq. react to yield different oxidation products. This secondary process could be the proposed homolysis of the peroxide bond. Given that this secondary process is also a first-order reaction, it would explain why the observed peroxide consumption fits first-order kinetics so well.

### 3.3.2. Kinetic Model of $Et_2BOOEt$ Decomposition

To validate if the experimental observations align with a mixture of heterolytic and homolytic peroxide decomposition, a kinetic model was constructed. This model was based on the first-order rate constants derived from fitting the experimental results to a first-order reaction (model detailed in section 6.9.1) (Scheme 34).

*Rearrangement*

$$Et_2BOOEt \xrightarrow{k = ?} EtB(OEt)_2$$

*Homolysis*

$$Et_2BOOEt \xrightarrow{k = ?} EtO\cdot + \cdot OBEt_2$$

$$EtO\cdot + Et_2BOOEt \xrightarrow[M^{-1}s^{-1}]{k = 3 \times 10^5} \text{Oxidation}$$

$$\cdot OBEt_2 + Et_2BOOEt \xrightarrow[M^{-1}s^{-1}]{k = 3 \times 10^5} 2\ \text{Oxidation}$$

$$EtO\cdot + EtB(OEt)_2 \xrightarrow[M^{-1}s^{-1}]{k = 3 \times 10^5} \text{Oxidation}$$

$$\cdot OBEt_2 + EtB(OEt)_2 \xrightarrow[M^{-1}s^{-1}]{k = 3 \times 10^5} 2\ \text{Oxidation}$$

*Scheme 34. Reactions included in the kinetic model of $Et_2BOOEt$ decomposition in hexane, under $N_2$ and at 25 °C.*

The model accurately predicted the decomposition of $EtOOBEt_2$ and the formation of $EtB(OEt)_2$ (Figure 15).

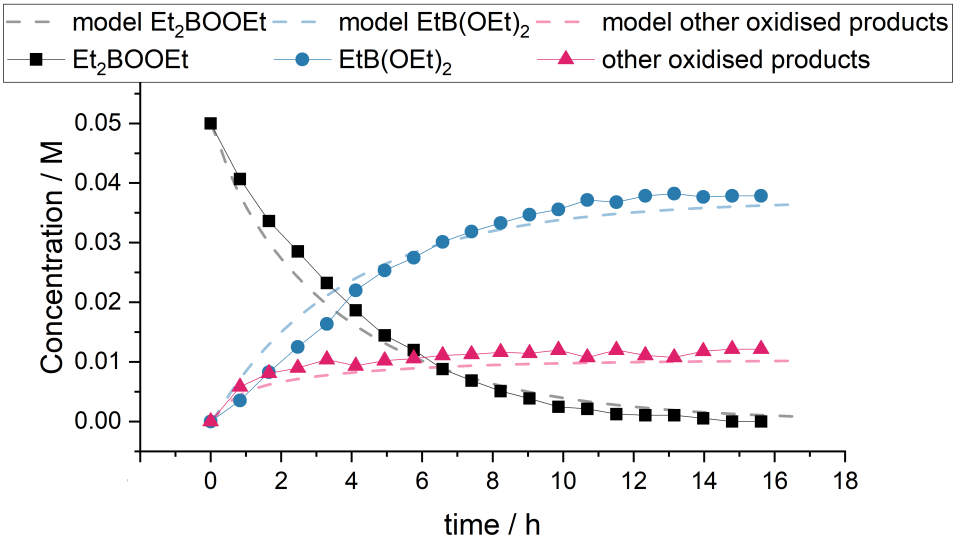


*Figure 15. Kinetic profile for the decomposition of $Et_2BOOEt$ from the experiment detailed in section 6.5.3 fitted to the kinetic model consisting of the reactions described in Scheme 34.*

We have estimated the rate constants for the reactions of peroxide decomposition at 25 °C (Scheme 35). The unimolecular rate constant of rearrangement of $Et_2BOOEt$ derived from fitting is $6 \times 10^{-5}$ $s^{-1}$, and the rate constant for the homolysis of the peroxide is estimated to be $4 \times 10^{-6}$ $s^{-1}$.

$$Et_2BOOEt \xrightarrow[s^{-1}]{k \approx 6 \times 10^{-5}} EtB(OEt)_2$$

$$Et_2BOOEt \xrightarrow[s^{-1}]{k \approx 4 \times 10^{-6}} EtO\cdot + \cdot OBEt_2$$

*Scheme 35. Reactions with their respective rate constants involved in the decomposition of $Et_2BOOEt$ in hexane at 25 °C.*

The autoinitiation of $Et_3B$ autoxidation refers to the ability of the products of $Et_3B$ to act as radical initiators themselves (e.g. homolysis of $Et_2BOOEt$). This autoinitiation in the $Et_3B/O_2$ system is the least understood part of the mechanism of oxidation. There is only one other report in the literature where the rate of $Et_2BOOEt$ homolysis is described. In 2017 S. Maeda proposed a value for the rate of the homolysis based on DFT calculations. The rate they suggested differs significantly, by two orders of magnitude, from the one we found ($k \approx 6.4 \times 10^{-4}$ $s^{-1}$ and $4 \times 10^{-6}$ $s^{-1}$ respectively).[99] Additionally, the total rate constant for degradation of $Et_2BOOEt$ that we measured is $6 \times 10^{-5}$, therefore there is a big discrepancy between our experimental data and the literature value.

Our observations indicate that the major process in $Et_2BOOEt$ decomposition is the rearrangement of the peroxide. It is also evident that more than one process is involved in the decomposition of $Et_2BOOEt$. We assumed that the second process was the homolysis of the peroxide. However, it is possible, albeit unlikely, that there is more than one secondary process since it is challenging to identify the other products of decomposition. This implies that the rate of homolysis could be much lower than the one we estimated, but not higher, and certainly not as high as the literature value of $6.4 \times 10^{-4}$ $s^{-1}$.

When the literature value ($6.4 \times 10^{-4}$ $s^{-1}$) was used in our kinetic model, the peroxides were consumed in 50 minutes, and the product of rearrangement, $EtB(OEt)_2$, was minor compared to other oxidation products (model detailed in section 6.9.2) (Figure 16).

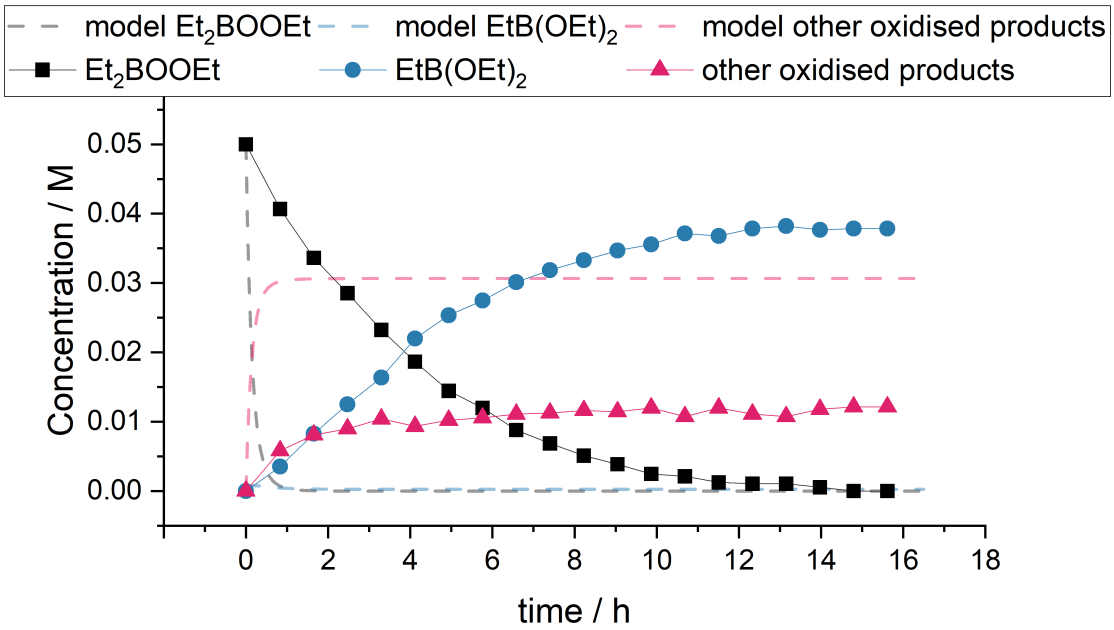


*Figure 16. Kinetic profile for the decomposition of $Et_2BOOEt$ from the experiment detailed in section 6.5.3 fitted to the kinetic model consisting of the reactions described in Scheme 34 where the rate of $Et_2BOOEt$ homolysis was changed to the value reported in the literature ($6.4 \times 10^{-4}\ s^{-1}$).*

### 3.3.3. Radical Trapping

We have concluded that at least 0.8 eq. of the peroxide decomposes via a rearrangement. We have estimated the rate constant of the rearrangement. However, there might or might not be homolysis of the peroxide $Et_2BOOEt$. To investigate this possibility, we turned to radical trapping.

A solution of $Et_2BOOEt$ was prepared in hexane, radical trap CHANT was added under $N_2$ and the solution was followed by $^{11}B$ and $^{1}H$ NMR (25 mM $Et_2BOOEt$, 25 mM CHANT, 1 mL hexane. Experiment detailed in section 6.3.7.). After complete decomposition of $Et_2BOOEt$, there were no trapped ethyl radicals. Moreover, the concentration of the unreacted trap remained constant throughout the reaction (Figure 17). However, MS analysis showed trapped ethyl and ethoxyl radicals (Table 10).

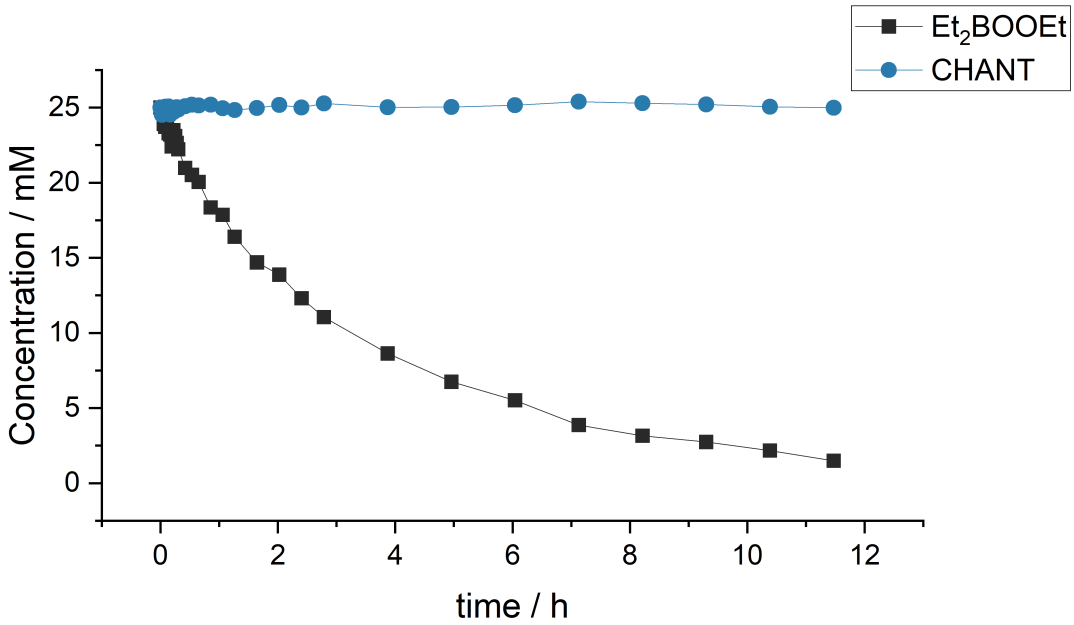


*Figure 17. Kinetic profile for the decomposition of $Et_2BOOEt$ in hexane in the presence of CHANT. The reaction was run at 25 °C, and under $N_2$ and was followed by $^{11}B$ and $^{1}H$ NMR using the initial concentration as reference. Measurements were taken at the indicated timestamps. Experiment detailed in section 6.3.7.*

*Table 10. Trapped radicals using CHANT from the decomposition of $Et_2BOOEt$ in hexane, at 25 °C and under $N_2$. Experiment detailed in section 6.3.7.*

$$Et_2BOOEt \xrightarrow{\text{CHANT}} EtO\cdot + \cdot OBEt_2$$

| Species | | m/z | MS peak intensity |
|---|---|---|---|
| Unreacted Trap | $[CHANT+H]^+$ | 323.2699 | 130965 |
| | $[CHANT+Na]^+$ | 345.2519 | 675 |
| Trapped Et· | $[CHANT+Et\cdot+Na]^+$ | 218.1518 | 54 |
| | $[TEMPO+Et\cdot+H]^+$ | 186.1855 | 11 |
| Trapped EtO· | $[CHANT+EtO\cdot+H]^+$ | 212.1648 | 5 |

These results indicate that the system generates enough radicals to be detected by a highly sensitive technique such as MS. However, it does not generate sufficient radicals to be detected by a less sensitive technique like NMR.

### 3.3.4. Conclusions $Et_2BOOEt$ Decomposition

The results clarified the mechanism of $Et_2BOOEt$ decomposition. We have confirmed that at 25 °C, the dominant pathway is a heterolytic rearrangement yielding $EtB(OEt)_2$ with the first order rate constant of $6 \times 10^{-5}$ $s^{-1}$.

There is a homolytic component to this reaction, as verified by our trapping experiment. However, this homolytic reaction plays a minor role, producing very few initiating radicals. Additionally, the rate of this reaction is very slow, with a rate constant equal to or smaller than $4 \times 10^{-6}$ $s^{-1}$.

Overall, it is likely that the homolysis has a negligible contribution to the autoinitiating properties of $Et_3B$ autoxidation, considering the speed and efficiency of $Et_3B$ autoxidation.

## 3.4. $Et_2BOOEt$ Reaction with $Et_3B$

We have seen how a semi-oxidised solution of $Et_3B$ under $N_2$ continues reacting and the reaction generates radicals (Section 2.4). This property is called autoinitiation, where the products of oxidation of $Et_3B$ can themselves become radical initiators. We have already discussed that the homolysis of $Et_2BOOEt$ is unlikely to play a significant role in the autoinitiation of $Et_3B$, thus, there must be a different process that generates radicals in a semi oxidised solution of $Et_3B$ under $N_2$.

As mentioned in section 2.5, it is thought that the product of oxidation $Et_2BOOEt$ can react with $Et_3B$ in a molecule-assisted homolysis of the peroxide bond. However, there is no consensus on whether the reaction $Et_3B/Et_2BOOEt$ is a homolytic or heterolytic process, or a combination of both (Scheme 36).

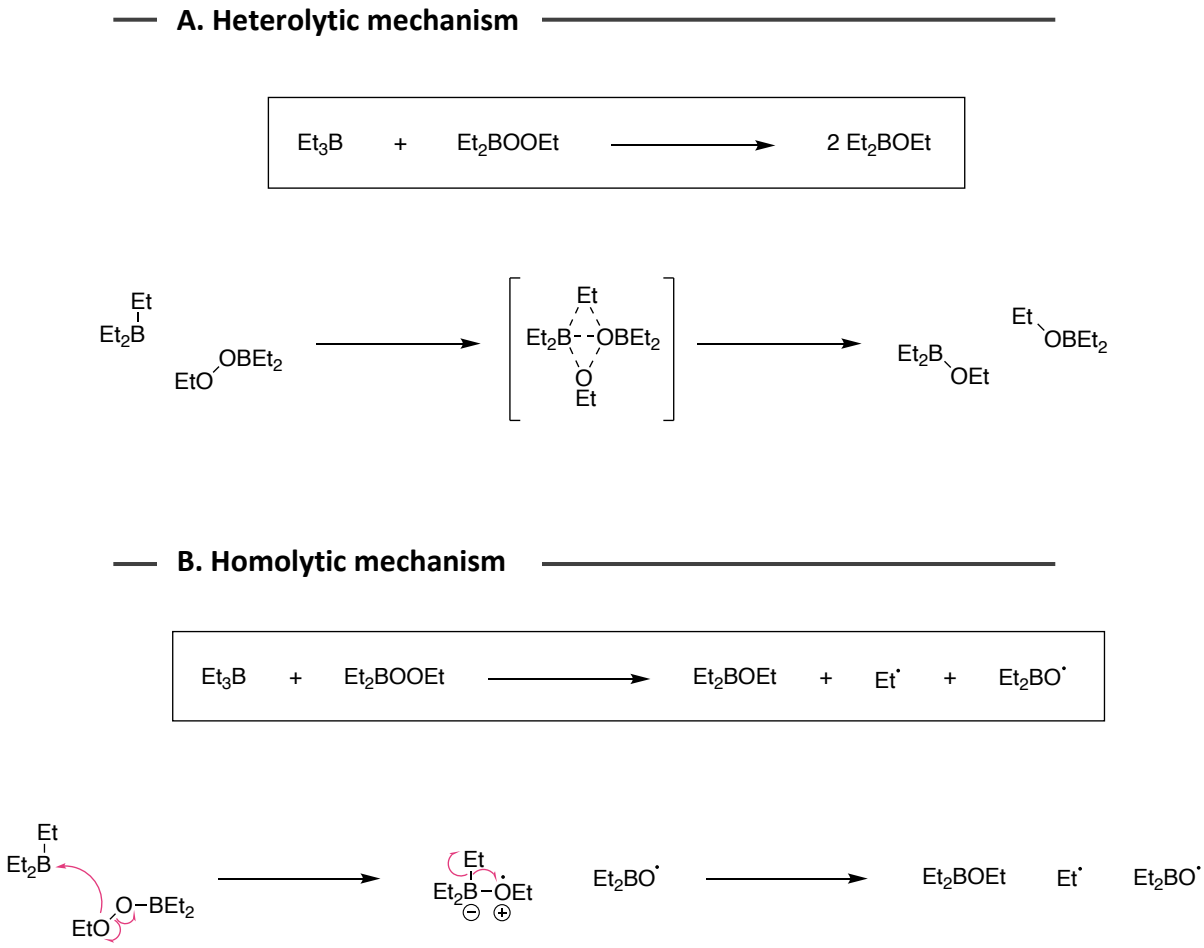


*Scheme 36. Proposed mechanism for the reaction between $Et_3B/Et_2BOOEt$. (A) heterolytic reaction, (B) homolytic reaction.*

### 3.4.1. Reaction Products

Initially, our aim was to identify the products formed in the reaction between $Et_3B$ and $Et_2BOOEt$, as this would provide valuable insights into the underlying mechanism. A purely heterolytic mechanism would yield 2 eq. of $Et_2B(OEt)$, with no other expected products. Conversely, a purely homolytic mechanism would yield at least 1 eq. of $Et_2B(OEt)$, with the potential for other products formed from the reaction of radicals Et· and $Et_2BO$· with other system components.

A solution of $Et_2BOOEt$ and $Et_3B$ was mixed in hexane and under $N_2$ and the reaction was followed by $^1H$ and $^{11}B$ NMR (25 mM $Et_2BOOEt$, 25 mM $Et_3B$, 1 mL hexane. Experiment detailed in section 6.5.4, Entry 1) (Figure 18). $^{11}B$ NMR reveals that the reaction generates more than one product, indicating that we are not dealing with a purely heterolytic process, which would produce only 2 eq. of $Et_2B(OEt)$.

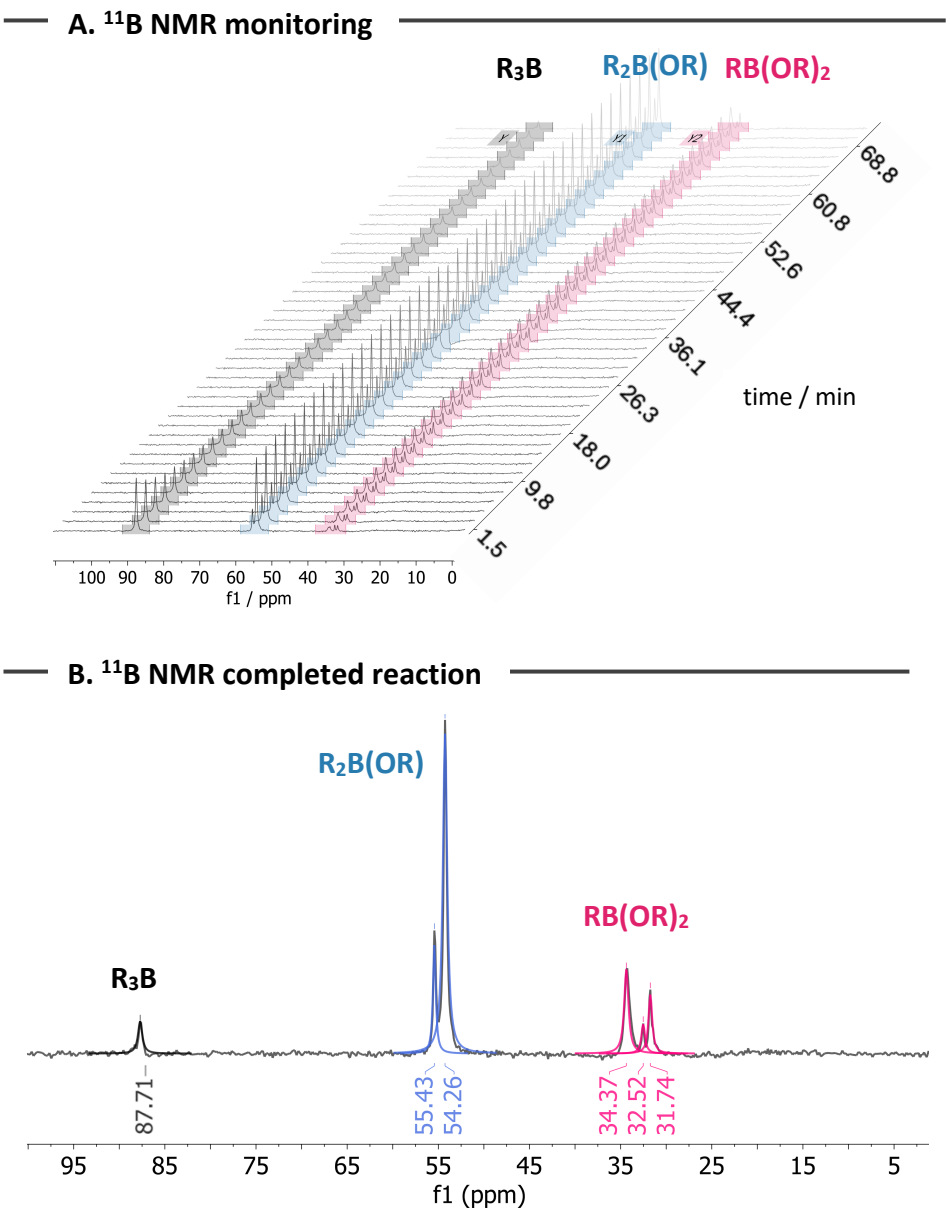


*Figure 18. Reaction between $Et_3B$ and $Et_2BOOEt$ in hexane, at 25 °C, under $N_2$. Experiment detailed in section 6.5.4 (Entry 1). (A) $^{11}B$ NMR monitoring of the reaction over time (B) $^{11}B$ NMR of the reaction after completion.*

Our earlier experiments on the synthesis of $Et_2BOOEt$ (Section 2.5) allowed us to assign the peaks for $Et_3B$ (87.7 ppm) and $Et_2BOOEt$ (54.2 ppm) in $^{11}B$ NMR. We expect to form at least 1 eq. of $Et_2B(OEt)$ which would appear in the $R_2B(OR)$ region (50 - 60 ppm). In this region, we observe two peaks that evolve very little over time. We know that at the beginning of the reaction, the larger peak in this region at 54 ppm corresponds to $Et_2BOOEt$.

We can monitor the evolution of $Et_2BOOEt$ via $^1H$ NMR as the characteristic peaks for this compound in $^1H$ NMR were also assigned in section 2.5. It can be observed that $Et_2BOOEt$ reacts close to 1:1 with $Et_3B$ (Figure 19). The difference in reactivities is likely the result of a slow decomposition of $Et_2BOOEt$.

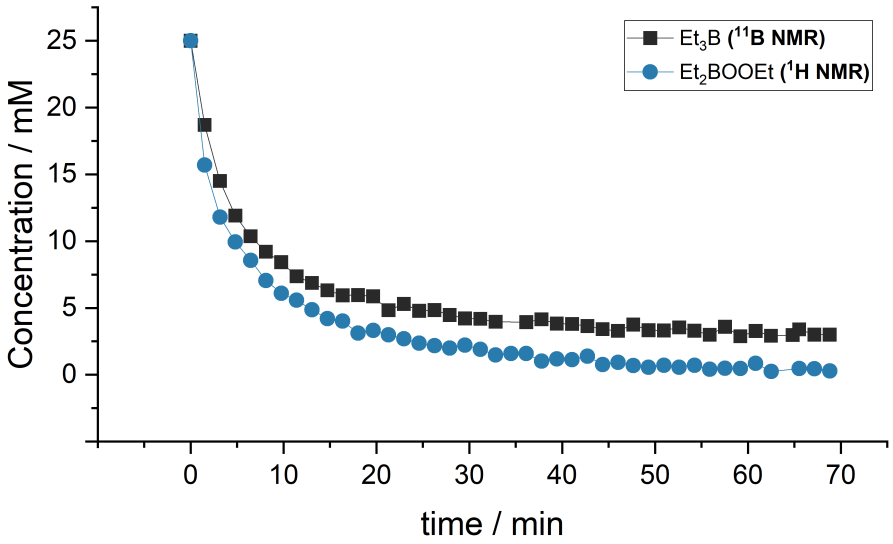


*Figure 19. Kinetic profile for the reaction between $Et_3B$ and $Et_2BOOEt$ in hexane, at 25 °C, under $N_2$. Experiment detailed in section 6.5.4 (Entry 1). The reaction was followed by $^{11}B$ and $^1H$ NMR using the initial concentrations as reference. Measurements were taken at the indicated timestamps.*

Since all $Et_2BOOEt$ has reacted, the persistence of the peak at 54 ppm in $^{11}B$ NMR indicates that a second species is slowly forming at a very similar chemical shift to $Et_2BOOEt$. Due to the similarity of boron environment in between $Et_2BOOEt$ and $Et_2B(OEt)$, it is likely that the species that is forming is the expected $Et_2B(OEt)$.

We can confirm this by following the kinetics of this reaction by $^{1}H$ and $^{11}B$ NMR (Figure 20). If we assume that the peak at 54 ppm in $^{11}B$ NMR corresponds to $Et_2BOOEt$ + $Et_2B(OEt)$, and we know the concentration of $Et_2BOOEt$ alone thanks to $^{1}H$ NMR, we can subtract the concentration of $Et_2BOOEt$ to the concentration of the peak at 54 ppm in $^{11}B$ NMR ($Et_2BOOEt$+$Et_2B(OEt)$) to give the concentration of $Et_2B(OEt)$ alone. This concentration can be plotted against time, and we can see that it matches the formation of a quartet at 4.5 ppm in $^{1}H$ NMR (Figure 20). It is likely that this quartet at 4.5 ppm in $^{1}H$ NMR corresponds to the $Et_2BO$-C**H$_2$**-$CH_3$ in $Et_2B(OEt)$ because it appears close to the quartet that corresponds to EtBO-(C**H$_2$**-$CH_3$) in $EtB(OEt)_2$ and both proton environments are very similar. We are certain that we are forming product $Et_2B(OEt)$ as this is confirmed later by MS analysis in Figure 23, and the quartet at 4.5 ppm in $^{1}H$ NMR can only correspond to $Et_2BO$-C**H$_2$**-$CH_3$ since there are no other unassigned quartets forming in the right chemical shift. Together with the close match shown in Figure 20 (B) between 4.5 ppm $^{1}H$ NMR quartet and (54 ppm $^{11}B$ NMR singlet - $Et_2BOOEt$) we can confidently assign both of these NMR peaks to $Et_2B(OEt)$.

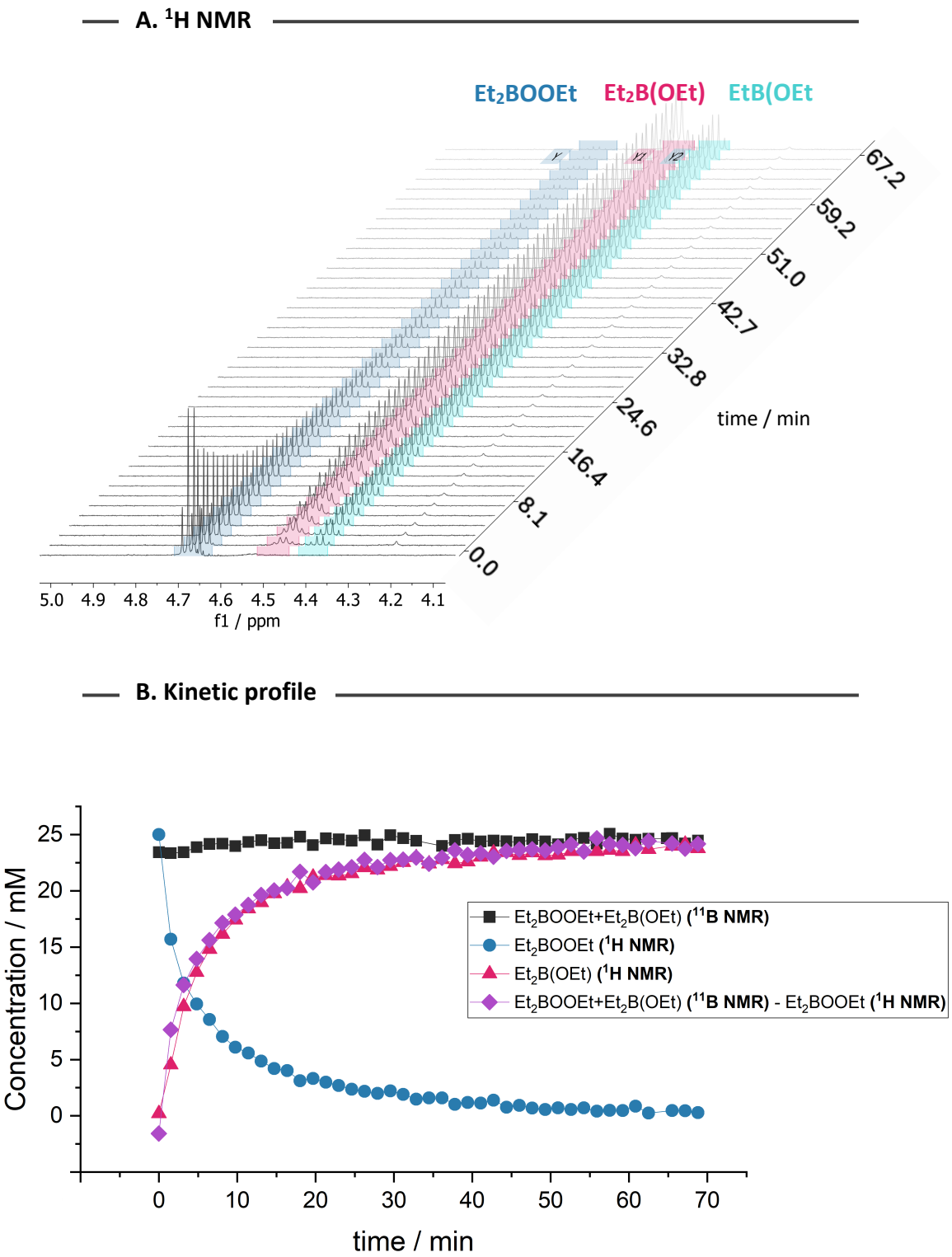


*Figure 20. (A) $^{1}H$ NMR monitoring of the reaction between $Et_3B$ and $Et_2BOOEt$ in hexane, at 25 °C, under $N_2$. Experiment detailed in section 6.5.4 (Entry 1). (B) Kinetic profile for the reaction followed by $^{11}B$ and $^{1}H$ NMR using the initial concentrations as reference. Measurements were taken at the indicated timestamps.*

We observe the formation of only 1 eq. of product $Et_2B(OEt)$. As explained above, the formation of less than 2 eq. of this product indicates that the mechanism is not heterolytic. Moreover, the formation of exactly 1 eq. of $Et_2B(OEt)$ strongly suggests that the mechanism is homolytic and that the formed radicals can escape the solvent cage before recombining. In the homolytic mechanism, we form Et· and $Et_2BO$· radicals. If these radicals do not have time to escape the solvent cage upon formation, they would recombine to give $Et_2B(OEt)$. If this were the case, we would observe the formation of more than 1 eq. of $Et_2B(OEt)$, but we observe the formation of exactly 1 eq. of this product. Additionally, the fact that the radicals escape the solvent cage instead of recombining indicates that they can serve as radical initiators.

Having identified and quantified the major product and discussed its implications, we turned to the other products formed. As shown in the $^1$H NMR monitoring displayed in Figure 20, we observe the formation of $EtB(OEt)_2$. This structure was assigned on the basis of our studies on $Et_2BOOEt$ decomposition (Section 2.5). We tentatively attribute the formation of $EtB(OEt)_2$ observed here to the unimolecular rearrangement of $Et_2BOOEt$. This is because at the end of the reaction between $Et_3B$ and $Et_2BOOEt$, there is some $Et_3B$ remaining. This occurs even though the reaction should be stoichiometric and both $Et_3B$ and $Et_2BOOEt$ are added in equal amounts. This indicates that a second process is consuming a small proportion of $Et_2BOOEt$, and this is likely to be $Et_2BOOEt$ rearrangement, which explains the formation of $EtB(OEt)_2$ (Figure 21).

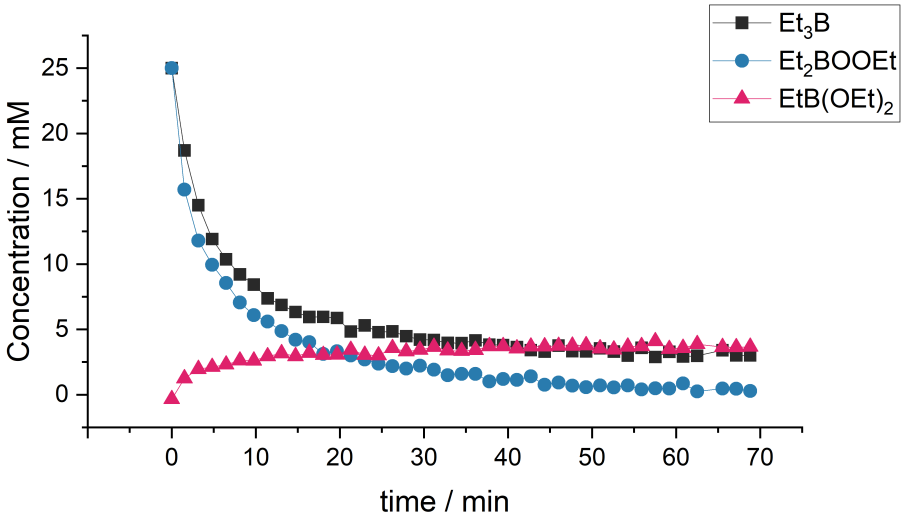


*Figure 21. Kinetic profile the reaction between $Et_3B$ and $Et_2BOOEt$ in hexane. The reaction was run at 25 °C, and under $N_2$ and was followed by $^{11}B$ and $^{1}H$ NMR using the initial concentration as reference. Measurements were taken at the indicated timestamps. Experiment detailed in section 6.5.4 (Entry 1).*

It is clear that the reaction between $Et_3B$ with $Et_2BOOEt$ is faster than the decomposition of $Et_2BOOEt$ by just looking at kinetic plots. This is intriguing since we have assumed that the decomposition of $Et_2BOOEt$ to yield few radicals, and we are beginning to see that the $Et_3B/Et_2BOOEt$ system might be a good source of radicals. The fact that $Et_3B/Et_2BOOEt$ is faster than $Et_2BOOEt$ decomposition further suggests that in the presence of $Et_3B$, $Et_2BOOEt$ homolysis will be an insignificant process in terms of radical initiation and puts $Et_3B/Et_2BOOEt$ as a strong candidate for the hypothesized autoinitiation of $Et_3B$ autoxidation.

To gain a better understanding of the different species formed in $^{11}B$ NMR, we carried out MS analysis of the reaction. In the 1950s, Law, R. W. studied the ion fragments of small boron molecules by electron ionisation (EI), a hard ionisation method that leads to extensive fragmentation and is typically useful for organic compounds with a low molecular weight.[122] This technique, usually coupled with gas chromatography (GCEI), allowed us to successfully ionise commercially available triethylborate ($B(OEt)_3$) as a test sample. We used this technique to study the products of the reaction between $Et_3B$ and $Et_2BOOEt$.

The expected products, $Et_3B$ and $Et_2B(OEt)$, were observed as the major products, consistent with the NMR (Figure 23). Another major product was identified with 93% probability as ethylboroxine $(EtOB)_3$. This compound likely corresponds to a major product in the $^{11}B$ NMR in the region of $RB(OR)_2$ at **34.37** ppm (Figure 22). The relative integrations between $(EtOB)_3$ and $Et_2BOEt$ in GCEI are very similar to the relative integrations of $Et_2B(OEt)$ and peak at 34.37 ppm in $^{11}B$ NMR.

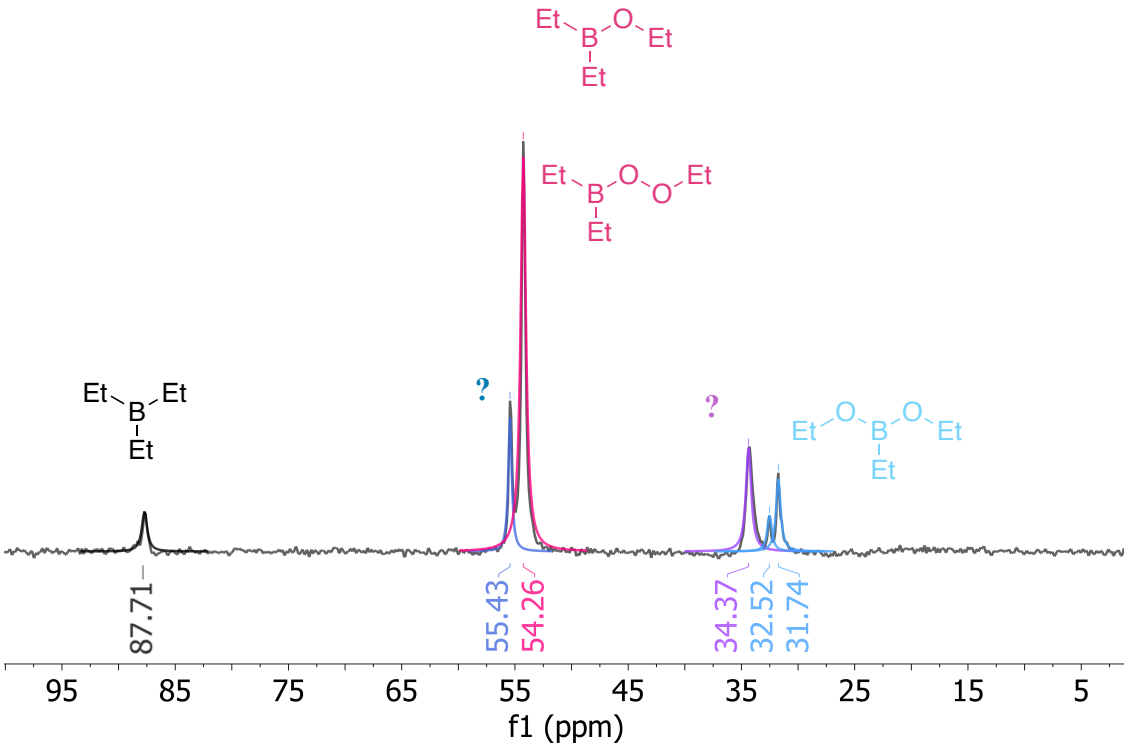


*Figure 22. Partially assigned $^{11}B$ NMR of the reaction between $Et_3B$ and $Et_2BOOEt$ in hexane, at 25 °C, under $N_2$, after reaction completion. Experiment detailed in section 6.5.4 (Entry 1).*

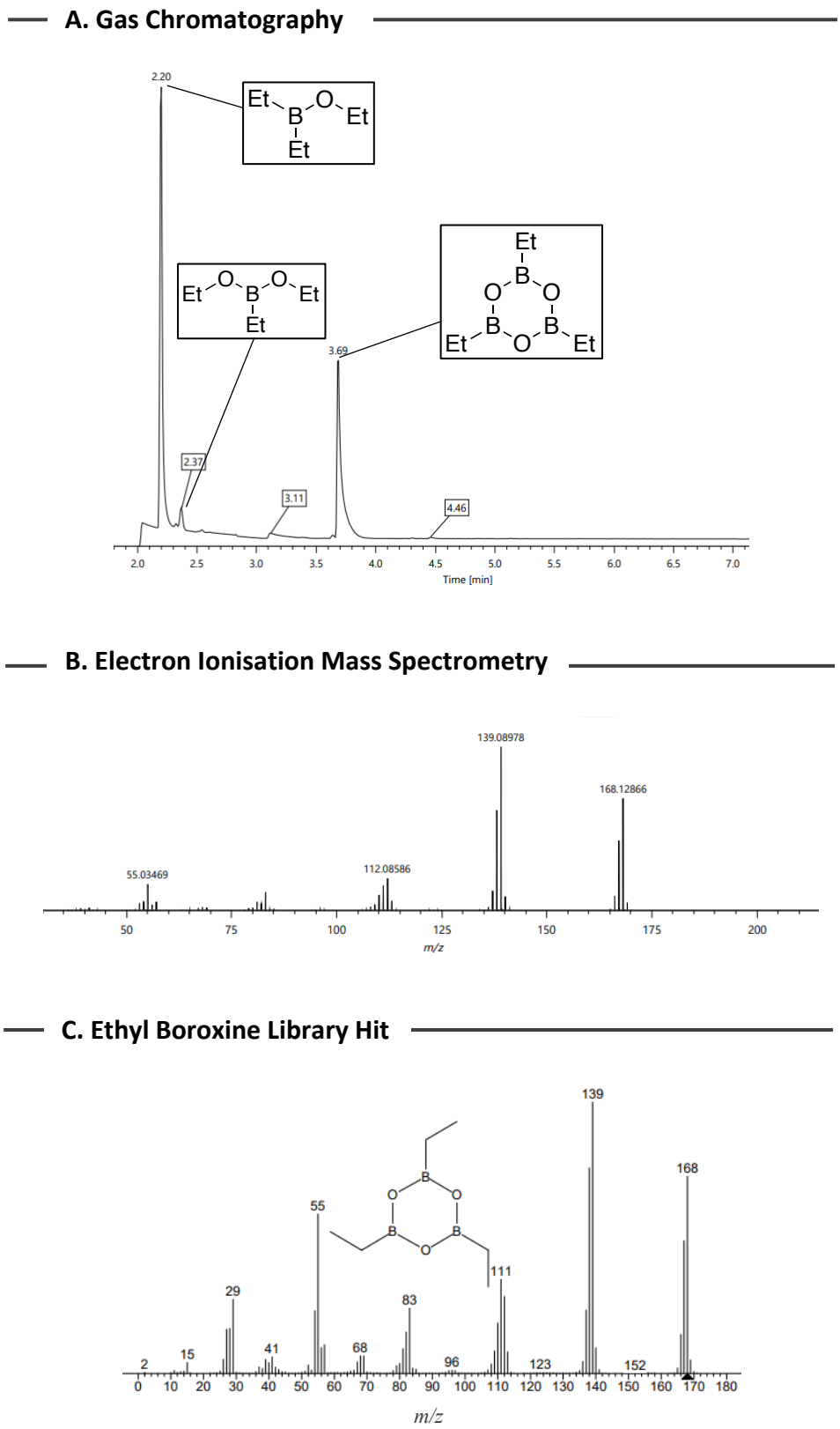


*Figure 23. (A) Gas chromatogram of the reaction between $Et_3B$ and $EtOOBEt_2$ after reaction completion. (B) MS of the peak at 3.69 min in the GC. (C) Library fragmentation pattern of triethyl boroxine.*

We validated the assignment of the boroxine in $^{11}B$ NMR reaction by counting oxygen atoms. Given that our experiment is conducted under $O_2$ free conditions, all oxygen present in the products originates from peroxide $Et_2BOOEt$. As we know the amount of reacted $Et_2BOOEt$ at any given time, we can measure the moles of oxygen that have reacted to form products. This is particularly useful due to the unique structure of boroxine where, despite having a boron environment $RB(OR)_2$, there is only one oxygen per boron as opposed to two oxigens per boron. We can use this to differentiate between $EtB(OEt)_2$ and boroxine ($(BOEt)_3$) by plotting the moles of oxygen reacted (from $Et_2BOOEt$) together with moles of oxygen formed (from the products formed) (Figure 24).

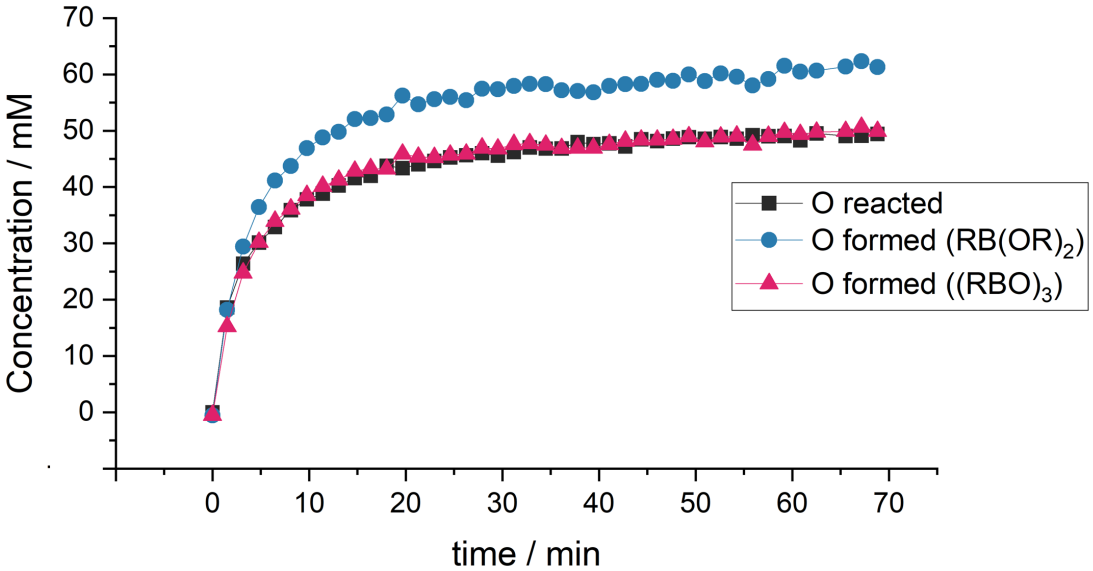


*Figure 24. Kinetic profile the reaction between $Et_3B$ and $Et_2BOOEt$ in hexane at 25 °C, and under $N_2$ Experiment detailed in section 6.5.4 (Entry 1). O reacted was calculated from $Et_2BOOEt$ reacted. O formed was calculated from the products formed: $Et_2BOEt$, $EtB(OEt)_2$, and $RB(OR)_2$ or $(EtBO)_3$.*

The plot reveals that if the peak at 34.37 ppm in $^{11}B$ NMR corresponds to boroxine ($(RBO)_3$), the moles of oxygen reacted match the moles of oxygen formed in products. However, this is not the case for a different molecule with structure $RB(OR)_2$ with 2 moles of oxygen per mole of boron.

This leads us to the question, how is triethyl boroxine formed? From our observations so far, it is plausible that the molecule-assisted homolysis is the dominant process in the $Et_3B/Et_2BOOEt$ reaction. If this holds true, it is likely the reaction products are diethyl(ethoxy)borane ($Et_2BOEt$), ethyl radical (Et·) and diethylboroxyl radical ($Et_2BO$·). ß-eliminations are well-documented for alkoxyl radicals, with rate constants of the order of $10^4$ $s^{-1}$;[1] however, little is known about boroxyl species. Nevertheless, it is plausible that the unstable radical $Et_2BO$· will undergo ß-elimination to form ethyl radical and Et-B=O. The driving force of this would be the formation of a stronger B-O bond and breaking of a weaker B-C bond. Three moles of the formed molecule can combine to form the more stable boroxine. The driving force for this would be the formation of the low energy boroxine (Scheme 37).

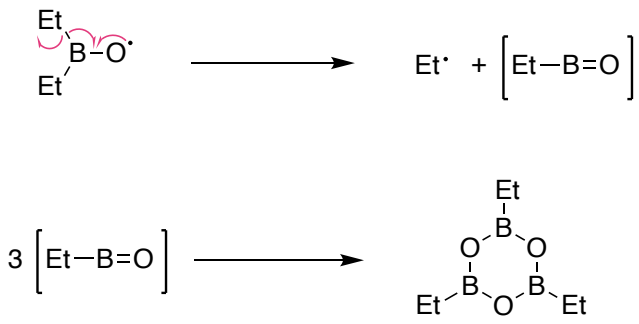


*Scheme 37. Proposed mechanism for the formation of triethyl boroxine. ß-elimination of Et· from Et2BO·, producing EtB=O and subsequent combination of three EtB=O molecules, results in the observed boroxine.*

Thus far, we have successfully identified the majority of the products generated in the reaction. The remaining product corresponds to the NMR peak at **54.43** ppm (Figure 25), which is indicative of a B environment in a $R_2BOR$ structure. Given that $Et_2BOEt$ and $Et_2BOOEt$ have already been identified, the remaining compounds that could fit this structure are likely to be $Et_2BOBEt_2$ or $Et_2BOH$.[123, 124]

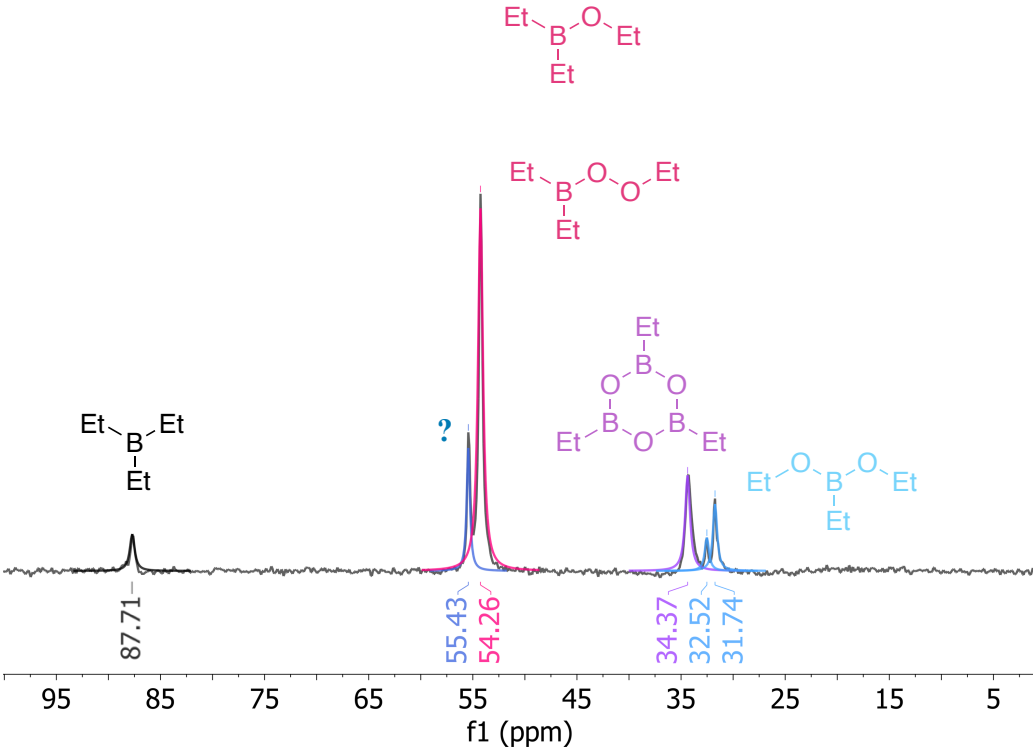


*Figure 25. Partially assigned $^{11}B$ NMR of the reaction between $Et_3B$ and $Et_2BOOEt$ in hexane, at 25 °C, under $N_2$, after reaction completion. Experiment detailed in section 6.5.4 (Entry 1).*

The ability to observe B species by MS would greatly facilitate the assignment of peaks to compound structures. We found that the conditions for APCI can be optimised to detect these elusive compounds (Section 6.10.2). To this end, we used $Bu_3B$, the butyl analogue to $Et_3B$, to study this reaction. This choice was made by the fact that the compound $Et_3BOH$, which we aim to observe, has a mass of 86.09 amu, while the mass spectrometer used can only detect masses above 100 amu. By using $Bu_3B$, the expected compound, $Bu_2BOH$, would have a mass of 142.15 amu, making it detectable by our instrument.

The reaction products of $Bu_3B$ and $Bu_2BOOBu$ were analysed by MS, which confirmed the formation of both $Bu_2BOBu_2$ and $Bu_2BOH$ (50 mM $Bu_3B$, 50 mM $Bu_2BOOBu$, 1 mL hexane. Experiment detailed in section 6.4.1.) (Table 11). In addition, we observed all previously identified products, such as Butyl boroxine ($(BuBO)_3$), $Bu_2B(OBu)$, and $BuB(OBu)_2$. The $^{11}B$ NMR of the reaction mirrors that of the reaction with ethyl analogues. We can therefore

assume that in the analogous reaction $Et_3B$ and $Et_2BOOEt$ we will be forming the corresponding product $Et_2BOH$.

*Table 11. MS analysis of the products formed in the reaction between $Bu_3B$ and $Bu_2BOOBu$ in hexane, at 25 °C and under $N_2$. Experiment detailed in section 6.4.1.*

| Species | | m/z | MS peak intensity/Noise |
|---|---|---|---|
| $Bu_2BOH$ | $[Bu_2BOH+H]^+$ | 143.1607 | 12649 |
| $Bu_2BOBBu_2$ | $[Bu_2BOBBu_2+H]^+$ | 267.3030 | 3281 |
| $(BuBO)_3$ | $[(BuBO)_3+H]^+$ | 253.2318 | 12340 |
| $Bu_2B(OBu)$ | $[Bu_2B(OBu)+H]^+$ | 199.2233 | 251 |
| | $[Bu_2B(OBu)+Na]^+$ | 221.2053 | 54 |
| $BuB(OBu)_2$ | $[BuB(OBu)_2+H]^+$ | 215.2182 | 30 |
| | $[BuB(OBu)_2+Na]^+$ | 237.2002 | 19 |

Given that we are forming the $Et_2BOH$ product, we expected to detect the OH proton by $^1H$ NMR. A broad peak appears at the right chemical shift at 5.6 ppm, which could correspond to this species (Figure 26).

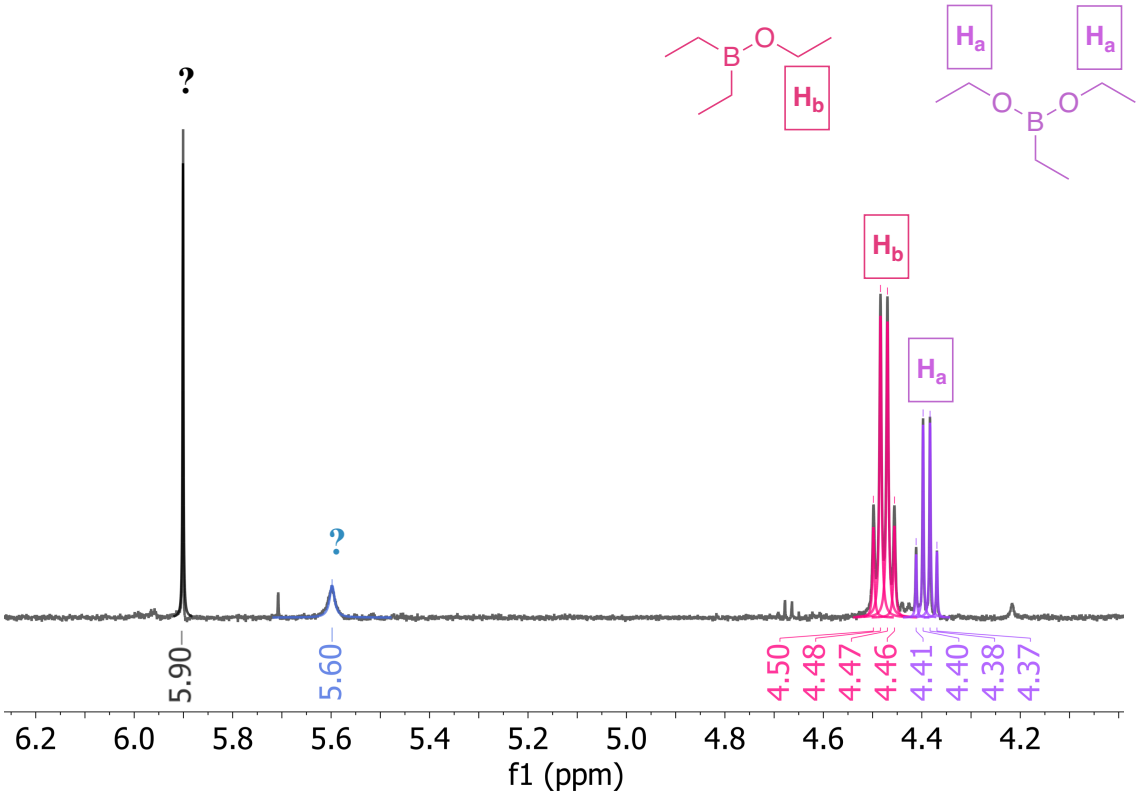


*Figure 26. Assigned $^{1}H$ NMR of the reaction between $Et_3B$ and $Et_2BOOEt$ in hexane, at 25 °C, under $N_2$, after reaction completion. Experiment detailed in section 6.5.4 (Entry 1).*

To confirm that this peak corresponds to the same species, we can monitor the evolution of this $^{1}H$ NMR peak at **5.60** ppm as the reaction progresses and compare it to the formation of the $^{11}B$ NMR peak at **55.43** ppm (Figure 27).

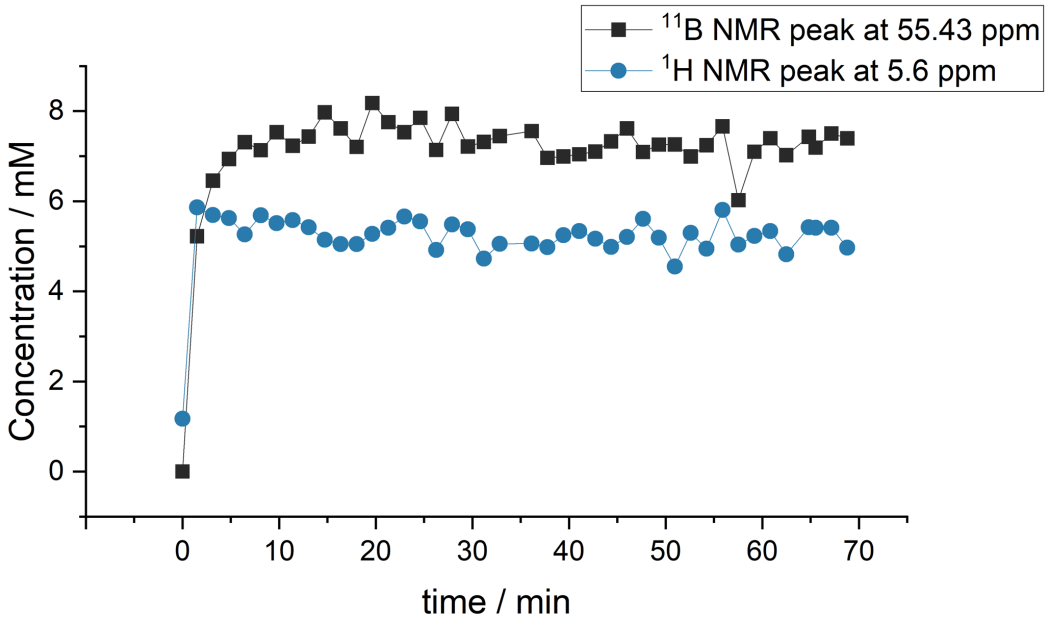


*Figure 27. Kinetic profile the reaction between $Et_3B$ and $Et_2BOOEt$ in hexane. The reaction was run at 25 °C, and under $N_2$ and was followed by $^{11}B$ and $^{1}H$ NMR using the initial concentration as reference. Measurements were taken at the indicated timestamps. Experiment detailed in section 6.5.4 (Entry 1).*

We observe how both peaks increase rapidly in the first minutes of reaction. $^{11}B$ NMR peak continues increasing slowly as the reaction progresses, whereas $^{1}H$ NMR peak remains at a similar intensity throughout. This discrepancy can be tentatively assigned to the formation of $Et_2BOBEt_2$ in $^{11}B$ NMR under a similar chemical shift. We know that $Et_2BOBEt_2$ is formed in the reaction thanks to MS analysis, and we also know that the chemical shift for this compound must be near 53 ppm.[123] If this is the case it is possible to calculate the amount of $Et_2BOH$ and $Et_2BOBEt_2$ separately, forming 0.21 eq. of $Et_2BOH$ and 0.04 eq. of $Et_2BOBEt_2$. However, with no further evidence to confirm the structures it is possible that the assignment is not correct.

The remaining question is how these products are formed. The formation of $Et_2BOBEt_2$ is likely a result of the reaction of the radical $Et_2BO\cdot$ with $Et_3B$. Given that all O-centred radicals are expected to react quickly with trialkylboranes ($k \approx 10^6$ $M^{-1}$ $s^{-1}$),[88, 90] it is plausible that if the radical $Et_2BO\cdot$ is formed in the system, it would readily react to form the product $Et_2BOBEt_2$ (Scheme 38).[90]

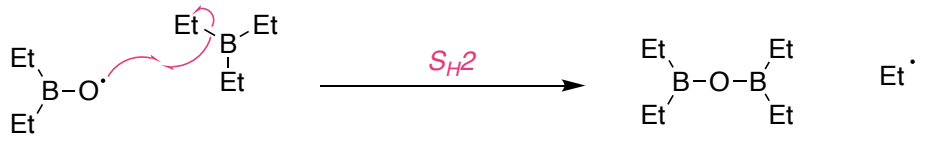


*Scheme 38. $S_H2$ reaction between $Et_2BO\cdot$ and $Et_3B$ to yield the observed product $Et_2BOBEt_2$ and ethyl radical.*

The formation of $Et_2BOH$ presents an intriguing case. The product $Et_2BOEt$ could undergo hydrolysis to yield $Et_2BOH$ and EtOH, a known reactivity pathway in the synthesis of alcohols from boronic esters.[96, 125] However, the water solubility in hexane is 3.6 mM,[126] which would only allow for a maximum formation of 3.6 mM of $Et_2BOH$, and we observe a concentration of 5.4 mM.

To investigate this possibility, we conducted the reaction under anhydrous conditions. The $^1$H NMR peak for $Et_2BOH$ was observed again, with a similar final concentration of 5.1 mM. No other changes were noted under strictly anhydrous conditions, suggesting that the small amount of water in hexane does not significantly influence this reaction or the products observed. Thus, $Et_2BOH$ must be formed via a different pathway. One possibility is that the $Et_2BO\cdot$ radical abstracts a hydrogen atom from a hydrogen donor.

Upon further analysis of the $^1$H NMR, we noted the formation of a peak that could correspond to ethene (Figure 28).

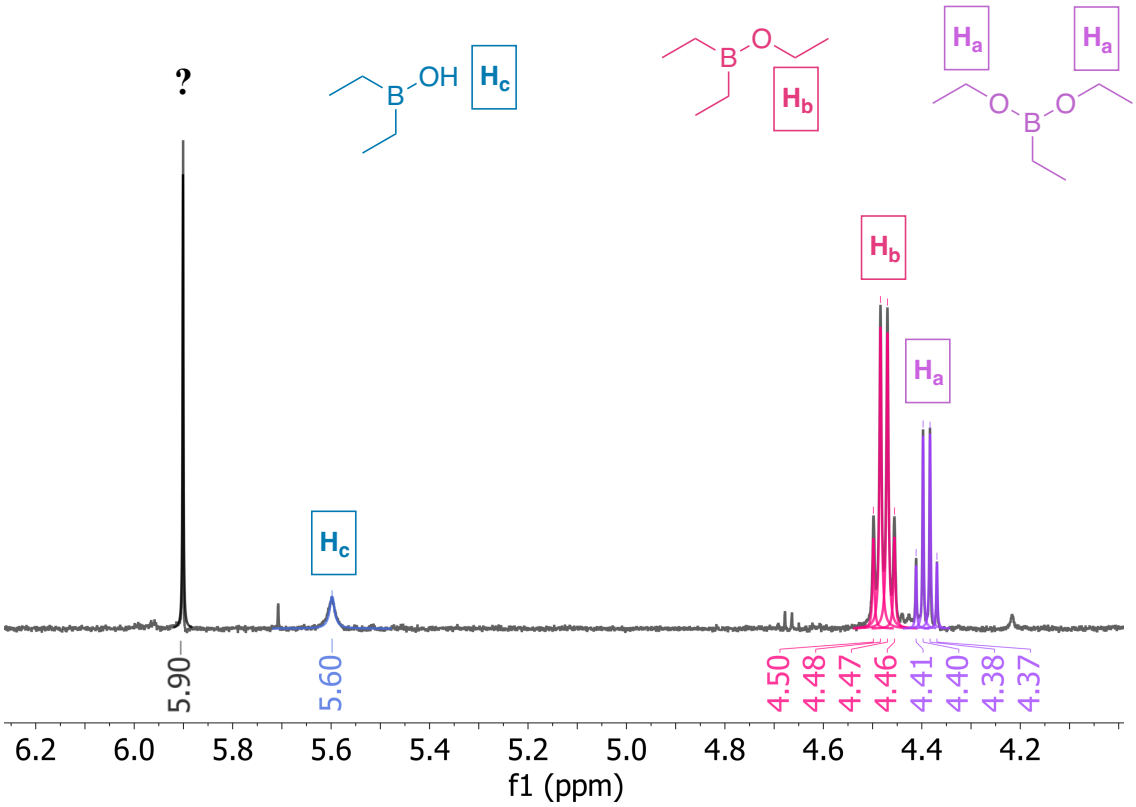


*Figure 28. Assigned $^1$H NMR of the reaction between $Et_3B$ and $Et_2BOOEt$ in hexane, at 25 °C, under $N_2$, after reaction completion. Experiment detailed in section 6.5.4 (Entry 1).*

The simultaneous formation of ethene and $Et_2BOH$ could be tentatively explained by the disproportionation of $Et_2BO\cdot$ and $Et\cdot$ radicals to yield $Et_2BOH$ and ethene (Scheme 39). This radical-radical reaction would be rare, however at the beginning of the reaction radical flux is high, especially for $Et_2BO\cdot$ and $Et\cdot$, facilitating the radical-radical reaction.

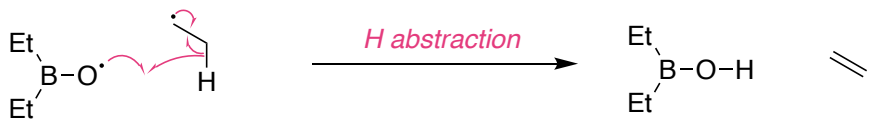


*Scheme 39. Termination reaction between $Et\cdot$ and $Et_2BO\cdot$ to yield products $Et_2BOH$ and ethene.*

This reaction pathway aligns with the observed trend of product formation. As seen in Figure 27, all the $Et_2BOH$ is formed before the first NMR spectrum can be recorded (2 minutes). This rapid formation is characteristic of a radical-radical termination reaction, which would be fastest at high radical concentrations. If the reaction proceeds via a homolytic mechanism, the flux of radicals would be highest at the beginning of the reaction and decrease as the reaction progresses. Therefore, it is logical that products resulting from termination ($Et_2BOH$ and ethene) are formed quickly when the radical flux is high.

To confirm that the singlet at 5.9 ppm corresponded to ethene, we reacted $Bu_3B$ + $Bu_2BOOBu$ (50 mM $Bu_3B$, 50 mM $Bu_2BOOBu$, 1 mL hexane. Experiment detailed in section 6.4.1(Entry 1)). $^1$H NMR after reaction completion showed the formation of 1-butene instead of the singlet for ethene (Figure 29). This can be assigned by comparing to the $^1$H NMR of butene reported in the literature.[127] This evidence suggests that the reaction $Et_3B$ + $Et_2BOOEt$ does indeed form ethene and the peak observed at 5.9 ppm $^1$H NMR corresponds to ethene.

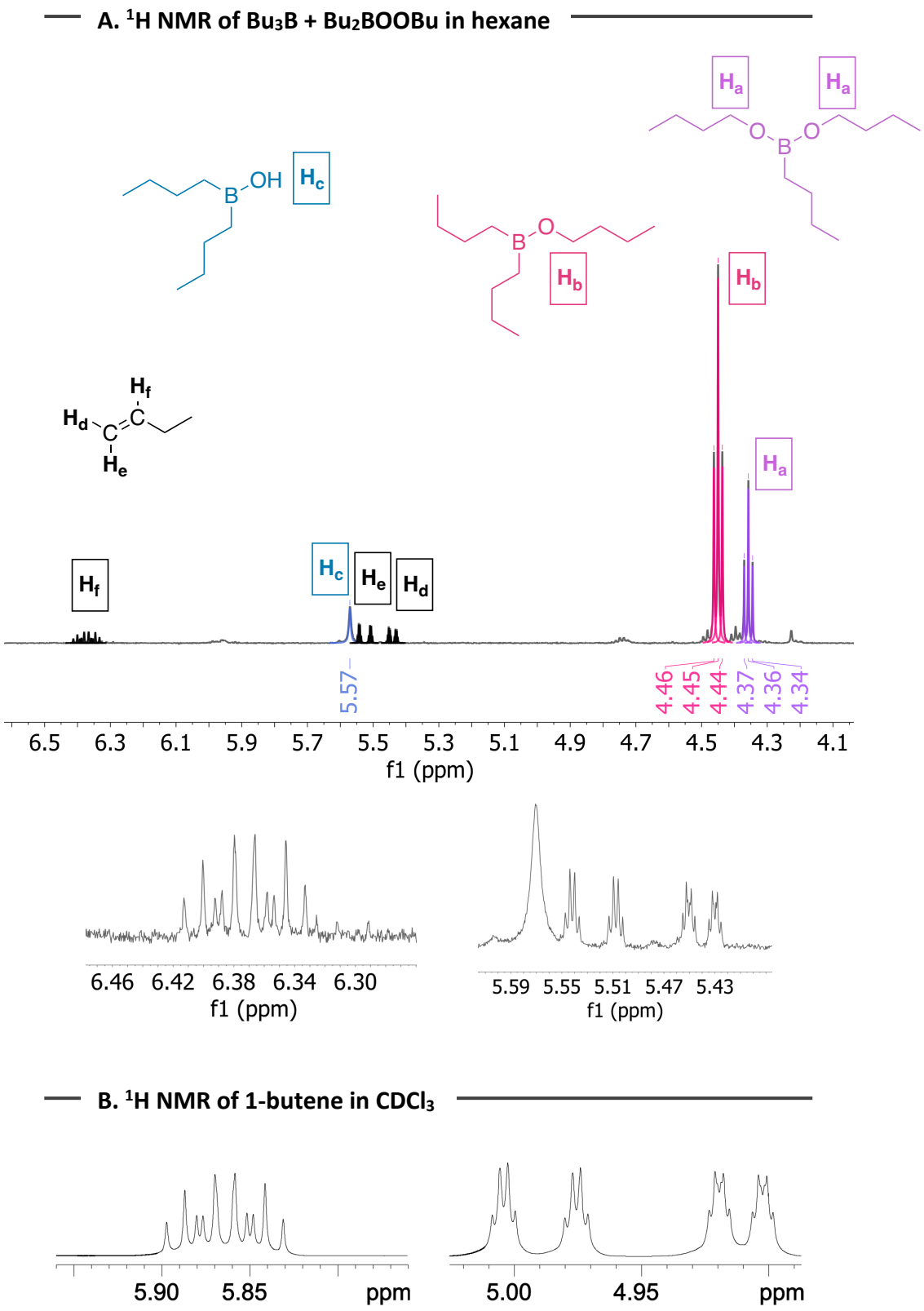


*Figure 29. (A) Assigned $^{11}H$ NMR of the reaction between $Bu_3B$ and $Bu_2BOOEt$ in hexane, at 25 °C, under $N_2$, after reaction completion. Experiment detailed in section 6.4.1(Entry 1). (B) $^{1}H$ NMR of 1-butene in $CDCl_3$.*[127]

With the last species assigned we can now assign most of the $^{1}H$ and $^{11}B$ NMR peaks to the products formed in this reaction (Figure 30).

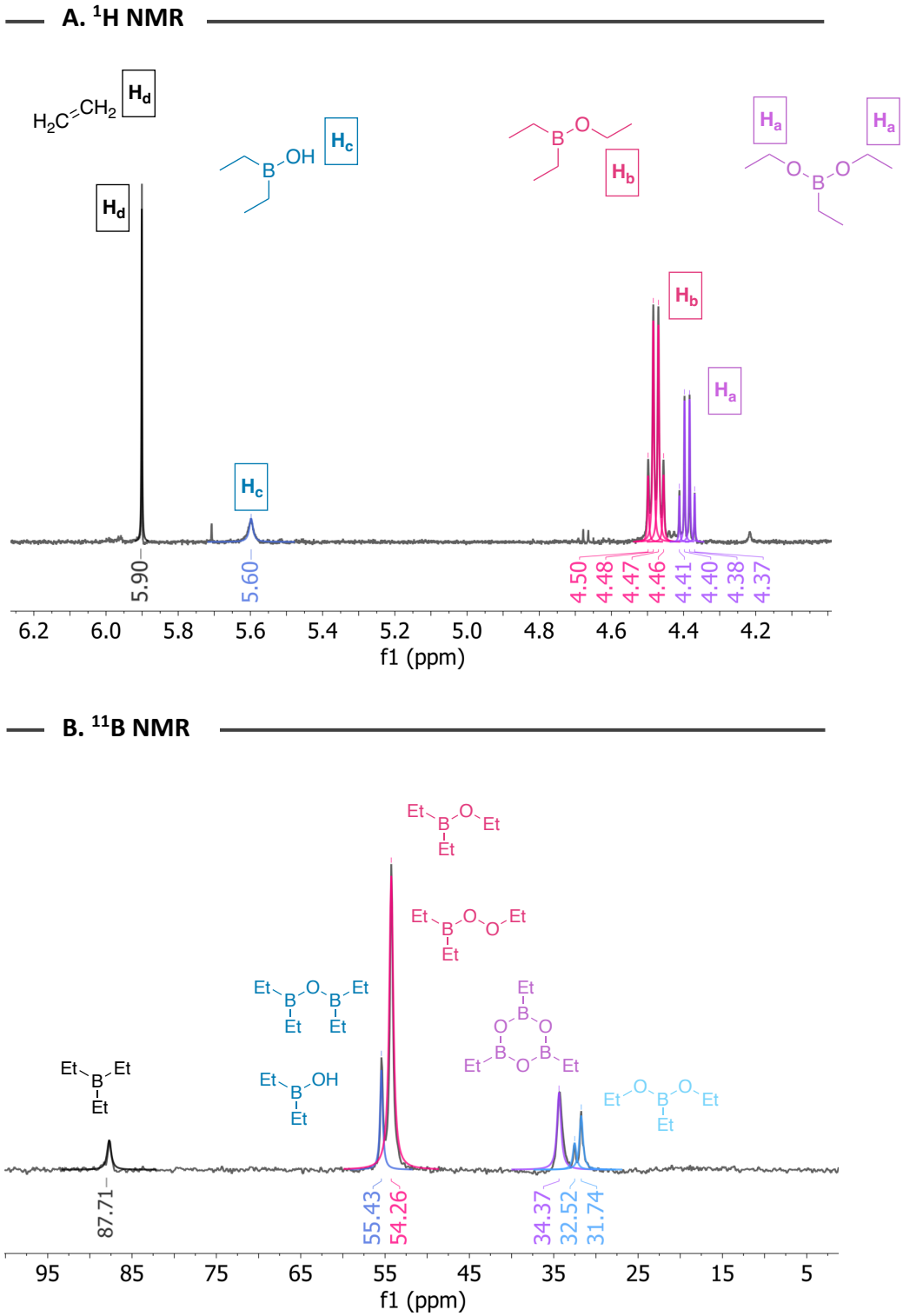


*Figure 30. Assigned $^{1}H$ (A) and $^{11}B$ (B) NMR of the reaction between $Et_3B$ and $Et_2BOOEt$ in hexane, at 25 °C, under $N_2$, after reaction completion. Experiment detailed in section 6.5.4 (Entry 1).*

The reactions leading to the formation of the products observed have been discussed and they are summarised in Scheme 40.

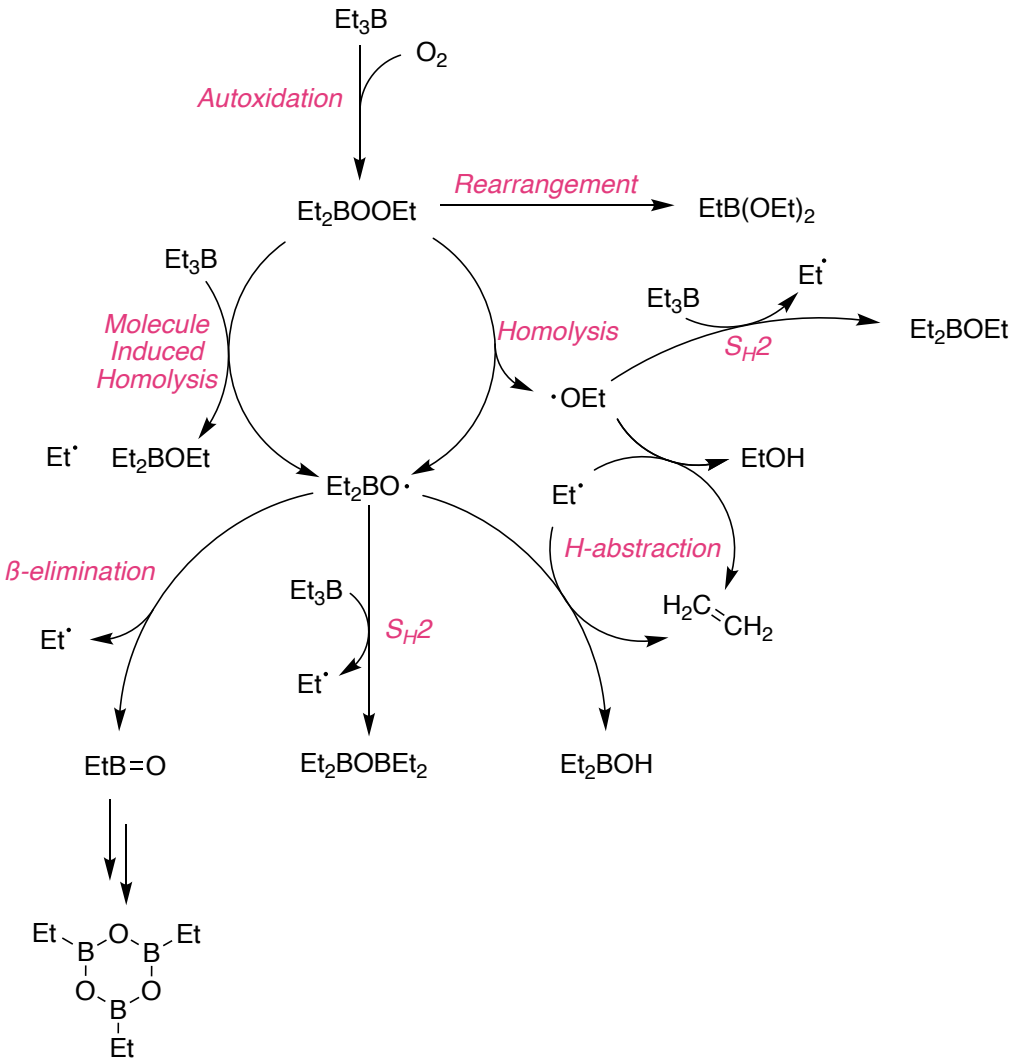


*Scheme 40. Reactions involved in the autoxidation of $Et_3B$.*

### 3.4.2. Reaction Kinetics

The kinetics of the reaction between $Et_3B$ and $Et_2BOOEt$ were also investigated in order to determine the kinetic order and determine the contribution of this reaction to the overall radical production in $Et_3B$ autoxidation. The reaction was monitored at four different concentrations of $Et_3B$ and $Et_2BOOEt$ in order to calculate the reaction rate constant. (Figure 31).

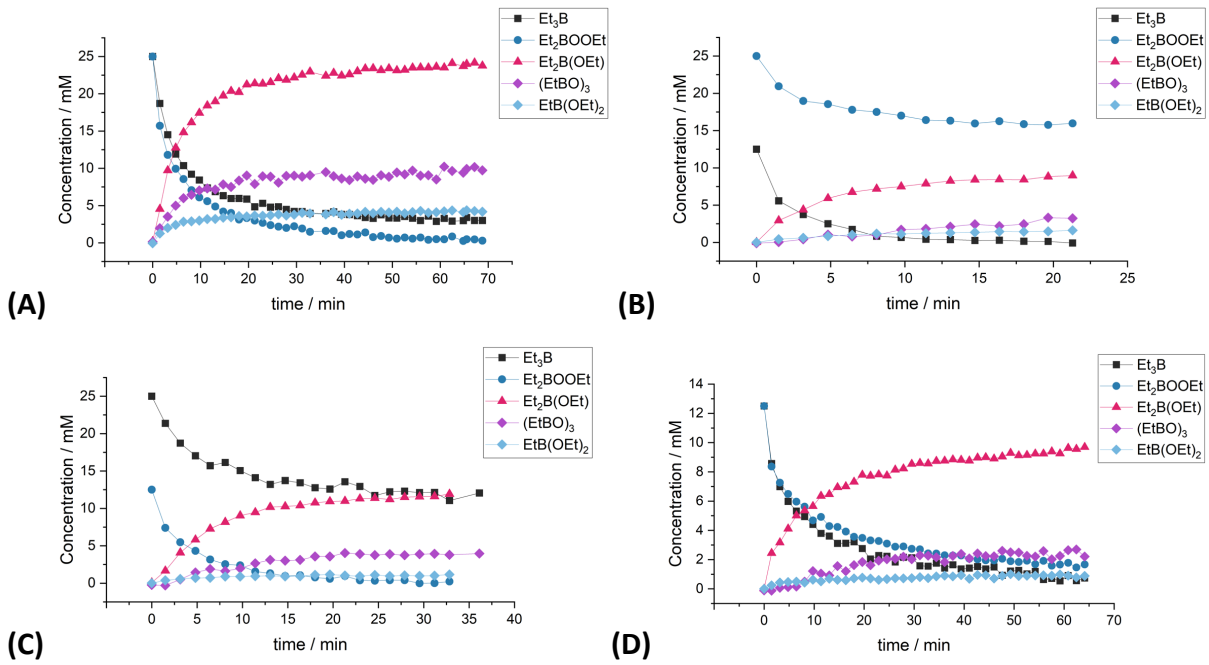


*Figure 31. Kinetic profiles for the reaction between $Et_3B$ and $Et_2BOOEt$ at 25 °C, under $N_2$ at different initial concentrations: (A) 25 mM $Et_3B$ / 25 mM $Et_2BOOEt$, (B) 12.5 mM $Et_3B$ / 25 mM $Et_2BOOEt$, (C) 25 mM $Et_3B$ / 12.5 mM $Et_2BOOEt$ and (D) 12.5 mM $Et_3B$ / 12.5 mM $Et_2BOOEt$. Reactions were followed by $^1H$ and $^{11}B$ NMR and measurements were taken at the indicated timestamps. After reaction completion triethylborate was added to the crude mixture and used as internal standard. Experiment detailed in section 6.5.4.*

All four measurements yielded approximately one equivalent of the product $Et_2B(OEt)$, consistent with a homolytic mechanism. These measurements were used to fit the consumption of $Et_2BOOEt$ and $Et_3B$ to a bimolecular reaction (Figure 32). The experimental rate constants for the consumption of $Et_3B$ and $Et_2BOOEt$ and the formation of $Et_2B(OEt)$ at different starting concentrations were obtained from these fittings (Table 12). The average rate constant for the reaction was determined to be 0.19 ± 0.08 $M^{-1}s^{-1}$.

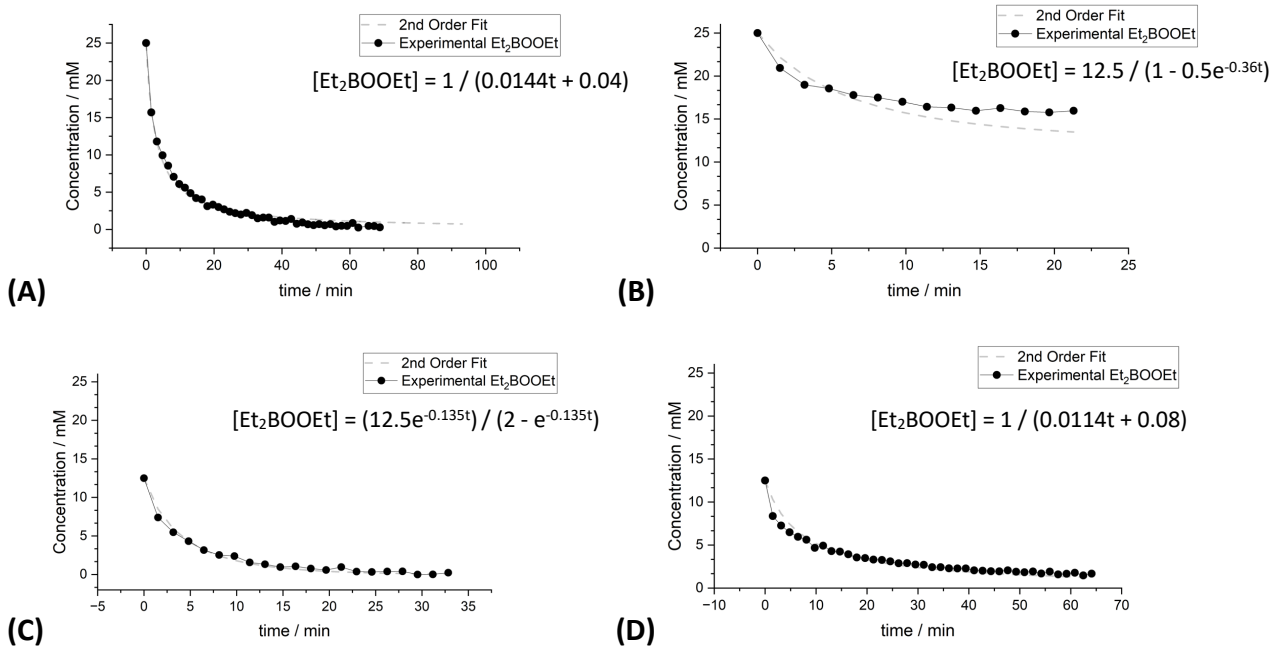


*Figure 32. Kinetic profiles for the consumption of $Et_2BOOEt$ in the reaction with $Et_3B$ at 25 °C, under $N_2$ fitted to a second order reaction. (A) 25 mM $Et_3B$ / 25 mM $Et_2BOOEt$, (B) 12.5 mM $Et_3B$ / 25 mM $Et_2BOOEt$, (C) 25 mM $Et_3B$ / 12.5 mM $Et_2BOOEt$ and (D) 12.5 mM $Et_3B$ / 12.5 mM $Et_2BOOEt$. Reactions were followed by $^1H$ and $^{11}B$ NMR and measurements were taken at the indicated timestamps. After reaction completion triethylborate was added to the crude mixture and used as* Type equation here.*internal standard. Experiment detailed in section 6.5.4.*

*Table 12. Experimental rate constants for the bimolecular reaction between $Et_3B$ and $Et_2BOOEt$ in hexane under $N_2$ at 25 °C. Constants calculated for the consumption of $Et_3B$ and $Et_2BOOEt$ and formation of $Et_2BOEt$ at different concentrations: (A) 25 mM $Et_3B$ / 25 mM $Et_2BOOEt$, (B) 12.5 mM $Et_3B$ / 25 mM $Et_2BOOEt$, (C) 25 mM $Et_3B$ / 12.5 mM $Et_2BOOEt$ and (D) 12.5 mM $Et_3B$ / 12.5 mM $Et_2BOOEt$. The rate constants are given in $M^{-1}$ $s^{-1}$.*

| | $Et_3B$ | $Et_2BOOEt$ | $Et_2BOEt$ |
|---|---|---|---|
| A) | 0.20 | 0.24 | 0.22 |
| B) | 0.27 | 0.09 | 0.18 |
| C) | 0.19 | 0.18 | 0.16 |
| D) | 0.21 | 0.19 | 0.17 |

The rate constant for the reaction will change depending on the solvent used. It is particularly important here were $Et_3B$ is a strong Lewis acid and can coordinate with solvent molecules, thus, making it less reactive to other reactions. The effect of different solvents on the reaction rate was also studied. $Et_3B$ was reacted with $Et_2BOOEt$ in four different solvents (Hexane, diethylether ($Et_2O$), dichloromethane (DCM), and toluene), and the kinetic profile was fitted to a second-order reaction (Figure 33). The rate constants for the reaction in different solvents were estimated from these fittings (Table 13).

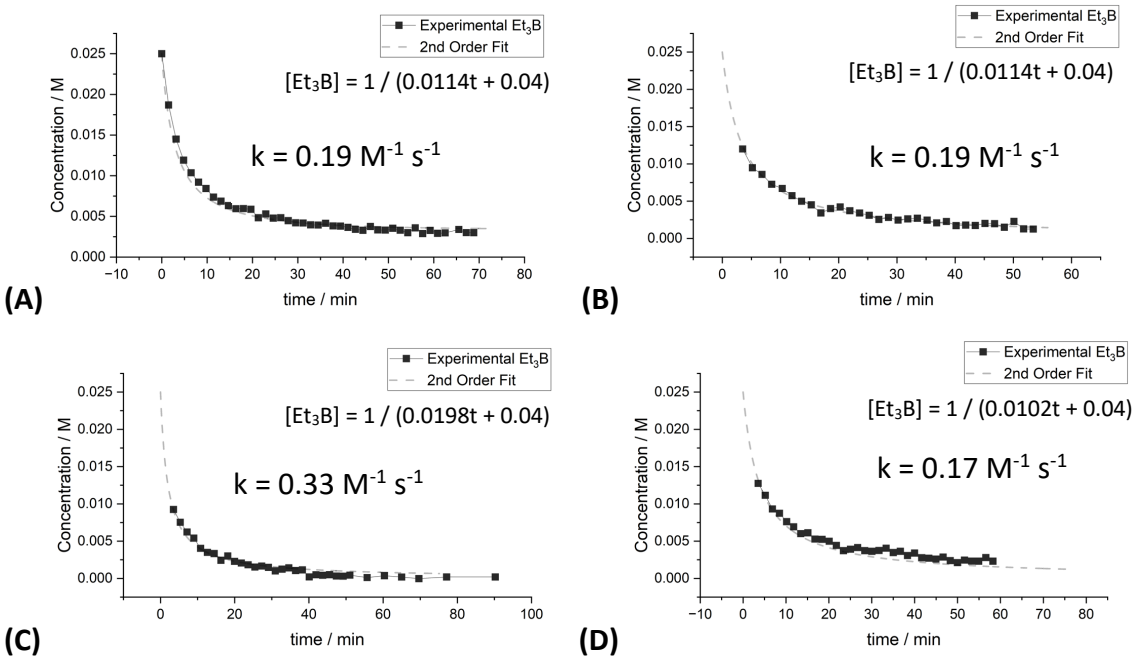


*Figure 33. Kinetic profiles for the consumption of $Et_3B$ in the reaction with $Et_2BOOEt$ at 25 °C, under $N_2$ fitted to a second order reaction in (A) Hexane, (B) $Et_2O$, (C) DCM and (D) toluene. Reactions were followed by $^1H$ and $^{11}B$ NMR and measurements were taken at the indicated timestamps. After reaction completion triethylborate was added to the crude mixture and used as internal standard. Experiment detailed in section 6.5.5.*

*Table 13. Experimental rate constants for the bimolecular reaction between $Et_3B$ and $Et_2BOOEt$ under $N_2$ at 25 °C in four different solvents. The rate constants are given in $M^{-1}$ $s^{-1}$. Experiment detailed in section 6.5.5.*

| Solvent | k / $M^{-1}$ $s^{-1}$ |
|---|---|
| Hexane | 0.19 |
| $Et_2O$ | 0.19 |
| DCM | 0.33 |
| Toluene | 0.18 |

The results revealed a minimal solvent effect on this reaction, with DCM having the most significant impact. This is surprising given that $Et_3B$ is a strong Lewis acid and ethereal solvents such as $Et_2O$ could act as Lewis bases, potentially forming a complex with $Et_3B$, however this does not seem to affect the reaction rate. If such complexation does occur, it appears to be insufficient to significantly affect the observed reactivity.

Reaction stoichiometry suggests that this reaction might proceed via a homolytic mechanism. If this is the case, and the radicals formed can act as radical initiators, this reaction would serve as a secondary initiation mechanism in $Et_3B/O_2$ initiation. Given that peroxide $Et_2BOOEt$ is the primary product formed in the autoxidation cycle, and considering its rapid reaction rate with $Et_3B$, this secondary initiation process could be quite significant in the overall success of $Et_3B/O_2$ as a radical initiator. We find that the rate constant for secondary initiation is about 300 times greater than the rate constant for primary initiation (Scheme 41), of course they are not directly comparable as primary initiation depends on the concentration of $O_2$ whereas secondary initiation is dependent on the concentration of $Et_2BOOEt$. However, in a later section (Section 3.5.1) we model the reaction find that secondary initiation is responsible for the majority of radicals formed under realistic concentrations of each product.

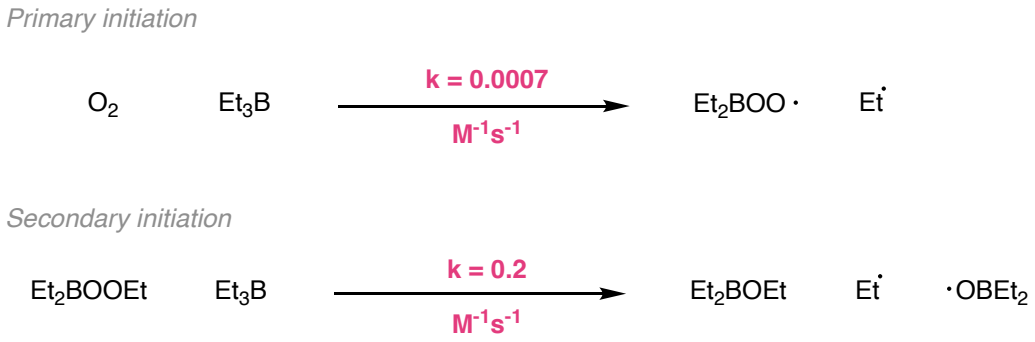


*Scheme 41. Reactions for primary initiation and secondary initiation in $Et_3B$ autoxidation with their respective rate constants.*

Before drawing any conclusions, we need to gather more evidence to confirm that the reaction between $Et_3B$ and $Et_2BOOEt$ proceeds via a homolytic mechanism and that the generated radicals can act as radical initiators. To address these questions, we employed radical trapping.

### 3.4.3. Radical Trapping

Trapping radicals generated in the reaction between $Et_3B$ and $Et_2BOOEt$ in the absence of $O_2$ would provide evidence that this reaction could be responsible for autoinitiation. Indeed, the trapping reaction of an initiator radical with our allyl-TEMPO trap can be considered a mimic of a chain initiation.

The experiment had to be conducted in the absolute absence of oxygen. Initial experiments showed that the presence of trace $O_2$ in the solvent would react with $Et_3B$, yielding Et· and showing trapped ethyl radicals in the controls. To circumvent this reaction, the solutions were purged by bubbling Ar for 30 seconds, followed by a freeze-Pump-Thaw before the addition of $Et_3B$.

This method enabled the recording of a control containing $Et_3B$ and trap that reproductively yielded very small peaks (8 times noise level) for trapped ethyl radicals, thereby ensuring that the procedure was successfully carried out under $O_2$-free conditions. With the method

validated, $Et_3B$ was reacted with $Et_2BOOEt$ in the presence of CHANT (50 mM $Et_3B$, 50 mM $Et_2BOOEt$, 5 mM CHANT. Experiment detailed in section 6.3.8, Entry 1), and the solution was analysed by MS (Table 14).

*Table 14. Trapped radicals using CHANT in the reaction between $Et_3B$ and $Et_2BOOEt$ in hexane, at 25 °C and under $N_2$. Experiment detailed in section 6.3.8 (Entry 1).*

| Species | | m/z | MS peak intensity | |
|---|---|---|---|---|
| | | | Control[a] | Sample[b] |
| Unreacted Trap | $[CHANT+H]^+$ | 323.2699 | 2411 | 9 |
| Trapped Et· | $[CHANT+Et\cdot+H]^+$ | 196.1697 | - | 18 |
| | $[CHANT+Et\cdot+Na]^+$ | 218.1518 | 8 | 431 |
| | $[TEMPO+Et\cdot+H]^+$ | 186.1855 | 7 | 3831 |
| | $[TEMPO+Et\cdot Na]^+$ | 208.1674 | - | 6 |

*[a] Control consisted of $Et_3B$ and CHANT (0.1 eq.) with no $Et_2BOOEt$. [b] Sample consisted of $Et_3B$ + $Et_2BOOEt$ (1:1) in the presence of CHANT (0.1 eq.). Control detailed in section 6.3.8 (Entry 1).*

We successfully trapped ethyl radicals generated by this reaction. This provides evidence that the reaction generates radicals, and these radicals can act as radical initiators. A closer examination revealed that the peak for the unreacted trap had a very low intensity. Moreover, there were various peaks of multiple additions of radicals to the trap (Table 15). This occurs when the concentration of the trap decreases, and the generated radicals start reacting with the accumulated trapped adducts.

*Table 15. MS peaks for multiple additions of radicals to CHANT in the radical trapping of the reaction between $Et_3B$ and $Et_2BOOEt$ in hexane, at 25 °C and under $N_2$. Experiment detailed in section 6.3.8.*

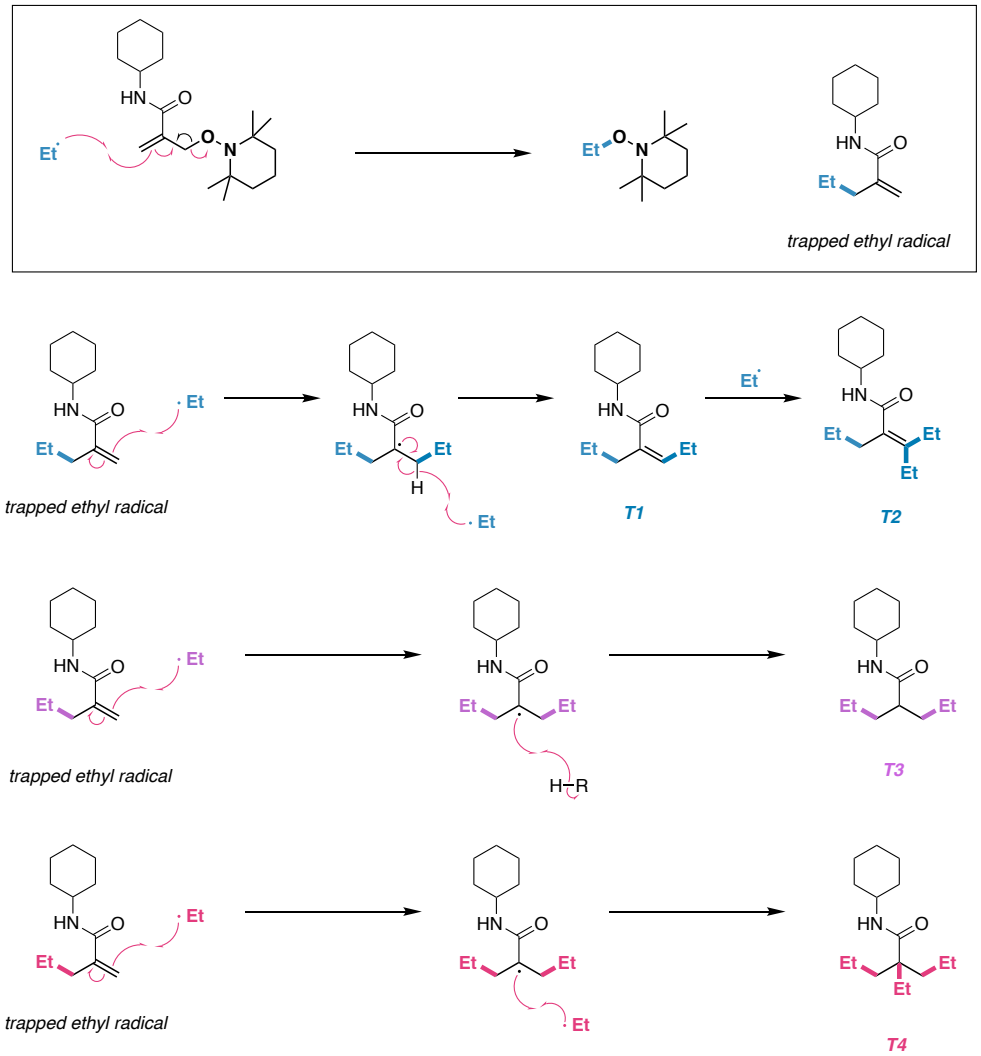


| Species | | m/z | MS peak intensity | |
|---|---|---|---|---|
| | | | Control | Sample |
| **T1** | $[T1+H]^+$ | 224.201 | - | 199 |
| | $[T1+Na]^+$ | 246.183 | - | 467 |
| **T2** | $[T2+H]^+$ | 252.2323 | - | 43 |
| | $[T2+Na]^+$ | 274.2142 | - | 41 |
| **T3** | $[T3+H]^+$ | 226.2166 | - | 174 |
| | $[T3+Na]^+$ | 248.1986 | - | 398 |
| **T4** | $[T4+H]^+$ | 254.248 | - | 396 |
| | $[T4+Na]^+$ | 276.2299 | - | 683 |

This is usually a hindrance since the trapped adducts start degrading, making them more difficult to detect. However, in this case, it is an encouraging observation as it suggests that the studied reaction might produce a large number of radicals.

To obtain a quantitative analysis of the trapped radicals, we attempted to use NMR to detect the trapped adduct. The initial concentration of CHANT was increased to 1 eq., up from the previous 0.1 eq, to reduce the formation of products of multiple addition (50 mM $Et_3B$, 50 mM $Et_2BOOEt$, 50 mM CHANT. Experiment detailed in section 6.3.8, Entry 2).

MS analysis showed the expected peaks, and the trapped adduct was also observed by NMR and with high intensities as shown in Figure 34.

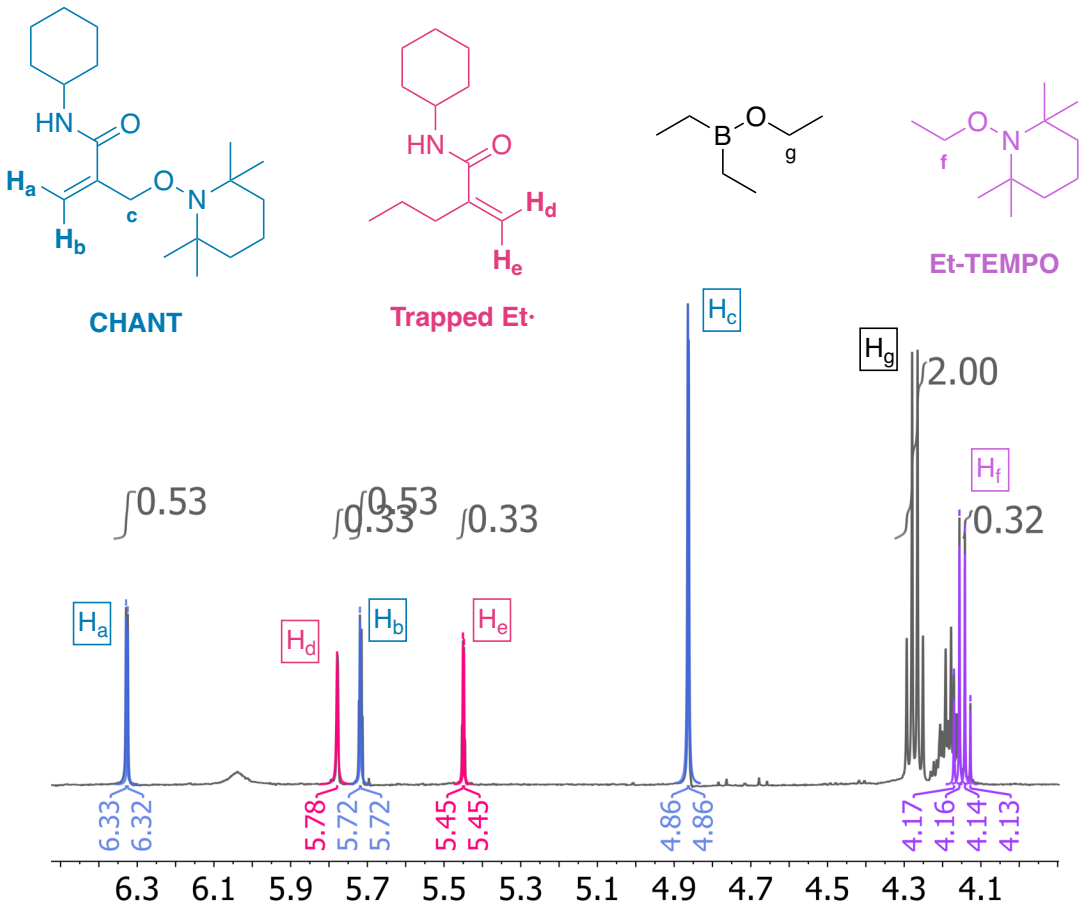


*Figure 34. $^1H$ NMR of radical trapping in reaction between $Et_3B$ and $Et_2BOOEt$ in hexane using CHANT, at 25 °C, under $N_2$, after reaction completion. Experiment detailed in section 6.3.8 (Entry 2).*

NMR provides a quantitative measurement of the radicals trapped in this reaction. Approximately 0.33 eq. of trapped ethyl radical was observed relative to 1 eq. of initial $Et_3B$, along with 0.33 eq. of TEMPO trapped ethyl radicals (Et-TEMPO). This adds up to a total of 0.66 eq. of trapped ethyl radicals relative to the 1 eq. of initial $Et_3B$.

Additionally, 0.5 eq. of the trap had reacted. There was more reacted trap than trapped ethyl radicals, which could be due to other types of radicals reacting with the trap or multiple additions of ethyl radicals to trapped adducts (as observed in MS analysis). Either way, this is an indication that the reaction generates at least 0.66 eq. of radicals. This confirms our earlier suspicion that the reaction between $Et_3B$ and $Et_2BOOEt$ is likely responsible for the autoinitiation in $Et_3B$ autoxidation.

The efficiency of the reaction in generating ethyl radicals was so high that these radicals were directly observable via EPR (Figure 35). A solution of $Et_2BOOEt$ and $Et_3B$ in hexane was reacted under $N_2$ (25 mM $Et_3B$, 25 mM $Et_2BOOEt$, 1 mL hexane. Experiment detailed in section 6.6.3). The EPR analysis was rapidly conducted after mixing, capturing the spectrum at the peak of the reaction when the radical concentration was at its highest.

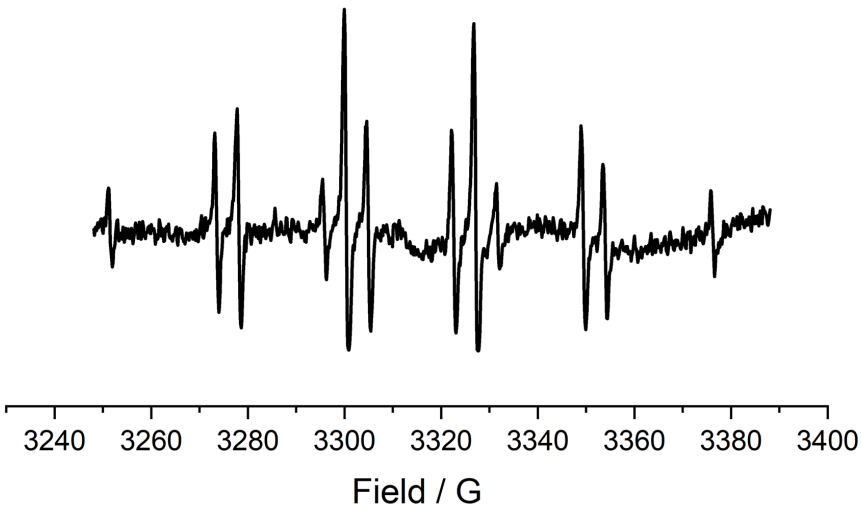


*Figure 35. EPR spectrum of a solution of $Et_3B$ and $Et_2BOOEt$ (1:1) in hexane, under $N_2$ and at 25 °C. The spectrum was recorded 1.5 minutes after $Et_3B$ was added to the solution of $Et_2BOOEt$. Experiment detailed in section 6.6.3.*

The spectrum revealed a quartet of triplets from the $CH_2CH_3$ of the ethyl radicals, aligning with the literature hyperfine coupling constants for ethyl radicals (Table 16).

*Table 16. EPR coupling constants of ethyl radical in gauss.*

| Coupling constant | Experimental | Literature[128] |
|---|---|---|
| $a(H_\alpha)$ | 22.31 | 22.38 |
| $a(H_\beta)$ | 26.86 | 26.87 |

The detection limit of EPR under these conditions is ca. 1 µM. Reactive radicals, such as alkyl radicals like ethyl radicals, can usually only be observed in flow or with very efficient continuous initiation, e.g., by high power photolysis at high initiator concentrations. These radicals usually need to be trapped with spin traps to form more stable spin adducts for EPR observation. However, in this case, the reactive species were observable via EPR without trapping, indicating a high concentration of radicals produced by the system.

Based on the observations on the products of this reaction (Section 3.4.1), specifically the formation of 1 eq. of product $Et_2B(OEt)$, it is plausible that the reaction of $Et_3B$ with $Et_2BOOEt$ proceeds via the molecule-assisted homolysis proposed by Friebolin.[97] This homolytic mechanism suggests that the ethyl radicals originate from the $Et_3B$ species (Scheme 42).

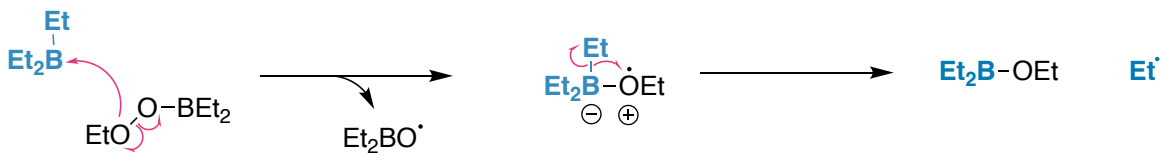


*Scheme 42. Homolytic mechanism of the reaction between $Et_3B$ and $Et_2BOOEt$. The mechanism consists of a molecule assisted homolysis of the peroxide bond, which is then followed by a ß-elimination that results in the expulsion of an ethyl radical from the resulting oxygen-centred radical.*

To confirm the mechanism we decided to use $Bu_3B$ as an homologue of $Et_3B$. When $Bu_3B$ is reacted with $Et_2BOOEt$, Bu· radical will be observed if they originate from $R_3B$, and Et· radicals will be observed if they originate from $R_2BOOR$. An experiment was conducted where $Bu_3B$ was reacted with $Et_2BOOEt$ in the presence of CHANT (50 mM $Bu_3B$, 50 mM $Et_2BOOEt$, 50 mM CHANT. Experiment detailed in section 6.3.9.).

MS analysis revealed the presence of both trapped ethyl and butyl radicals (Table 17). However, the intensities of trapped butyl were over 16 times higher than trapped ethyl. Compared to the control reaction ($Et_3B$/$Et_2BOOEt$), the amount of trapped ethyl radicals was minimal, although it does not rule out the production of some amount of ethyl radicals.

*Table 17. Trapped radicals using CHANT in the reaction between $Bu_3B$ and $Et_2BOOEt$ in hexane, at 25 °C and under $N_2$. Experiment detailed in section 6.3.9.*

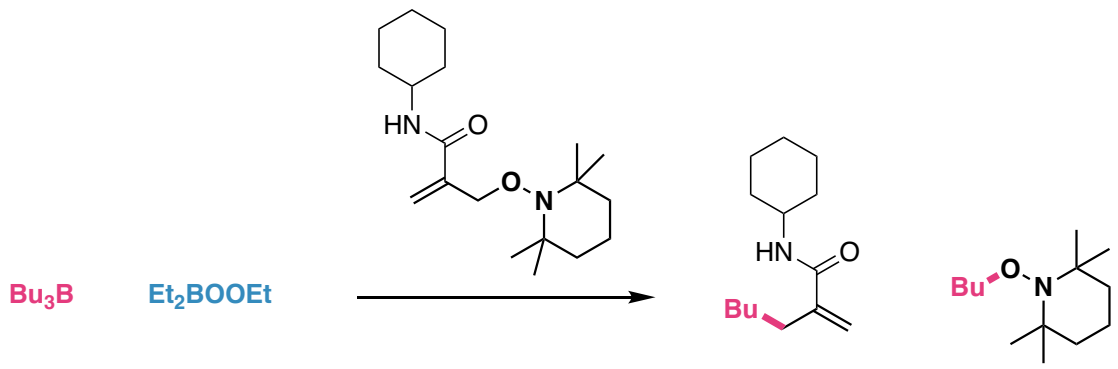


| | Species | m/z | MS peak intensity/Noise | |
|---|---|---|---|---|
| | | | Control[a] | Sample[b] |
| Trapped Et· | [CHANT+Et·+H]$^+$ | 196.1697 | 18 | 31 |
| | [CHANT+Et·+Na]$^+$ | 218.1518 | 431 | - |
| | [TEMPO+Et·+H]$^+$ | 186.1855 | 3831 | 203 |
| Trapped Bu· | [CHANT+Bu·+H]$^+$ | 224.2012 | - | 498 |
| | [TEMPO+Bu·+H]$^+$ | 214.2169 | - | 6797 |

*[a]Control: $Et_3B$ + $Et_2BOOEt$ + CHANT (1:1:1) (Experiment detailed in section 6.3.8). [b]Sample: $Bu_3B$ + $Et_2BOOEt$ + CHANT (1:1:1). (Experiment detailed in section 6.3.9)*

NMR analysis only detected trapped butyl radicals (Figure 36). These were distinguished from ethyl radicals by the splitting of the alkyl-TEMPO trapped species where Et-TEMPO gives a quartet in the $CH_2$ adjacent to the O and Bu-TEMPO gives a triplet in the same region. The NMR peak characterisation was confirmed by recording separate NMR spectra of Bu-TEMPO and Et-TEMPO, achieved by bubbling air in two separate solutions of $Et_3B$/TEMPO and $Bu_3B$/TEMPO.

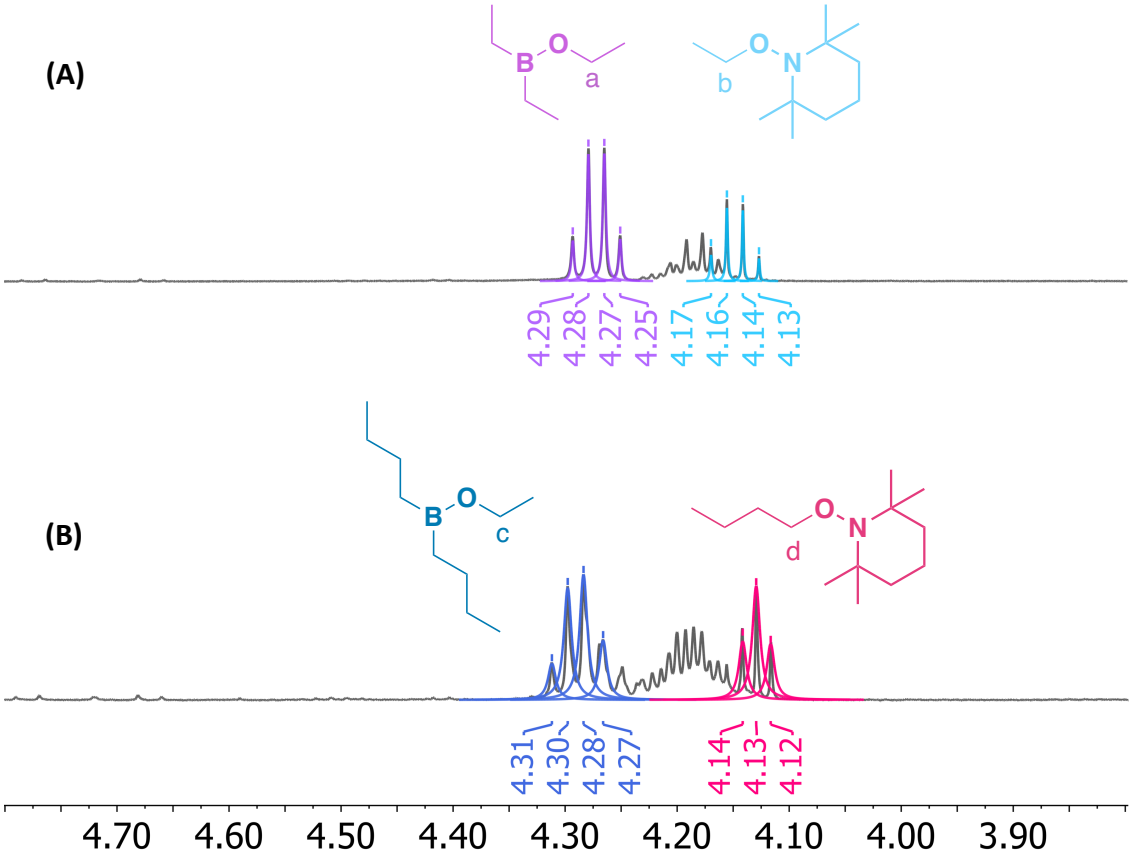


*Figure 36. $^1$H NMR of radical trapping in reaction between (A) $Et_3B$ and $Et_2BOOEt$ and (B) $Bu_3B$ and $Et_2BOOEt$. Both reactions were run in hexane using CHANT as radical trap, at 25 °C, and under $N_2$. Experiment detailed in section 6.3.9.*

Both techniques used to study this $Bu_3B$ experiment show that most of the radicals generated are butyl radicals, consistent with the homolytic mechanism proposed by Friebolin.

The small amount of ethyl radicals formed are likely a result of the subsequent reactions of the diethylboroxyl radical ($R_2BO\cdot$) formed in this reaction. As discussed in the previous section (Section 3.4.1), $R_2BO\cdot$ can either react with $R_3B$ in a $S_H2$ reaction forming $R_2BOBR_2$, undergo H atom abstraction to form $R_2BOH$ or decay through ß-elimination to form RB=O. Both the formation of $R_2BOBR_2$ through $S_H2$, and the formation of RB=O through ß-elimination, generate an alkyl radical. However, only in the ß-elimination does this radical originate from the $R_2BO\cdot$ species. In the $S_H2$, the radical is expelled from the $R_3B$ species. This distinction is crucial in this experiment since the $R_3B$ is tributylborane $Bu_3B$ and $R_2BO\cdot$ is diethylboroxyl radical $Et_2BO\cdot$, therefore $S_H2$ leads to the formation of butyl radical ($Bu\cdot$) and ß-elimination leads to the formation of ethyl radical ($Et\cdot$) (Scheme 43).

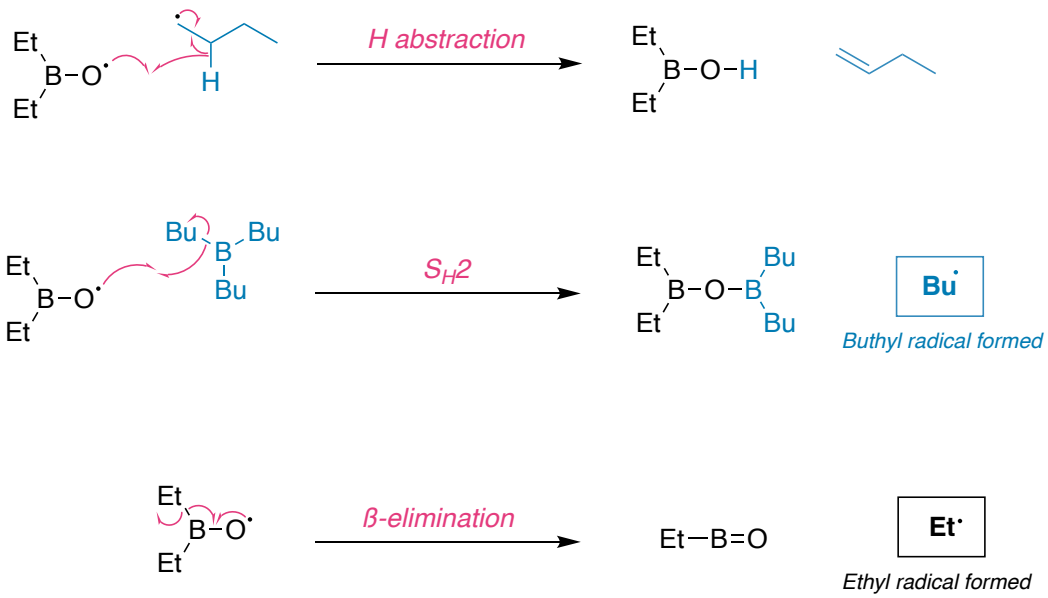


*Scheme 43. Possible reactions that radical $Et_2BO\cdot$ can undergo upon formation in the $Bu_3B/Et_2BOOEt$ reaction.*

The various outcomes of $Et_2BO\cdot$ dictate the formation of specific products and radicals. Consequently, the minimal presence of ethyl radicals detected by MS is attributed to the ß-elimination of this radical.

Additionally, it's worth noting that the formation of butene has been observed in $^{1}H$ NMR, which is a result of the H abstraction process. This observation provides further evidence of the H abstraction reaction (Experiment detailed in section 6.4.1).

### 3.4.4. Conclusions for $Et_2BOOEt$ Reaction with $Et_3B$

We have clarified the mechanism of reaction between $Et_2BOOEt$ and $Et_3B$. This section provides evidence supporting the homolytic mechanism for this reaction, as proposed by Friebolin. Although his work was done in the 1970s, the relevance of this work to the $Et_3B/O_2$ initiation has been overlooked.

Our findings indicate that the reaction products and the substantial presence of radicals are consistent with a strictly homolytic mechanism, with no notable heterolytic contribution. The rate constant for this reaction, determined experimentally, is approximately 0.2 $M^{-1}$ $s^{-1}$.

## 3.5. Kinetic Model of $Et_3B$ Initiation

The complexity of $Et_3B$ autoxidation, with its intricate network of reactions, poses challenges in visualizing and understanding the system. This complexity also hinders fidning optimal conditions and rational predictions for $Et_3B/O_2$ initiation. To overcome these challenges, we resort to kinetic modelling, leveraging our understanding of the reactions and rate constants involved. The objectives of this model are two:

1. Enhance understanding: Kinetic modelling allows us to manipulate the system, altering parameters and species, and tracking the consumption of reagents and formation of intermediates and products. This can help identifying the most important processes in this complex system, thereby guiding our future efforts in $Et_3B$ initiation.

2. Facilitate predictions: The model can simulate various reaction conditions, helping us identify conditions that optimise initiation efficiency.

### 3.5.1. Building the Model

The model is grounded in our current understanding of the $Et_3B$ initiation mechanism (Scheme 44).

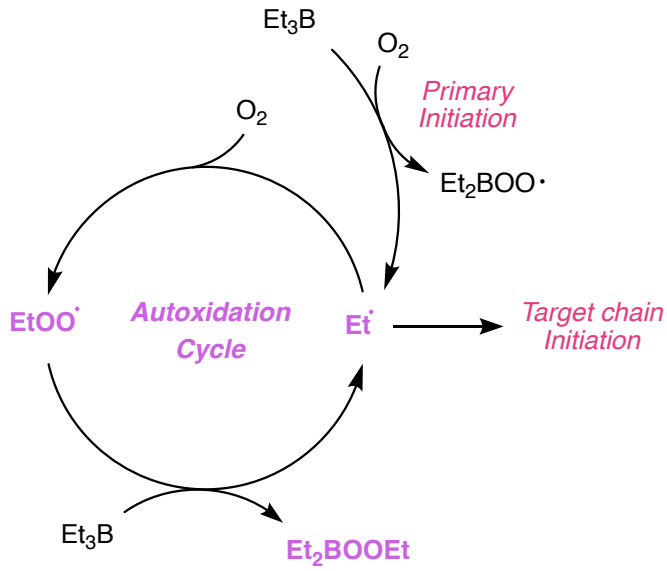


*Scheme 44. Mechanism of $Et_3B/O_2$ as it is currently understood in the literature.*

Our mechanistic investigations have revealed a secondary initiation mechanism resulting from the reaction between $Et_3B$ and the intermediate $Et_2BOOEt$, adding an extra step to the existing mechanism (Scheme 45).

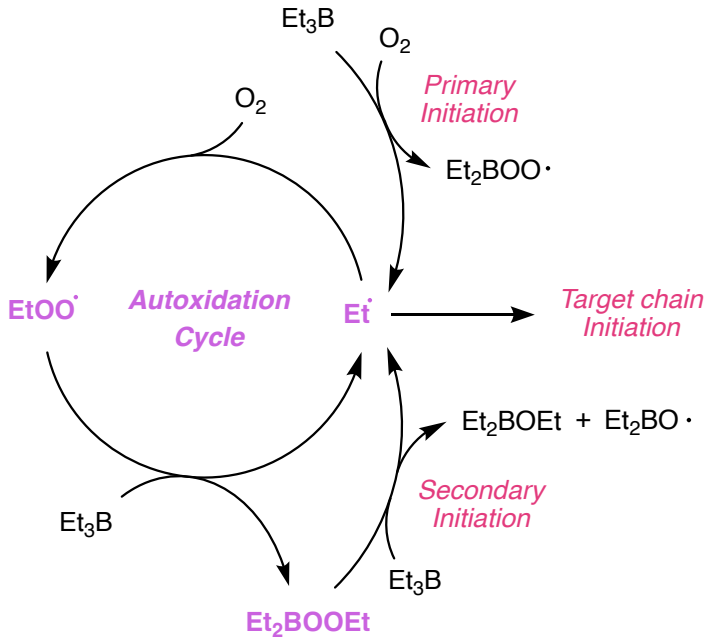


*Scheme 45. New proposal for the mechanism of $Et_3B/O_2$ initiation which includes the reaction between $Et_3B$ and $Et_2BOOEt$ as a process of secondary initiation.*

The $Et_3B/O_2$ initiating system was then simulated computationally (Table 18).

*Table 18. Reactions and rates used in the kinetic simulation of the $Et_3B/O_2$ initiation. The software used for the simulation was Kintecus 6.01. Initial species and concentrations: $Et_3B$ (50 mM), and A (1000 mM).*

| Reaction | Rate | Annotation |
|---|---|---|
| A ==> $O_2$ | $6.6 \times 10^{-6}$ | Slow diffusion of $O_2$ into the system |
| $Et_3B + O_2$ ==> $Et_2BOO\cdot + Et\cdot$ | $7.0 \times 10^{-4}$ | Primary initiation[87] |
| $Et\cdot + O_2$ ==> $EtOO\cdot$ | $2.0 \times 10^{9}$ | Autoxidation cycle of radicals formed in primary initiation[88, 90, 129] |
| $EtOO\cdot + Et_3B$ ==> $EtOOBEt_2 + Et\cdot$ | $2.0 \times 10^{6}$ | |
| $Et_2BOO\cdot + Et_3B$ ==> $Et_2BOOBEt_2 + Et\cdot$ | $2.0 \times 10^{6}$ | $S_H2$[88, 90] |
| $Et\cdot$ + Trap ==> EtTrap | $2.5 \times 10^{5}$ | Target chain initiation of radicals formed through primary initiation[130] |
| $Et_3B + EtOOBEt_2$ ==> $Et_2BOEt + Et'\cdot + Et_2BO\cdot$ | $1.9 \times 10^{-1}$ | Secondary initiation |
| $Et_2BO\cdot + Et_3B$ ==> $Et_2BOBEt_2 + Et'$ | $2.0 \times 10^{6}$ | $S_H2$[88, 90] |
| $Et'\cdot + O_2$ ==> $EtOO'\cdot$ | $2.0 \times 10^{9}$ | Autoxidation cycle of radicals formed in secondary initiation[88, 90, 129] |
| $EtOO'\cdot + Et_3B$ ==> $EtOOBEt_2 + Et'\cdot$ | $2.0 \times 10^{6}$ | |
| $Et'\cdot$ + Trap ==> Et'Trap | $2.5 \times 10^{5}$ | Target chain initiation of radicals formed through secondary initiation[130] |
| $EtOOBEt_2$ ==> $(EtO)_2BEt$ | $5.0 \times 10^{-5}$ | Peroxide rearrangement |

In the reactions outlined in Table 18, a distinction is made between ethyl radicals generated via the primary mechanism (Et) and those produced through the secondary mechanism (Et'). This distinction enables a comparison of the total number of radicals produced by the two mechanisms.

We previously questioned whether the secondary initiation mechanism would generate the majority of initiating radicals, based on the fact that the rate constant for secondary initiation ($Et_3B$+$Et_2BOOEt$) is approximately 300 times faster than the rate constant of primary initiation ($Et_3B + O_2$). This is of course dependent on the concentrations of $Et_2BOOEt$ and $O_2$, therefore

modelling the reaction allows us to work with realistic concentrations of both products. The kinetic model also allows us to plot separately the primary and the secondary initiations of the target chain (Figure 37). The model supports our hypothesis, showing over 7 x $10^4$ times more initiating ethyl radicals generated through secondary initiation compared to primary initiation.

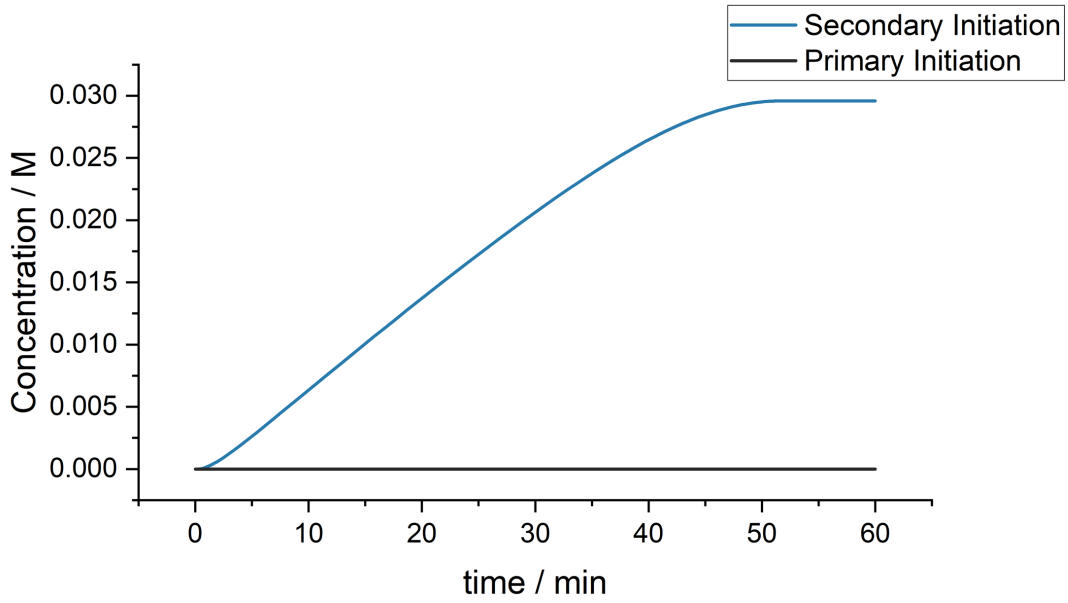


*Figure 37. Ethyl radicals generated in $Et_3B$ autoxidation via Primary initiation and Secondary initiation based on the kinetic model displayed in Table 18. Model detailed in section 6.9.1.*

### 3.5.2. Oxygen Regimes

One of the primary goals of building the model was to test different initiating conditions and predict the most efficient initiation. A key variable we can manipulate is the method of supplying $O_2$ to the system.

Synthetic chemists have employed a variety of methods to supply $O_2$ to an $Et_3B$ initiated reaction. Sometimes, ambient air in the solvent suffices to initiate reactions. Often, reactions are run open to air, or with controlled or uncontrolled admission of air. In some cases, chemists even resort to slowly blowing air over the solvent surface.[85] Despite the abundance of techniques to improve initiating conditions, most chemists use the method that works best

for them without considering the reaction mechanism, and this leads to very poor reproducibility.

When considering the mechanism, a kinetic analysis can be applied quantitatively to any chain reaction to predict whether and under what conditions $Et_3B/O_2$ will effectively initiate chains. However, the required rate constants for new radical reactions are often unknown. Moreover, in synthetic transformations, the concentration of $O_2$, a crucial variable, is usually unknown. Finally, the importance of the secondary initiation processes was not known.

A recent review study proposed a kinetic theory to simplify the process of choosing reaction conditions.[85] It was suggested that most synthetic transformations can be categorised as either strictly limited or unlimited oxygen. At these extremes, the rather complex kinetic analysis can be reduced to two limiting cases. It was suggested that most reactions that use $Et_3B$ and $O_2$ for initiation fall into either a low-oxygen regime or a high-oxygen regime.

It was concluded that in the low-oxygen regime (small amounts of $Et_3B$, ambient oxygen), $Et_3B/O_2$ can only be used to initiate long, efficient chains. In the high-oxygen regime (large amounts of $Et_3B$, air feed periodically or continuously), $Et_3B/O_2$ can be used to initiate less efficient chains, but these chains must constantly compete with autoxidation.

The end result with $Et_3B$ in the high-oxygen regime is rather wasteful of $Et_3B$. As the target chain becomes less efficient, more $Et_3B$ and $O_2$ have to be added because they are continuously consumed by autoxidation.

With the new kinetic data on the reaction mechanism, the efficiency of high and low $O_2$ regimes can be assessed quantitatively. We have modelled $Et_3B$ initiation in the two distinct oxygen regimes (Figure 38).[85]

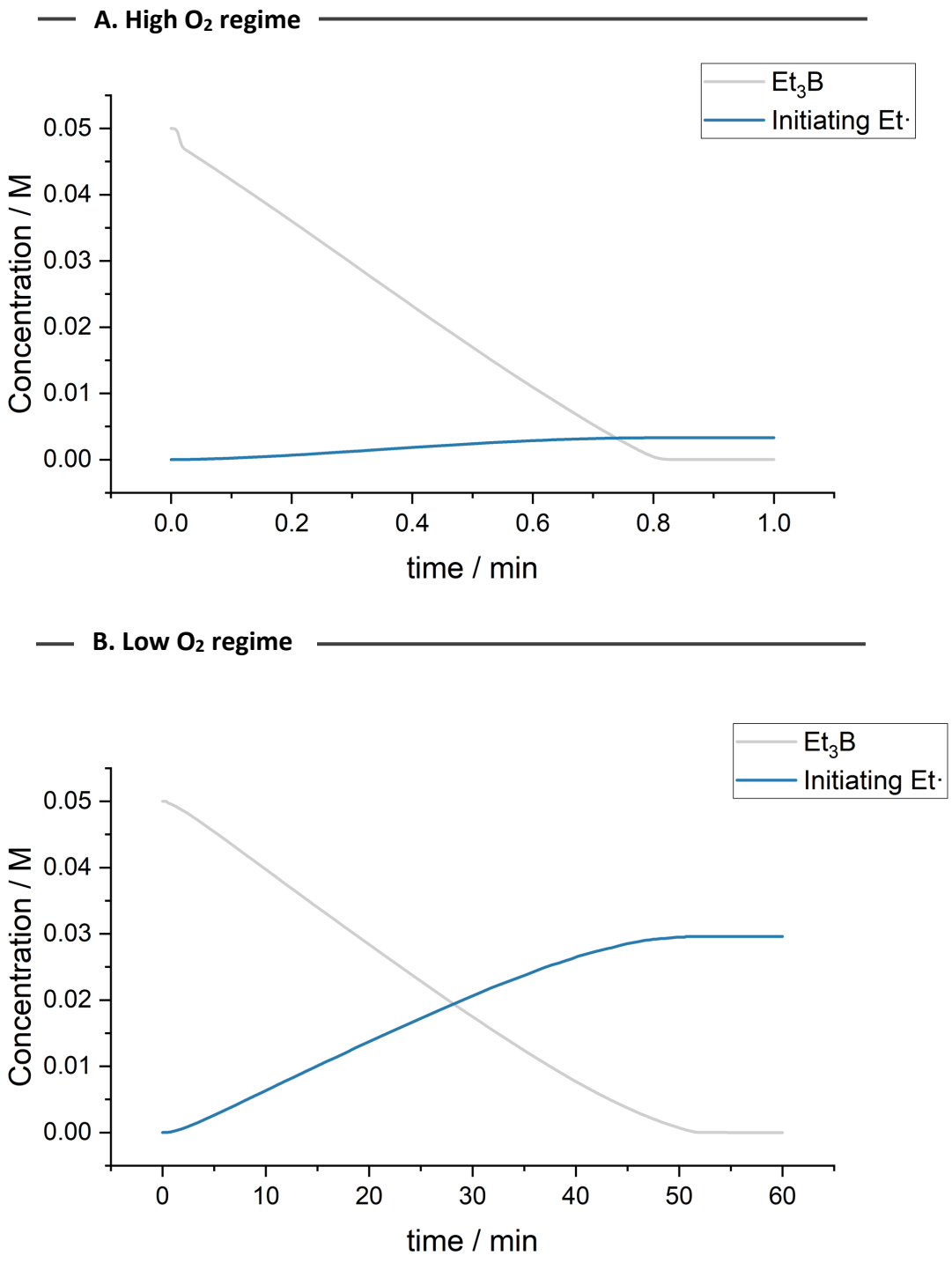


*Figure 38. Kinetic simulations of $Et_3B/O_2$ based on the kinetic model displayed in Table 18 for (A) 50 mM/min of $O_2$ provided (Model detailed in section 6.9.4) (B) 0.4 mM/min of $O_2$ provided (Model detailed in section 6.9.1).*

Our simulation revealed that the low $O_2$ regime generated tenfold initiating radicals compared to the high $O_2$ regime. This finding contradicts the prevailing belief that the high $O_2$ regime is the way to increase the flux of initiating radicals in the system. We only modelled $O_2$ being provided with a constant rate. It is possible that there are efficient initiation systems where $O_2$ is provided in a step-wise manner and slow diffusion of $O_2$ through the reaction mixture results in high initiator radical flux. Such poorly defined systems are very difficult to model and reproduce experimentally.

The poor performance of the high $O_2$ regime in our model can be attributed to overoxidation. As predicted by Curran, the propagation chain is promoted in reactions run at high $O_2$ regimes.[85] While this promotion generates more radicals due to autoxidation, the target chain must compete with the autoxidation cycle, a challenging task given the efficiency of the autoxidation process, particularly in high $O_2$ regimes.

Kinetic analysis shows that secondary mechanism is also most efficient at low concentrations of oxygen. In high $O_2$ regimes, it is possible to overoxidise $Et_3B$ to form $Et_2BOOEt$. Although this might seem beneficial as $Et_2BOOEt$ is a component of the secondary initiation mechanism, excessive formation could deplete all $Et_3B$, leaving none for the secondary initiation mechanism. This is precisely what occurs in the high $O_2$ regime simulation (Figure 39).

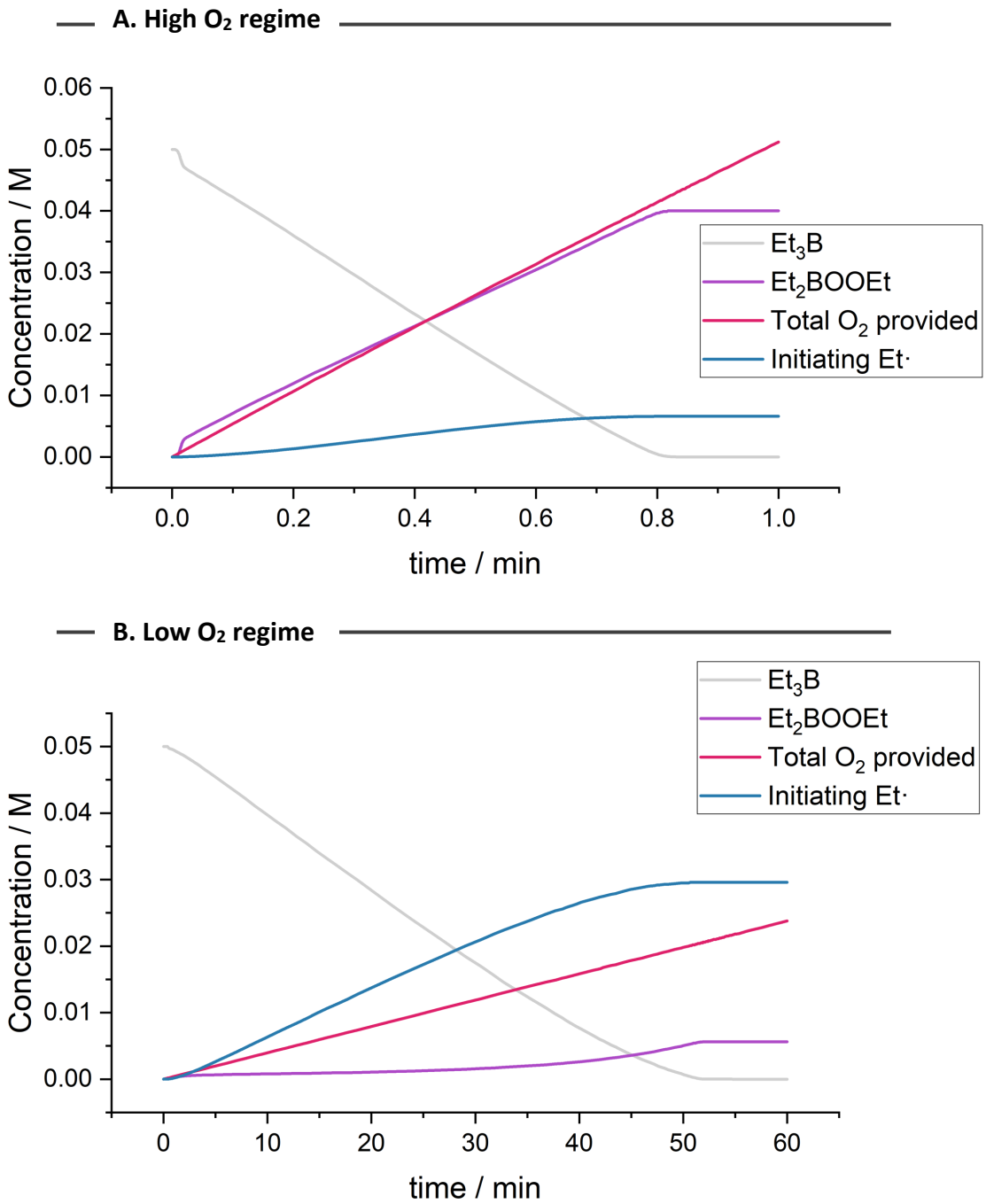


*Figure 39. Kinetic simulations of $Et_3B/O_2$ based on the kinetic model displayed in Table 18 for (A) 50 mM/min of $O_2$ provided (Model detailed in section 6.9.4). (B) 0.4 mM/min of $O_2$ provided (Model detailed in section 6.9.1). The figure shows the same simulation as the above Figure 38 with additional species displayed.*

In contrast, a lower rate of $O_2$ supply to the system resulted in an increased total number of initiating ethyl radicals. Under low $O_2$ regimes, the autoxidation cycle is moderated, allowing $Et_3B$ to react with $Et_2BOOEt$ as it forms slowly, thereby creating favourable conditions for enhancing secondary initiation.

Time is another critical factor. In high $O_2$ regimes, radicals are produced in a shorter time due to enhanced autoxidation, leading to a high radical concentration. This high concentration increases both the initiation and termination rates, rendering the system less efficient at producing the initiating radicals. Conversely, in low $O_2$ regimes, radicals are generated over a longer period, resulting in a lower radical concentration at any given time but a higher total number of radicals produced by the initiator.

The mechanistic differences between high and low $O_2$ regimes are visualized in Scheme 46. The schemes are an oversimplification of the model outcome. Real systems are much more complex as the reactions are heterogeneous probably forming a gradient of $O_2$ concentrations in the solution, with $O_2$ diffusion dominating the kinetics. It is therefore very difficult to model (and reproduce) such systems, and it is possible that some configurations of high $O_2$ regime could lead to efficient initiation.

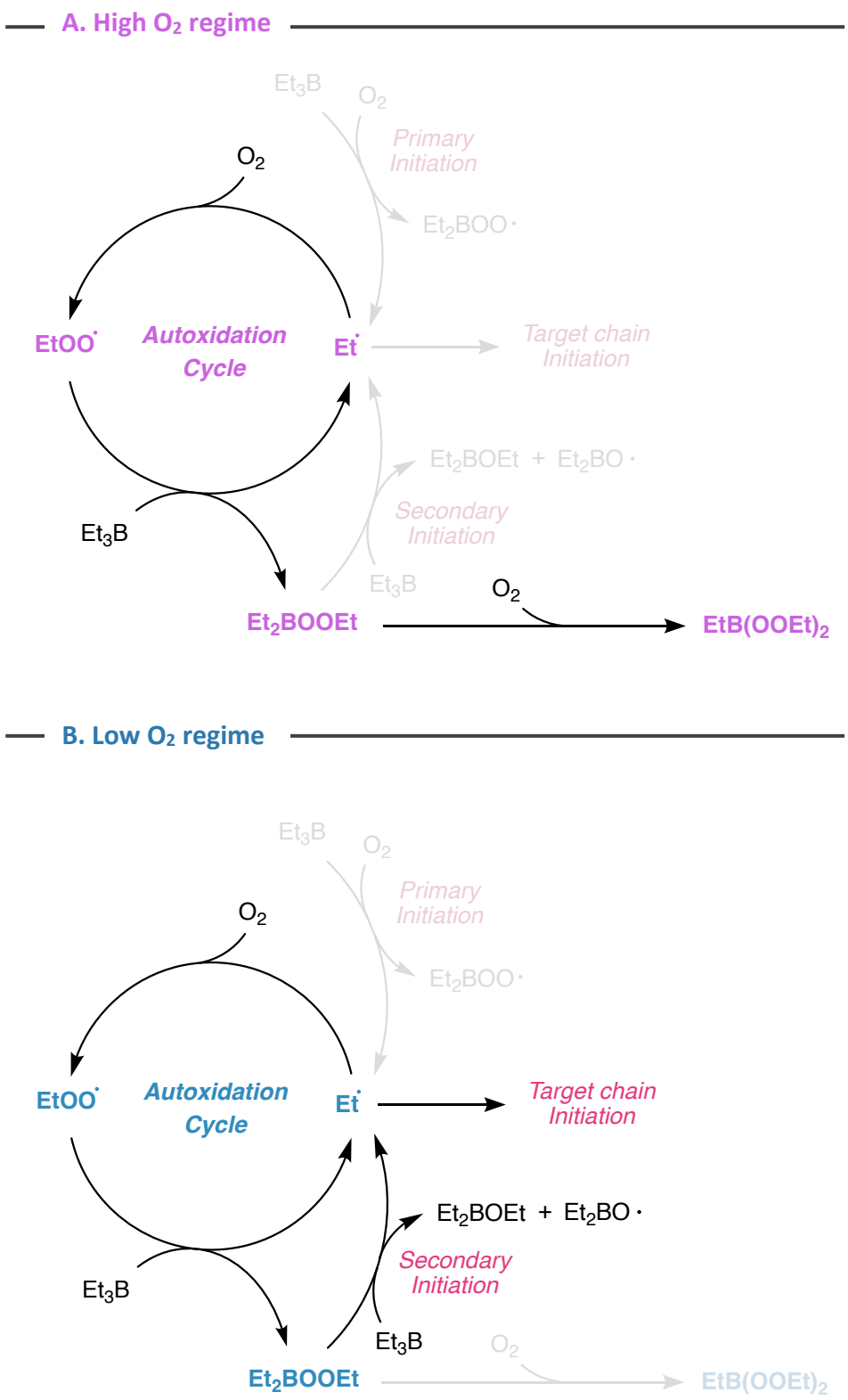


*Scheme 46. Main reactions involved in the mechanism of $Et_3B$ autoxidation depending on $O_2$ regime.*

The superior performance of the low $O_2$ regime over the high $O_2$ regime can be attributed to its promotion of efficient secondary initiation, as opposed to the autoxidation promoted in the high $O_2$ regime. This raises an intriguing question: would it be more beneficial to employ secondary initiation directly as a radical initiator?

Simulations of the initiation by $Et_3B/Et_2BOOEt$ in an $O_2$-free environment revealed that secondary initiation alone could generate approximately 1.6 times more initiating ethyl radicals than the low $O_2$ regime (Figure 40).

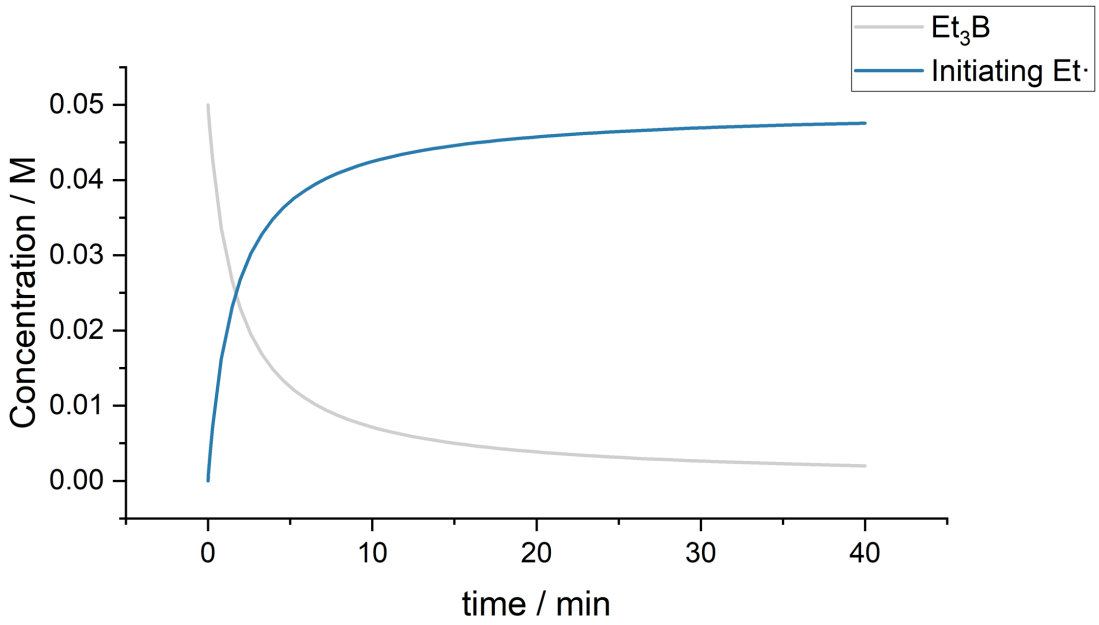


*Figure 40. Kinetic simulation of the radicals produced by $Et_3B/Et_2BOOEt/N_2$ based on the kinetic model displayed in Table 18. Model detailed in section 6.9.5.*

Figure 41 presents a comparison of the three different systems ($Et_3B$/High $O_2$, $Et_3B$/Low $O_2$, and $Et_3B/Et_2BOOEt/N_2$) in terms of the number of initiating radicals produced.

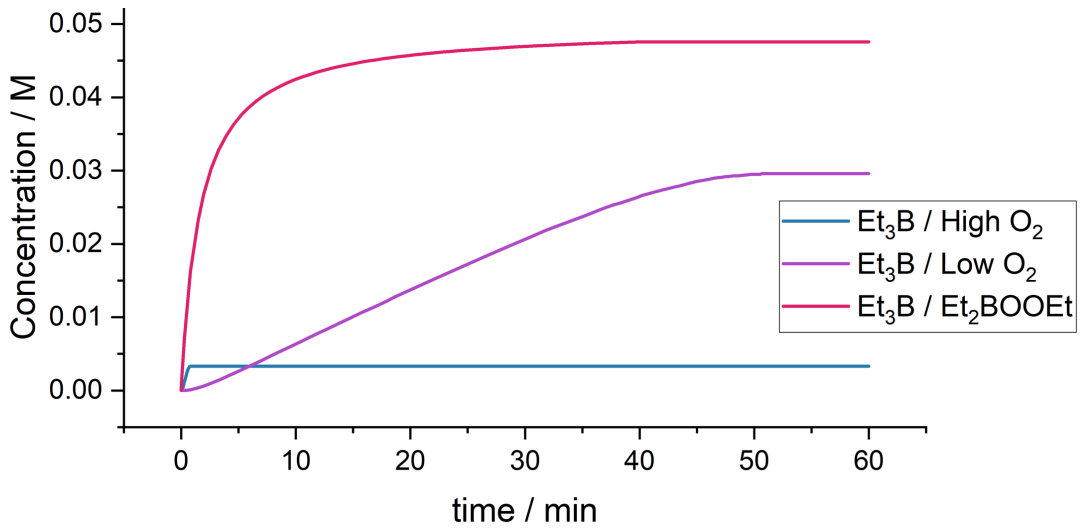


*Figure 41. Kinetic simulation of the radicals produced by $Et_3B$/High $O_2$ (Model in section 6.9.4), $Et_3B$/Low $O_2$ (Model in section 6.9.1), and $Et_3B/Et_2BOOEt/N_2$ (Model in section 6.9.5) based on the kinetic model displayed in Table 18.*

The model predicts that the $Et_3B$/High $O_2$ system would perform the worst, with the $Et_3B$/Low $O_2$ system producing 10 times more initiating radicals. The $Et_3B/Et_2BOOEt/N_2$ system is predicted to be the most effective, generating 16 times more initiating radicals than the $Et_3B$/High $O_2$ system and 1.6 times more than the $Et_3B$/Low $O_2$ system. In addition, it is a homogeneous reaction therefore it is easy to reproduce and control. A notable disadvantage is that it $Et_3B/Et_2BOOEt$ is a 2nd order reaction, which leads to an uneven radical generation.

### 3.5.3. Model Validation; Radical Trapping

The model, which is based on the novel understanding of $Et_3B$ autoxidation developed in this thesis, requires validation. This validation, which will provide evidence supporting the theory and overall understanding of $Et_3B$ initiation, can be achieved using our newly developed method of radical trapping.

In section 3.4.3 we introduced a method for quantifying the radicals produced by secondary initiation using allyl TEMPO radical traps and NMR spectroscopy. A similar approach can be employed to experimentally compare the radical flux produced by the $Et_3B$/High $O_2$, $Et_3B$/Low

$O_2$, and $Et_3B/Et_2BOOEt/N_2$ systems. The radicals generated by these three systems were trapped and measured using NMR (Figure 42).

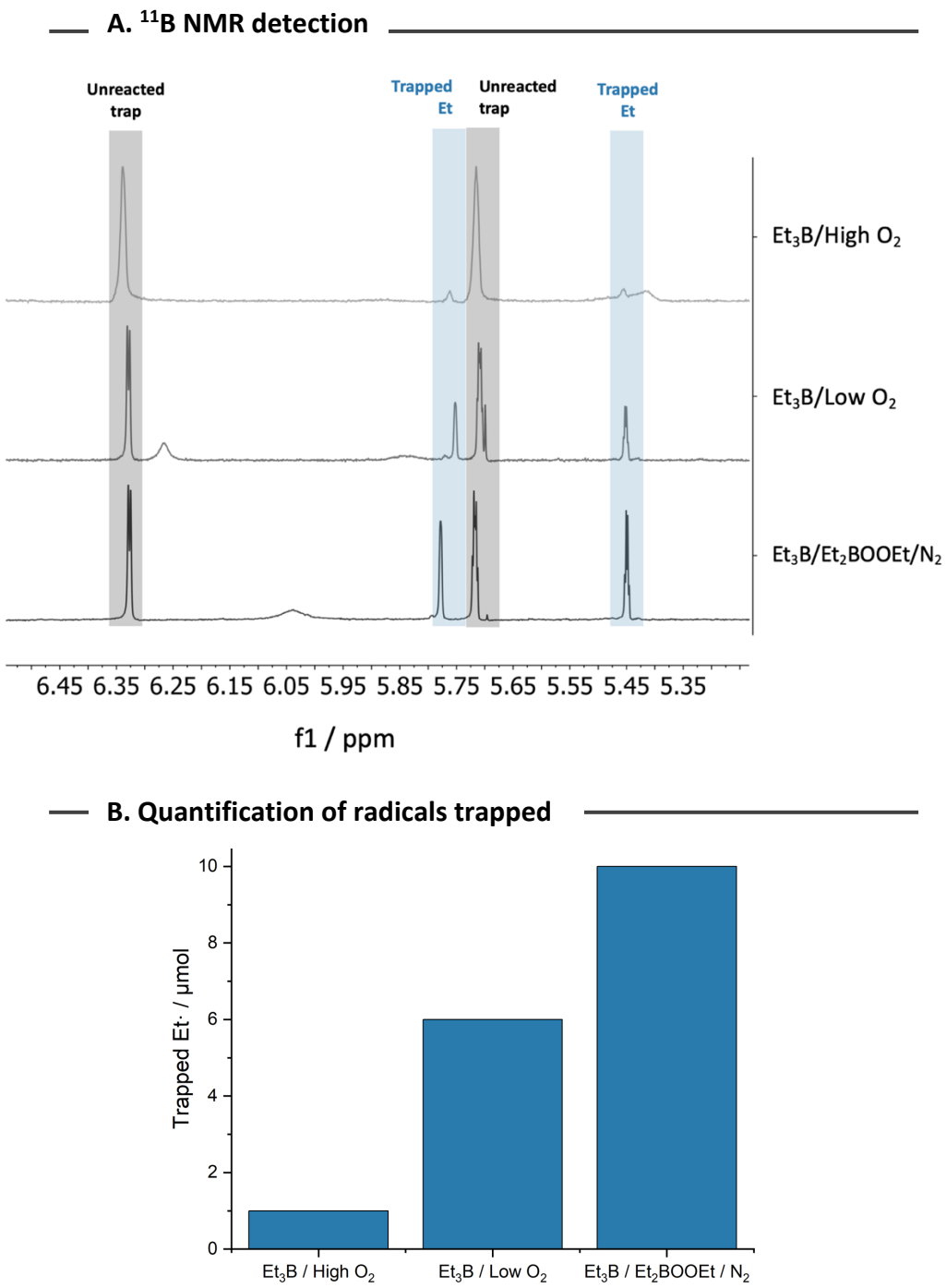


*Figure 42. Radicals trapped in three different initiating systems $Et_3B$/High $O_2$ (Experiment detailed in section 6.3.10), $Et_3B$/Low $O_2$ (Experiment detailed in section 6.3.11), and $Et_3B/Et_2BOOEt/N_2$ (Experiment detailed in section 6.3.8). Here trapped Et refers to the sum of TEMPO and CHANT trapped radicals.*

The experimental data aligns with our predictions. The high $O_2$ regime performed the worst, trapping only 1 µmol of ethyl radicals. This was followed by the low $O_2$ regime, which trapped 6 µmol of ethyl radicals. As anticipated, the direct use of secondary initiation resulted in the highest number of trapped radicals, with 10 µmol of ethyl radicals trapped.

Interestingly, when the low $O_2$ regime was monitored over time by NMR, we observed the initial accumulation of $Et_2BOOEt$ followed by steady state and the decrease due to reaction with $Et_3B$, which aligns with the predicted behaviour for this species (Figure 43).

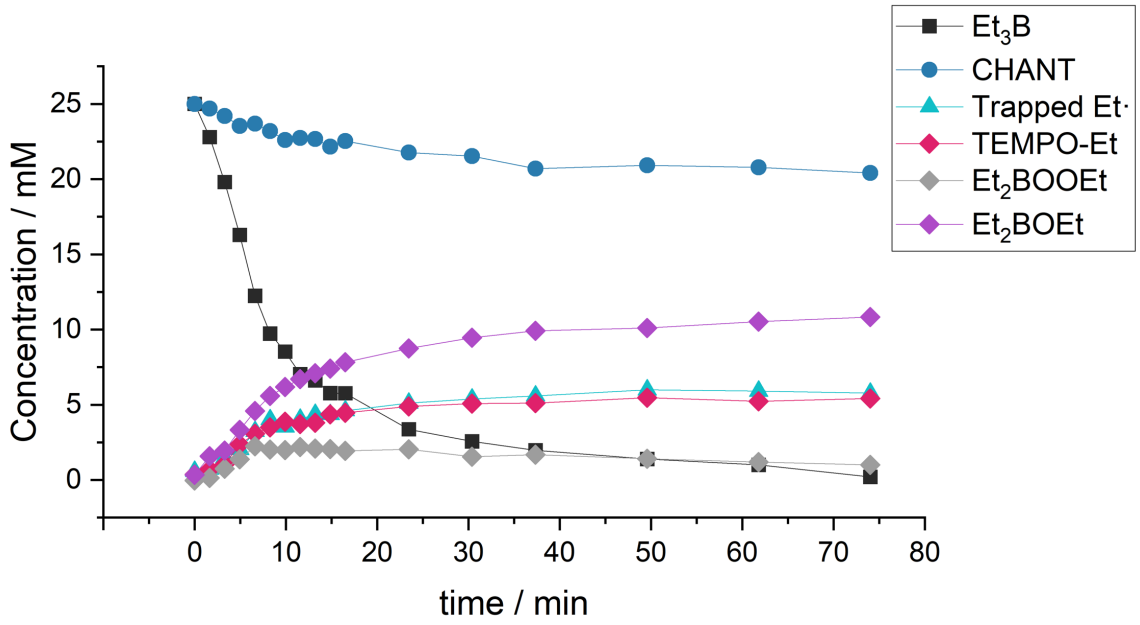


*Figure 43. Kinetic profile the autoxidation of $Et_3B$ under conditions of low $O_2$ regime. The reaction was run at 25 °C, and was followed by $^{11}B$ and $^{1}H$ NMR using the initial concentration as reference. Measurements were taken at the indicated timestamps. Experiment detailed in section 6.3.11.*

At the end of the reaction, we observed the formation of 0.5 eq. of $Et_2BOEt$. Given our understanding of this reaction, $Et_2BOEt$ only forms in the reaction between $Et_3B$ and $Et_2BOOEt$. If this is indeed the case, the formation of exactly 0.5 eq. of this product indicates that 0.5 eq. of $Et_3B$ has been converted into 0.5 eq. of $Et_2BOOEt$ through autoxidation, and the resulting peroxide has reacted 1:1 with the remaining 0.5 eq. of $Et_3B$. This process occurs progressively

as the $Et_3B$ oxidises. The key to success here is to ensure a sufficiently slow oxidation rate to allow the formed $Et_2BOOEt$ to react with $Et_3B$.

### 3.5.4. Conclusions for Kinetic Model

The kinetic modelling of $Et_3B$ initiation has deepened our understanding of the underlying processes. Our findings indicate that secondary initiation is the primary source of radicals in this system, which has informed our predictions about the optimal conditions for $Et_3B$ initiation.

Our reasoning suggests that if the majority of radicals originate from the secondary mechanism, optimal initiation conditions should favour secondary initiation over autooxidation to enhance the initiating power of $Et_3B$. Our model and experimental data both support the superiority of the low $O_2$ regime in promoting secondary initiation compared to the high $O_2$ regime.

These findings challenge the prevailing belief that the low $O_2$ regime is necessary for initiating efficient chains that do not require of a powerful initiator, and that the high $O_2$ regime is a brute force method for generating a high flux of radicals required for inefficient chains. We cannot rule out efficient initiation with high $O_2$ regime using different methods such as stepwise addition of $O_2$ or establishment of $O_2$ gradient in the reaction mixture, however, these conditions would be hard to reproduce in a heterogeneous system.

Furthermore, we propose that if the secondary mechanism is the driving force behind $Et_3B$ initiation, it could be directly employed for anaerobic initiation. Our model predicts that direct use of the secondary initiation mechanism ($Et_3B/Et_2BOOEt/N_2$) would result in the production of more initiating ethyl radicals, specifically 1.6 times more than the low $O_2$ regime. This prediction was confirmed experimentally, with 1.7 times more radicals trapped in secondary initiation compared to the $Et_3B$/low $O_2$ regime. This insight provides us with a new tool for future investigations, enabling us to directly use $Et_3B/Et_2BOOEt/N_2$ to initiate challenging chains.

Additionally, the direct use of $Et_3B/Et_2BOOEt/N_2$ would provide a homogeneous method for $Et_3B$ initiation which would make the initiation more reproducible. A potential disadvantage to this initiation is the second order nature of the reaction which leads to an uneven formation of radicals.

### 3.6. Conclusions Chapter 3

There has not been a clear understanding of the role of secondary initiation in $Et_3B/O_2$ initiation. The primary initiation reaction generates new radicals, but it is slow, and the propagation chain, despite its efficiency, does not yield new radicals, necessitating the existence of a secondary initiation process. Our findings suggest that the homolysis of $Et_2BOOEt$ is not an efficient radical generator. Our research indicates that the decomposition of $Et_2BOOEt$ primarily occurs via a heterolytic rearrangement, with only a minor component of peroxide homolysis.

Our study did uncover a secondary initiation process within $Et_3B$ autoxidation. We observed that the reaction between $Et_3B$ and $Et_2BOOEt$ generates ethyl radicals. This process proved to be both rapid and highly efficient in producing radicals, leading us to propose a mechanism for this reaction that involves molecule-assisted homolysis.

Incorporating these findings into a kinetic model enabled us to gain a deeper understanding of the overall initiation mechanism. Our model revealed that the majority of radicals in $Et_3B/O_2$ initiation are produced by this secondary mechanism.

The model also facilitated a comparison of system behaviour under varying $O_2$ conditions. Our findings suggest that lower $O_2$ regimes are more efficient at the production of initiating radicals compared to high $O_2$ conditions. Furthermore, we found evidence to suggest that the direct implementation of the secondary mechanism as a radical initiator in the absence of $O_2$ could yield improved results.

The next chapter will put the theory of radical initiation to the test, as we apply the insights gained in this chapter to initiate synthetic reactions.

# 4. Applying Mechanistic Insights to Triethylborane Initiation

## 4.1. Introduction

### 4.1.1. $Et_3B/O_2$ as a Radical Initiator

The $Et_3B/O_2$ system has been used as a radical initiator for over 35 years, since the first time it was used by Utimoto and Oshima.[82, 131] The system quickly emerged as a highly efficient and versatile initiator. One of the most notable features of this system is its ability to function efficiently at temperatures as low as −78 °C. This low-temperature capability is particularly beneficial for stereoselective radical reactions and for reactions involving thermally unstable intermediates or products.[83]

The ethyl radicals generated by the system can then abstract halogen atoms from various substrates, initiating a chain reaction. The mild conditions under which this system operates make it an attractive alternative to traditional thermal initiators, which often require higher temperatures and can lead to unwanted side reactions.

### 4.1.2. Applications in Organic Synthesis

The utility of $Et_3B/O_2$ as a radical initiator has been demonstrated in numerous organic transformations, here we will show some selected recent examples. $Et_3B/O_2$ has been effectively employed in the hydrostannylation of alkynes, a reaction that traditionally requires thermal initiation.[82] The $Et_3B/O_2$ system allows this reaction to proceed at room temperature or below, providing high yields and selectivity (Table 19). This method has been successfully applied to the synthesis of complex molecules such as dehydroiridodiol and α-methylene-γ-butyrolactone.

*Table 19. $Et_3B$ initiated hydrostannylation of alkynes.*[82]

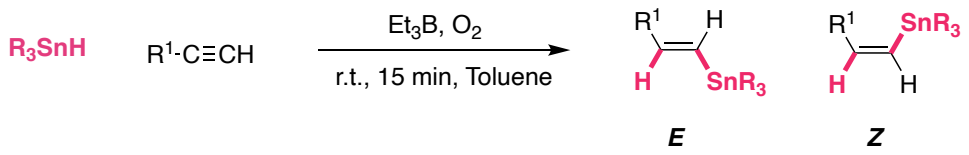


| $R^1$ | Yield | **E/Z** |
|---|---|---|
| Ph | 75% | 100/0 |
| $Me_3Si$ | 83% | 100/0 |
| $HOCH_2CH_2$ | 87% | 82/18 |
| $^nC_{10}H_{21}$ | 80% | 79/21 |

Another significant application of $Et_3B/O_2$ is in the radical cyclisation of alkenyl sulfoxides (Scheme 47).[132] This reaction, which avoids the formation of conjugated dienes by thermal elimination of sulfinic acid, proceeds smoothly under the mild conditions offered by the $Et_3B/O_2$ system. Similarly, the radical cyclisation of anomeric selenides to synthesize 2-amino-2-deoxy-α-D-C-glucopyranoside has been achieved with high efficiency using this initiator (Scheme 48).[133]

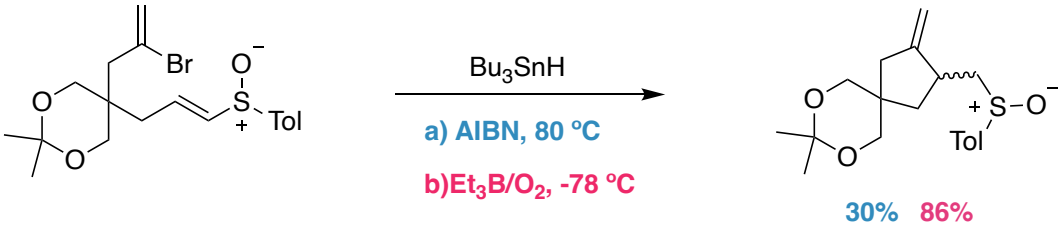


*Scheme 47. $Et_3B/O_2$ initiated radical cyclisation of alkenyl sulfoxides.*

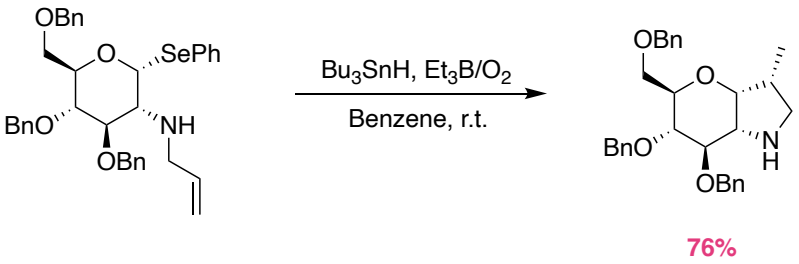


*Scheme 48. Synthesis of 2-amino-2-deoxy-R-D-C-glucopyranoside by radical cyclisation of an anomeric selenide initiated by $Et_3B/O_2$*

$Et_3B/O_2$ has also been utilised in the reduction of alkyl and alkenyl halides. For example, the reduction of alkyl iodides and bromides by $Bu_3SnH$ in the presence of a catalytic amount of $Et_3B$ at low temperatures has been shown to proceed with high efficiency (Scheme 49).[134] This method has been extended to the reduction of alkenyl and aryl halides, further demonstrating the versatility of the $Et_3B/O_2$ system.

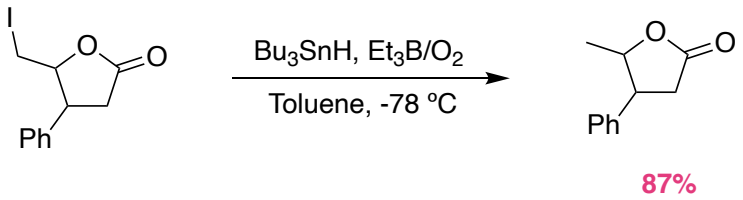


*Scheme 49. Reduction of alkyl halides by $Bu_3SnH/Et_3B/O_2$.*

### 4.1.3. Atom-Transfer Reactions

$Et_3B/O_2$ also excels in atom-transfer reactions, particularly iodine atom transfers. The ethyl radicals generated by $Et_3B/O_2$ can abstract iodine atoms from alkyl iodides, initiating a chain process that leads to the formation of various radical intermediates.[135, 136] This mechanism has been utilised in the addition of perfluoroalkyl iodides,[137] α-iodoesters (Scheme 50),[138] and simple alkyl iodides[131] to alkenes and alkynes, even in aqueous media (Scheme 51).[139]

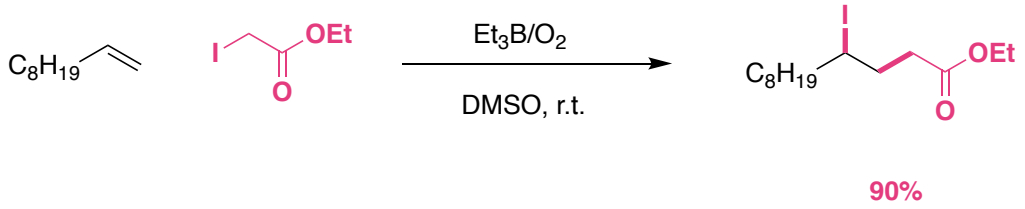


*Scheme 50. Atom transfer radical addition of α-iodoesters to alkene.*

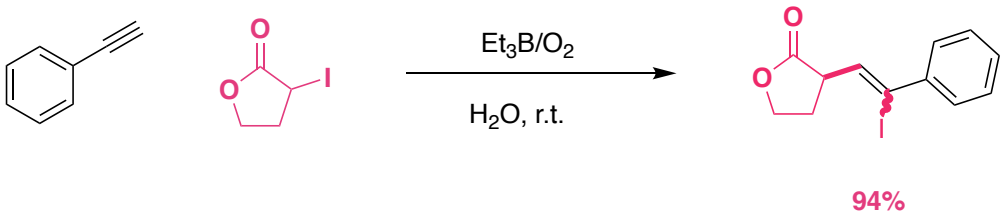


*Scheme 51. Atom transfer radical addition of α-iodoesters to alkyne in $H_2O$.*

The ability of $Et_3B/O_2$ to initiate radical reactions in aqueous media is particularly noteworthy, as it opens up new possibilities for conducting radical reactions under environmentally benign conditions. This feature has been used in the synthesis of various complex molecules, including dioxatriquinanes and tricyclic gluconjugates, through elegant cascade cyclisations.

This system is also suitable for tandem atom transfer reactions under mild conditions (Scheme 52).[139]

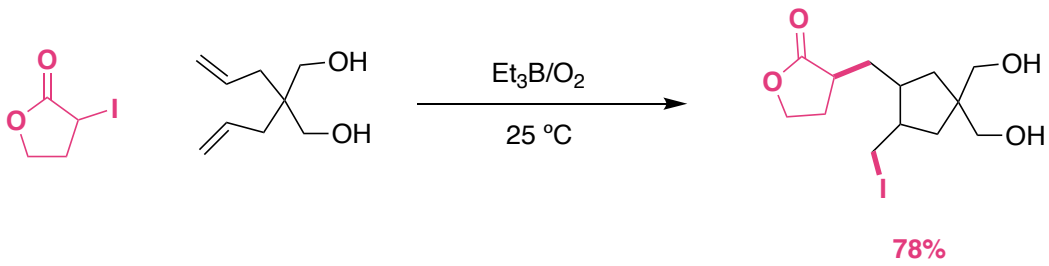


*Scheme 52. Tandem atom transfer radical addition of α-iodoesters to alkenes.*

### 4.1.4. Issues with $Et_3B/O_2$ Initiation

Despite its success, $Et_3B$ does not always lead to successful initiations. Often, substantial amounts of $Et_3B$ and $O_2$ are required to sustain the reaction.[85] This is associated with the efficiency of the target chain; inefficient chains struggle to compete with the highly efficient autoxidation cycle of $Et_3B$.

A radical chain is typically inefficient due to the presence of a slow propagation step. This inefficiency has two primary consequences:

1. The slow step becomes the rate-determining step, meaning the overall reaction rate is limited by this step. Consequently, if the step is slow, the reaction will take a prolonged time to convert reagents into products.

2. The slow step leads to the accumulation of the intermediate preceding it. In a radical chain, this intermediate is usually a radical, resulting in an accumulation of radicals. This accumulation is problematic as it increases the rate of terminations and side reactions.

The optimal approach to initiating these radical chains involves a slow and continuous supply of initiating radicals over an extended period:

1. A slow and continuous initiation aligns with the slow pace of the radical chain, providing the necessary initiating radicals throughout the duration of the transformation.

2. Slow initiation maintains a low flux of radicals, thereby minimizing the rate of termination.

Unfortunately, $Et_3B$ reacts quickly with $O_2$, generating a strong radical flux that rapidly diminishes once all the $O_2$ or $Et_3B$ is consumed. This rapid reaction makes $Et_3B$ challenging to use for initiating less efficient chains.

Synthetic chemists often address this challenge by continuously supplying more $Et_3B$ and O2, ensuring continuous initiation throughout the duration of the reaction.[85] However, this approach does not resolve the termination issue, as having more initiator will only increase the rate of termination. This is why $Et_3B$ has generally not been a very successful initiator for these types of chains.

The primary issue with $Et_3B$ is the inefficiency of autoxidation in terms of radical production. As previously discussed (section 2.1), the autoxidation of triethylborane is a double-edged sword for generating radicals. On one hand, it extends the life of initiating ethyl radicals by cycling them in the chain and accumulates peroxides that can become radical initiators. On the other hand, the chain rapidly consumes $Et_3B$ and $O_2$ without generating new radicals.

For inefficient chains, many chemists employ a high $O_2$ regime to maintain a continuous radical supply. However, this approach promotes the autoxidation chain, often leading to inefficient consumption of $Et_3B$ and $O_2$. A low $O_2$ regime offers more optimal initiation conditions but often results in quick $O_2$ consumption, stopping initiation. Ideally, a low concentration of $O_2$ would be continuously supplied slowly into the reaction, but this complicates experimental setup and reproducibility.

Given this paradigm, we explored the possibility of directly using the secondary initiation mechanism ($Et_3B$ + $Et_2BOOEt$) as a radical initiator. This approach could offer several advantages over traditional $Et_3B$ initiation:

1. Autoxidation would no longer occur under $O_2$-free conditions, circumventing issues associated with inefficient and rapid consumption of initiator.

2. $O_2$ would no longer be needed, allowing for better control of initiator concentration, thus improving reproducibility. Additionally, $O_2$-free initiation would benefit $O_2$-sensitive reagents or intermediates.

These improvements would be compatible with the low-temperature initiation characteristic of $Et_3B$, thereby enhancing the effectiveness of the initiator.

## 4.2. Chapter 4 Aims

1. Implement secondary initiation ($Et_3B$ + $Et_2BOOEt$) to initiate radical chains.
2. Compare traditional $Et_3B/O_2$ initiation with $Et_3B/Et_2BOOEt$.
3. Use the experimental data to corroborate the kinetic model built in the previous chapter.

### 4.3. Atom Transfer Radical Addition of Alkyl Iodides to Acetylenes

Following the mechanistic investigations and development of an improved initiation method, we proceeded to test the new method in synthetic applications. Specifically, we initiated radical reactions to evaluate the performance of the new system in terms of scope and yields. The first experiment involved the atom transfer radical addition (ATRA) of alkyl iodides to alkynes (Scheme 53).

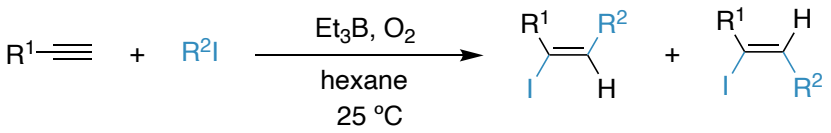


*Scheme 53. $Et_3B$ initiated addition of alkyl iodides to alkynes.*

This reaction served as a suitable initial candidate for several reasons:

1. The reaction is well-documented and has been extensively studied using $Et_3B/O_2$ as an initiator[3, 131, 135, 140, 141]. This provides a solid foundation, minimizing the need for extensive optimisation or troubleshooting.

2. The yields reported in previous studies are high[131], indicating that the reaction is reliable and can be easily reproduced, providing a good starting point to evaluate the new initiator.

3. The reaction is straightforward, requiring only two starting materials in addition to the initiator. Both reagents are commercially available, eliminating the need to synthesize precursors.

The mechanism follows the generally accepted pathway for most atom transfer additions (Scheme 54). $Et_3B$ + $O_2$ generates ethyl radicals, which abstract an iodine atom form alkyl

iodide in the initiating step. The alkyl radical generated in the initiation adds to the acetylene followed by atom transfer, constituting the two steps of the chain propagation.

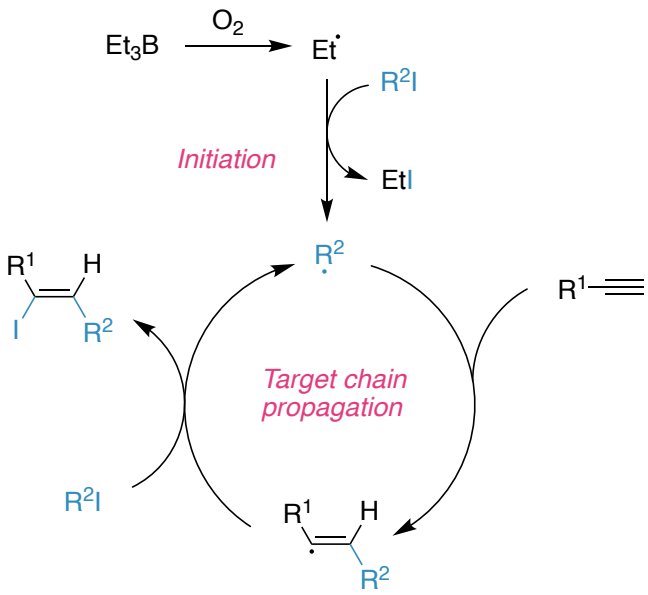


*Scheme 54. General mechanism for $Et_3B/O_2$ initiated atom transfer addition of alkyl iodides to alkynes.*

### 4.3.1. Atom Transfer Radical Addition of Ethyl Iodide to TMS Acetylene

In our initial experiments, we tested the ability of our system to initiate the addition of ethyl iodide (EtI) to trimethylsilylacetylene (TMS acetylene). We employed the same conditions as those reported in existing literature,[131] with the modification of substituting $Et_3B/O_2$ for $Et_3B/Et_2BOOEt/N_2$.

NMR analysis of the completed reaction indicated a 27% yield (Table 20, entry 1). This preliminary result was promising, suggesting that our system was capable of initiating the reaction under $N_2$. Recognising the potential for yield improvement, we proceeded to optimise the reaction.

*Table 20. Optimisation of $Et_3B/Et_2BOOEt$ initiated ATRA of EtI to TMS acetylene under $N_2$. Experiment detailed in section 6.7.1.*

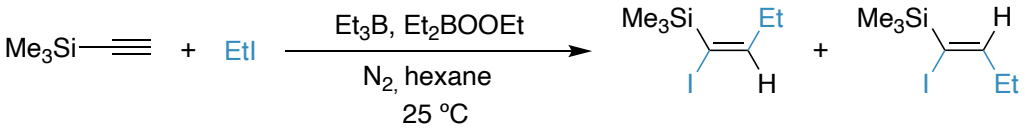


| Entry | TMS acetylene (µmol) | EtI (µmol) | $Et_3B$ (µmol) | $Et_2BOOEt$ (µmol) | T | Yield[a] (%) | E/Z |
|---|---|---|---|---|---|---|---|
| 1 | 250 | 50 | 25 | 25 | rt | 27 | 0/100 |
| 2 | 300 | 250 | 25 | 25 | rt | 11 | 0/100 |
| 3 | 300 | 250 | 50 | 50 | rt | 14 | 0/100 |
| 4 | 300 | 250 | 25 | 25 | 0 °C | 1 | 0/100 |
| 5 | 125 | 12.5 | 25 | 25 | rt | 47 | 0/100 |
| 6 | 62.5 | 12.5 | 25 | 25 | rt | 28 | 0/100 |
| 7 | 250 | 50 | 50 | 50 | rt | **96**[b,c] | 0/100 |

*[a] Yields calculated by $^1H$ NMR using EtI as reference. [b] Yield calculated by $^1H$ NMR using 1,2-dichloroethane as internal standard. [c] Initiator $Et_3B/Et_2BOOEt$ was delivered at the beginning of reaction as a 25 µmol /25 µmol batch and a second batch of 25 µmol /25 µmol was delivered after 1h.*

Despite these variations in reaction conditions, the formation of the E isomer was not observed. This is consistent with literature reports of the same reaction initiated by $Et_3B/O_2$[131].

Initially, we found that an increase in the concentration of the starting materials led to a decrease in yield (entry 2). The reaction did not achieve complete conversion, suggesting that an increase in the concentration of initiator might further drive the unreacted reagents towards the formation of products. Indeed, a higher concentration of initiator led to an increase of conversion and yield (entry 3). However, the reaction remained far from completion at 1 eq. of initiator, so a different approach was attempted.

Lowering the reaction temperature would slow down the rate of initiation. This would in turn result in a lower concentration of radicals that is favourable for promoting chain initiation over radical termination[142]. Contrary to our expectations, this modification led to a significant decrease in yield (entry 4). This is likely the result of the decrease in temperature also affecting the rates of the reactions involved in the target chain.

Interestingly, a decrease in the concentration of starting materials resulted in a substantial increase in yield (entry 5). However, further reduction in the concentration of TMS acetylene began to decrease the yield (entry 6). In a final set of experiments, we returned to the original concentrations and introduced a second batch of initiator. This adjustment resulted in a remarkable increase in yield, reaching an impressive 96%.

A noteworthy observation was the substantial increase in yield from 27% to 96% upon doubling the initiator concentration in entry 7. This contrasted sharply with the results from entries 2 to 3, where a similar doubling resulted in a marginal yield increase from 11% to 14%. A critical difference was that in entry 7, the initiator was added in two separate aliquots, whereas in entry 3, it was introduced in a single batch. This raises the question: why does distributing the initiator over multiple additions enhance the reaction yield compared to a single, initial addition?

A notable characteristic of this initiator is its second order kinetics, which distinguishes it from many other radical initiators. This characteristic has significant implications for the implementation and optimisation of initiation. Bimolecular kinetics follow a hyperbolic plot, as shown in section 3.4.2. This implies that the reaction rate will be highest at the start and decrease as the reaction progresses. The same is true for unimolecular reactions, however the dependence on the concentration is stronger for the 2nd order reactions. In the context of radical initiation, the initiator generates radicals, leading to a high initial radical flux that decreases rapidly with the consumption of $Et_3B$ and $Et_2BOOEt$. Although doubling the initiator quantity theoretically doubles the radical count, this does not translate to improved yields. High radical flux can decrease the yield due to an increased rate of termination[142].

By providing the initiator in two separate batches, the radical concentration is lowered while maintaining the overall number of initiating radicals. This strategy accounts for the observed yield improvement when the initiator is delivered in divided batches.

The successful initiation of a reaction solely through secondary initiation under $N_2$ underscores the efficacy of this method. In the previous chapter we proposed that secondary initiation can provide a higher amount of radicals per mole of initiator compared to classic $Et_3B/O_2$ methods. To prove this claim, we tested it experimentally.

ATRA of ethyl iodide to TMS acetylene was initiated using $Et_3B/O_2$ in high $O_2$ regime and in low $O_2$ regime. The results are displayed in Table 21 and compared to the initiation using secondary mechanism $Et_2BOOEt/Et_3B/N_2$.

*Table 21. ATRA of ethyl iodide to TMS acetylene under different conditions of $Et_3B$ initiation. Experiment detailed in section 6.7.2.*


| Entry | Initiator | Atmosphere | Yield (%) [a] | E/Z |
|---|---|---|---|---|
| 1 | $Et_3B$ | High $O_2$ [b] | 0 | 0/100 |
| 2 | $Et_3B$ | Low $O_2$ [c] | 28 | 0/100 |
| 3 | $Et_3B+Et_2BOOEt$ | $N_2$ | 96 | 0/100 |

*[a] Yields calculated by $^1H$ NMR using 1,2-dichloroethane as internal standard. [b] Reaction was carried out open to air with unrestricted $O_2$ (See experimental section 6.7.2. for more details). [c] Reaction was carried out with restricted $O_2$ (See experimental section 6.7.2. for more details).*

With a yield of 96%, initiator $Et_3B/Et_2BOOEt$ under $N_2$ performed markedly better than low $O_2$ regime which gave a yield of only 28%. This regime, in turn, outperformed the high $O_2$ regime, which failed to show any measurable initiation. These findings align with the predictions of

the kinetic model discussed in section 3.5, giving further evidence to the theoretical framework presented.

In the original work by Utimoto, the ATRA reaction of ethyl iodide with TMS acetylene, initiated by $Et_3B/O_2$, yielded 84% of the desired product.[95] Contrasting sharply with this figure, our experiments yielded only 28%. This is a clear example of the reproducibility issues associated with heterogeneous $Et_3B/O_2$ initiation discussed in the introduction to this chapter (Section 4.1). This variability is a recognised challenge in $Et_3B/O_2$ initiated reactions, however, the alternative initiation system of $Et_3B/Et_2BOOEt/N_2$ can overcome these issues.

### 4.3.2. Atom Transfer Radical Addition of Isopropyl Iodide to Phenylacetylene

In this study, we extended our investigation into the ATRA of alkyl iodides to acetylenes. We initiated a reaction between isopropyl iodide ($^{i}PrI$) and phenylacetylene using the $Et_3B/Et_2BOOEt/N_2$ system, as detailed in Table 22. This particular reaction was selected due to its similarity to our previous work, with a reported yield of 81%. However, the selectivity for the E/Z isomer (21/79) was worse than the previous example (0/100) making this as an opportunity to improve it.

*Table 22. Optimisation of $Et_3B/Et_2BOOEt$ initiated ATRA of $^iPrI$ to phenylacetylene under $N_2$. Experiment detailed in section 6.7.3.*

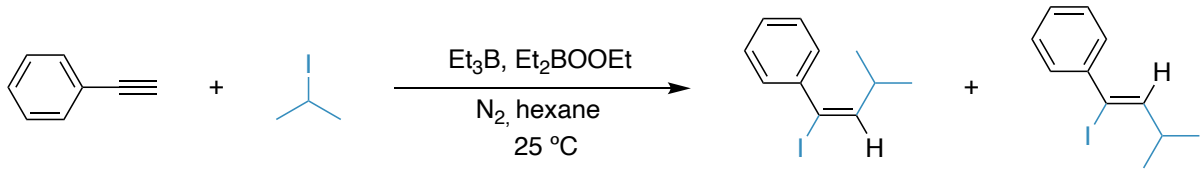


| Entry | Phenylacetylene (µmol) | $^iPrI$ (µmol) | $Et_3B$ (µmol) | $Et_2BOOEt$ (µmol) | Yield (%) [a] | E/Z |
|---|---|---|---|---|---|---|
| 1 | 250 | 50 | 50 | 50 | 12[b,c] | 55/45 |
| 2 | 50 | 200 | 25 | 25 | 24 | 50/50 |
| 3 | 50 | 200 | 50 | 50 | **56**[c] | 37/63 |

*[a] Yields calculated by $^1H$ NMR using 1,2-dichloroethane as internal standard. [b] Yield calculated by $^1H$ NMR using $^iPrI$ as reference. [c] Initiator $Et_3B/Et_2BOOEt$ was delivered at the beginning of reaction as a 25/25 mmol batch and a second batch of 25/25 mmol was delivered after 1h.*

Initially, we sought to replicate the optimised conditions used in the previous example in section 3.3.1 (Entry 1). However, the yield was disappointingly low. Consequently, we adapted the protocol to mirror the conditions reported in the literature for $Et_3B/O_2$ initiation, substituting the initiator for $Et_3B/Et_2BOOEt/N_2$ (Entry 2). This modification led to a doubling of the yield. Further increase in yield was achieved by dividing the initiator into two separate additions (Entry 3).

Once more, the secondary initiation mechanism demonstrated its efficacy in the absence of $O_2$. A comparative analysis of the optimised initiation conditions across the three different $Et_3B$ initiation methods was attempted (Table 23).

*Table 23. ATRA of ethyl iodide to TMS acetylene under different conditions of $Et_3B$ initiation. Experiment detailed in section 6.7.4.*

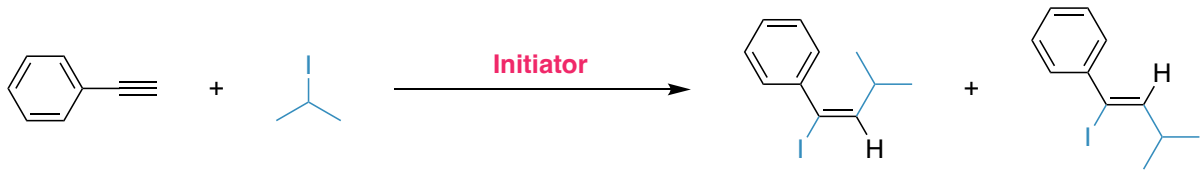


| Entry | Initiator | Atmosphere | Yield (%) [a] | E/Z |
|---|---|---|---|---|
| 1 | $Et_3B$ | High $O_2$ [b] | 1 | 62/38 |
| 2 | $Et_3B$ | Low $O_2$ [c] | 22 | 51/49 |
| 3 | $Et_3B$+$Et_2BOOEt$ | $N_2$ | **56** | 37/63 |

*[a] Yields calculated by $^1H$ NMR using 1,2-dichloroethane as internal standard. [b] Reaction was carried out open to air with unrestricted $O_2$ (See experimental section for more details). [c] Reaction was carried out with restricted $O_2$ (See experimental section for more details).*

Similar results were observed as in the previous section: secondary initiation (Entry 3) showed better performance than $Et_3B/O_2$ in low $O_2$ regime (Entry 2), which in turn was better than high $O_2$ regime (Entry 1). These findings lend further support to our proposed theory.

It is worth noting that as the yield of the reaction increased, the E/Z ratio changed. It appears that, lower conversion rates predominantly yielded the E isomer, while higher conversion rates favoured the Z isomer. This phenomenon is tentatively attributed to the competition between chain propagation and radical isomerisation mechanisms. Initially, a high concentration of iPrI favours rapid chain propagation. However, as iPrI is depleted over the course of the reaction, propagation rates diminish. Efficient propagation correlates with shorter radical lifespans, decreasing the opportunity for rearrangement, specifically of the vinyl radical. Consequently, the E isomer, as the kinetic product, is predominantly formed in the early phase of the reaction.

However, as the reaction progresses, concentration of $^{i}$PrI will decrease, thus the propagation of the chain will slow down. As the propagation of the chain slows down this gives the time to the vinyl radical to rearrange and favour the thermodynamic isomer Z. This theory is also consistent with the results reported by Utimoto where they reported an 81% yield and 21/79 E/Z ratio.[95] Again, the higher the yield, the higher formation of the Z isomer.

The replication of this reaction lead to a markedly lower yields than the one reported in the literature, even when using $Et_3B/Et_2BOOEt/N_2$. Utimoto reported an 81% whereas we achieved a yield of 56% with $Et_3B/Et_2BOOEt/N_2$, and even less (22%) with $Et_3B/O_2$. This touches again on the issues with reproducibility using $Et_3B/O_2$ initiation. As per $Et_3B/Et_2BOOEt/N_2$ initiation, further optimisation of the system might have led to higher conversions.

### 4.3.3. Atom Transfer Radical Addition of Tris(trimethylsilyl)silane to Phenylacetylene

The last of the ATRA reactions to acetylenes that were initiated was the ATRA of tris(trimethylsilyl)silane ($(TMS)_3SiH$) to phenylacetylene (Table 24). This reaction provided a similar example of ATRA to acetylene, but using $(TMS)_3SiH$ instead of an iodide.

*Table 24. $Et_3B/Et_2BOOEt$ initiated ATRA of $(TMS)_3SiH$ to phenylacetylene under $N_2$. Experiment detailed in section 6.7.5.*

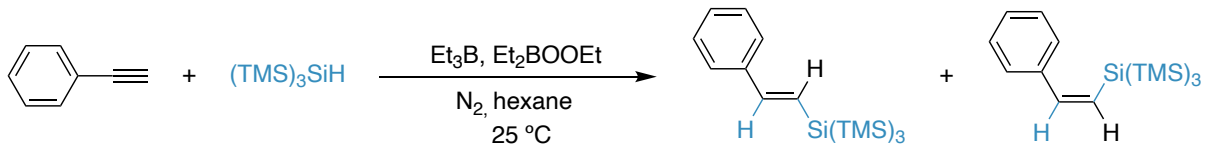


| Entry | Phenylacetylene (µmol) | $(TMS)_3SiH$ (µmol) | $Et_3B$ (µmol) | $Et_2BOOEt$ (µmol) | Yield (%) [a] | E/Z |
|---|---|---|---|---|---|---|
| 1 | 50 | 100 | 25 | 25 | 96 | 0/100 |

[a] *Yield calculated by $^1$H NMR using 1,2-dichloroethane as internal standard.*

The reaction was initiated following the literature procedure for $Et_3B/O_2$ initiation and substituting the initiator for $Et_3B/Et_2BOOEt/N_2$.[143] The conditions were sufficient to yield the Z product with a 96% NMR yield. The selectivity for the Z isomer is presumably because in the phenyl substituted radical, the bulky tris(trimethylsilyl)silyl group hinders syn attack.

The $Et_3B/Et_2BOOEt/N_2$ initiation was compared $Et_3B/O_2$ with the two different $O_2$ regimes (Table 25).

*Table 25. ATRA of ethyl iodide to TMS acetylene under different conditions of $Et_3B$ initiation. Experiment detailed in section 6.7.5.*

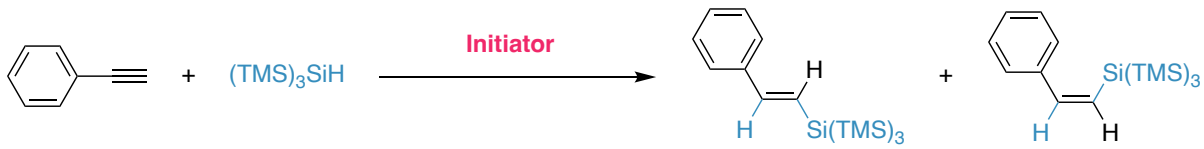


| Entry | Initiator | Atmosphere | Yield (%) [a] | E/Z |
|---|---|---|---|---|
| 1 | $Et_3B$ | High $O_2$ [b] | 30 | 0/100 |
| 2 | $Et_3B$ | Low $O_2$ [c] | 88 | 0/100 |
| 3 | $Et_3B+Et_2BOOEt$ | $N_2$ | **96** | 0/100 |

*[a] Yields calculated by $^1H$ NMR using 1,2-dichloroethane as internal standard. [b] Reaction was carried out open to air with unrestricted $O_2$. [c] Reaction was carried out with restricted $O_2$. See experimental section 6.7.5 for more details.*

In this example, secondary initiation performed similarly to $Et_3B$ initiation under low $O_2$ regime (Entries 3 and 4) both with excellent yields. In stark contrast, the high $O_2$ regime significantly underperformed, yielding a mere 30% (Entry 1).

Upon comparison with the initiation reactions detailed in sections 4.3.1 and 4.3.2, the present reaction demonstrated a lower threshold for initiation, requiring only half the amount of initiator previously utilised, while still achieving superior yields. This enhancement in yield can

be attributed to the highly efficient propagation of the reaction chain, shown by the comparable performance of the $Et_3B/Et_2BOOEt/N_2$ initiation system to the $Et_3B/O_2$ system under a low $O_2$ regime. The inherent efficiency of the reaction chain negates the need for optimisation of the initiation process, as even minimal initiation seams sufficient. This is presumably driven by the weakness of the Si-H bond (377 kJ $mol^{-1}$) and formation of stronger Si-C bond (435 kJ $mol^{-1}$).[144]

Giese's findings of an 85% yield from this reaction initiated by $Et_3B/O_2$ align closely with our results, which demonstrated an 88% yield under a low $O_2$ regime. This establishes the present reaction as the most reproducible reported here. The high reproducibility is likely attributed to the efficiency of the reaction chain.

### 4.3.4. Conclusions Atom Transfer Radical Addition to Acetylenes

The results of ATRA to acetylenes are summarised in Scheme 55:

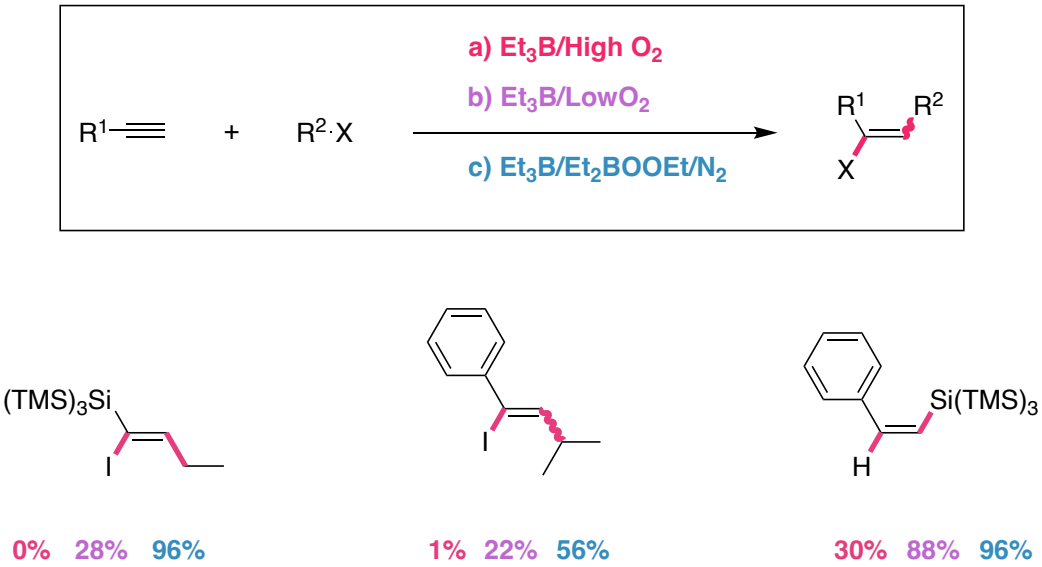


*Scheme 55. Summary of $Et_3B$ initiated ATRA to acetylenes.*

In this section, we have elucidated the potential of $Et_3B$ oxidation product $Et_2BOOEt$, to act in tandem with $Et_3B$ under $N_2$ to initiate radical chain reactions. Our findings indicate that the

$Et_3B/Et_2BOOEt/N_2$ system, to our knowledge, represents a novel approach to radical chain initiation. This discovery paves the way for the development of this system as an efficient radical initiator.

Comparative analysis revealed that the secondary mechanism, employing $Et_3B/Et_2BOOEt/N_2$ directly as a radical initiator, exhibits greater efficiency than the traditional $Et_3B/O_2$ system. Additionally, our results demonstrate that when utilising $Et_3B$ as a radical initiator, operating under a low $O_2$ regime gives increased yields.

These observations were predicted in the previous chapter, where the kinetic model accurately predicted the superior performance of the secondary mechanism over $Et_3B$ autoxidation, and the preference for a low $O_2$ regime over a high $O_2$ regime.

The new system offers advantages like low temperature initiation, reproducible homogeneous conditions, no need for oxygen, and higher initiation radical flux. In order to test the efficiency of initiation, we wanted to explore inefficient radical chains which could not be initiated by standard $Et_3B/O_2$ system.

### 4.4. Initiating Atom Transfer Radical Addition to TCP

It is widely acknowledged that $Et_3B$ often falls short in initiating some radical chains.[85] In instances where the target chain lacks efficiency (i.e. slow rates of propagation and high rates of termination), $Et_3B$ has been inadequate in maintaining consistent initiation.[145-148] With $Et_3B/O_2$, initiation always competes with $Et_3B$ autoxidation. Therefore, if propagation rates of the target chain are slow, initiation will not be efficient even if the termination of the target chain is slow. This has compelled synthetic chemists to opt for alternative initiators.[149] Although this is not necessarily problematic if the alternative initiator accomplishes the task, many chemists prefer $Et_3B$ due to its mild reaction conditions. Switching the initiator implies giving up the gentle initiating conditions of $Et_3B$ for potentially harsher treatments.

In this last section, our objective was to investigate a reaction that is inefficient and challenging to initiate with $Et_3B$. The initial step was to identify an example of such reaction

which prompted chemists to seek an alternative initiator. In 2018, Caputo et al. reported a method for synthesizing highly functionalized 1-halo-3-substituted bicyclo[1.1.1]pentanes (Scheme 56).[150]

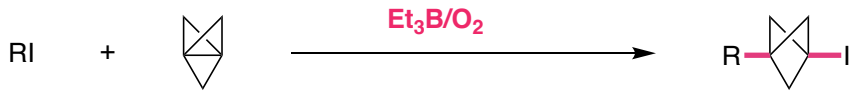


*Scheme 56. $Et_3B/O_2$ initiated ATRA of alkyl iodides to tricyclopropane.*

This method involved an ATRA reaction, with triethylborane serving as the chemical initiator. The authors noted that the success of this method hinged on the mildness of the conditions employed. Indeed, previous methods were hindered by the need for large excesses of radical precursor or suffered from the formation of oligomeric byproducts due to multiple insertions into the radical acceptor.[151, 152] The use of mild conditions for triethylborane initiation facilitated the successful development of this method and its application for the late-stage functionalisation of complex molecules.

Despite the undeniable utility of $Et_3B/O_2$ initiation, which demonstrated a broad scope and functional group compatibility with good to excellent yields (38 – 98%), there were issues with substrate compatibility. $Et_3B/O_2$ initiation showed limitations in functional group tolerance (e.g., amines and aldehydes) and could not be used to access products with $sp^2$ substituents such as arenes and heteroarenes. The authors attributed these limitations to the inefficient chain propagation of certain substrates, a problem that aligns with other reports in the literature concerning $Et_3B$ initiation.[85] Some of the reactions that could not be initiated by $Et_3B/O_2$ in the original publication were again reported in a second publication where they successfully used photoredox catalysis.[149]

The two publications offer an excellent opportunity to test our new methodology: The second publication provides a range of examples of substrates that could not be initiated with triethylborane due to inefficient chain propagation. These can be directly compared to the successful substrates reported in the original publication. This provides us with a method to

compare how our system behaves in both efficient and inefficient chains under identical reaction conditions.

### 4.4.1. Synthesis of TCP

[1.1.1]Propellane, also known as tricyclopropane (TCP), was synthesized from the commercially available 1,1-dibromo-2,2-bis(chloromethyl)cyclopropane (Scheme 57). This method for TCP synthesis was originally reported by Wiberg and Walker in 1982.[153]

**A. Synthesis of TCP**

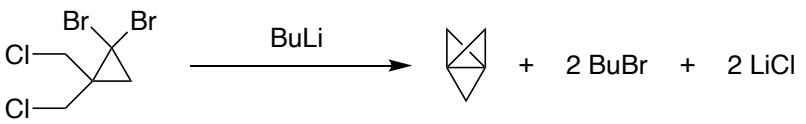


**B. Reaction Mechanism**

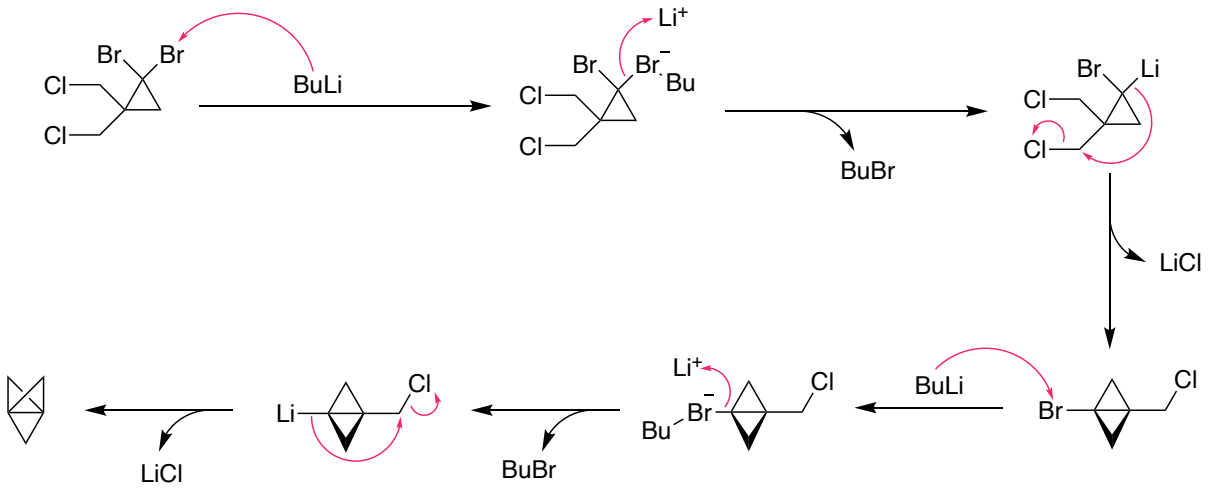


*Scheme 57. (A) Synthesis of TCP from 1,1-dibromo-2,2-bis(chloromethyl)cyclopropane using BuLi Synthesis detailed in section 6.8.4. (B) Scheme of the reaction mechanism.*

The reactant undergoes a double transmetallation with Butyl Lithium (BuLi) to form TCP. BuLi attacks one of the bromines forming an ate complex. The carbon-bromine bond electrons take up the lithium and displace the butyl bromide. The carbon-lithium bond electrons then attack the carbon adjacent to one of the chlorines, displacing one of the chlorines to form

lithium chloride and intermediate bycyclopropane. Intermediate byciclopropane undergoes the same set of reactions to form the final product, [1.1.1]propellane (TCP).

The synthesized TCP was then purified by distillation and recovered as a solution in diethyl ether ($Et_2O$) with a concentration ranging between 0.6 to 0.9 M. The reactant can be stored for several months under an inert atmosphere, and at –20 °C.

### 4.4.2. $Et_3B/Et_2BOOEt$ Initiated Atom Transfer Radical Addition to TCP

In this section, we will explore two specific examples from Anderson's papers on $Et_3B$-initiated ATRA to TCP.[150] The first example involves a reaction successfully initiated by $Et_3B$. From the extensive range of examples provided in Anderson's first paper, we selected (2-iodoethyl)benzene (Scheme 58).[150] This iodide gave a reported yield of 87%, under standard reaction conditions (1.3 eq. TCP, 10% $Et_3B$ at room temperature). Furthermore, the starting iodide is commercially available making it a suitable example for the successful reaction.

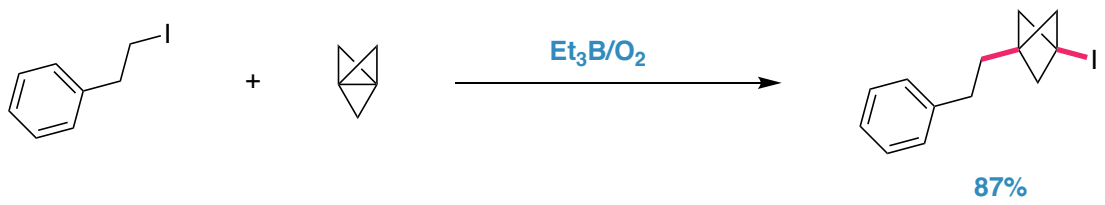


*Scheme 58. $Et_3B/O_2$ initiated ATRA of (2-iodoethyl)benzene to TCP.*

The second example is the ATRA of benzyl iodide (BnI) to TCP. The reaction could not be initiated with $Et_3B/O_2$, However, an optimised yield of 87% was achieved using photoredox catalysis (Scheme 59).[149]

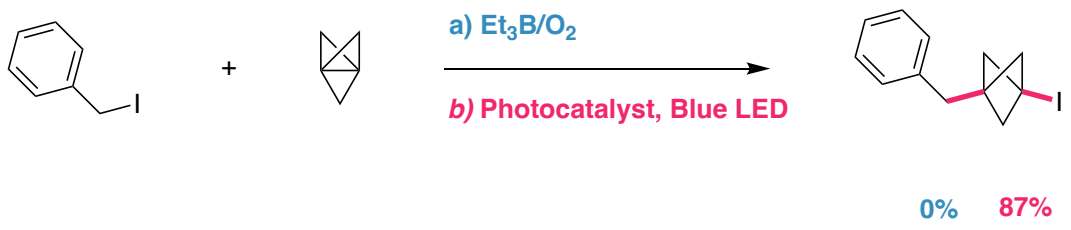


*Scheme 59. ATRA of BnI to TCP initiated using (a) $Et_3B/O_2$, (b) photoredox catalysis.*

The BnI was readily prepared through the Finkelstein reaction from commercially available benzyl bromide (Scheme 60).

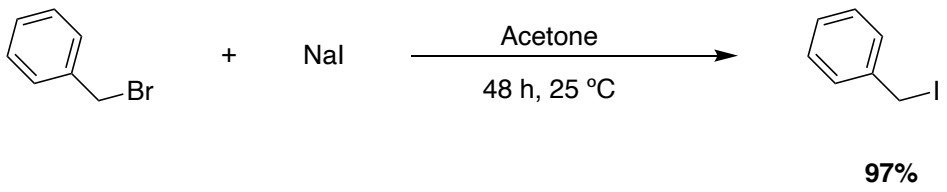


*Scheme 60. Finkelstein reaction of Benzyl bromide to Benzyl iodide. Synthesis detailed in section 6.8.12.*

What is intriguing about these examples ((2-iodoethyl)benzene and benzyl iodide) is the similarity of the starting materials. The only difference is that (2-iodoethyl)benzene from the efficient reaction has an additional $CH_2$ group. This small structural difference leads to a significant difference in reactivity.

The difference in reactivity can be tentatively attributed to the electronics of the radical intermediate. As previously discussed, the inefficiency of a reaction often stems from the slow propagation of the radical chain, fast rates of termination or both. This inefficiency is directly linked to the reactions involved in the propagation steps and, consequently, the intermediates involved in these steps (Scheme 61). In the example of the efficient reaction, the generated intermediate is an alkyl radical. This intermediate is highly reactive due to the radical being localized, not stabilised by resonance.

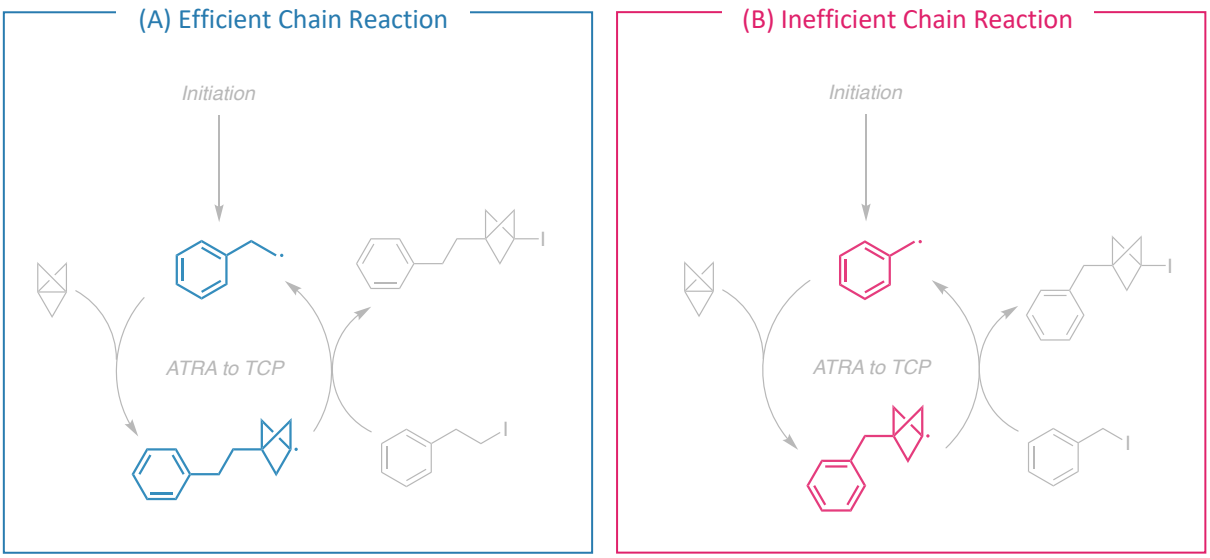


*Scheme 61. Radicals involved in the propagation chain of ATRA to TCP of (A) (2-iodoethyl)benzene (B) Benzyl iodide.*

In inefficient reactions, the intermediate benzyl radical is more stable due to its spin density being spread across the aromatic ring. This stability leads to inefficiency because stable radicals form quickly but react slowly. This slows down propagation and increases the steady state concentration of radicals, favouring termination over propagation and reducing chain efficiency.

This theory aligns with results reported in the literature and with our experimental results. When TCP was reacted with (2-iodoethyl)benzene, we obtained a 63% yield, calculated by NMR. However, when the same conditions were applied to benzyl iodide, no significant product formation was observed (Scheme 62).

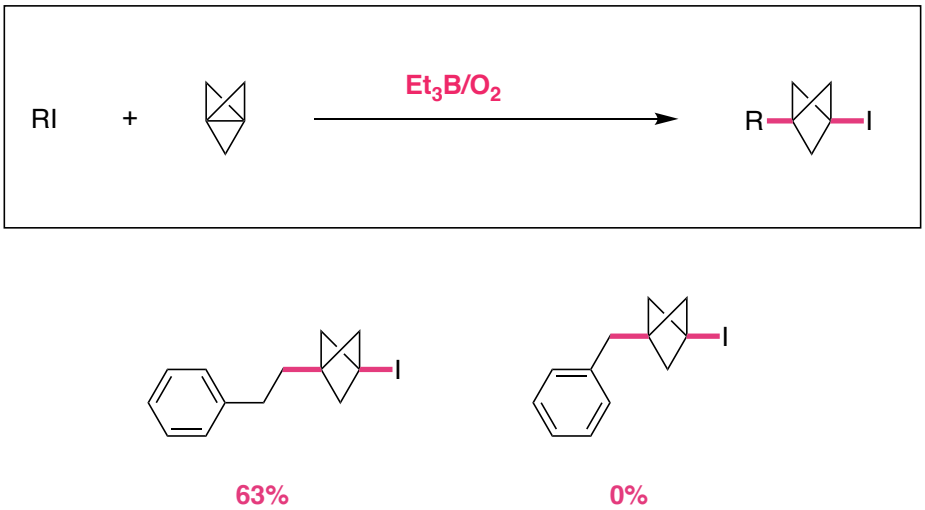


*Scheme 62. $Et_3B/O_2$ initiated ATRA to TCP of (2-iodoethyl)benzene (left) and Benzyl iodide (right). Yields were calculated by NMR using starting iodide as reference. Experiment detailed in section 6.7.6.*

After reproducing the reported results, we implemented the new system. To our delight, both reactions were successfully initiated by the new system (Experiment detailed in section 6.7.7). The efficient reaction was initiated with an NMR yield of 71%, and the inefficient reaction was also successfully initiated with an impressive 71% NMR yield (Scheme 63).

Following the success of these examples, we attempted to initiate more substrates that had previously been unreactive. We selected 2-iodopyridine and 4-iodotrifluorotoluene. Both substrates have been reported to be challenging to initiate with $Et_3B$, but they were both successfully initiated through photoredox catalysis with good yields (87% and 51% respectively).

Both substrates showed the desired reactivity when subjected to $Et_3B/Et_2BOOEt$ initiation, with yields of 29% for 2-iodopyridine and 28% for 4-iodotrifluorotoluene (Scheme 63).

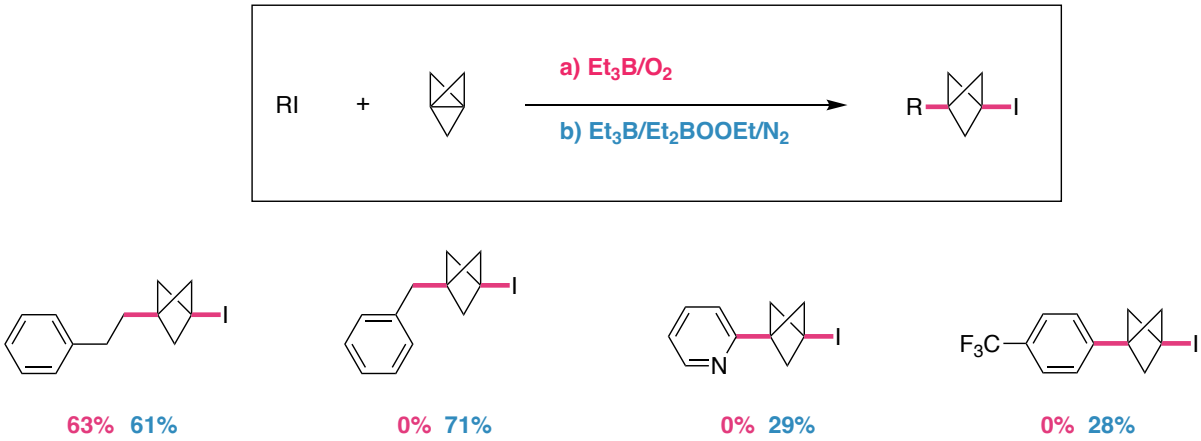


*Scheme 63. (a) $Et_3B/_{O2}$ and (b) $Et_3B/Et_2BOOEt/N_2$ initiated ATRA to TCP of (2-iodoethyl)benzene, and Benzyl iodide, 2-iodipyridine and 4-iodotrifluorotoluene (left to right). Yields were calculated by NMR using starting iodide as reference. Experiment detailed in section 6.7.7.*

This success with 2-iodopyridine and 4-iodotrifluorotoluene, despite the challenges associated with $Et_3B$, prompts further investigation into the underlying mechanisms.

### 4.4.3. Mechanism of $Et_3B/Et_2BOOEt$ Initiated Atom Transfer Radical Addition to TCP

As we delved deeper into the mechanism of $Et_3B/Et_2BOOEt$ initiated atom transfer radical addition to TCP, we encountered an unexpected reactivity pattern. When benzyl iodide (BnI) reacted with TCP in the presence of $Et_3B/Et_2BOOEt$, the correct product was obtained with the anticipated 71% yield. Interestingly, less than half of the initial $Et_3B$ had reacted, despite the reaction between $Et_3B$ and $Et_2BOOEt$ being stoichiometric. This discrepancy suggested an alternative reaction involving more than half of $Et_2BOOEt$ that had not reacted with $Et_3B$.

To investigate this additional reactivity, we monitored the reaction by $^{1}H$ and $^{11}B$ NMR. The decay of $Et_3B$ was particularly slow and $Et_2BOOEt$ also decayed less quickly in the presence of TCP/BnI than in the absence of these reagents (Figure 44).

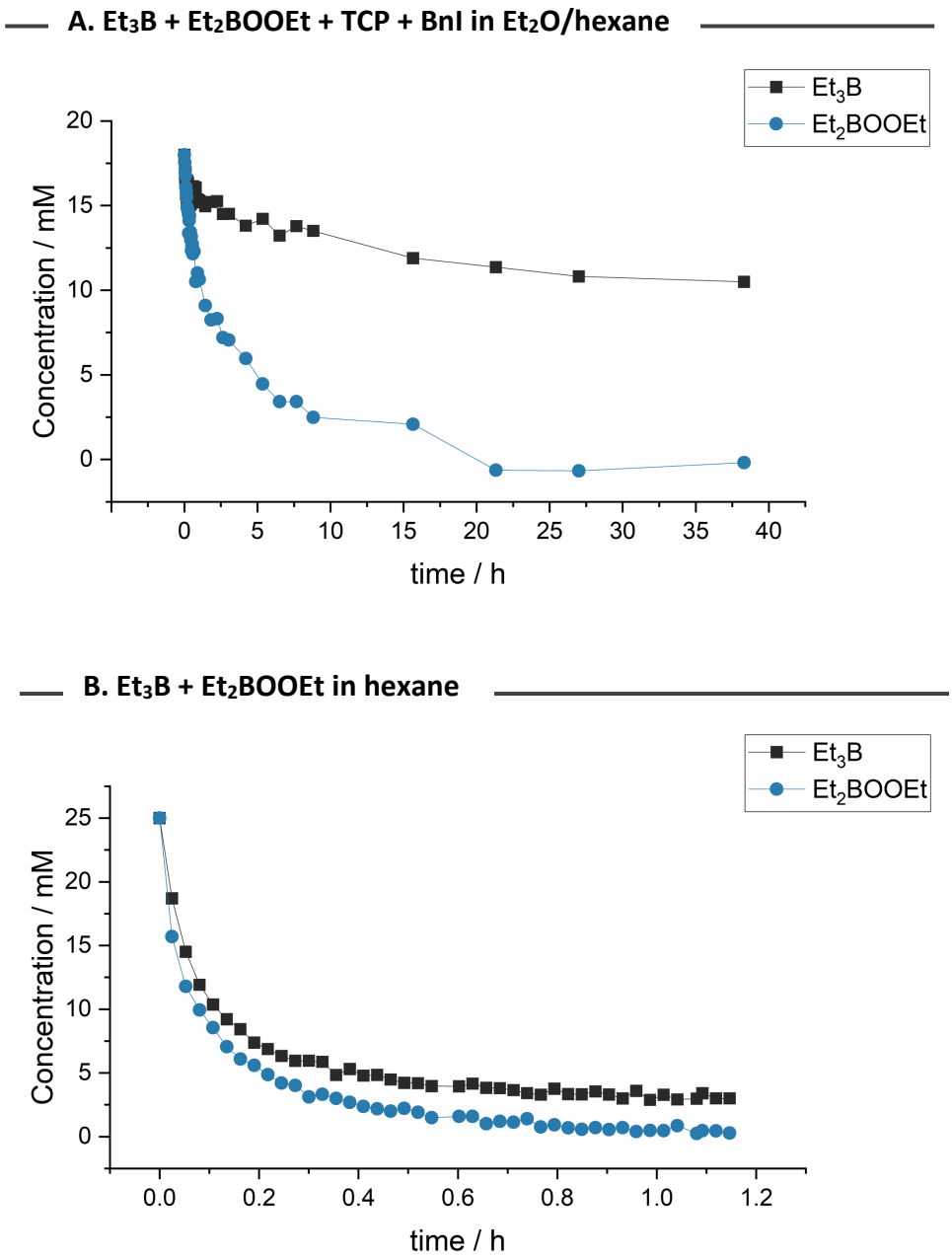


*Figure 44. Kinetic profiles for the reactions between (A) $Et_3B$ and $Et_2BOOEt$ in the presence of TCP and BnI in $Et_2O$ and hexane (Experiment detailed in section 6.7.7). (B) $Et_3B$ and $Et_2BOOEt$ in hexane (Experiment detailed in section 6.5.4). Both reactions were run at 25 °C, under $N_2$, and were followed by $^1H$ and $^{11}B$ NMR using the initial concentrations as reference. Measurements were taken at the indicated timestamps.*

The first potential factor to explain the discrepancy was the solvent system. All our previous mechanistic investigations on $Et_3B$ and $Et_3B/Et_2BOOEt$ were conducted in hexane. However, for the ATRA to TCP, a 5:2 hexane: $Et_2O$ mixture was used. The reason behind the change is that TCP is synthesised as an ethereal solution.

The change in solvent system can of course affect the rates of the reactions, especially in this case where $Et_2O$ possesses two lone pairs of electrons that could potentially donate to the empty p orbital of $Et_3B$ thus interfering with its reactivity.

To assess this potential effect, we monitored the $Et_3B/Et_2BOOEt$ reaction via NMR in $Et_2O$ (Figure 45). The observed reaction rate exhibited a negligible deviation from that in hexane, with a calculated rate constant of 0.19 $M^{-1}$ $s^{-1}$, closely approximating the 0.20 $M^{-1}$ $s^{-1}$ rate constant determined for the reaction in hexane alone. These findings suggest that the solvent system's electron-donating characteristics do not significantly influence the reaction kinetics under the studied conditions.

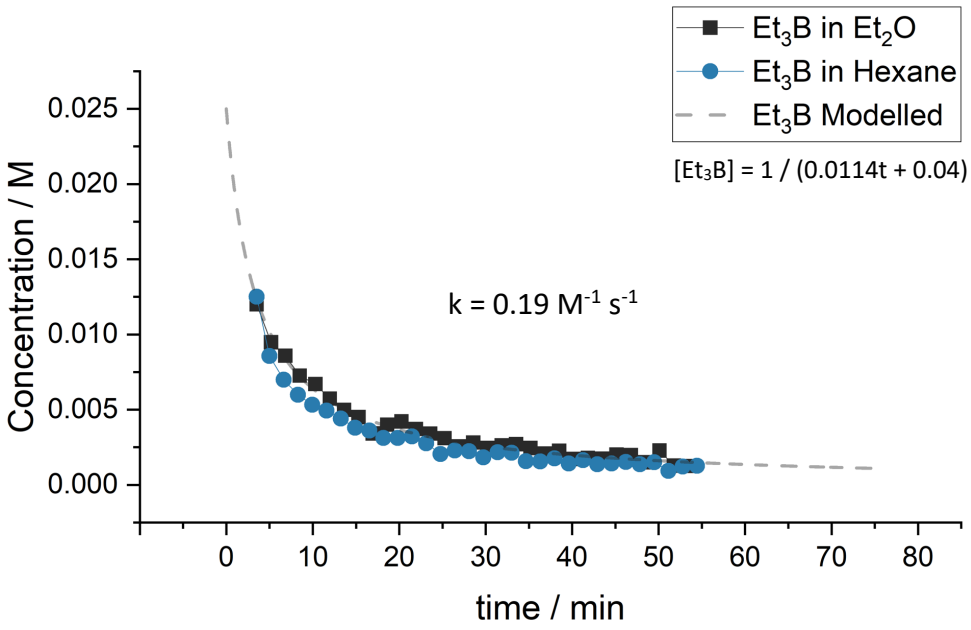


*Figure 45. Kinetic profile of $Et_3B$ in the reaction with $Et_2BOOEt$ in different solvents, at 25 °C, and under $N_2$. The reaction was followed by $^{11}B$ NMR using the initial concentration as reference and measurements were taken at the indicated timestamps. Experiment detailed in section 6.5.5.*

Upon eliminating $Et_2O$ as the factor responsible for the change in the rate of $Et_3B/Et_2BOOEt$ reaction in the presence of BnI and TCP, we opted for a different factor affecting the typical $Et_3B/Et_2BOOEt$ reactivity. The slow loss of $Et_3B$ in the reaction with $Et_2BOOEt$ / BnI / TCP could be due to $Et_2BOOEt$ consumption through a different pathway.

It is known that $Et_2BOOEt$ rearranges to $EtB(OEt)_2$ in solution and at room temperature. Normally this rearrangement progresses slowly and does not interfere with the rapid reaction of $Et_2BOOEt$ with $Et_3B$. The half-life for the rearrangement of $Et_2BOOEt$ is approximately 2.5 h, whereas the half-life for $Et_2BOOEt$ in the reaction with $Et_3B$ is 3 minutes, making reaction $Et_3B$ + $Et_2BOOEt$ the preferred pathway. Nevertheless, in the presence of $Et_3B$, BnI and TCP, the half-life of $Et_2BOOEt$ extends to 1.5 h, rendering $Et_2BOOEt$ rearrangement a competitive pathway.

$Et_2BOOEt$ rearrangement becoming a competitive pathway can explain the deviation from the 1:1 stoichiometry in $Et_3B/Et_2BOOEt$ reaction. This is evidenced by the observation of the expected rearranged product $EtB(OEt)_2$ in the corresponding quantity.

However, one question remains: why is the reaction between $Et_3B$ and $Et_2BOOEt$ slowed down in the presence of TCP and BnI? The most plausible explanation is the complexation of $Et_3B$ by another component in the system without significant changes to its NMR spectra. $Et_3B$ is a strong Lewis acid and can form a complex with a Lewis base present in the reaction mixture. If such complexation occurs, it could potentially suppress the reactivity of $Et_3B$.

To elucidate the nature of this interference with $Et_3B$ reactivity, we examined the reaction of $Et_3B$ with $Et_2BOOEt$ in the presence of the associated reagents (BnI, and TCP) separately.

Given that iodides can act as a Lewis base, possessing three lone pairs of electrons capable of complexing with $Et_3B$, it was plausible that BnI could inhibit the reactivity of $Et_3B$. Moreover, the concentration of BnI was tenfold that of $Et_2BOOEt$, potentially promoting the reaction between $Et_3B$/BnI over the reaction between $Et_3B/Et_2BOOEt$. However, monitoring the reaction between $Et_3B$ and $Et_2BOOEt$ in the presence of BnI revealed no difference compared

to the control (Figure 46). The presence of BnI did not significantly influence the reaction rate of $Et_3B$ with $Et_2BOOEt$.

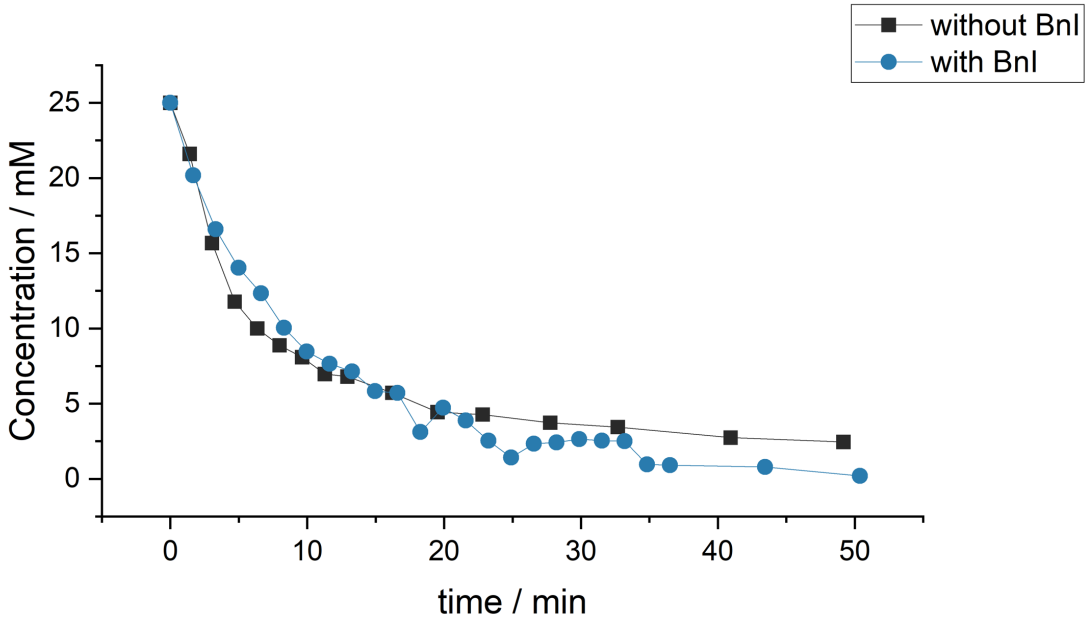


*Figure 46. Kinetic profile of $Et_3B$ in reaction with $Et_2BOOEt$ in hexane in the presence of BnI (experiment detailed in section 6.5.7) compared to $Et_3B$ in reaction with $Et_2BOOEt$ in the absence of BnI (experiment detailed in section 6.5.4, Entry 1). Both reactions run in hexane and at 25 °C, and under $N_2$. The reaction was followed by $^{11}B$ NMR using the initial concentration as reference and measurements were taken at the indicated timestamps.*

Neither $Et_2O$ nor BnI were responsible for the strange reactivity in the $Et_3B/Et_2BOOEt$/BnI/TCP which left TCP as the only possible responsible species. The reaction between $Et_3B$ and $Et_2BOOEt$ was monitored in the presence of TCP and showed a remarkable decrease in reactivity between $Et_3B/Et_2BOOEt$ (Figure 47).

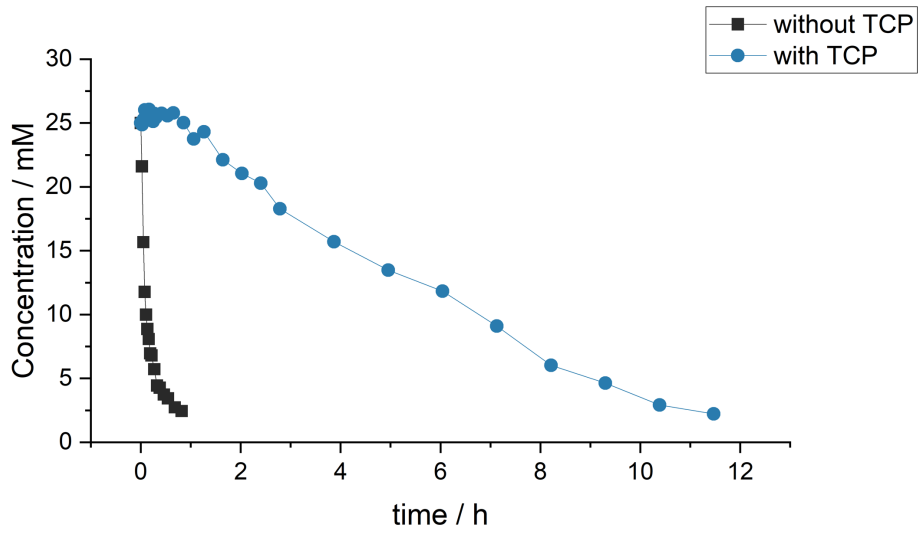


*Figure 47. Kinetic profile of $Et_2BOOEt$ in reaction with $Et_3B$ in $Et_2O$ and hexane in the presence of TCP (experiment detailed in section 6.5.8) compared to $Et_2BOOEt$ in reaction with $Et_3B$ in the absence of TCP (Experiment detailed in section 6.5.4, Entry 1). Both reactions run at 25 °C, and under $N_2$. The reaction was followed by $^1H$ NMR using the initial concentration as reference, and measurements were taken at the indicated timestamps.*

Analysis of $^{11}B$ NMR data for this kinetic run showed a broad doublet at the region of $R_3B$ that disappeared rapidly (in 41 min) (Figure 48).

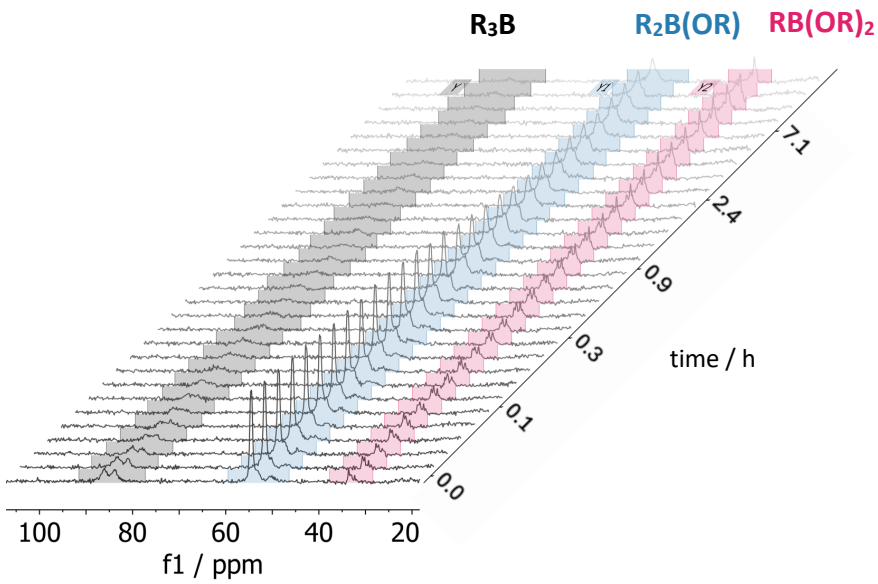


*Figure 48. $^{11}B$ NMR monitoring of a solution of $Et_3B/Et_2BOOEt$ in the presence of TCP in $Et_2O$/hexane, at 25 °C, under $N_2$ over 11 h. Experiment detailed in section 6.5.8.*

This observation was originally attributed to experimental error, we suspected $O_2$ had leaked into the system causing the quick decay of $Et_3B$. However, after repeating the experiment in triplicate, we confirmed that $O_2$ was not the issue and that the observations were valid.

TCP appeared to react with $Et_3B$, consuming the borane quickly, and thus competing with the $Et_3B/Et_2BOOEt$ reaction.

#### 4.4.4. Reaction Between $Et_3B$ and TCP.

We have observed an interaction between TCP and $Et_3B$, however the nature of this reaction is unknown and there are no reports in the literature of such reaction. Understanding this process might shine some light on the results with $Et_3B/Et_2BOOEt$ initiated ATRA to TCP.

To gain a deeper insight, TCP was reacted with $Et_3B$ in the absence of other reagents, and the reaction was monitored by NMR under $N_2$ (1 M TCP, 1 M $Et_3B$. Experiment detailed in section 6.5.9.) (Figure 49). The experiment revealed a clear reaction between TCP and $Et_3B$. Specifically, $Et_3B$ partially reacted to form an unidentified product. This was evidenced by the $^{11}B$ NMR, which showed not only the peak for $Et_3B$ at 87.4 ppm but also a second peak at 84.8 ppm. The emergence of this second peak indicates the presence of a second B environment in the mixture. Since $Et_3B$ is the only source of B, the second B peak could only originate from the reacted $Et_3B$. This doublet appeared as a single peak in earlier work carried out at lower $Et_3B$ concentration. This is why it appeared that most of $Et_3B$ remained unreacted in the reaction with $Et_2BOOEt$/TCP/BnI.

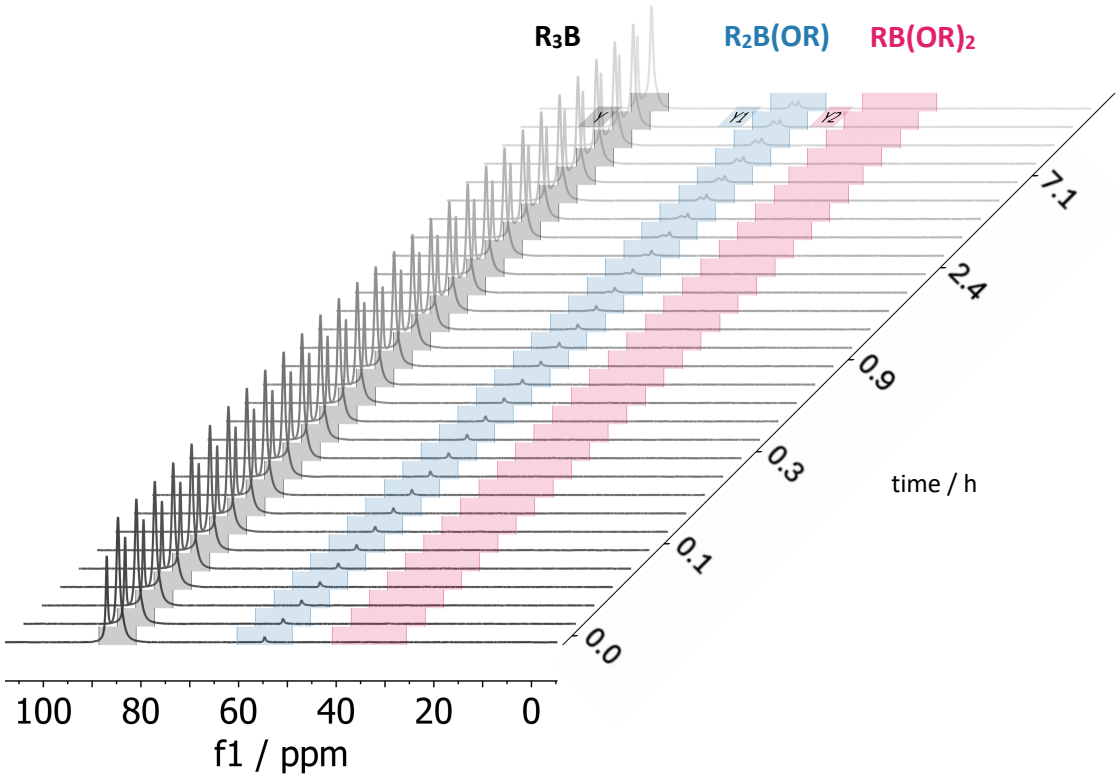


*Figure 49. $^{11}B$ NMR monitoring of a solution of $Et_3B$ and TCP in $Et_2O$, at 25 °C, under $N_2$ over 11 h. Experiment detailed in section 6.5.9.*

Furthermore, TCP was completely consumed in the first measurement, as indicated by the disappearance of the TCP peak in $^1H$ NMR.

This experiment confirms that TCP reacts with $Et_3B$, but the exact nature of the reaction remains unknown. However, the $^{11}B$ NMR provides some insight into the products formed. Starting with 1 eq. of $Et_3B$, at the end of the reaction time, the reaction mixture contained 0.25 eq. of $Et_3B$, 0.68 eq. of product 1 (P1), and 0.07 eq. of products 2 (P2) and 3 (P3) (Figure 50). The chemical shifts of these peaks provide structural information about the compounds. P1, appearing at 84.8 ppm (the region of $R_3B$), corresponds to a trialkyl boron species that is not $Et_3B$ and is the major product of the reaction. P2 and P3, appearing at 56.1 and 54.7 ppm (the region of **$R_2B(OR)$**), have incorporated at least one O, likely from the solvent $Et_2O$ as there is no other source of oxygen in the reaction mixture.

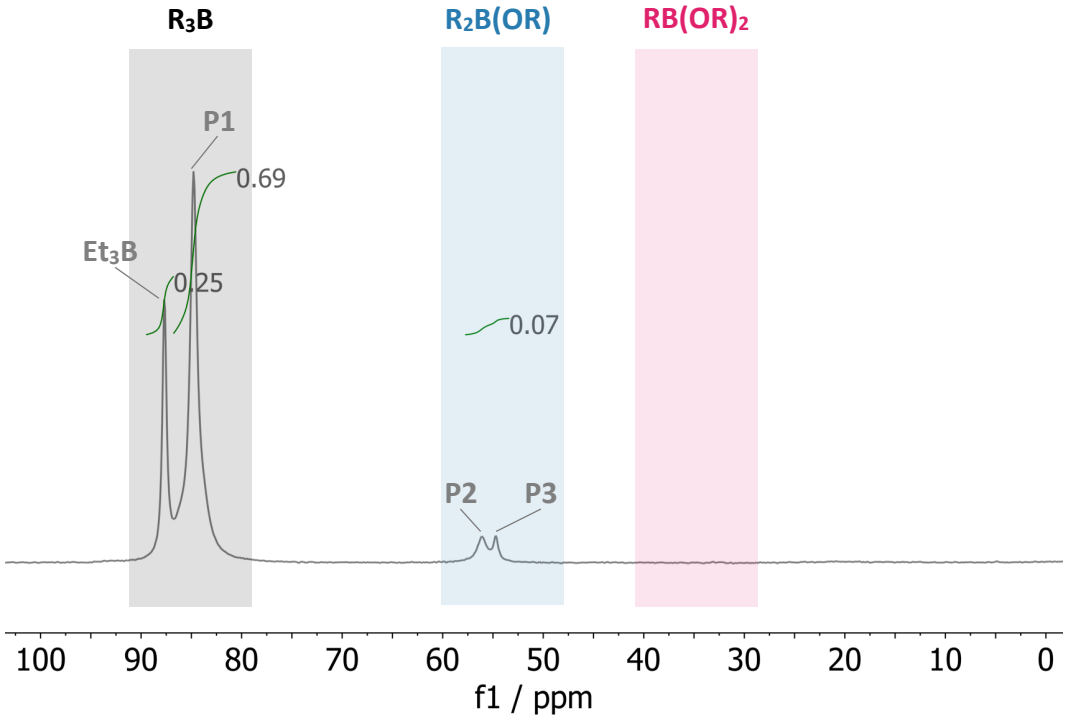


*Figure 50. $^{11}B$ NMR of $Et_3B$ + TCP in $Et_2O$, at 25 °C and under $N_2$ after reaction completion. Experiment detailed in section 6.5.9.*

To gain a deeper understanding of this reaction, we performed radical trapping, and the trapped radicals were analysed by MS (experiment detailed in section 6.3.13). The details of the trapped radicals are presented in Table 26.

*Table 26. Trapped radicals using CHANT from the reaction between TCP and $Et_3B$ in $Et_2O$/hexane. Experiment detailed in section 6.3.13.*

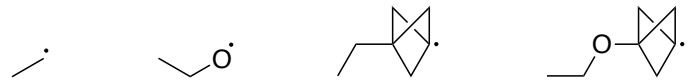

(Et·) (EtO·) (EtTCP·) (EtOTCP·)

| Species | | m/z | MS peak Intensity/Noise |
|---|---|---|---|
| Unreacted Trap | $[CHANT+H]^+$ | 323.2699 | 22582 |
| | $[CHANT+Na]^+$ | 345.2519 | 10 |
| Trapped Et· | $[CHANT+Et\cdot+H]^+$ | 196.1697 | 52 |
| | $[CHANT+Et\cdot+Na]^+$ | 218.1517 | 98 |
| | $[TEMPO+Et\cdot+H]^+$ | 186.1854 | 836 |
| Trapped EtO· | $[CHANT+EtO\cdot+H]^+$ | 212.1648 | 1197 |
| | $[CHANT+EtO\cdot+Na]^+$ | 234.1466 | 88 |
| Trapped EtTCP· | $[CHANT+EtTCP\cdot+H]^+$ | 262.2168 | 314 |
| | $[CHANT+EtTCP\cdot+Na]^+$ | 284.1988 | 26 |
| | $[TEMPO+EtTCP\cdot+Na]^+$ | 252.2324 | 654 |
| Trapped EtOTCP· | $[CHANT+EtOTCP\cdot+H]^+$ | 278.2118 | 19 |

The identified radical intermediates in the reaction provide further insight. Consequently, we now possess knowledge regarding the nature of reagents, intermediates and products involved in this reaction (Scheme 64).

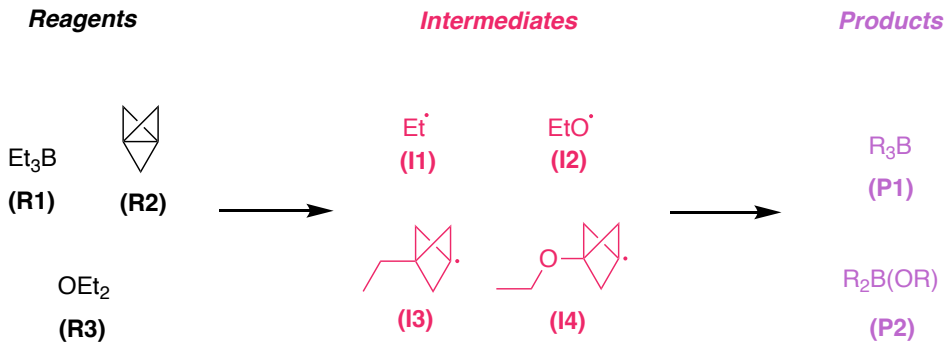


*Scheme 64. Reagents, radical intermediates and products involved in the reaction between TCP and $Et_3B$ in the presence of $Et_2O$.*

Based on the gathered information a mechanism can be tentatively proposed (Scheme 65).

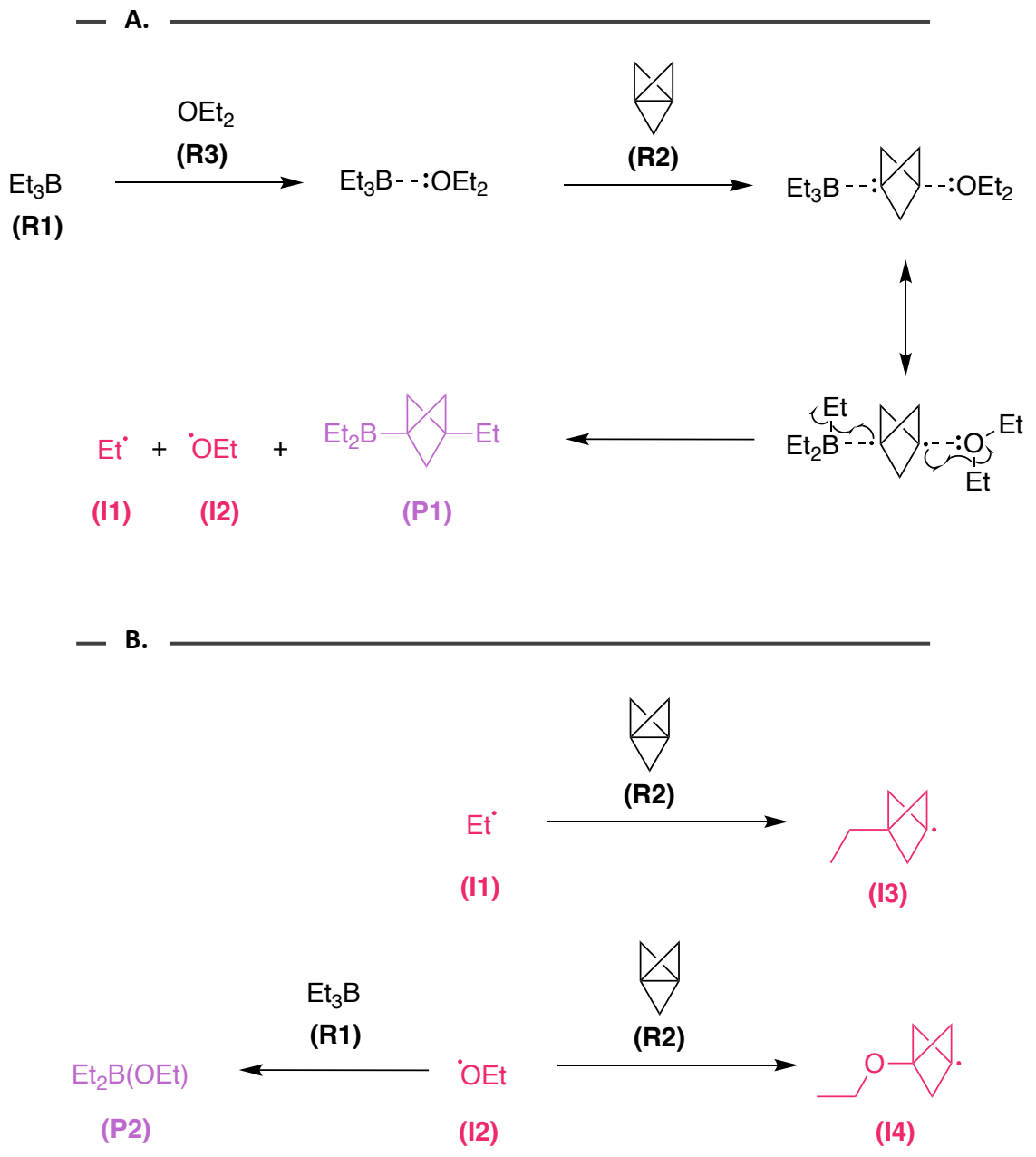


*Scheme 65. Mechanism of reaction between $Et_3B$ and TCP in the presence of $Et_2O$.*

$Et_3B$ initially coordinates with the solvent $Et_2O$. The key step involves the insertion of TCP between $Et_3B$ and $Et_2O$, which is facilitated by the unique nature of TCP's central bond. This bond is characterised as a charge-shift bond, which is neither purely covalent nor purely ionic.[154] In these types of bonds, the covalent-ionic resonance energy plays the major role.

The ionic character of the central bond can facilitate the insertion of TCP in between $Et_3B$ and $Et_2O$.

Post-insertion, the central bond undergoes homolysis, reacting with triethylborane on one side, forming an ethyl radical, and with $Et_2O$ on the other side, generating an ethoxyl radical. The driving force behind this reaction is the release of strain from the central bond of TCP, which has a highly energetic inverted tetrahedral geometry. Consequently, the reaction favours the formation of more stable C-C and C-B bonds.

The primary product of this homolytic process is **P1**. Its presence was confirmed as the major product through NMR, were it exhibited the expected chemical shift.

The reaction also generates ethyl and ethoxyl radicals (**I1** and **I2**), both of which were trapped and detected by MS. Both ethyl and ethoxyl radicals can react with TCP to form radicals **I3** and **I4** respectively, both of which were trapped and observed by MS.

Additionally, ethoxyl radical (**I2**) can also react with $Et_3B$ to form $Et_2B(OEt)$ (**P2**) which was identified by NMR.

The unexpected reactivity between $Et_3B$ and TCP interfered with our initial plan to use $Et_3B$ in combination with $Et_2BOOEt$ to initiate challenging chains. However, we were able to identify the source of this unusual reactivity and propose a reaction mechanism.

Interestingly, during these experiments, we observed that $Et_2BOOEt$ alone could initiate the inefficient reaction (experiment detailed in section 6.5.10). Moreover, the yields observed were excellent, reaching up to 90% (Scheme 66).

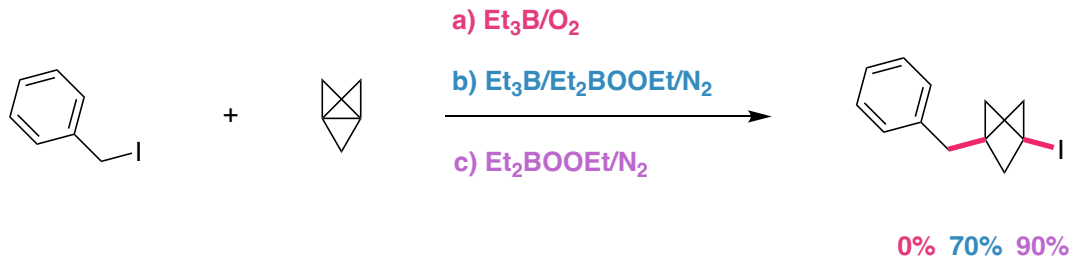


*Scheme 66. Initiation of the inefficient ATRA to TCP using different initiating systems. Experiments detailed in sections (a) 6.7.6, (b) 6.7.7, and (c) 6.7.8.*

The unusual reactivity observed between TCP and $Et_3B$, the lack of precedent for successful $Et_2BOOEt$ initiation, and the excellent yields observed for this initiation prompted us to investigate further the unusual reactivity occurring with these reagents. In the following section, we will explore the extent of this reactivity and propose a reaction mechanism.

### 4.4.5. $Et_2BOOEt$ Initiated Atom Transfer Radical Addition to TCP

Contrary to our initial hypothesis, the addition of $Et_2BOOEt$ to a mixture of BnI and TCP successfully initiated the ATRA reaction. Remarkably, the reaction yield was 90%, a substantial improvement over the 71% yield previously achieved using the $Et_2BOOEt/Et_3B$ system.

Having observed the unusual reactivity of $Et_2BOOEt$, we decided to explore the scope of this reaction. Scheme 67 shows the yields of different ATRA reactions to TCP initiated by classic $Et_3B/O_2$, the new $Et_3B/Et_2BOOEt$, and $Et_2BOOEt$ alone.

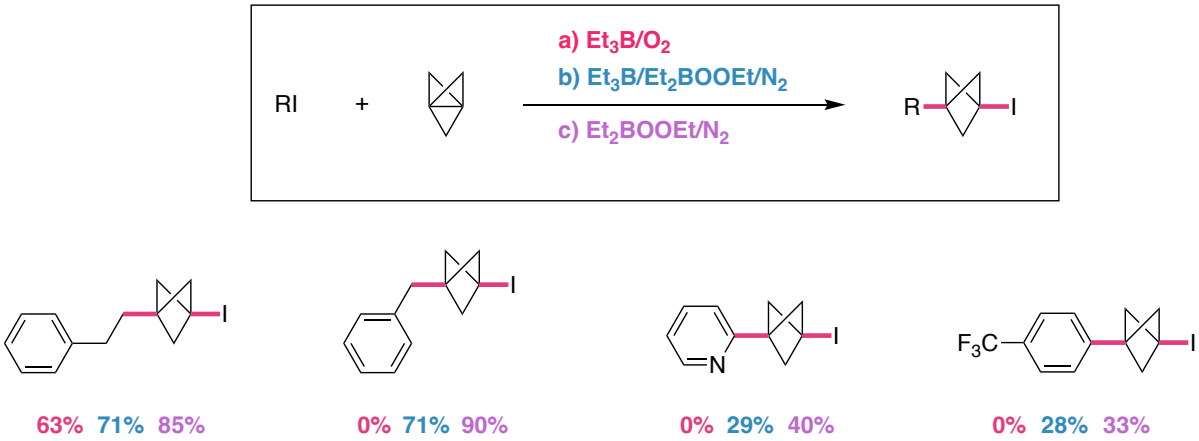


*Scheme 67. (a) $Et_3B/O_2$, (b) $Et_3B/Et_2BOOEt/N_2$, and (c) $Et_2BOOEt$ initiated ATRA to TCP of (2-iodoethyl)benzene, and Benzyl iodide, 2-iodipyridine and 4-iodotrifluorotoluene (left to right). Yields were calculated by NMR using starting iodide as reference. Experiments detailed in sections (a) 6.7.6, (b) 6.7.7, and (c) 6.7.8.*

Peroxide alone was successful in initiating reactions, including the previously reported challenging to initiate with $Et_3B$. In the cases of (2-iodiethyl)benzene and benzyl iodide the yields were excellent reaching a remarkable 90%. In all the examples $Et_2BOOEt$ decomposition alone proved to be the most effective initiator. Intrigued by these unexpected results we decided to look deeper into the mechanism of initiation.

### 4.4.6. Mechanism of $Et_2BOOEt$ Initiated Atom Transfer Radical Addition to TCP

Our initial hypothesis was that the decomposition of $Et_2BOOEt$ would not initiate radical reactions efficiently. We have evidence that there is a small contribution of homolytic reaction competing with the rearrangement. However, a notable advantage of this homolysis is its relatively slow rate ($k \approx 4 \times 10^{-6}\ s^{-1}$, at 25 °C in hexane). As discussed previously, an ideal initiator would provide a steady stream of radicals over an extended duration, optimising initiation and minimizing termination, thereby boosting initiation efficiency.

However, the homolysis of the peroxide bond is likely a minor process in $Et_2BOOEt$ decomposition. This was demonstrated on prior radical trapping experiments (Section 3.3.3), showing minimal radical trapping from $Et_2BOOEt$ decomposition alone. Thus, while the homolysis of $Et_2BOOEt$ could serve as a good initiator due to its sustained radical supply, the quantity of radicals it provides might not be sufficient to yield the excellent results observed in the previous section.

Additionally, we attempted to initiate ATRA to acetylenes using $Et_2BOOEt$, and as anticipated the initiation was unsuccessful yielding no observable amount of product. Therefore, the 90% yield observed in the $Et_2BOOEt$ initiated ATRA to TCP was a surprising result.

A possibility is that TCP interacts with $Et_2BOOEt$ increasing the radical production of the system. This hypothesis is sustained on our previous observations of $Et_3B$ interacting with TCP in an unpredicted fashion. However, $Et_2BOOEt$ should be less reactive towards TCP than $Et_3B$ due to the empty p orbital in the boron being partially occupied by the lone pairs of the oxygen.

Nevertheless, we decided to put the hypothesis to test, and we examined the decomposition of the peroxide in the presence of TCP. We trapped the radicals formed in the decomposition of $Et_2BOOEt$ when TCP was present in the mixture and compared the results to a control: the decomposition of $Et_2BOOEt$ in the absence of TCP (19 mM $Et_2BOOEt$, 248 mM TCP, 19 mM CHANT. Experiment detailed in section 6.3.13) (Table 27).

*Table 27. Trapped radicals using CHANT from the decomposition of $Et_2BOOEt$ alone and in the presence of TCP. Experiment detailed in section 6.3.13.*

| Species | | m/z | MS peak intensity | |
|---|---|---|---|---|
| | | | $Et_2BOOEt$ | $Et_2BOOEt$+TCP |
| Unreacted Trap | $[CHANT+H]^+$ | 323.2699 | 130965 | 89334 |
| | $[CHANT+Na]^+$ | 345.2519 | 675 | 5 |
| Trapped Et· | $[CHANT+Et\cdot+Na]^+$ | 218.1518 | 54 | 0 |
| | $[TEMPO+Et\cdot+H]^+$ | 186.1855 | 11 | 0 |
| Trapped EtO· | $[CHANT+EtO\cdot+H]^+$ | 212.1648 | 5 | 0 |

In the absence of TCP, the decomposition of $Et_2BOOEt$ resulted in the detection of small amounts of trapped ethyl and ethoxyl radicals. However, no radicals were observed in the $Et_2BOOEt$ decomposition in the presence of TCP, suggesting that TCP does not enhance the initiating ability of $Et_2BOOEt$.

Next, we aimed to investigate how $Et_2BOOEt$ performs in the presence of the target chain. If TCP alone does not influence the initiating ability of $Et_2BOOEt$, does the target chain (TCP + BnI) affect $Et_2BOOEt$ initiation? The radicals formed in $Et_2BOOEt$ initiated ATRA to TCP were trapped and compared to the radicals trapped in $Et_2BOOEt$ decomposition alone (19 mM $Et_2BOOEt$, 248 mM TCP, 188 mM BnI, 19 mM CHANT. Experiment detailed in section 6.3.14) (Scheme 68) (Table 28).

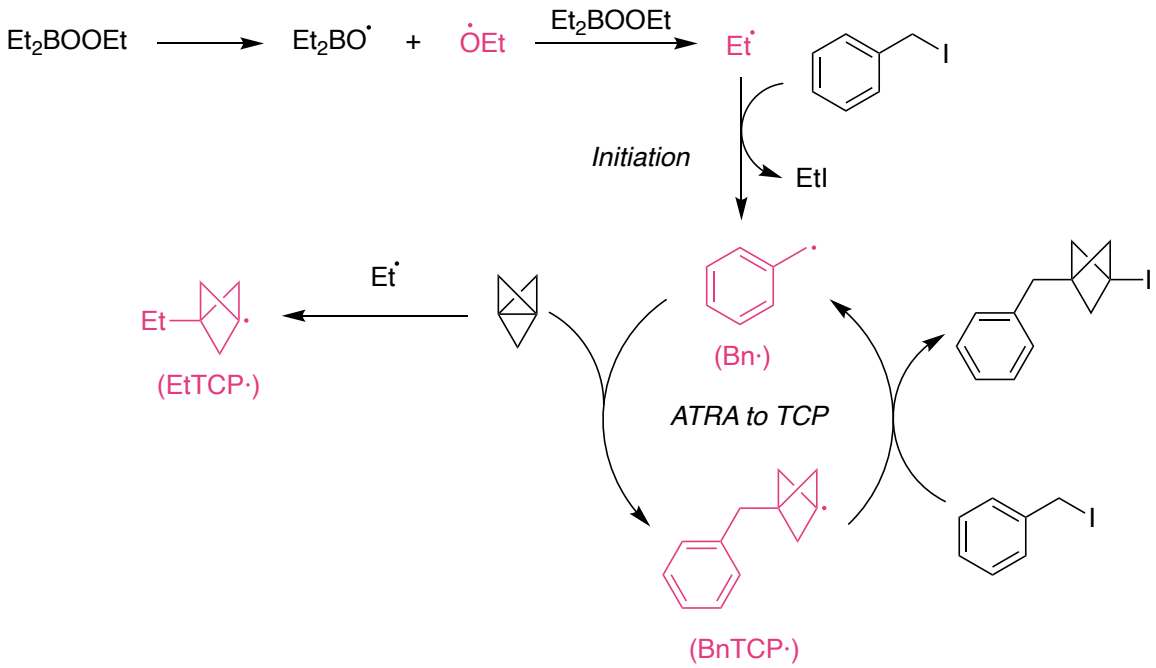


*Scheme 68. Mechanism and radicals involved in the $Et_2BOOEt$ initiated ATRA to TCP.*

*Table 28. Trapped radicals using CHANT from the decomposition of $Et_2BOOEt$ alone and in the $Et_2BOOEt$ initiated ATRA to TCP. Experiment detailed in section 6.3.14.*

| Species | | m/z | MS peak intensity | |
|---|---|---|---|---|
| | | | $Et_2BOOEt$ | $Et_2BOOEt$+TCP+BnI |
| Unreacted Trap | [CHANT+H]$^+$ | 323.2699 | 130965 | 123139 |
| | [CHANT+Na]$^+$ | 345.2519 | 675 | 378 |
| Trapped Et· | [CHANT+Et·+Na]$^+$ | 218.1518 | 54 | 7 |
| | [TEMPO+Et·+H]$^+$ | 186.1855 | 11 | 3 |
| Trapped EtO· | [CHANT+EtO·+H]$^+$ | 212.1648 | 5 | 0 |
| Trapped EtTCP· | [CHANT+EtTCP·+H]$^+$ | 262.217 | 0 | 6 |
| Trapped Bn· | [CHANT+Bn·+H]$^+$ | 258.1856 | 0 | 242 |
| | [CHANT+Bn·+Na]$^+$ | 280.1677 | 0 | 268 |
| | [TEMPO+Bn·+H]$^+$ | 248.2011 | 0 | 10298 |
| | [TEMPO+Bn·+Na]$^+$ | 270.1833 | 0 | 11 |
| Trapped BnTCP· | [CHANT+BnTCP·+H]$^+$ | 324.2329 | 0 | 25 |
| | [CHANT+BnTCP·+Na]$^+$ | 346.2149 | 0 | 28 |
| | [TEMPO+BnTCP·+H]$^+$ | 314.2484 | 0 | 31 |

As anticipated, both the radical intermediates involved in the reaction chain and the radicals formed during initiation were detected (Scheme 68). The intensities of the trapped adducts for the radicals within the reaction chain are significantly higher than those for initiation. This difference can be attributed to the lifetimes of these radicals.

In the studied system, all detected radicals originate from a single source, the initiation via $Et_2BOOEt$ decomposition. However, the concentration of benzyl radicals, which are part of the propagation step, is much higher than that of initiator radicals like ethyl radicals. This is due to their longer survival and recycling within the reaction chain, leading to a higher steady-state concentration. Ethyl radicals, on the other hand, are only generated during initiation

and are not recycled. They either initiate the target chain or get trapped, and are not regenerated until the next initiation.

The competition between radical trapping and target chain initiation provides an explanation for the observed higher intensity of trapped radical adducts involved in initiation (Et·, and EtO·) when studying $Et_2BOOEt$ decomposition in isolation (Table 27) as opposed to when the target chain is present (Table 28). In the absence of the target chain, the radical trap does not compete with the chain to capture the radicals produced during initiation. Consequently, this leads to the observed increase in the intensities of trapped Et· and EtO· in the absence of the competing chain.

Quantitative analysis of radicals via MS trapping is challenging; despite observing the anticipated radicals, their correlation with the target chain's influence on radical initiation needs to be treated with caution.

In order to measure whether there is an effect of target chain in $Et_2BOOEt$ decomposition, we monitored the decomposition of $Et_2BOOEt$ by NMR, both with and without the target chain (experiment detailed in section 6.5.10). The results indicated that the target chain does not significantly impact the decomposition rate of $Et_2BOOEt$ (Figure 51). Had the target chain facilitated an additional initiation reaction, an cahnge in the decomposition kinetics of $Et_2BOOEt$ would be expected, yet such changes were not observed. Furthermore, the formation of $EtB(OEt)_2$ remained consistent, reinforcing the conclusion that the target chain does not significantly promote any secondary initiation reactions that would otherwise alter the decomposition product distribution, particularly affecting the formation of $EtB(OEt)_2$, a heterolytic rearrangement product.

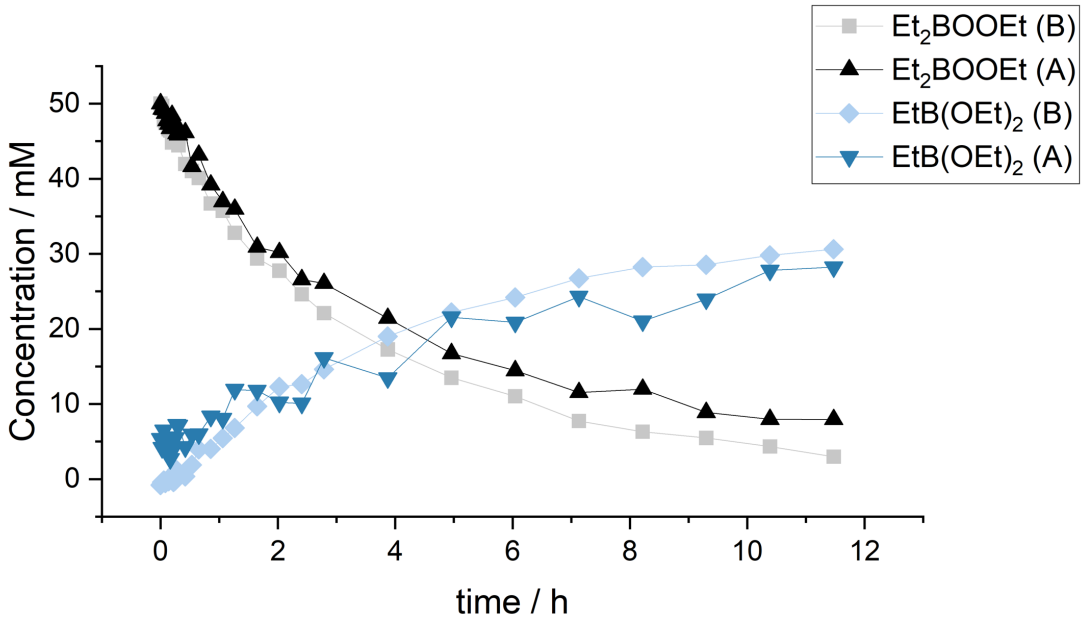


*Figure 51. Kinetic profile for the decomposition of $Et_2BOOEt$ in a solution of hexane (50 mM) at 25 °C, under $N_2$. (A) $Et_2BOOEt$ + TCP + BnI + CHANT (experiment detailed in section 6.5.10). (B) $Et_2BOOEt$ + CHANT (experiment detailed in section 6.3.7). The reaction was followed $^{11}B$ NMR using the initial concentration as reference and measurements were taken at the indicated timestamps.*

Our investigation into the mechanism of $Et_2BOOEt$ initiated ATRA to TCP has yielded significant insights. Contrary to our initial hypothesis, we found no evidence suggesting that TCP or the target chain increases the initiating ability of $Et_2BOOEt$. This observation suggests that the remarkable initiation efficiency may be an intrinsic property of $Et_2BOOEt$ itself. Despite this, we approach this conclusion with caution. Our attempts to initiate more efficient chains such as ATRA of alkyl iodides to acetylenes, with $Et_2BOOEt$ decomposition alone have consistently been unsuccessful. This outcome aligns with the known low radical yield from $Et_2BOOEt$ decomposition. Therefore it seems improbable that the current chain, previously characterised as less efficient, would exhibit such good results solely with $Et_2BOOEt$ initiation. Moreover, given the reported interactions between TCP and alkyl boranes in section 4.4.4, and considering the chemical resemblance between $Et_3B$ and $Et_2BOOEt$, one might anticipate a similar reactivity pattern with $Et_2BOOEt$.

In light of these findings, we propose that either $Et_2BOOEt$ is solely responsible for the initiation process, or the combination of TCP/BnI plays a role in enhancing the initiating efficiency of $Et_2BOOEt$.

Alternatively, it could be that the chain propagates slowly but it is very efficient. This could explain why it does not work with $Et_3B/O_2$, but works with $Et_2BOOEt$. Further research is needed to elucidate these mechanisms.

### 4.4.7. Conclusions Atom Transfer Radical Addition to TCP

This section's objective was to determine the feasibility of using $Et_3B/Et_2BOOEt/N_2$ to initiate ATRA reactions to TCP, particularly those that are difficult to start with $Et_3B$ alone. Our experiments successfully initiated these challenging reactions, achieving yields as high as 71%.

During our research, we uncovered a novel reaction between TCP and $Et_3B$. The mechanistic studies, coupled with the new radical trapping technique, allowed us to suggest a plausible mechanism for this reaction. However, the products of this reaction were not directly characterised.

Furthermore, our research indicates that $Et_2BOOEt$ might be a superior initiator on its own for this reaction. We observed a dramatic increase in yield from 0% to 90%. However, it is not yet clear if this remarkable yield is exclusively due to the initiation by $Et_2BOOEt$ or if there is an underlying interaction with one or more system components enhancing the initiation process. Further research is necessary to clarify this aspect.

## 4.5. Conclusions Chapter 4

In this study, we have established that the radicals generated in the reaction between $Et_3B$ and $Et_2BOOEt$ can function as an effective radical initiator. This novel initiation system employs the same chemicals as the conventional $Et_3B/O_2$ method but introduces several significant advantages. These include a homogeneous initiation, which ensures reproducible reaction conditions, high radical flux, and inert atmosphere. The disadvantage is that $Et_2BOOEt$ needs to be formed prior to initiation. Also, as the initiation is a second order process, the initiator is best added in batches.

The previous chapter outlined a kinetic model predicting this enhanced initiation. The empirical data presented herein corroborates these predictions, thereby providing experimental validation for our kinetic model. This, in turn, corroborates the theoretical principles behind the model.

Unexpectedly, we discovered that $Et_2BOOEt$ can act as a potent radical initiator in ATRA of alkyl iodides to TCP. This serendipitous finding prompts further investigation into the reactivity of $Et_2BOOEt$, potentially offering a novel initiation mechanism when $Et_3B$ is rendered ineffective, as evidenced by the superior yields documented in our experiments.

## 5. Conclusions

This thesis aimed to elucidate the initiation mechanism of $Et_3B$ using the newly developed allyl-TEMPO radical traps. By systematically exploring the radical intermediates, reaction kinetics, and secondary initiation processes, we aimed to establish a comprehensive model that would enhance the efficiency of radical generation. This research has expanded our understanding of $Et_3B/O_2$ initiation systems, offering significant insights into both primary and secondary initiation mechanisms.

Our studies revealed that the reaction between $Et_3B$ and air generates primarily ethyl radicals (Et·), with ethoxyl (EtO·) and ethylperoxyl (EtOO·) radicals playing a smaller role. We observed that the reaction between $Et_3B$ and $O_2$ rapidly depletes oxygen from the environment, but oxidation products continue to form even in the absence of $O_2$. This observation led us to suspect an additional radical-generating reaction independent of $O_2$. To further investigate this phenomenon, we synthesized $Et_2BOOEt$ and conducted a quantitative mechanistic study on its reactivity.

We aimed to understand the role of $Et_2BOOEt$ in the $Et_3B/O_2$ initiation system. Our research indicated that the homolysis of $Et_2BOOEt$ is not an efficient radical generator. Instead, we proposed that $Et_2BOOEt$ undergoes heterolytic rearrangement, with only a minor component of peroxide homolysis. Despite this, we discovered a secondary initiation process within $Et_3B$ autoxidation, where the reaction between $Et_3B$ and $Et_2BOOEt$ generates ethyl radicals. This molecule-assisted homolysis is rapid and efficient. Our kinetic model revealed that this secondary mechanism is a significant source of radicals in the $Et_3B/O_2$ system, particularly under low $O_2$ conditions.

We applied the insights gained from the mechanistic studies to synthetic reactions. We found that the novel initiation system using $Et_3B$ and $Et_2BOOEt$ offers several advantages over the traditional $Et_3B/O_2$ method. These include a homogeneous initiation environment, high radical flux, and an inert atmosphere. However, the formation of $Et_2BOOEt$ prior to initiation and the need for batch addition due to it being a second-order process are considerations to be managed. Our experimental data supported the kinetic model's predictions,

demonstrating the effectiveness of the secondary initiation mechanism and validating the newly proposed mechanism.

In conclusion, here we have successfully identified and characterised both the primary and secondary initiation mechanisms of $Et_3B$. The novel initiation system developed ($Et_3B/Et_2BOOEt/N_2$) has the potential to enhance the efficiency of $Et_3B$ initiation as well as the reproducibility of the reactions. Future research should explore the reactivity of $Et_2BOOEt$ as a radical initiator, potentially unlocking new pathways for radical initiation. This work lays a comprehensive understanding of $Et_3B/O_2$ initiation, providing a framework for future advancements in the field.

# 6. Experimental

## 6.1. General

Except where stated, all reagents and solvents were purchased from commercial sources and used without further purification. A full list of chemicals used is available in section 6.2. Anhydrous solvents were obtained from an Innovative Technology Inc. PureSolv® solvent purification system.

All chemical reactions and analyses were acquired at room temperature (293 K) unless stated otherwise. Thin layer chromatography was carried out on Merck silica gel 60F254 pre-coated aluminium foil sheets and were visualised using UV light (254 nm) or stained with basic aqueous potassium permanganate, as indicated. Flash column chromatography was carried out using slurry packed Fluka silica gel ($SiO_2$), 35–70 µm, 60 Å under a light positive pressure, eluting with the specified solvent system. Melting points were Stuart Scientific SMP3 apparatus and are uncorrected. $^{1}H$ and $^{13}C$ nuclear magnetic resonance (NMR) spectra were recorded in $CDCl_3$ (unless specified otherwise) on a JEOL ECX400 operating at 400 MHz. Chemical shifts (δ) are quoted in parts per million (ppm). The residual solvent peaks were used as references in $^{1}H$ and $^{13}C$[116] NMR spectroscopy were δH 7.26 ppm and δC 77.0 ppm respectively. Coupling constants (J) are reported in Hertz (Hz) to the nearest 0.1 Hz. The multiplicity abbreviations used are: s singlet, d doublet, t triplet, br broad, dd double doublet, dt double triplet, td triple doublet, ddd double double doublet and m multiplet. Signal assignment was achieved by analysis of DEPT, COSY, HMQC and HMBC experiments where required. Mass spectra synthesis products were recorded using positive electrospray ionisation (Pos ESI) on a Bruker compact QTOF MS (compact) mass spectrometer (±0.001 m/z precision, 30000 resolution), unless otherwise stated. Mass spectra of trapping reactions were recorded using positive electrospray ionisation (Pos ESI) on a high resolution solariX XR FTMS (solariX) mass spectrometer (±0.0001 m/z precision, $>10^7$ maximum resolution, mass accuracy 600 ppb (internal)), unless stated otherwise. The peroxides $Et_2BOOEt$ and $Bu_2BOOBu$ were used immediately after synthesis, or they were stored frozen in liquid $N_2$. EPR analysis were conducted using X-band measurements on a JEOL X320.

## 6.2. Chemicals

All chemicals in this list were used without further purification. 2,2,6,6-tetramethylpiperidine 1-oxyl (TEMPO, 98%, Fluorochem), pyrrolidine (99%, Sigma-Aldrich), sodium sulfite (≥98%, Sigma-Aldrich), O-(benzotriazol-1-yl)-N,N,N',N'-tetramethyluronium hexafluorophosphate (HBTU, 98%, Fluorochem), N,N-diisopropylethylamine (DIPEA, ≥99%, Fluorochem), sodium iodide (>99%, Thermo Scientific), methyl 2-(bromomethyl)acrylate (>97%, Fluorochem), cyclohexylamine (>98%, Alfa Aesar), triethylborane solution (1.0 M in THF, Sigma-Aldrich), triethylborane solution (1.0 M in hexane, Sigma-Aldrich), tributylborane solution (1.0 M in THF, Sigma-Aldrich), benzyl bromide (98%, Sigma-Aldrich), iodoethane (99%, Sigma-Aldrich), trimethylsilylacetylene (98%, Thermo Scientific), 2-iodopropane (>99%, Sigma Aldrich), phenylacetylene (98%, Sigma Aldrich), tris(trimethylsilyl)silane (97%, Sigma Aldrich), (2-iodoethyl)benzene (97%, Sigma Aldrich), 2-iodopyridine (98%, Sigma Aldrich), 4-iodobenzotrifluoride (97%, Sigma Aldrich), 1,1-dibromo-2,2-bis(chloromethyl)cyclopropane (90%, Sigma Aldrich), phenyllithium solution (1.9 M in dibutyl ether, Sigma Aldrich), 1,2-dichloroethane anhydrous (99.8%, Sigma Aldrich) sodium hydroxide (98%, Thermo Scientific), formaldehyde solution (37 wt% in water, Thermo Scientific), 2-propylmalonic acid (≥98%, Chemscene).

Water (LC-MS grade, ≥99.9%, Fischer Chemical), acetonitrile (LC-MS grade, ≥99.9%, Fischer Chemical), formic acid (LC-MS grade, ≥99%, Fischer Chemical), were used for MS characterisation without further purification.

## 6.3. Radical trapping Experiments

### 6.3.1. Radical Trapping of $Et_3B/O_2$ Method 1

CHANT (1.5 mg, 0.1 eq., 0.005 mmol) was weighed in an 8 mL vial. The solid was dissolved in THF (1 mL, 0.05 M). A solution of 1M $Et_3B$ in THF (0.05 mL, 1 eq., 0.05 mmol) was added. The solution was sealed and left stirring under air for 2 h. An aliquot of 10 µL was extracted and diluted in 2 mL of MS solvent 1 (1:1 MeCN/$H_2O$, 0.1% formic acid) and the solution was analysed by MS following MS protocol detailed in section 6.10.1.

### 6.3.2. Radical Trapping of $Et_3B/O_2$ Method 2

CHANT (1.5 mg, 0.1 eq., 0.005 mmol) was weighed in an 8 mL vial. The solid was dissolved in DCM (1 mL, 0.05 M). A solution of 1M $Et_3B$ in THF (0.05 mL, 1 eq., 0.05 mmol) was added. The solution was sealed and left stirring under air for 2 h. An aliquot of 10 µL was extracted and diluted in 2 mL of MS solvent 1 (1:1 MeCN/$H_2O$, 0.1% formic acid) and the solution was analysed by MS following MS protocol detailed in section 6.10.1.

### 6.3.3. Radical Trapping of $Et_3B/O_2$ Method 3

CHANT (5 mg, 0.32 eq., 0.016 mmol) was weighed in an 8 mL vial. The solid was dissolved in DCM (1 mL, 0.05 M). A solution of 1M $Et_3B$ in THF (0.05 mL, 1 eq., 0.05 mmol) was added. The solution was sealed and left stirring under air for 2 h. An aliquot of 10 µL was extracted and diluted in 2 mL of MS solvent 1 (1:1 MeCN/$H_2O$, 0.1% formic acid) and the solution was analysed by MS following MS protocol detailed in section 6.10.1.

### 6.3.4. Radical Trapping of $Et_3B/O_2$ Method 4

CHANT (5 mg, 0.32 eq., 0.016 mmol) was weighed in an 8 mL vial. The solid was dissolved in DCM (1 mL, 0.05 M). A solution of 1M $Et_3B$ in THF (0.05 mL, 1 eq., 0.05 mmol) was added. The

solution was sealed and left stirring under air for 2 h. An aliquot of 10 µL was extracted and diluted in 2 mL of MS solvent 2 (MeCN, 0.1% formic acid) and the solution was analysed by MS following MS protocol detailed in section 6.10.1.

### 6.3.5. Radical Trapping of $Et_3B/O_2$ Method 5

**Control**

1M $Et_3B$ in THF (0.05 mL, 0.05 mmol) was dissolved in anhydrous and degassed DCM (1 mL) in an 8 mL glass vial inside the glovebox. CHANT (5.2 mg, 0.016 mmol) was dissolved in degassed DCM (1 mL) and it was added to the solution. The reaction was left for 1 h without stirring. TEMPO (78 mg, 0.5 mmol) was added to the solution. An aliquot of 10 µL was extracted and diluted in 2 mL of degassed MS solvent 2 (MeCN, 0.1% formic acid) and the solution was analysed by MS following MS protocol detailed in section 6.10.1.

**Sample**

1M $Et_3B$ in THF (0.05 mL, 0.05 mmol) was dissolved in anhydrous and degassed DCM (1 mL) in an 8 mL glass vial inside the glovebox. The mixture was sealed and taken outside the glovebox and air was bubbled through it for 4 seconds. $N_2$ was bubbled through the solution for 15 seconds, CHANT (5.2 mg, 0.016 mmol) was dissolved in DCM (1 mL), purged with $N_2$, added to the reaction mixture and it was left for 1 h under $N_2$ without stirring. TEMPO (78 mg, 0.5 mmol) was added to the solution under $N_2$. An aliquot of 10 µL was extracted and diluted in 2 mL of degassed MS solvent 2 (MeCN, 0.1% formic acid) and the solution was analysed by MS following MS protocol detailed in section 6.10.1.

### 6.3.6. Radical Trapping of $Bu_3B/O_2$

CHANT (5.2 mg, 0.32 eq., 0.016 mmol) was weighed in an 8 mL vial. The solid was dissolved in DCM (1 mL, 0.05 M). A solution of 1M $Bu_3B$ in THF (0.05 mL, 1 eq., 0.05 mmol) was added. The solution was sealed and left stirring under air for 2 h. An aliquot of 10 µL was extracted and diluted in 2 mL of MS solvent 1 (1:1 MeCN/$H_2O$, 0.1% formic acid) and the solution was analysed by MS following MS protocol detailed in section 6.10.1.

### 6.3.7. Radical Trapping of $Et_2BOOEt$ Decomposition

25 mM $Et_2BOOEt$ in hexane (1 mL, 0.025 mmol) was synthesised using the method described in section 6.8.2. The solution was brought inside the glove box and CHANT (8 mg, 0.025 mM) was added to the solution. The reaction was monitored by $^{11}B$ and $^{1}H$ NMR for 12h without stirring. After reaction completion the solution was analysed by MS following MS protocol detailed in section 6.10.1.

### 6.3.8. Radical Trapping of $Et_3B/Et_2BOOEt/N_2$

**Control**

1M $Et_3B$ in hexane (0.05 mL, 0.05 mmol) was dissolved in hexane (freeze-pump-thaw degassed) (1 mL) and CHANT (Table 29) was added under $N_2$. The solution was left stirring for 10 minutes and an aliquot of 10 µL was extracted and diluted in 2 mL of degassed MS solvent 1 (1:1 MeCN/$H_2O$, 0.1% formic acid) and the solution was analysed by MS following MS protocol detailed in section 6.10.1.

**Sample**

50 mM $Et_2BOOEt$ in hexane (1 mL, 0.05 mmol) was synthesised following the procedure described in section 6.8.2. The solution was brought inside the glovebox, and 1M $Et_3B$ in hexane (0.05 mL, 0.05 mmol) and CHANT (Table 29) were added under $N_2$. The solution was left stirring for 40 minutes and the reaction was analysed by $^{1}H$ and $^{11}B$ NMR. An aliquot of 10 µL was extracted and diluted in 2 mL of degassed MS solvent 1 (1:1 MeCN/$H_2O$, 0.1% formic acid) and the solution was analysed by MS following MS protocol detailed in section 6.10.1.

*Table 29. Different concentrations of CHANT used in the experiment detailed in section 6.3.8.*

| Entry | CHANT / mmol |
|---|---|
| 1 | 0.005 |

| | |
|---|---|
| 2 | 0.05 |

### 6.3.9. Radical Trapping of $Bu_3B/Et_2BOOEt/N_2$

**Control**

1M $Et_3B$ in hexane (0.05 mL, 0.05 mmol) was dissolved in hexane (freeze-pump-thaw degassed) (1 mL) and CHANT (16 mg, 0.05 mmol) was added under $N_2$. The solution was left stirring for 10 minutes and an aliquot of 10 µL was extracted and diluted in 2 mL of degassed MS solvent 1 (1:1 MeCN/$H_2O$, 0.1% formic acid) and the solution was analysed by MS following MS protocol detailed in section 6.10.1.

**Sample**

50 mM $Et_2BOOEt$ in hexane (1 mL, 0.05 mmol) was synthesised using the method described in section 6.8.2. The solution was brought inside the glove box and 1.11M $Bu_3B$ in hexane (0.045 mL, 0.05 mmol) was added to the solution. CHANT (16 mg, 0.05 mmol) was added, and the reaction was left reacting inside the NMR tube for 2 h without stirring. The reaction was analysed $^1H$ and $^{11}B$ NMR. An aliquot of 10 µL was extracted and diluted in 2 mL of degassed MS solvent 1 (1:1 MeCN/$H_2O$, 0.1% formic acid) and the solution was analysed by MS following MS protocol detailed in section 6.10.1.

### 6.3.10. Radical Trapping of $Et_3B$/High $O_2$ Regime

CHANT (16 mg, 0.05 mmol) was dissolved in hexane (1 mL). The solution was stirred open to air for 3 min. 1M $Et_3B$ in hexane (0.05 mL, 0.05 mmol) was added to the solution, needle tip into the solution. The solution was left stirring for 1.5 h and then analysed by $^1H$ NMR. An aliquot of 10 µL was extracted and diluted in 2 mL of degassed MS solvent 1 (1:1 MeCN/$H_2O$, 0.1% formic acid) and the solution was analysed by MS following MS protocol detailed in section 6.10.1.

### 6.3.11. Radical Trapping of $Et_3B$/Low $O_2$ Regime

CHANT (16 mg, 0.05 mmol) was dissolved in hexane (1 mL) and transferred into a Young's tap NMR Tube. The solution was degassed using-freeze-pump thaw. The NMR was brought inside the glovebox and 1M $Et_3B$ in hexane (0.05 mL, 0.05 mmol) was added. The sealed NMR was taken outside the glovebox, and degassed by freeze-pump-thaw leaving the headspace under $10^{-2}$ mbar pressure. Air was let into the headspace by opening the lid of the NMR tube and the tube was sealed again. The reaction was followed by $^{11}B$ and $^{1}H$ NMR over 16 h without stirring. An aliquot of 10 µL was extracted and diluted in 2 mL of degassed MS solvent 1 (1:1 MeCN/$H_2O$, 0.1% formic acid) and the solution was analysed by MS following MS protocol detailed in section 6.10.1.

### 6.3.12. Radical Trapping of $Et_3B$/TCP under $N_2$

1 M TCP in $Et_2O$ (0.33 mL, 0.33 mmol) was transferred to a young's tap NMR tube. The solution was degassed via freeze pump thaw and brought into the glovebox. CHANT (16 mg, 0.025 mmol) and 1M $Et_3B$ in hexane (0.33 ml, 0.33 mmol) was added. The solution was taken outside the glovebox and the reaction was followed by $^{11}B$ and $^{1}H$ NMR without stirring. At the end of the reaction the solution was brought back inside the glovebox and an aliquot of 10 µL was extracted and diluted in 2 mL of MS solvent 1 (1:1 MeCN/$H_2O$, 0.1% formic acid) and the solution was analysed by MS following MS protocol detailed in section 6.10.1.

### 6.3.13. Radical Trapping of $Et_2BOOEt$/TCP under $N_2$

25 mM $Et_2BOOEt$ in hexane (1 mL, 0.025 mmol) was prepared following method described in section 6.8.2. 1 M TCP in $Et_2O$ (0.33 mL, 0.33 mmol) was added to the solution and it was degassed via freeze pump thaw and brought into the glovebox. CHANT (16 mg, 0.025 mmol) was added under $N_2$, and the solution was taken outside the glovebox and the reaction was followed by $^{11}B$ and $^{1}H$ NMR without stirring. At the end of the reaction the solution was brought back inside the glovebox and an aliquot of 10 µL was extracted and diluted in 2 mL of MS solvent 1 (1:1 MeCN/$H_2O$, 0.1% formic acid) and the solution was analysed by MS following MS protocol detailed in section 6.10.1.

### 6.3.14. Radical Trapping of $Et_2BOOEt$ Initiated ATRA of Benzyl Iodide to TCP under $N_2$

25 mM $Et_2BOOEt$ in hexane (1 mL, 0.025 mmol) was prepared following method described in section 6.8.2. Benzyl iodide (54 mg, 0.25 mmol) and TCP 1 M in $Et_2O$ (0.33 mL, 0.33 mmol) were added to the solution and it was degassed via freeze pump thaw and brought into the glovebox. CHANT (16 mg, 0.025 mmol) was added under $N_2$, and the solution was taken outside the glovebox and the reaction was followed by $^{11}B$ and $^{1}H$ NMR without stirring. At the end of the reaction the solution was brought back inside the glovebox and an aliquot of 10 µL was extracted and diluted in 2 mL of MS solvent 1 (1:1 MeCN/$H_2O$, 0.1% formic acid) and the solution was analysed by MS following MS protocol detailed in section 6.10.1.

## 6.4. MS Experiments

### 6.4.1. APCI of $Bu_3B/Bu_2BOOEt$

50 mM $Bu_2BOOBu$ in hexane (1 mL, 0.05 mmol) was synthesised following the procedure described in section 6.8.3. The solution was transferred to Young's tap NMR tube, and it was degassed by bubbling Ar for 30 seconds followed by freeze-pump-thaw. The solution was analysed by $^{11}B$ and $^{1}H$ NMR. The solution was brought inside the glovebox and 1.11M $Bu_3B$ in hexane (0.045 mL, 0.05 mmol) was added to the solution. The reaction was left reacting without stirring and analysed by $^{11}B$ and $^{1}H$ NMR, and APCI-MS after completion following MS protocol detailed in section 6.10.2.

## 6.5. Reaction Kinetics by NMR

### 6.5.1. Kinetics of $Et_3B/O_2$ reaction in the Presence of TEMPO

A solution of 0.1 mM TEMPO in anhydrous and degassed DCM (2 mL, 0.2 µmol) was prepared inside the glovebox under $N_2$. 1M $Et_3B$ in THF (0.001 mL, 10 µmol) was measured with a Hamilton syringe and added to the solution. The solution was transferred to a Young's tap NMR tube and taken outside the glovebox. Air was bubbled through it for 10 seconds and

argon was quickly bubbled through the solution for 20 seconds. The NMR tube was sealed, and the reaction was followed by $^{11}B$ NMR without stirring until reaction completion (40 minutes).

### 6.5.2. Kinetics of Partially Oxidised $Et_3B$ under $N_2$

1M $Et_3B$ in hexane (0.05 ml, 0.05 mmol) was dissolved in anhydrous and degassed hexane (1 mL) in an 8 mL glass vial inside the glovebox. The mixture was transferred into a Young's tap NMR tube, taken outside the glovebox and air was bubbled through it for 4 seconds. $N_2$ was bubbled through the solution for 15 seconds, and the NMR tube was sealed, and the solution was followed by $^{11}B$ and $^{1}H$ NMR without stirring.

### 6.5.3. Kinetics of $Et_2BOOEt$ Decomposition under $N_2$

50 mM $Et_2BOOEt$ in hexane (2 mL, 0.1 mmol) was synthesised using the method described in section 6.8.2. and the reaction was followed by $^{1}H$ and $^{11}B$ NMR without stirring.

### 6.5.4. Kinetics of $Et_3B/Et_2BOOEt$ reaction in hexane under $N_2$

50 mM $Et_2BOOEt$ in hexane (2 mL, 0.1 mmol) was synthesised following the procedure described in section 6.8.2. An aliquot of the solution (Table 30) was diluted in hexane making up to 1 mL. The diluted solution was transferred to Young's tap NMR tube and it was degassed by bubbling Ar for 30 seconds followed by freeze-pump-thaw. The solution was analysed by $^{11}B$ and $^{1}H$ NMR. The solution was brought inside the glovebox and 1M $Et_3B$ in hexane (Table 30) was added to the solution. The solution was taken outside the glovebox and the reaction was followed by $^{11}B$ and $^{1}H$ NMR without stirring. Once the kinetic run was finished, triethoxyborane (8.5 µL, 0.050 mmol, 2 eq.) was added as internal standard.

*Table 30. Different amounts of $Et_3B$ and $Et_2BOOEt$ used in the experiment detailed in section 6.5.4.*

| Entry | $Et_3B$ | $Et_2BOOEt$ |
|---|---|---|
| 1 | 25 µL (25 µmol) | 0.5 mL (25 µmol) |
| 2 | 12.5 µL (12.5 µmol) | 0.5 mL (25 µmol) |
| 3 | 25 µL (25 µmol) | 0.25 mL (12.5 µmol) |
| 4 | 12.5 µL (12.5 µmol) | 0.25 mL (12.5 µmol) |

### 6.5.5. Kinetics of $Et_3B/Et_2BOOEt$ in Different Solvents under $N_2$

25 mM $Et_2BOOEt$ in hexane (1 mL, 0.025 mmol) was synthesised following the procedure described in section 6.8.2. Solvent (0.4 mL) (Table 31) was added to the solution and it was degassed by bubbling Ar for 30 seconds followed by freeze-pump-thaw. The solution was brought inside the glovebox and 1M $Et_3B$ in hexane (0.025mL, 0.025 mmol) was added to the solution. The solution was taken outside the glovebox and the reaction was followed by $^{11}B$ and $^{1}H$ NMR without stirring.

*Table 31. Different solvents used in the experiment detailed in section 6.5.5.*

| Entry | Solvent |
|---|---|
| 1 | Hexane |
| 2 | $Et_2O$ |
| 3 | DCM |
| 4 | Toluene |

### 6.5.6. Kinetic Run of $Et_3B/Et_2BOOEt/N_2$ Initiated ATRA of Benzyl Iodide to TCP

25 mM $Et_2BOOEt$ in hexane (1 mL, 0.025 mmol) was prepared following method described in section 6.8.2. Benzyl iodide (54 mg, 0.25 mmol) and 1M TCP in $Et_2O$ (0.33 mL, 0.33 mmol)

were added to the solution containing $E_2BOOEt$. The solution was degassed via freeze pump thaw and brought into the glovebox and 1M $Et_3B$ in hexane (0.025 mL, 0.025 mmol) was added. The solution was taken outside the glovebox and the reaction was followed by $^{11}B$ and $^{1}H$ NMR without stirring.

### 6.5.7. Kinetic Run of $Et_3B/Et_2BOOEt/N_2$ in the Presence of Benzyl Iodide

25 mM $Et_2BOOEt$ in hexane (1 mL, 0.025 mmol) was prepared following method described in section 6.8.2. Benzyl iodide (54 mg, 0.25 mmol) was added to the solution. The solution was degassed via freeze pump thaw and brought into the glovebox and 1M $Et_3B$ in hexane (0.025 mL, 0.025 mmol) was added. The solution was taken outside the glovebox and the reaction was followed by $^{11}B$ and $^{1}H$ NMR without stirring.

### 6.5.8. Kinetic Run of $Et_3B/Et_2BOOEt/N_2$ in the Presence of TCP

25 mM $Et_2BOOEt$ in hexane (1 mL, 0.025 mmol) was prepared following method described in section 6.8.2. 1M TCP in $Et_2O$ (0.33 mL, 0.33 mmol) was added to the solution. The solution was degassed via freeze pump thaw and brought into the glovebox and 1M $Et_3B$ in hexane (0.025 mL, 0.025 mmol) was added. The solution was taken outside the glovebox and the reaction was followed by $^{11}B$ and $^{1}H$ NMR without stirring.

### 6.5.9. Kinetic Run of $Et_3B$/TCP under $N_2$

1M TCP in $Et_2O$ (0.33 mL, 0.33 mmol) was transferred to a young's tap NMR tube. The solution was degassed via freeze pump thaw and brought into the glovebox and 1M $Et_3B$ in hexane (0.33 mL, 0.33 mmol) was added. The solution was taken outside the glovebox and the reaction was followed by $^{11}B$ and $^{1}H$ NMR without stirring.

### 6.5.10. Kinetic Run of $Et_2BOOEt$ Initiated ATRA of Benzyl Iodide to TCP under $N_2$

25 mM $Et_2BOOEt$ in hexane (1 mL, 0.025 mmol) was prepared following method described in section 6.8.2. Benzyl iodide (54 mg, 0.25 mmol) and 1M TCP in $Et_2O$ (0.33 mL, 0.33 mmol) were added to the solution and it was degassed via freeze pump thaw and the reaction was followed by $^{11}B$ and $^{1}H$ NMR without stirring.

## 6.6. EPR Experiments

### 6.6.1. EPR of $Et_3B/O_2$ in the Presence of TEMPO

All the materials for the sample preparation were introduced in the glovebox and the samples were prepared inside the glovebox under $N_2$. All the solvents used were anhydrous and degassed via freeze-pump-thaw. A solution of 1mM TEMPO in hexane (Table 32) was dissolved in DCM (2 mL) inside an 8 mL glass vial. A solution of 1M $Et_3B$ in THF (Table 32) was measured in a Hamilton syringe and added to the solution containing TEMPO. The solution was transferred to an EPR cell, and the cell was sealed and brought outside the glovebox. Air was bubbled through the solution for 4-6 seconds and the cell was sealed again, and the sample was analysed by EPR. The solution was left reacting without stirring and measurements were taken every minute during the course of 2 hours.

*Table 32. Different amounts of a solution of 1mM TEMPO in DCM and 1M $Et_3B$ in THF used in the experiment detailed in section 6.6.1.*

| Entry | TEMPO | $Et_3B$ / µmol |
|---|---|---|
| 1 | 0.06 mL (0.06 µmol) | 0.02 mL (20 µmol) |
| 2 | 0.2 mL (0.2 µmol) | 0.01 mL (10 µmol) |

### 6.6.2. EPR of a Partially Oxidised Solution of $Et_3B$ in the Presence of TEMPO under $N_2$

All the materials for the sample preparation were introduced in the glovebox and the samples were prepared inside the glovebox under $N_2$. All the solvents used were anhydrous and

degassed via freeze-pump-thaw. TEMPO (0.5 µmol) was dissolved in DCM (2 mL) inside an 8 mL glass vial. A solution of 1M $Et_3B$ in THF (0.05 mmol) was measured in a Hamilton syringe and added to the solution containing TEMPO. The solution was transferred to an EPR cell, and the cell was sealed and brought outside the glovebox. Air was bubbled through the solution for 4-6 seconds and the cell was sealed again, and the sample was analysed by EPR. The solution was left reacting without stirring and measurements were taken every minute during the course of 95 minutes. $N_2$ was then bubbled though the solution, the cell was sealed under $N_2$ and analysed by EPR taking measurements every minute for 40 minutes.

### 6.6.3. EPR of $Et_3B/Et_2BOOEt/N_2$

25 mM $Et_2BOOEt$ in hexane (1 mL, 0.025 mmol) was prepared following method described in section 6.8.2. The solution was brought inside the glovebox, and 1M $Et_3B$ in hexane (0.025 mmol) was added under $N_2$. The solution was transferred to an EPR tube, sealed under $N_2$ and immediately analysed by EPR.

## 6.7. $Et_3B$ Initiation Reactions

### 6.7.1. ATRA of Ethyl Iodide to TMS Acetylene Optimisation

$Et_2BOOEt$ (Table 33) was prepared in a solution of hexane (1 mL) following method described in section 6.8.2. Acetylene and alkyl iodide (Table 33) were added to the solution. The solution was degassed via freeze pump thaw and brought into the glovebox and 1M $Et_3B$ in hexane (Table 33) was added and left reacting overnight without stirring at T (Table 33).

*Table 33. Different conditions used in the experiment detailed in section 6.7.1.*

| Entry | TMS acetylene (µmol) | EtI (µmol) | $Et_3B$ (µmol) | $Et_2BOOEt$ (µmol) | T | Yield[a] (%) | E/Z |
|---|---|---|---|---|---|---|---|
| 1 | 250 | 50 | 25 | 25 | rt | 27 | 0/100 |

| | | | | | | | |
|---|---|---|---|---|---|---|---|
| 2 | 300 | 250 | 25 | 25 | rt | 11 | 0/100 |
| 3 | 300 | 250 | 50 | 50 | rt | 14 | 0/100 |
| 4 | 300 | 250 | 25 | 25 | 0 °C | 1 | 0/100 |
| 5 | 125 | 12.5 | 25 | 25 | rt | 47 | 0/100 |
| 6 | 62.5 | 12.5 | 25 | 25 | rt | 28 | 0/100 |
| 7 | 250 | 50 | 50 | 50 | rt | **96** | 0/100 |

### 6.7.2. ATRA of Ethyl Iodide to TMS Acetylene with Different Initiating Methods

**$Et_3B/Et_2BOOEt/N_2$ initiation**

50 mM $Et_2BOOEt$ in hexane (1 mL, 0.05 mmol) was prepared following method described in section 6.8.2. TMS acetylene (24.5 mg, 0.25 mmol) and EtI (7.8 mg, 0.05 mmol) were added to the solution. The solution was degassed via freeze pump thaw and brought into the glovebox and 1M $Et_3B$ in hexane (0.05 mL, 0.05 mmol) was added and left reacting overnight without stirring at room temperature. After reaction completion, 1,2-dichloroethane (5 µL, 63.3 µmol) was added as internal standard and the solution was analysed by $^{11}B$ and $^{1}H$ NMR. $^{1}H$ NMR yield 96%.

**$Et_3B$/Low $O_2$ initiation**

TMS acetylene (24.5 mg, 0.25 mmol) and EtI (7.8 mg, 0.05 mmol) were dissolved in hexane (1 mL). The solution was degassed via freeze pump thaw, brought into the glovebox and 1M $Et_3B$ in hexane (0.05 mL, 0.05 mmol) was added. The solution was degassed via freeze pump thaw leaving the headspace under $10^{-2}$ mbar pressure and it was analysed by $^{11}B$ and $^{1}H$ NMR. Air was allowed into the headspace and the reaction was monitored by $^{11}B$ and $^{1}H$ NMR without stirring until reaction completion. After reaction completion, 1,2-dichloroethane (5 µL, 63.3 µmol) was added as internal standard and the solution was analysed by $^{11}B$ and $^{1}H$ NMR. $^{1}H$ NMR yield 28%.

**$Et_3B$/High $O_2$ initiation**

TMS acetylene (24.5 mg, 0.25 mmol) and EtI (7.8 mg, 0.05 mmol) were dissolved in hexane (1 mL) 1M $Et_3B$ in hexane (0.05 mL, 0.05 mmol) was added. The solution stirred open to air for 15 minutes and the reaction was analysed by $^1H$ and $^{11}B$ NMR. No measurable product formation was observed.

### 6.7.3. ATRA of Isopropyl Iodide to Phenylacetylene Optimisation

$Et_2BOOEt$ (Table 34) was prepared in a solution of hexane (1 mL) following method described in section 6.8.2. Acetylene and alkyl iodide (Table 34) were added to the solution. The solution was degassed via freeze pump thaw and brought into the glovebox and 1M $Et_3B$ in hexane (Table 34) was added and the solution was left reacting overnight without stirring at T (Table 34). After reaction completion the solution was analysed by $^{11}B$ and $^1H$ NMR. $^1H$ NMR.

*Table 34. Different conditions and yields for the experiment detailed in section 6.7.3.*

| Entry | Phenylacetylene (µmol) | $^iPrI$ (µmol) | $Et_3B$ (µmol) | $Et_2BOOEt$ (µmol) | Yield (%) | E/Z |
|---|---|---|---|---|---|---|
| 1 | 250 | 50 | 50 | 50 | 12 | 55/45 |
| 2 | 50 | 200 | 25 | 25 | 24 | 50/50 |
| 3 | 50 | 200 | 50 | 50 | **56** | 37/63 |

### 6.7.4. ATRA of Isopropyl Iodide to Phenylacetylene with Different Initiating Methods

**$Et_3B/Et_2BOOEt/N_2$ initiation**

50 mM $Et_2BOOEt$ in hexane (1mL, 0.05 mmol) was prepared following method described in section 6.8.2. Phenylacetylene (5.1 mg, 0.05 mmol) and iPrI (34 mg, 0.2 mmol) were added to the solution. The solution was degassed via freeze pump thaw and brought into the glovebox and 1M $Et_3B$ in hexane (0.05 mL, 0.05 mmol) was added and left reacting overnight without stirring at room temperature. After reaction completion, 1,2-dichloroethane (5 µL, 63.3 µmol)

was added as internal standard and the solution was analysed by $^{11}B$ and $^{1}H$ NMR. $^{1}H$ NMR yield 56%.

**$Et_3B$/Low $O_2$ initiation**

Phenylacetylene (5.1 mg, 0.05 mmol) and iPrI (34 mg, 0.2 mmol) were dissolved in hexane (1 mL). The solution was degassed via freeze pump thaw, brought into the glovebox and 1M $Et_3B$ in hexane (0.05 mL, 0.05 mmol) was added. The solution was degassed via freeze pump thaw leaving the headspace under $10^{-2}$ mbar pressure and it was analysed by $^{11}B$ and $^{1}H$ NMR. Air was allowed into the headspace and the reaction was monitored by $^{11}B$ and $^{1}H$ NMR without stirring until reaction completion. After reaction completion, 1,2-dichloroethane (5 µL, 63.3 µmol) was added as internal standard and the solution was analysed by $^{11}B$ and $^{1}H$ NMR. $^{1}H$ NMR yield 22%.

**$Et_3B$/High $O_2$ initiation**

Phenylacetylene (5.1 mg, 0.05 mmol) and iPrI (34 mg, 0.2 mmol) were dissolved in hexane (1 mL) open to air. 1M $Et_3B$ in hexane (0.05 mL, 0.05 mmol) was added and the reaction was left stirring for 30 minutes. 1,2-Dichloroethane (5 µL, 63.3 µmol) was added as internal standard, and the solution was analysed by $^{11}B$ and $^{1}H$ NMR. $^{1}H$ NMR yield 1%.

### 6.7.5. ATRA of Tris(trimethylsilyl)silane to Phenylacetylene with Different Initiating Methods

**$Et_3B$/$Et_2BOOEt$/$N_2$ initiation**

25 mM $Et_2BOOEt$ in hexane (1 mL, 0.025 mmol) was prepared following method described in section 6.8.2. Phenylacetylene (5.1 mg, 0.05 mmol) and tris(trimethylsilyl)silane (24.9 mg, 0.1 mmol) were added to the solution. The solution was degassed via freeze pump thaw and brought into the glovebox and 1M $Et_3B$ in hexane (0.025 mL, 0.025 mmol) was added and left reacting overnight without stirring at room temperature. After reaction completion, 1,2-dichloroethane (5 µL, 63.3 µmol) was added as internal standard and the solution was analysed by $^{11}B$ and $^{1}H$ NMR. $^{1}H$ NMR yield 96%.

**$Et_3B$/Low $O_2$ initiation**

Phenylacetylene (5.1 mg, 0.05 mmol) and tris(trimethylsilyl)silane (24.9 mg, 0.1 mmol) were dissolved in hexane (1 mL). The solution was degassed via freeze pump thaw, brought into the glovebox and 1M $Et_3B$ in hexane (0.025 mL, 0.025 mmol) was added. The solution was degassed via freeze pump thaw leaving the headspace under $10^{-2}$ mbar pressure and it was analysed by $^{11}B$ and $^{1}H$ NMR. Air was allowed into the headspace and the reaction was monitored by $^{11}B$ and $^{1}H$ NMR without stirring until reaction completion. After reaction completion, 1,2-dichloroethane (5 µL, 63.3 µmol) was added as internal standard and the solution was analysed by $^{11}B$ and $^{1}H$ NMR. $^{1}H$ NMR yield 88%.

**$Et_3B$/High $O_2$ initiation**

Phenylacetylene (5.1 mg, 0.05 mmol) and tris(trimethylsilyl)silane (24.9 mg, 0.1 mmol) were dissolved in hexane (1 mL) open to air. 1M $Et_3B$ in hexane (0.025 mL, 0.025 mmol) was added and the reaction was left stirring for 30 minutes. 1,2-Dichloroethane (5 µL, 63.3 µmol) was added as internal standard and the solution was analysed by $^{11}B$ and $^{1}H$ NMR. $^{1}H$ NMR yield 30%.

### 6.7.6. $Et_3B/O_2$ Initiated ATRA of Alkyl Iodides to TCP

To a screw-capped vial containing alkyl iodide (Table 35) (0.25 mmol) was added TCP 1 M in $Et_2O$ (0.33 mL, 0.33 mmol) The vial was capped and the mixture was stirred at 0 °C for 3 min. 1M $Et_3B$ in hexane (0.025 mL, 0.025 mmol) was then added to the solution via syringe (needle tip in the solution), and the mixture was stirred at 0 °C for 2 h in the dark.

*Table 35. Different alkyl iodides used for the experiment detailed in section 6.7.6.*

| Entry | Alkyl iodide |
|---|---|
| 1 | (2-iodoethyl)benzene |
| 2 | benzyl iodide |

### 6.7.7. $Et_3B/Et_2BOOEt/N_2$ Initiated ATRA of Alkyl Iodides to TCP

25 mM $Et_2BOOEt$ in hexane (1 mL, 0.025 mmol) was prepared following method described in section 6.8.2. Alkyl iodide (Table 36) (0.25 mmol) and 1M TCP in $Et_2O$ (0.33 mL, 0.33 mmol) were added to the solution containing $E_2BOOEt$. The solution was degassed via freeze pump thaw and brought into the glovebox and 1M $Et_3B$ in hexane (0.025 mL, 0.025 mmol) was added and left reacting in the NMR tube without stirring overnight at room temperature. The reaction was analysed by $^{11}B$ and $^{1}H$ NMR and yields were calculated using starting iodide as reference.

*Table 36. Different alkyl iodides used for the experiment detailed in section 6.7.7.*

| Entry | Alkyl iodide |
|---|---|
| 1 | (2-iodoethyl)benzene |
| 2 | benzyl iodide |
| 3 | 2-iodopyridine |
| 4 | 4-iodotrifluorotoluene |

### 6.7.8. $Et_2BOOEt$ Initiated ATRA of Alkyl Iodides to TCP under $N_2$

25 mM $Et_2BOOEt$ in hexane (1 mL, 0.025 mmol) was prepared following method described in section 6.8.2. Alkyl iodide (Table 37) (0.25 mmol) and 1M TCP in $Et_2O$ (0.33 mL, 0.33 mmol) were added to the NMR tube containing the solution of $Et_2BOOEt$. The solution was degassed via freeze pump thaw and the reaction was followed by $^{11}B$ and $^{1}H$ NMR without stirring.

*Table 37. Different alkyl iodides used for the experiment detailed in section 6.7.8.*

| Entry | Alkyl iodide |
|---|---|
| 1 | (2-iodoethyl)benzene |
| 2 | benzyl iodide |
| 3 | 2-iodopyridine |
| 4 | 4-iodotrifluorotoluene |

## 6.8. Synthesis

### 6.8.1. Optimisation of the Synthesis of $Et_2BOOEt$

1M $Et_3B$ in hexane (Table 38) was measured with a syringe inside the glovebox, the needle was sealed by piercing it into a suba-seal and it was taken outside the glovebox. hexane (2 mL) was measured into an 8 mL glass vial and air was slowly bubbled through it. The measured $Et_3B$ was injected into the solvent using a syringe pump over time (Table 38) at temperature (Table 38). The solution was transferred into a Young's tap NMR tube, purged with argon and analysed by $^{1}H$ and $^{11}B$ NMR.

*Table 38. Different conditions for the experiment detailed in section 6.8.1.*

| Entry | $Et_3B$ / µmol | Injection time / min | temperature / °C |
|---|---|---|---|
| 1 | 100 | 5 | 25 |
| 2 | 100 | 2 | 25 |
| 3 | 100 | 1 | 25 |
| 4 | 25 | 1 | 25 |
| 5 | 100 | 2 | 25 |
| 6 | 75 | 1.5 | 25 |
| 7 | 100 | 6.5 | -78 |

### 6.8.2. Synthesis of $Et_2BOOEt$

1M $Et_3B$ in hexane (0.1 mL, 0.1 mmol) was measured with a syringe inside the glovebox, the needle was sealed by piercing it into a suba-seal and it was taken outside the glovebox. hexane (2 mL) was measured into an 8 mL glass vial and air was slowly bubbled through it. The solvent was cooled down to –78 °C using an acetone/dry ice bath. The measured $Et_3B$ was injected into the solvent using a syringe pump (needle tip into the solvent) over 6.5 minutes at –78 °C. The solution was transferred into a Young's tap NMR tube, purged with

argon and degassed by freeze pump thaw giving the desired product $Et_2BOOEt$ as a 50 mM solution in hexane (96 % yield).

### 6.8.3. Synthesis of $Bu_2BOOBu$

1M $Bu_3B$ in THF (10 mL, 10 mmol) was transferred to a round bottomed flask under $N_2$. The flask was sealed, and the solvent was evaporated under Ar flow to yield a colourless oil. An aliquot of the oil (0.1 mL) was dissolved in 1 mL of hexane and $B(OEt)_3$ (29.2 mg, 0.2 mmol) was added as an internal standard and the solution was analysed by $^{11}B$ and $^{1}H$ NMR. The molarity of the solution of $Bu_3B$ in hexane was determined to be 1.11 M using $B(OEt)_3$ as internal standard.

An aliquot of the colourless oil (0.4 mL, 4.44 mmol) was diluted in 4 mL of degassed hexane inside the glovebox to give a solution 1.11 M $Bu_3B$ in hexane. An aliquot of this solution 1.11 M $Bu_3B$ in hexane (0.1 mL, 0.111 mmol) was measured with a syringe inside the glovebox, the needle was sealed by piercing it into a suba-seal and it was taken outside the glovebox. Hexane (2 mL) was measured into an 8 mL glass vial and air was slowly bubbled through it. The solvent was cooled down to −78 °C using an acetone/dry ice bath. The measured $Bu_3B$ was injected into the solvent using a syringe pump (needle tip into the solvent) over 6.5 minutes at −78 °C. The solution was transferred into a Young's tap NMR tube, purged with argon and degassed by freeze pump thaw and it was analysed by $^{11}B$ and $^{1}H$ NMR giving the desired product $Bu_2BOOBu$ as a 50 mM solution in hexane (96 % yield)

### 6.8.4. Synthesis of TCP[153]

To a flame-dried round-bottom flask (rbf) under $N_2$ equipped with a stirrer bar was added 1,1-dibromo-2,2-bis(chloromethyl)cyclopropane (5 g, 16.9 mmol). The reaction vessel was evacuated and back-filled with nitrogen three times, and then anhydrous $Et_2O$ (10 mL) was added. The reaction vessel was cooled to −45 °C (dry ice / isopropanol bath). Phenyllithium (17.8 mL, 1.9 M in $Bu_2O$, 33.7 mmol, 2.0 equiv.) was added dropwise over 15 min at –45 °C, and the resulting mixture was stirred for 15 min at −45 °C. The cooling bath was replaced with

an ice bath, and the reaction mixture was warmed to 0 °C, and then stirred at this temperature for 2 h.

The mixture was then distilled using a rotary evaporator. The rotary evaporator was washed thoroughly first with acetone and then $Et_2O$. The outlet was attached to a nitrogen line. The rotary evaporator was dried by putting small rbf on it and leaving it under vacuum for 20 minutes. The flask was back-filled with $N_2$, then put on pump down to evacuate, $N_2$ filling followed by evacuation was repeated 3 times before finally leaving it under $N_2$. The water bath was at room temperature and the receiving flask at −78 °C (immersed in a dry ice/acetone bath). The stirrer bar was removed from the reaction flask and the flask was put on the rotatory evaporator. The pressure was slowly brought down to around 200 mbar over 20 minutes and was left at that pressure for 20 more minutes. The TCP-containing distillate was then transferred in a flame-dried septum-sealed bottle under inert atmosphere, and stored at −20 °C. The yield was determined by $^1$H NMR spectroscopy with 1,2-dichloroethane as an internal standard. An aliquot of the solution of TCP (0.5 mL) was transferred to an NMR tube and 1,2-dichloroethane (70 µL, 0.886 mmol) was added and the solution was analysed by $^1$H NMR. The concentration of the TCP solution was determined to be 1 M (yield 61 %).


$^1$H NMR (400 MHz, $Et_2O$) δ 2.28 (s, 6H,)

### 6.8.5. Synthesis of CHANT (first step)

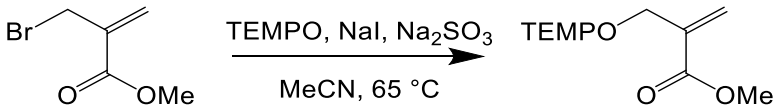


To a 250 mL round-bottomed flask was added methyl 2-(bromomethyl)acrylate (1.43 mg, 8.00 mmol, 1.0 eq.), TEMPO (1.50 g, 1.2 eq., 9.61 mmol), NaI (2.42 g, 2.0 eq., 16.16 mmol), $Na_2SO_3$

(2.02 g, 2.0 eq., 16,06 mmol) and MeCN (80 mL). The mixture was purged with nitrogen and stirred at 65 °C for 16 h. The solvent was evaporated under reduced pressure to give an orange oil. $H_2O$ (70 mL) was added to the oil and the mixture was extracted with ethyl acetate (3 x 70 mL). The organic phase was dried with $MgSO_4$, filtered and the solvent was evaporated in vacuo yielding an orange oil. The product was purified by flash silica column chromatography (2% $Et_2O$/DCM, Rf 0.35). The required fractions were combined and the solvent was evaporated under reduced pressure to give the desired product methyl 2-(((2,2,6,6-tetramethylpiperidin-1-yl)oxy)methyl)acrylate (1.67 g, 81% yield) as a colourless oil.

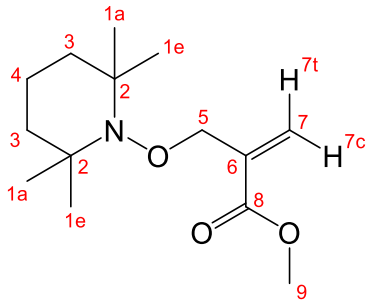


$^1$H NMR (400 MHz, Chloroform-d) δ 6.27 (q, J = 1.8 Hz, 1H, $H_{7c}$), 5.89 (q, J = 2.0 Hz, 1H, $H_{7t}$), 4.48 (t, J = 1.8 Hz, 2H, $H_5$), 3.74 (s, 3H, $H_9$), 1.58 – 1.40 (m, 4H, $H_3$), 1.45 (dd, J = 11.7, 3.4 Hz, 2H, $H_4$), 1.15 (s, 6H, $H_{1a}$), 1.10 (s, 6H, $H_{1e}$).

MS (Pos ESI): m/z 256.1907 ([M+H]$^+$, 100%); 256.1912 (calc. for $C_{14}H_{26}NO_3$, [M+H]$^+$).

### 6.8.6. Synthesis of CHANT (second step)

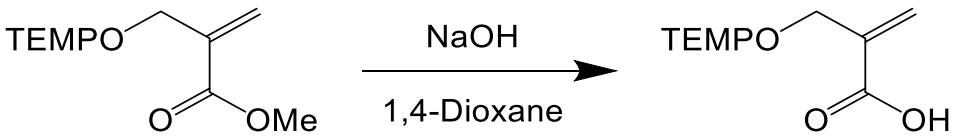


To a solution of methyl 2-(((2,2,6,6-tetramethylpiperidin-1-yl)oxy)methyl)acrylate (1.31 g, 5.13 mmol, 1 eq.) in 1,4-dioxane (20 mL) was added aqueous NaOH (1 M, 40 mL, 40 mmol, 7.35 eq.) and the solution was stirred for 4 h. The solution was acidified (pH 5) by adding an aqueous solution of HCl (1M, 40 mL, 40 mmol) and the resulting mixture was extracted with EtOAc (5x 40 mL). The organic phase was dried with $MgSO_4$, filtered and the solvent was evaporated under reduced pressure to yield a yellow oil. The oil was dissolved in DCM (5 mL) and purified by flash silica column chromatography (0.1% AcOH/5% MeOH/DCM, Rf 0.35) the

required fractions were combined, and the solvent was evaporated under reduced pressure to yield the desired product as a white solid 2-(((2,2,6,6-tetramethylpiperidin-1-yl)oxy)methyl)acrylic acid (1.25 g, 100%).

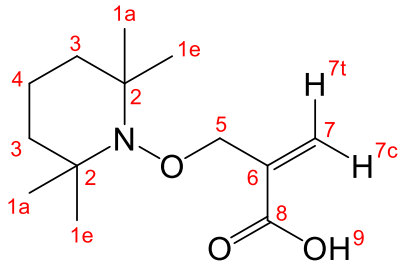


$^1$H NMR (400 MHz, Chloroform-d) δ 6.42 – 6.37 (m, 1H, $H_{7c}$), 5.97 (m, 1H, $H_{7t}$), 4.53 (s, 2H, $H_5$), 1.47-1.34 (m, 6H, $H_{3,4}$), 1.19 (s, 6H, $H_{7a}$), 1.13 (s, 6H, $H_{7e}$).

MS (Pos ESI): m/z 242.1751 ([M+H]$^+$, 100%), 264.1570 ([M+Na]$^+$, 18%); 242.1756 (calc. for $C_{13}H_{24}NO_3$, [M+H]$^+$).

### 6.8.7. Synthesis of CHANT (third step)

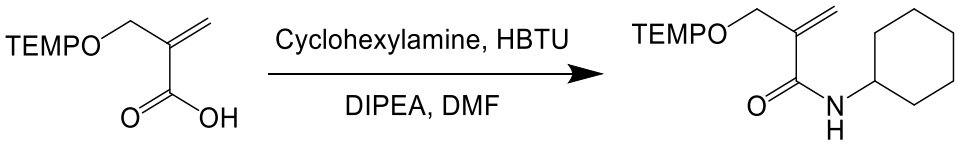


2-(((2,2,6,6-Tetramethylcyclohexyl)oxy)methyl)acrylic acid (1.25 g, 5,19 mmol, 1 eq.), cyclohexylamine (620 mg, 6.26 mmol, 1.2 eq.), N,N,N',N'-tetramethyl-O-(1H-benzotriazol-1-yl)uronium hexafluorophosphate (HBTU, 2.95 g, 7.78 mmol, 1.5 eq.) and N,N-diisopropylethylamine (DIPEA, 1.34 g, 10,38 mmol, 2.0 eq.) were dissolved in N,N-dimethylformamide (DMF, 50 mL). The solution was left stirring for 23 h. The reaction was quenched with a saturated solution of sodium bicarbonate (40 mL). 80 mL of $H_2O$ were added to the mixture to dissolve the precipitated $NaHCO_3$ and the aqueous phase was extracted with ethyl acetate (3x 80 mL). The organic phases were combined and washed with brine (2x 80 mL) and dried with $MgSO_4$. The solution was filtered, and the solvent was evaporated in vacuo to give an orange oil. The oil was dissolved in DCM (3 mL) and purified by flash silica column chromatography (20% ethyl acetate/petroleum ether, Rf 0.37). The required fractions were combined and the solvent was evaporated under reduced pressure to give the desired

product N-cyclohexyl-2-(((2,2,6,6-tetramethylpiperidin-1-yl)oxy)methyl)acrylamide as a white solid (630 mg, 37% yield).

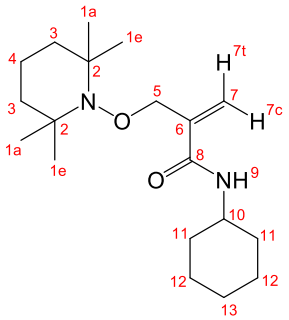


$^{1}$H NMR (400 MHz, Chloroform-d) δ 6.59 (d, J = 8.1 Hz, 1H, $H_9$), 6.06 (m, 1H, $H_{7c}$), 5.46 (m, 1H, $H_{7t}$), 4.46 (m, 2H, $H_5$), 3.89 – 3.75 (m, 1H, $H_{10}$), 1.97 (dq, J = 11.9, 3.9 Hz, 2H, $H_{11e}$), 1.81 – 1.67 (m, 2H, $H_{12e}$), 1.66 – 1.57 (m, 1H, $H_{13}$), 1.46 (dd, J = 8.9, 2.5 Hz, 4H, $H_3$), 1.36 (m, 2H, $H_4$), 1.18 (s, 6H, $H_{1a}$), 1.22 – 1.10 (m, 3H, $H_{11a,13}$), 1.09 (s, 6H, $H_{1e}$).

$^{13}$C NMR (101 MHz, CHLOROFORM-D) δ 166.01($C_8$), 139.96($C_6$), 124.05 ($C_7$), 77.80 ($C_5$), 60.09 ($C_2$), 48.34 ($C_{10}$), 39.77 ($C_3$), 33.48 ($C_{1a}$), 33.19 ($C_{11}$), 25.72 ($C_{12}$), 25.14 ($C_{13}$), 20.47 ($C_{1e}$), 17.14 ($C_4$).

MS (Pos ESI): m/z 323.2693 ($[M+H]^+$, 100%), 345.2512 ($[M+Na]^+$, 36%).; 323.2698 (calc. for $C_{19}H_{35}N_2O_2$, $[M+H]^+$).

### 6.8.8. Synthesis of Trapped Et (first step)

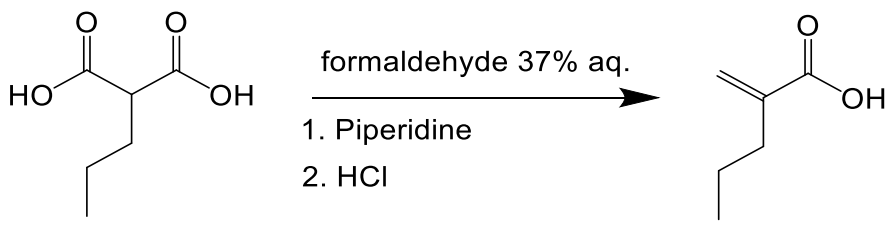


Piperidine (170 µL, 0.2 eq., 2.05 mmol), formaldehyde 37% in $H_2O$ (0.8 mL, 2 eq., 20.52 mmol) and 2-propylmalonic acid (1.55 g, 1 eq., 10.26 mmol) were dissolved in ethanol (35 mL). The mixture was heated at reflux for 18 h. The volatiles were evaporated under reduced pressure and the solution was diluted in water (30 mL) and treated with hydrochloric acid until the pH was between 3 and 4. The solution was extracted with ethyl acetate (3x 30 mL) and the combined organic phases were washed with brine (40 mL), dried over $MgSO_4$ and filtered.

The solvent was evaporated under reduced pressure to give the desired product 2-methylenepentenoic acid (1.11 g, 95% yield) as a yellow oil.

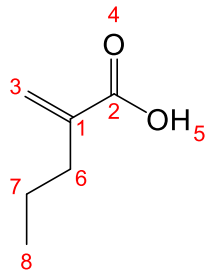


$^{1}$H NMR (400 MHz, Methanol-d4) δ 6.13 (d, J = 1.8 Hz, 1H, $H_3$), 5.56 (d, J = 1.8 Hz, 1H, $H_3$), 2.26 (t, J = 7.3 Hz, 2H, $H_6$), 1.59 – 1.43 (m, 2H, $H_7$), 0.93 (t, J = 7.4 Hz, 3H, $H_8$).

$^{13}$C NMR (101 MHz, Methanol-d4) δ 170.61 ($C_2$), 142.47 ($C_1$), 125.37 ($C_3$), 35.01 ($C_6$), 22.81 ($C_7$), 13.97 ($C_8$).

MS (Pos ESI): m/z 114.068 ($[M]^+$, 100%); 114.0680 (calc. for $C_6H_{10}O_2$, $[M]^+$).

### 6.8.9. Synthesis of Trapped Et (second step)

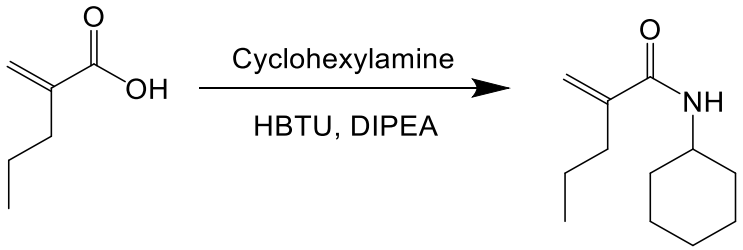


2-Methylenepentoic acid (1.11 g, 9.67 mmol, 1.0 eq.) was dissolved in N,N-dimethylformamide (DMF, 50 mL). Cyclohexylamine (1.05 g, 10.28 mmol, 1.0 eq.), N,N,N',N'-tetramethyl-O-(1Hbenzotriazol-1-yl)uronium hexafluorophosphate (HBTU, 4.5 g, 11.87 mmol, 1.1 eq.) and N,N-diisopropylethylamine (DIPEA, 2.75 g, 21.27 mmol, 2.0 eq.) were added and the solution was left stirring at room temperature for 24 h. A saturated solution of $NaHCO_3$ (40 mL) was added and the formation of a precipitate was observed. This was brought back into solution by adding water (100 mL). The mixture was extracted with EtOAc (3 x 70 mL), and the combined organic phases were washed with brine (3 x 40 mL), dried over $MgSO_4$ and filtered. The solvent was evaporated under reduced pressure to give an orange oil. The oil was dissolved in DCM (3 mL) and purified by flash silica column chromatography (20% ethyl acetate/hexane, Rf 0.37) the required fractions were combined and the solvent was

evaporated under reduced pressure to give the desired product N-cyclohexyl-2-methylenepentanamide as a white solid (1.38 g, 73% yield).

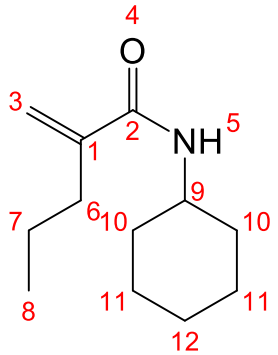


$^{1}$H NMR (400 MHz, Chloroform-d) δ 5.62 (s, 1H, $H_5$), 5.53 (s, 1H, $H_3$), 5.21 (s, 1H, $H_3$), 3.88 – 3.74 (m, 1H, $H_9$), 2.27 (t, J = 7.7 Hz, 2H, $H_6$), 1.93 (dq, J = 11.9, 4.0 Hz, 2$H_{10a}$), 1.97 (dq, J = 11.9, 4.0 Hz, 2H, $H_{10e}$), 1.81 – 1.67 (m, 2H, $H_{11e}$), 1.66 – 1.57 (m, 1H, $H_{12}$), 1.52 – 1.42 (m, 2H, $H_7$), 1.22 – 1.10 (m, 3$H_{11a,12}$, H), 0.92 (t, J = 7.3 Hz, 3H, $H_8$).

$^{13}$C NMR (101 MHz, Chloroform-d) δ 168.30 ($C_2$), 146.21 ($C_1$), 116.81 ($C_3$), 48.25 ($C_9$), 34.60 ($C_6$), 33.26 ($C_{10}$), 25.68 ($C_{12}$), 24.97 ($C_2$), 21.38 ($C_{11}$), 13.86 ($C_8$).

MS (Pos ESI): m/z 196.1696 ($[M+H]^+$, 16%), 218.1515 ($[M+Na]^+$, 100%); 196.1701 (calc. for $C_{12}H_{22}NO$, $[M+H]^+$).

### 6.8.10. Synthesis of TEMPO Et

A solution of TEMPO (4 mg, 0.025 mmol) was prepared in degassed hexane (1 mL). 1M $Et_3B$ in hexane (50 µL, 0.05 mmol) was added to the solution, and it was analysed by NMR. The solution was the opened to air for 1 h and analysed again by NMR. The desired product ethyl TEMPO was formed in a solution in hexane.

### 6.8.11. Synthesis of TEMPO Bu

A solution of TEMPO (4 mg, 0.025 mmol) was prepared in degassed hexane (1 mL). 0.056 M $Bu_3B$ in hexane (100 µL, 0.059 mmol) was added to the solution, and it was analysed by NMR. The solution was stirred open to air for 1h and analysed again by 1H NMR. The desired product butyl TEMPO was formed in a solution in hexane.

### 6.8.12. Synthesis of Benzyl Iodide

Benzyl bromide (3.6 mL, 30 mmol) was added to a solution of sodium iodide (9 g, 60 mmol) in acetone (40 mL). The mixture was stirred for 48 h in the dark at room temperature, then quenched with water (25 mL) and extracted with $Et_2O$ (2 x 50 mL). The combined organic layers were dried ($MgSO_4$), filtered and concentrated under reduced pressure to afford the product as orange oil. The oil was purified by flash column chromatography eluting with (5% DCM in hexane, Rf 0.32). The required fractions were combined, and the solvent was evaporated under reduced pressure to afford a light purple oil. The oil was dried under vaccum overnight to give the pure product benzyl iodide as a colourless oil (5.36 g, 24.6 mmol, 82% yield).

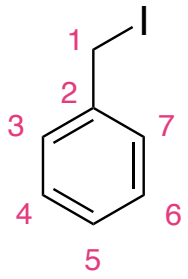


$^1$H NMR (400 MHz, Chloroform-d) δ 7.39 – 7.20 (m, 5H, $H_{3-7}$), 4.45 (s, 2H, $H_1$).

$^{13}$C NMR (101 MHz, Chloroform-d) δ 139.30 ($C_2$), 128.85 ($C_{3,7}$), 128.75 ($C_{4,6}$), 127.92 ($C_5$), 5.80 ($C_1$).

## 6.9. Kinetic Model

### 6.9.1. Kinetic Model $Et_2BOOEt$ Decomposition Method 1

*Table 39. Reactions and rate constants used in the Kineticus chemical simulation software. Initial species and concentrations: $Et_2BOOEt$ (50 mM)*

| Reaction | Rate | Annotation |
|---|---|---|

| | | |
|---|---|---|
| $Et_2BOOEt$ ==> $EtB(OEt)_2$ | 6 x $10^{-5}$ | Peroxide rearrangement |
| $Et_2BOOEt$ ==> $Et_2BO\cdot$ + $EtO\cdot$ | 4 x $10^{-6}$ | Peroxide homolysis |
| $EtO\cdot$ + $Et_2BOOEt$ ==> Oxidation | 3 x $10^5$ | $S_H2$[89] |
| $Et_2BO\cdot$ + $Et_2BOOEt$ ==> Oxidation | 3 x $10^5$ | $S_H2$[89] |
| $EtO\cdot$ + $EtB(OEt)_2$ ==> Oxidation | 3 x $10^5$ | $S_H2$[89] |
| $Et_2BO\cdot$ + $EtB(OEt)_2$ ==> Oxidation | 3 x $10^5$ | $S_H2$[89] |

### 6.9.2. Kinetic Model $Et_2BOOEt$ Decomposition Method 2

*Table 40. Reactions and rate constants used in the Kineticus chemical simulation software. Initial species and concentrations: $Et_2BOOEt$ (50 mM), $O_2$ (5 mM).*

| Reaction | Rate | Annotation |
|---|---|---|
| $Et_2BOOEt$ ==> $EtB(OEt)_2$ | 6 x $10^{-5}$ | Peroxide rearrangement |
| $Et_2BOOEt$ ==> $Et_2BO\cdot$ + $EtO\cdot$ | 4 x $10^{-6}$ | Peroxide homolysis |
| $EtO\cdot$ + $Et_2BOOEt$ ==> Oxidation | 3 x $10^5$ | $S_H2$[89] |
| $Et_2BO\cdot$ + $Et_2BOOEt$ ==> Oxidation | 3 x $10^5$ | $S_H2$[89] |
| $EtO\cdot$ + $EtB(OEt)_2$ ==> Oxidation | 3 x $10^5$ | $S_H2$[89] |
| $Et_2BO\cdot$ + $EtB(OEt)_2$ ==> Oxidation | 3 x $10^5$ | $S_H2$[89] |
| $O_2$ + $Et_2BOOEt$ | 7 x $10^{-4}$ | Oxidation of peroxide[87] |

### 6.9.3. Kinetic Model $Et_3B$/Low $O_2$

*Table 41. Reactions and rate constants used in the Kineticus chemical simulation software. Initial species and concentrations: $Et_3B$ (50 mM), and A (1000 mM).*

| Reaction | Rate | Annotation |
|---|---|---|
| A ==> $O_2$ | $6.6 \times 10^{-6}$ | Slow diffusion of $O_2$ into the system |
| $Et_3B + O_2$ ==> $Et_2BOO\cdot + Et\cdot$ | $7.0 \times 10^{-4}$ | Primary initiation[87] |
| $Et\cdot + O_2$ ==> $EtOO\cdot$ | $2.0 \times 10^{9}$ | Autoxidation cycle of radicals formed in primary initiation[88, 90, 129] |
| $EtOO\cdot + Et_3B$ ==> $EtOOBEt_2 + Et\cdot$ | $2.0 \times 10^{6}$ | |
| $Et_2BOO\cdot + Et_3B$ ==> $Et_2BOOBEt_2 + Et\cdot$ | $2.0 \times 10^{6}$ | $S_H2$[88, 90] |
| $Et\cdot$ + Trap ==> EtTrap | $2.5 \times 10^{5}$ | Target chain initiation of radicals formed through primary initiation[130] |
| $Et_3B + EtOOBEt_2$ ==> $Et_2BOEt + Et'\cdot + Et_2BO\cdot$ | $1.9 \times 10^{-1}$ | Secondary initiation |
| $Et_2BO\cdot + Et_3B$ ==> $Et_2BOBEt_2 + Et'$ | $2.0 \times 10^{6}$ | $S_H2$[88, 90] |
| $Et'\cdot + O_2$ ==> $EtOO'\cdot$ | $2.0 \times 10^{9}$ | Autoxidation cycle of radicals formed in secondary initiation[88, 90, 129] |
| $EtOO'\cdot + Et_3B$ ==> $EtOOBEt_2 + Et'\cdot$ | $2.0 \times 10^{6}$ | |
| $Et'\cdot$ + Trap ==> Et'Trap | $2.5 \times 10^{5}$ | Target chain initiation of radicals formed through secondary initiation[130] |
| $EtOOBEt_2$ ==> $(EtO)_2BEt$ | $5.0 \times 10^{-5}$ | Peroxide rearrangement |

### 6.9.4. Kinetic Model $Et_3B$/High $O_2$

*Table 42. Reactions and rate constants used in the Kineticus chemical simulation software. Initial species and concentrations: $Et_3B$ (50 mM), and A (1000 mM).*

| Reaction | Rate | Annotation |
|---|---|---|
| A ==> $O_2$ | $9 \times 10^{-4}$ | Slow diffusion of $O_2$ into the system |

| | | |
|---|---|---|
| $Et_3B + O_2$ ==> $Et_2BOO\cdot + Et\cdot$ | $7.0 \times 10^{-4}$ | Primary initiation[87] |
| $Et\cdot + O_2$ ==> $EtOO\cdot$ | $2.0 \times 10^{9}$ | Autoxidation cycle of radicals formed in primary initiation[88, 90, 129] |
| $EtOO\cdot + Et_3B$ ==> $EtOOBEt_2 + Et\cdot$ | $2.0 \times 10^{6}$ | |
| $Et_2BOO\cdot + Et_3B$ ==> $Et_2BOOBEt_2 + Et\cdot$ | $2.0 \times 10^{6}$ | $S_H2$[88, 90] |
| $Et\cdot$ + Trap ==> EtTrap | $2.5 \times 10^{5}$ | Target chain initiation of radicals formed through primary initiation[130] |
| $Et_3B + EtOOBEt_2$ ==> $Et_2BOEt + Et'\cdot + Et_2BO\cdot$ | $1.9 \times 10^{-1}$ | Secondary initiation |
| $Et_2BO\cdot + Et_3B$ ==> $Et_2BOBEt_2 + Et'$ | $2.0 \times 10^{6}$ | $S_H2$[88, 90] |
| $Et'\cdot + O_2$ ==> $EtOO'\cdot$ | $2.0 \times 10^{9}$ | Autoxidation cycle of radicals formed in secondary initiation[88, 90, 129] |
| $EtOO'\cdot + Et_3B$ ==> $EtOOBEt_2 + Et'\cdot$ | $2.0 \times 10^{6}$ | |
| $Et'\cdot$ + Trap ==> Et'Trap | $2.5 \times 10^{5}$ | Target chain initiation of radicals formed through secondary initiation[130] |
| $EtOOBEt_2$ ==> $(EtO)_2BEt$ | $5.0 \times 10^{-5}$ | Peroxide rearrangement |

### 6.9.5. Kinetic Model $Et_3B/Et_2BOOEt/N_2$

*Table 43. Reactions and rate constants used in the Kineticus chemical simulation software. Initial species and concentrations: $Et_3B$ (50 mM), and $Et_2BOOEt$ (50 mM).*

| Reaction | Rate | Annotation |
|---|---|---|
| $Et_3B + O_2$ ==> $Et_2BOO\cdot + Et\cdot$ | $7.0 \times 10^{-4}$ | Primary initiation[87] |
| $Et\cdot + O_2$ ==> $EtOO\cdot$ | $2.0 \times 10^{9}$ | Autoxidation cycle of radicals formed in primary initiation[88, 90, 129] |
| $EtOO\cdot + Et_3B$ ==> $EtOOBEt_2 + Et\cdot$ | $2.0 \times 10^{6}$ | |
| $Et_2BOO\cdot + Et_3B$ ==> $Et_2BOOBEt_2 + Et\cdot$ | $2.0 \times 10^{6}$ | $S_H2$[88, 90] |
| $Et\cdot$ + Trap ==> EtTrap | $2.5 \times 10^{5}$ | Target chain initiation of radicals formed through primary initiation[130] |
| $Et_3B + EtOOBEt_2$ ==> $Et_2BOEt + Et'\cdot + Et_2BO\cdot$ | $1.9 \times 10^{-1}$ | Secondary initiation |

| | | |
|---|---|---|
| $Et_2BO\cdot + Et_3B$ ==> $Et_2BOBEt_2 + Et'$ | $2.0 \times 10^6$ | $S_H2$[88, 90] |
| $Et'\cdot + O_2$ ==> $EtOO'\cdot$ | $2.0 \times 10^9$ | Autoxidation cycle of radicals formed in secondary initiation[88, 90, 129] |
| $EtOO'\cdot + Et_3B$ ==> $EtOOBEt_2 + Et'\cdot$ | $2.0 \times 10^6$ | |
| $Et'\cdot$ + Trap ==> Et'Trap | $2.5 \times 10^5$ | Target chain initiation of radicals formed through secondary initiation[130] |
| $EtOOBEt_2$ ==> $(EtO)_2BEt$ | $5.0 \times 10^{-5}$ | Peroxide rearrangement |

## 6.10. Analysis Protocols

### 6.10.1. ESI MS Protocol

Direct injection MS characterisation was performed using a solariX XR FTMS mass spectrometer in positive-ion mode ESI (m/z ±0.0001 precision, 30000 resolution, 1-50 Hz scan speed). Mass spectra were recorded over an m/z range of m/z 100-1000, averaging 16 scans. Ion transfer time (ToF) was set to 0.6 ms. In general, ESI settings were as follows: drying gas flow = 2.0 L min-1; nebulizer pressure: 2.0 bar; dry temperature: 180 °C, capillary voltage = 4500 V; spray shield voltage = –500 V; skimmer voltage = 15 V. For standard MS other settings used were injection speed = 2 µL $min^{-1}$; ion accumulation time = 0.2 s; drying gas temperature = 180 °C. The MS instrument was calibrated daily using a dilute solution of sodium trifluoroacetate (NaTFA) in a 1:1 MeCN/$H_2O$ mixture in ESI. Samples were injected in the spectrometer (2 µL $min^{-1}$) until stable signal was detected (typically within 5 min). A mass spectrum was then recorded, and the spectrometer was reflushed with the 1:1 MeCN/$H_2O$ mixture and the procedure was repeated. Accepted random m/z error was < 0.0000 - 0.0010.

### 6.10.2. APCI MS Protocol

Direct injection MS characterisation was performed using a solariX XR FTMS mass spectrometer in APCI mode (m/z ±0.001 precision, 30000 resolution, 1-50 Hz scan speed). Mass spectra were recorded over an m/z range of m/z 100-1000, averaging 16 scans. Ion transfer time (ToF) was set to 0.6 ms. APCI settings were as follows: Corona: 5 µA, source

temperature: 130 °C, drying gas flow: 1.8 L min-1; nebulizer pressure: 1.0 bar; dry temperature: 300 °C, capillary voltage = 2000 V. For standard MS other settings used were injection speed = 2 µL $min^{-1}$; ion accumulation time = 0.2 s; drying gas temperature = 180 °C. The MS instrument was calibrated using a dilute solution of sodium trifluoroacetate (NaTFA) in a 1:1 MeCN/$H_2O$ mixture in APCI. Samples were injected in the spectrometer (2 µL $min^{-1}$) until stable signal was detected (typically within 5 min). A mass spectrum was then recorded, and the spectrometer was reflushed with the 1:1 MeCN/$H_2O$ mixture and the procedure was repeated. Accepted random m/z error was < 0.0000 - 0.0010.

### 6.10.3. GCEI Protocol

GCEI was performed using an Agilent 7890B GC system. The GC method was 60 °C starting temp, hold 1 min, ramp 20 °C / min, final temperature 300 °C with a run time of 15 minutes. The flow rate was set at 1 mL /minute with helium as a carrier gas. The injector temperature was 280 °C. The column used was a Zebron ZB-5MSplus. MS was performed using an AccTOF GCx-plus mass EI mass spectrometer with an acquisition range from 0-750 Da, calibration using perfluoro tributylamine. The temperature source was set at 180 °C, the electron energy was 70 eV, and the trap current was 200 µA.

### 6.10.4. $^{1}H$ and $^{11}B$ NMR Kinetics Protocol

NMR characterisation was performed using a 500MHz AVIIIHD NMR spectrometer with a PA TBO 500S2 BB-H-F probe. Before the sample analysis the NMR was shimmed unlocked with hexane. When the reaction mixture was mixed, timer started, the solution was transferred to a Young's TAP NMR tube, sealed and the tube was immediately introduced inside the spectrometer. The sample was tuned to $^{1}H$ and $^{11}B$ nuclei and the magnet was shimmed unlocked from solvent. NMR spectra were recorded at the indicated timestamps alternating $^{1}H$ and $^{11}B$. $^{11}B$ NMR parameters: 32 scans, 1 s relaxation delay, 25 ms acquisition time, 64 kHz spectral width. $^{1}H$ NMR parameters: 8 scans, 1 s relaxation delay, 4 s acquisition time, 8 kHz spectral width. Unless stated otherwise all kinetic runs were recorded at 298.0 °C.

**Appendix**

**Contents**

## 7.1. Atom Transfer Radical Addition of Alkyl Iodides to Acetylenes

### 7.1.1. $Et_3B/Et_2BOOEt$ initiated ATRA of EtI to TMS acetylene

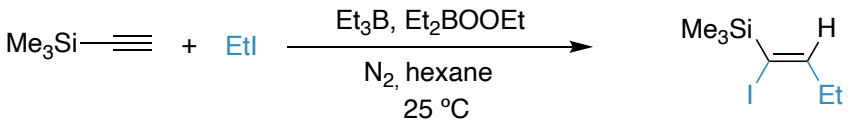


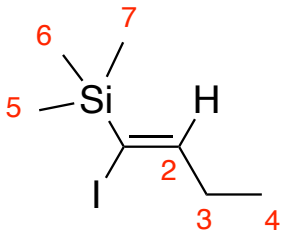


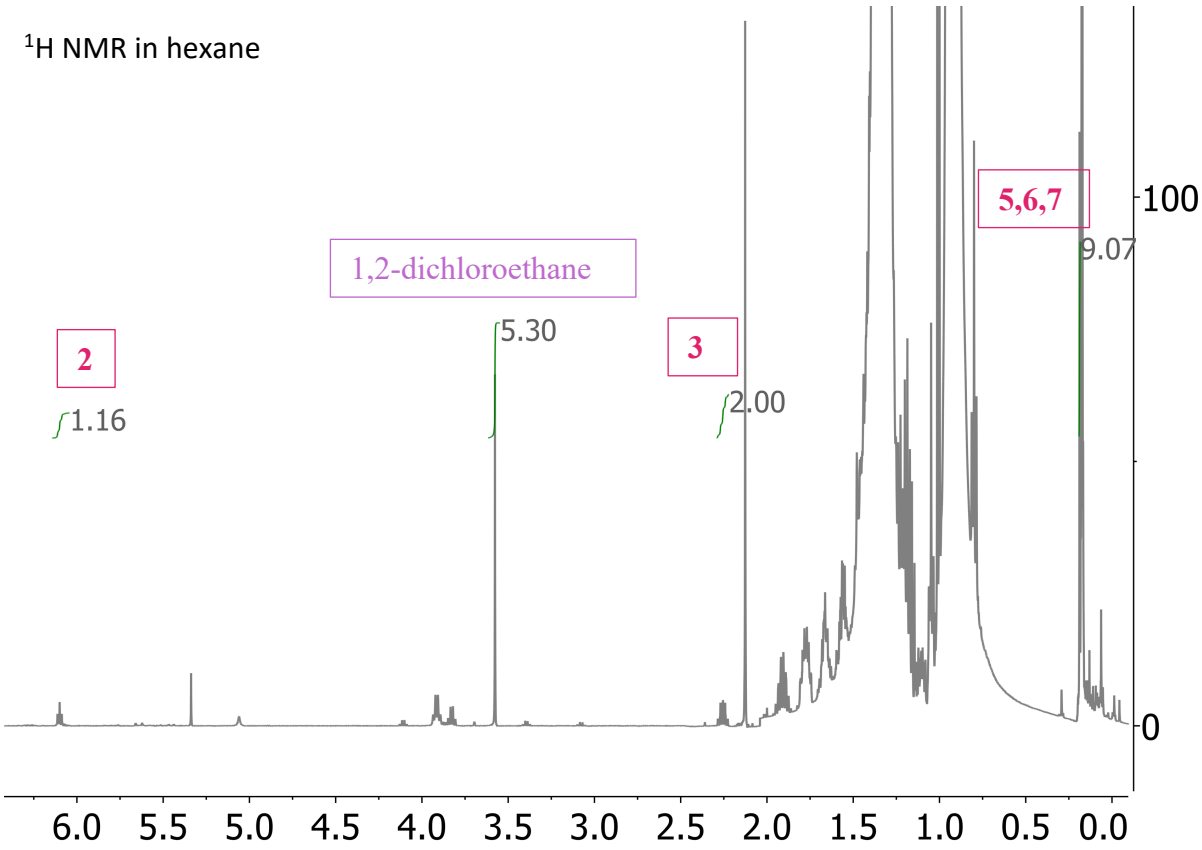

### 7.1.2. $Et_3B$/Low O2 initiated ATRA of EtI to TMS acetylene

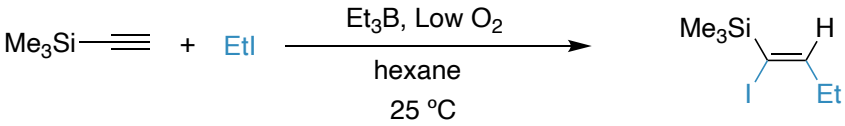


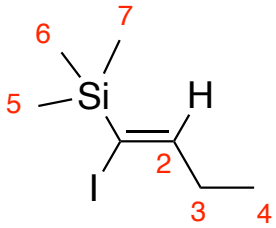


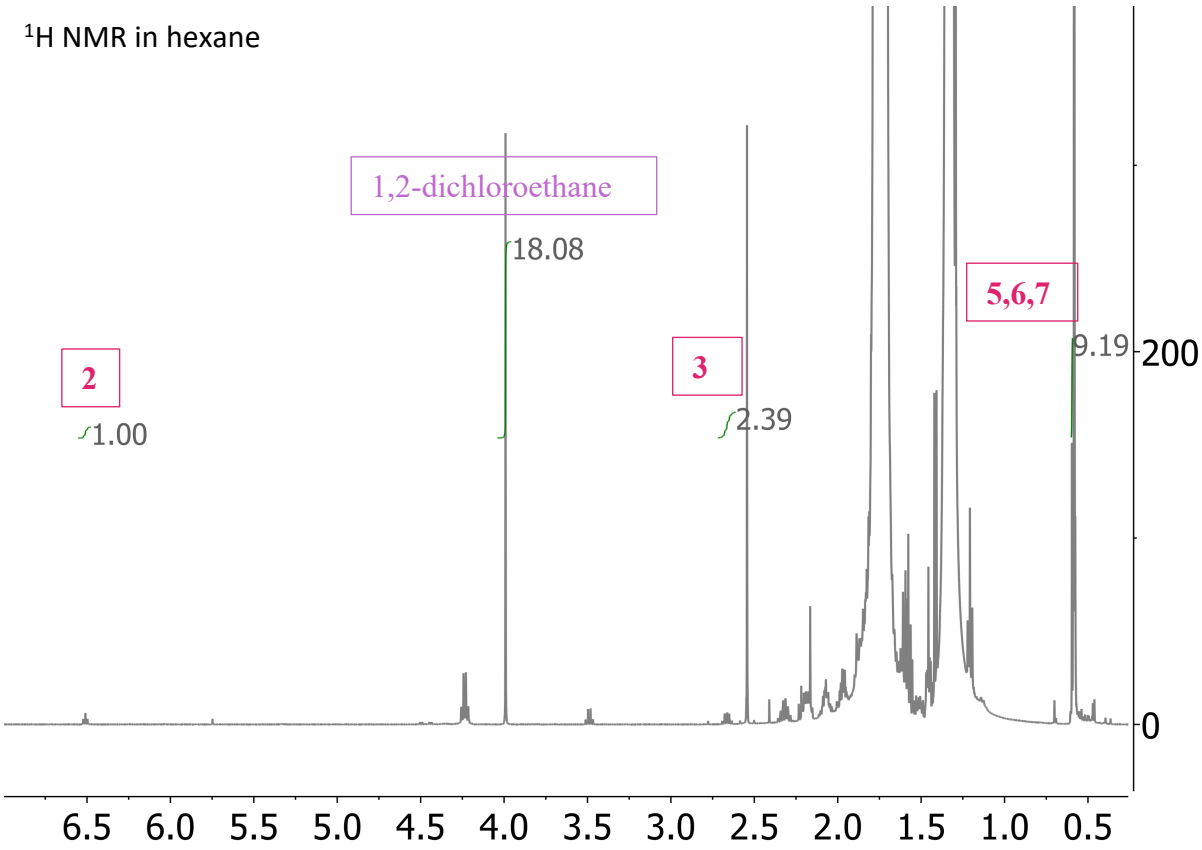

### 7.1.3. $Et_3B$/Et2BOOEt initiated ATRA of $^iPrI$ to phenylacetylene

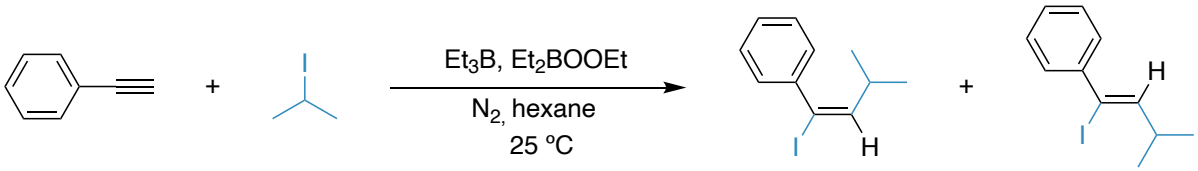



**E** **Z**

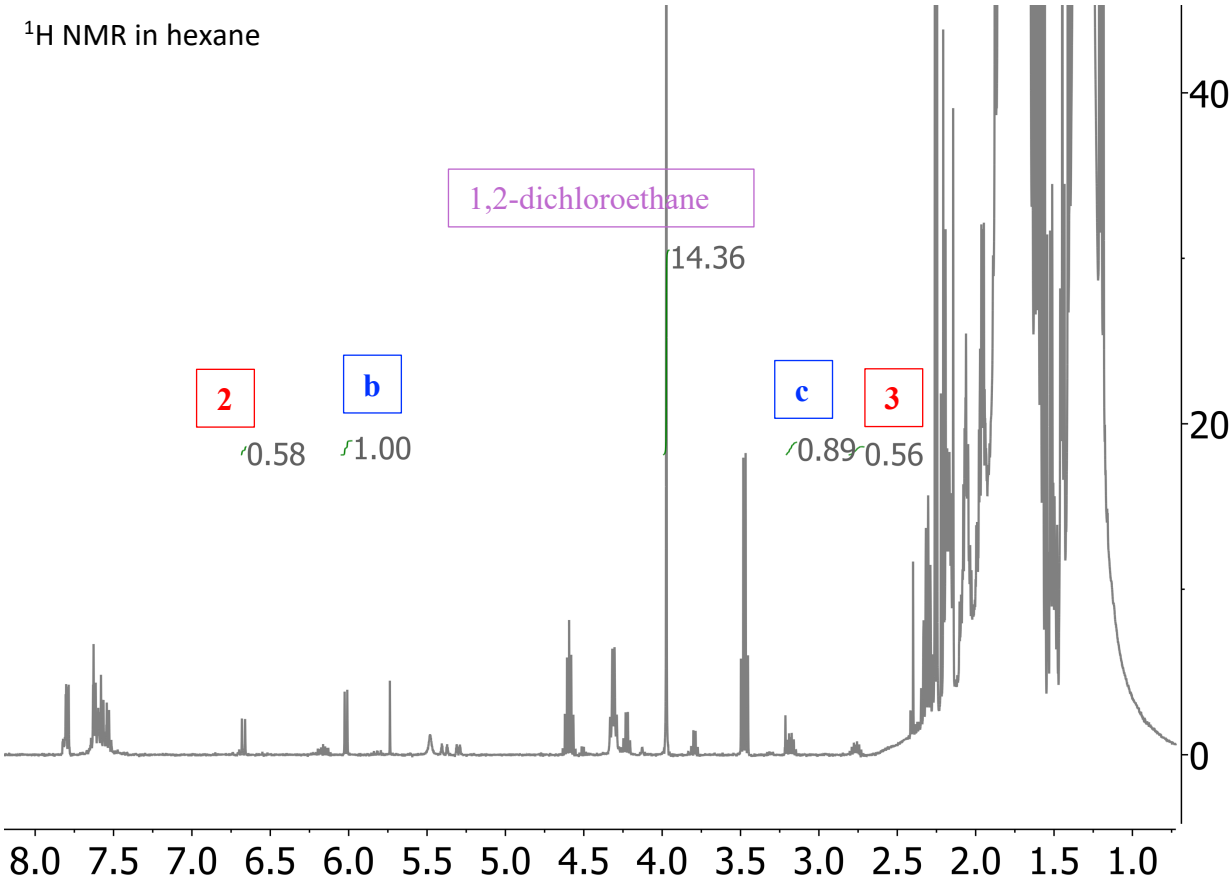

### 7.1.4. $Et_3B$/Low $O_2$ initiated ATRA of $^iPrI$ to phenylacetylene

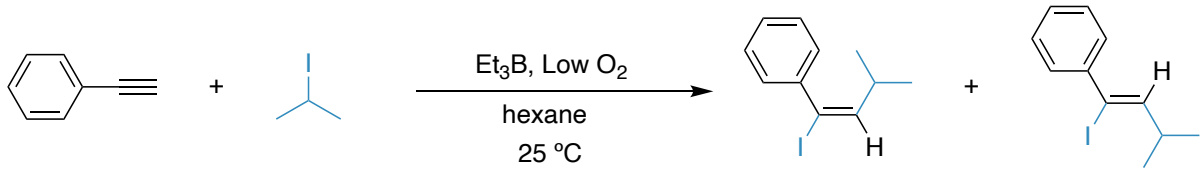



E Z

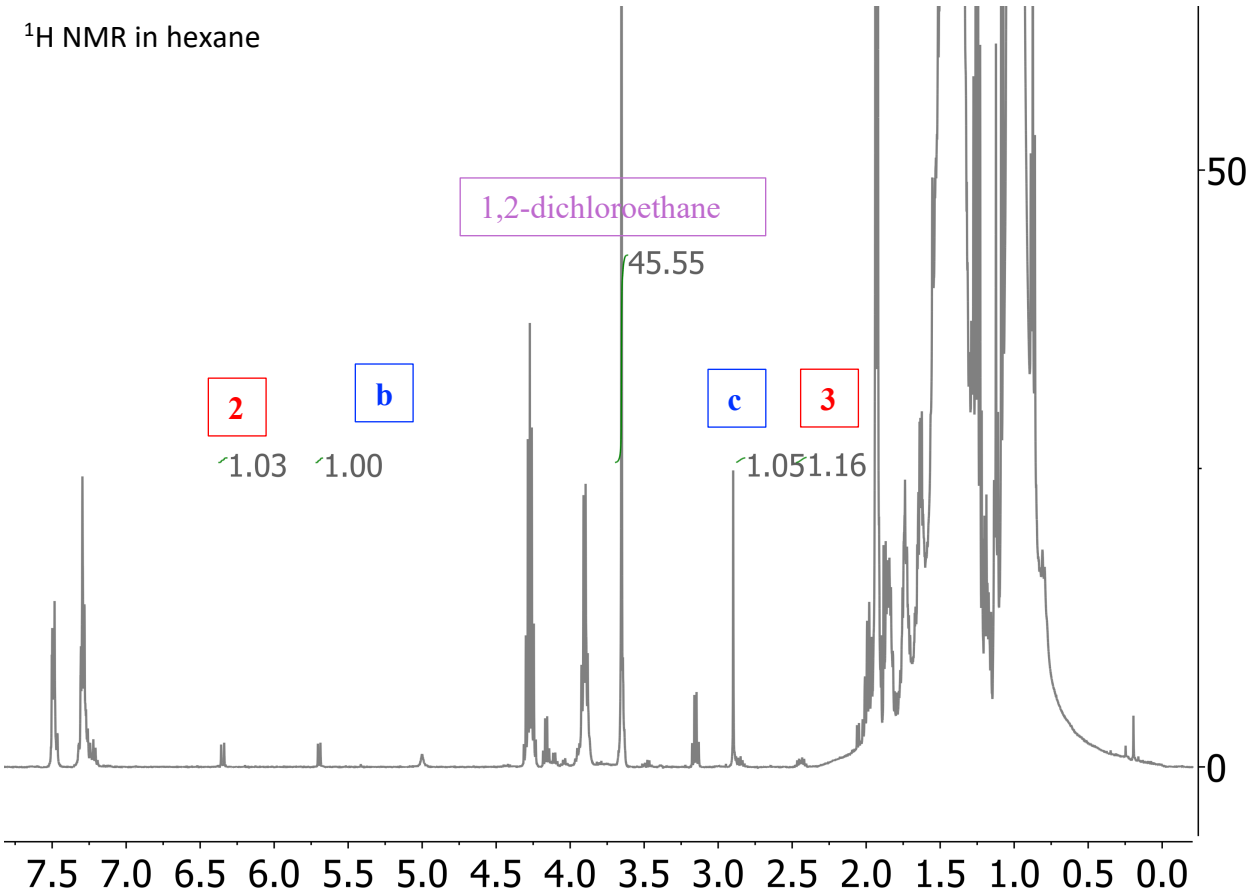

### 7.1.5. $Et_3B$/High $O_2$ initiated ATRA of $^iPrI$ to phenylacetylene

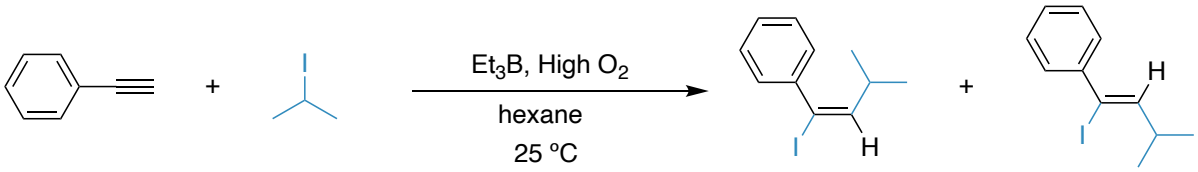


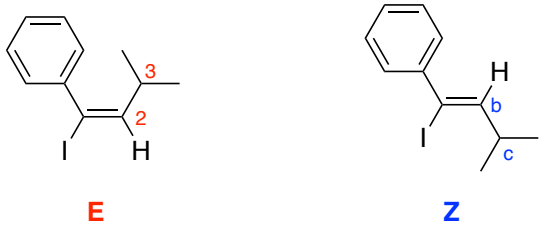


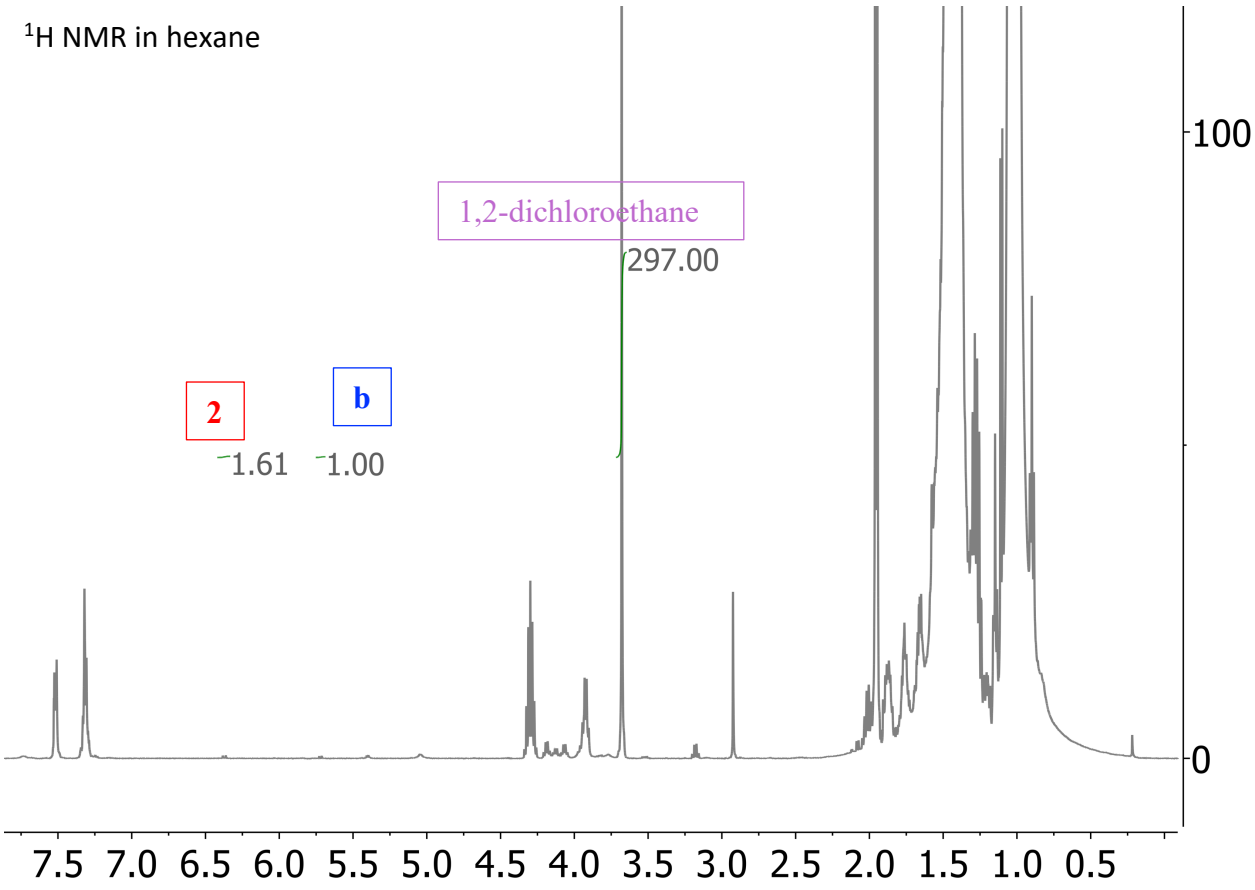

### 7.1.6. $Et_3B/Et_2BOOEt$ initiated ATRA of $(TMS)_3SiH$ to phenylacetylene

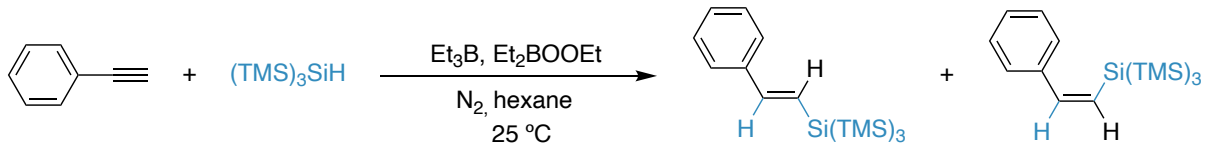


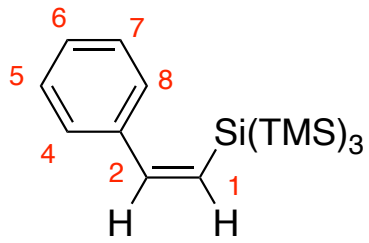


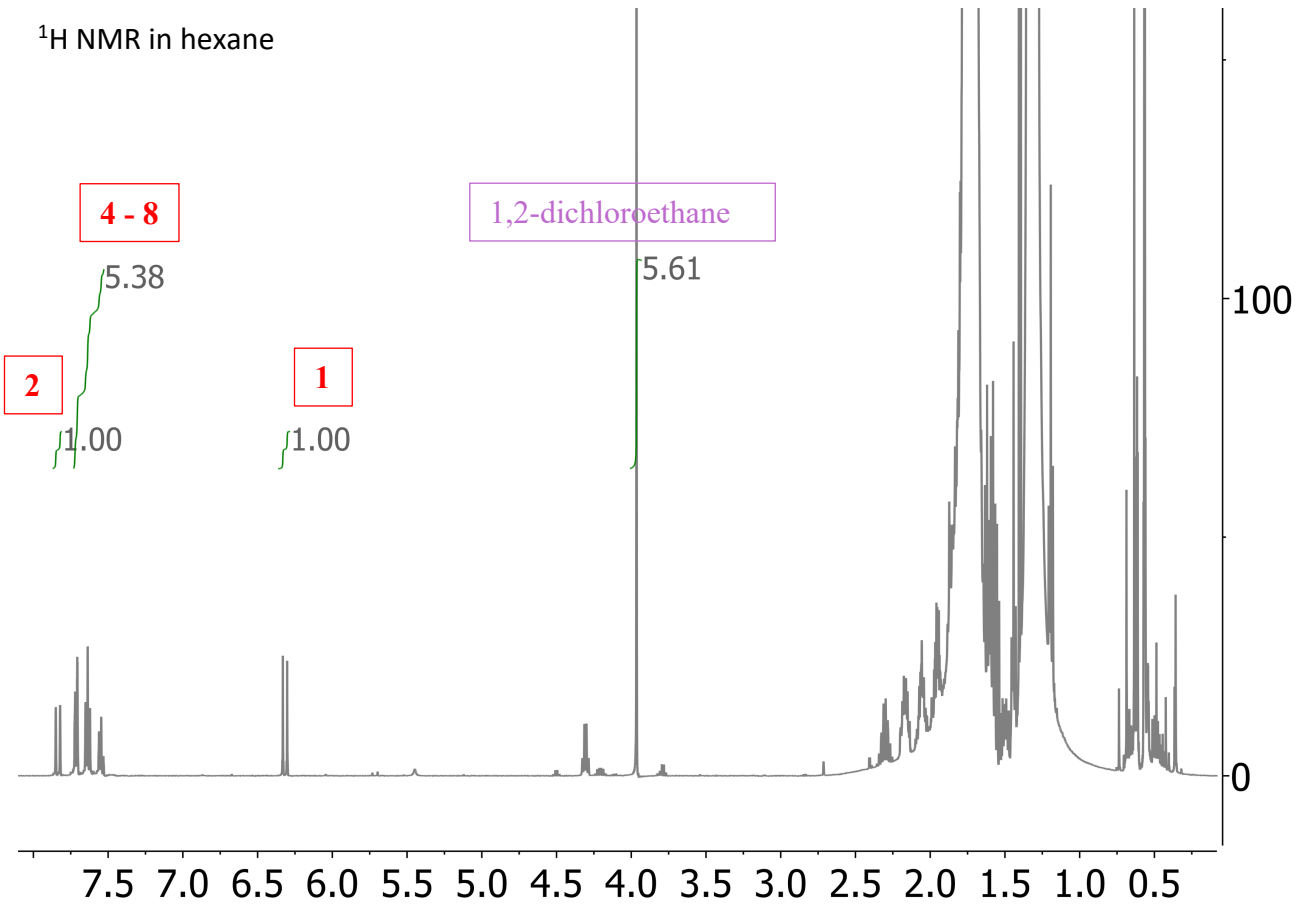

### 7.1.7. $Et_3B$/Low $O_2$ initiated ATRA of $(TMS)_3SiH$ to phenylacetylene

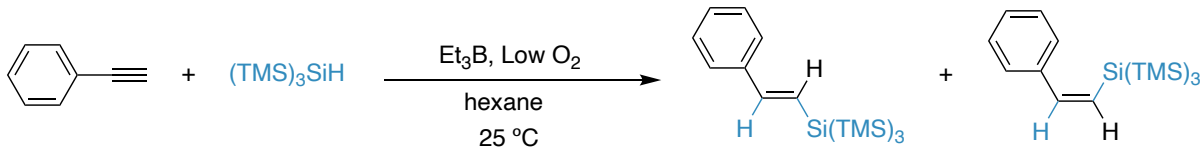


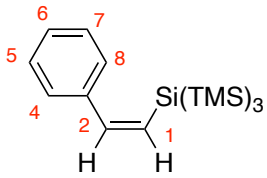


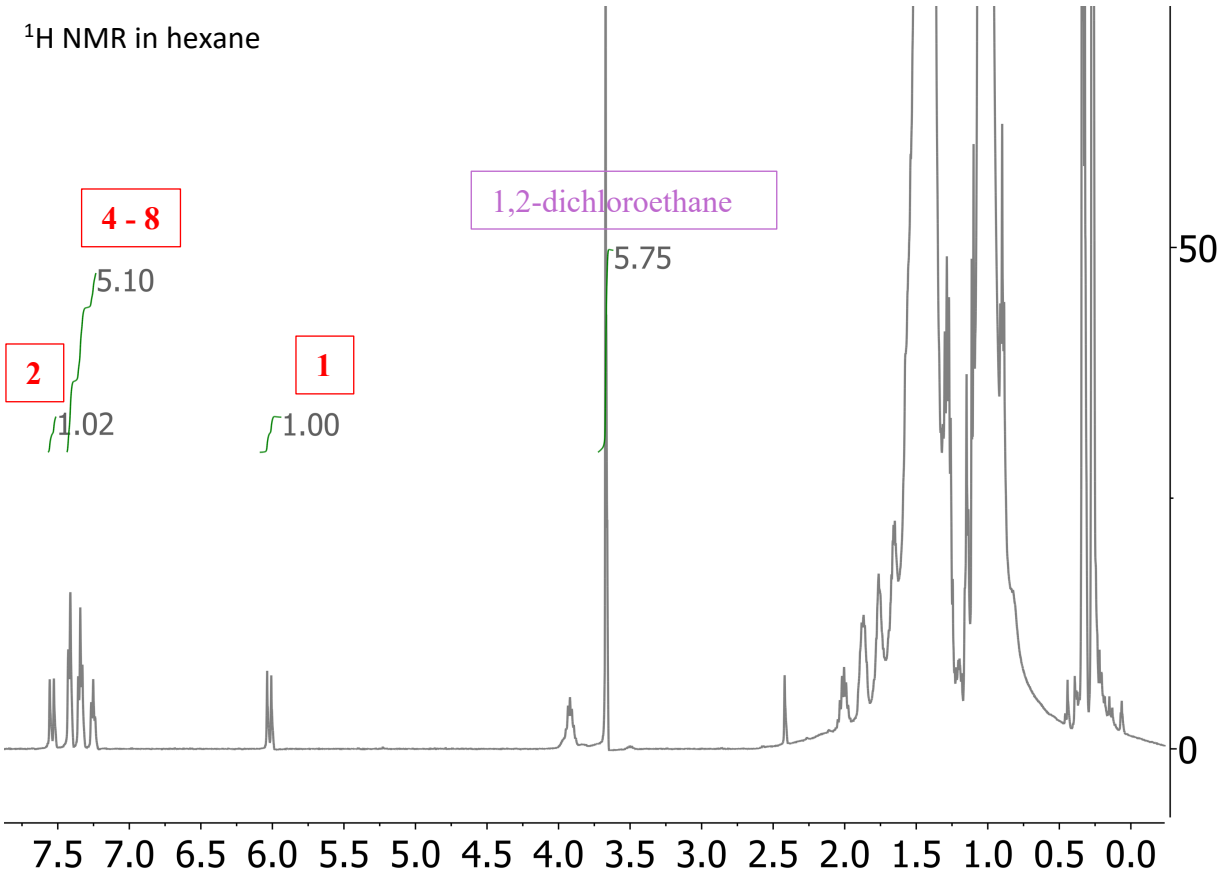

### 7.1.8. $Et_3B$/High $O_2$ initiated ATRA of $(TMS)_3SiH$ to phenylacetylene

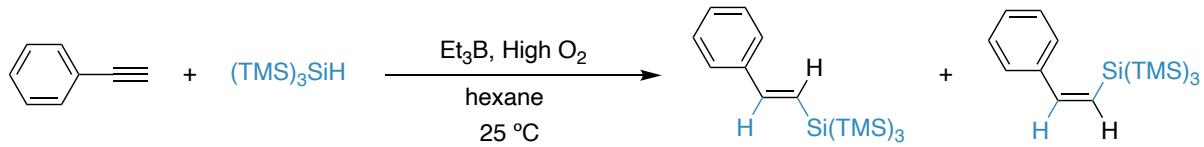


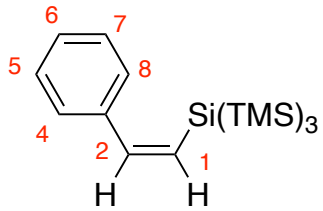


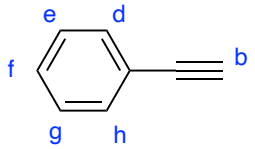


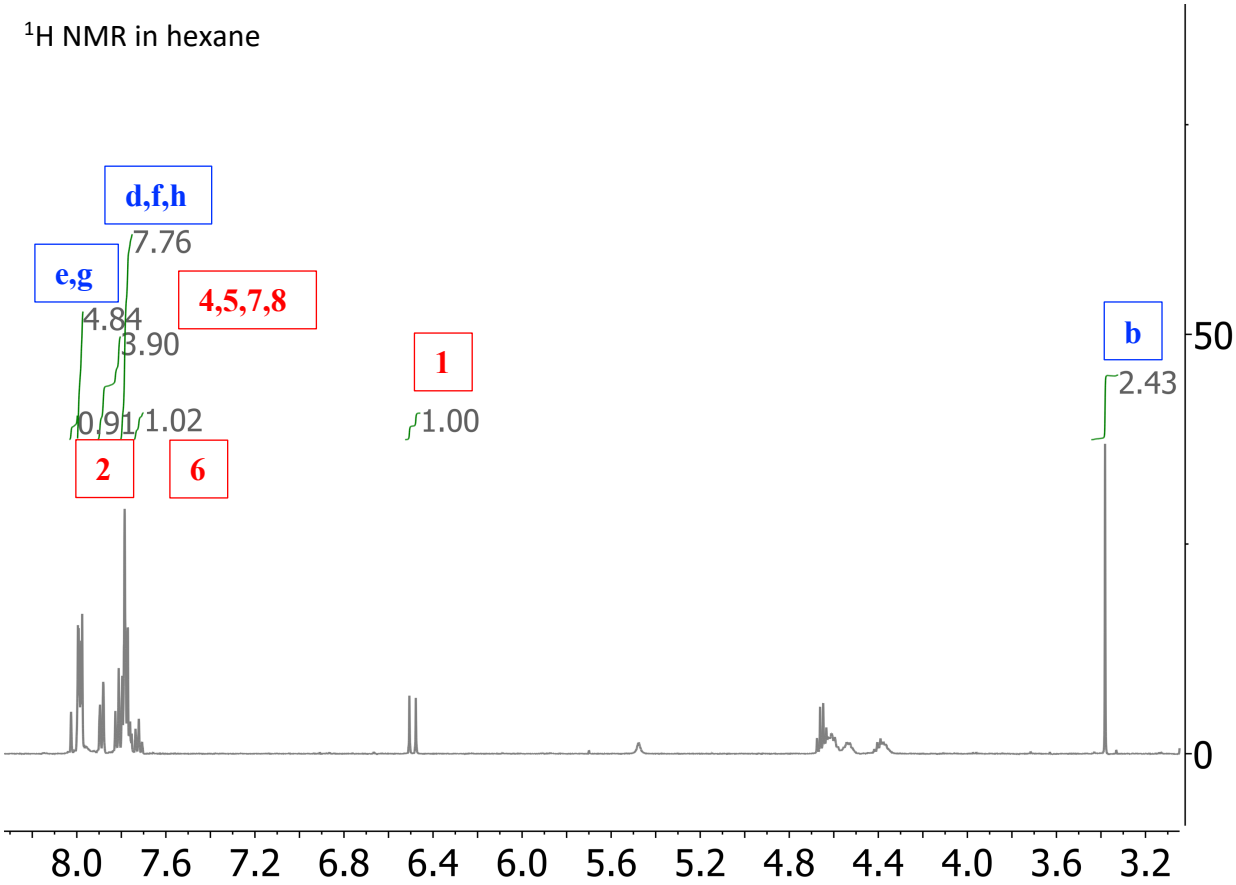

## 7.2. Atom Transfer Radical Addition of Alkyl Iodides to TCP

### 7.2.1. $Et_3B/Et_2BOOEt$ initiated ATRA of (2-iodoethyl)benzene to TCP

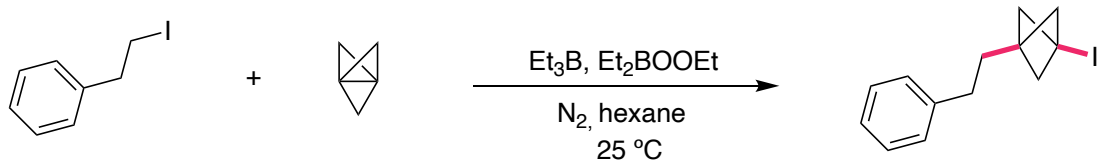


**71%**

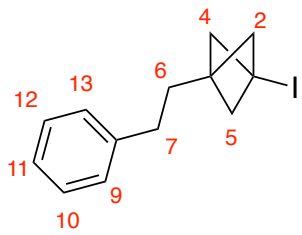


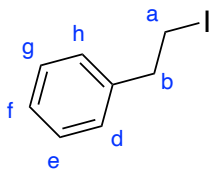


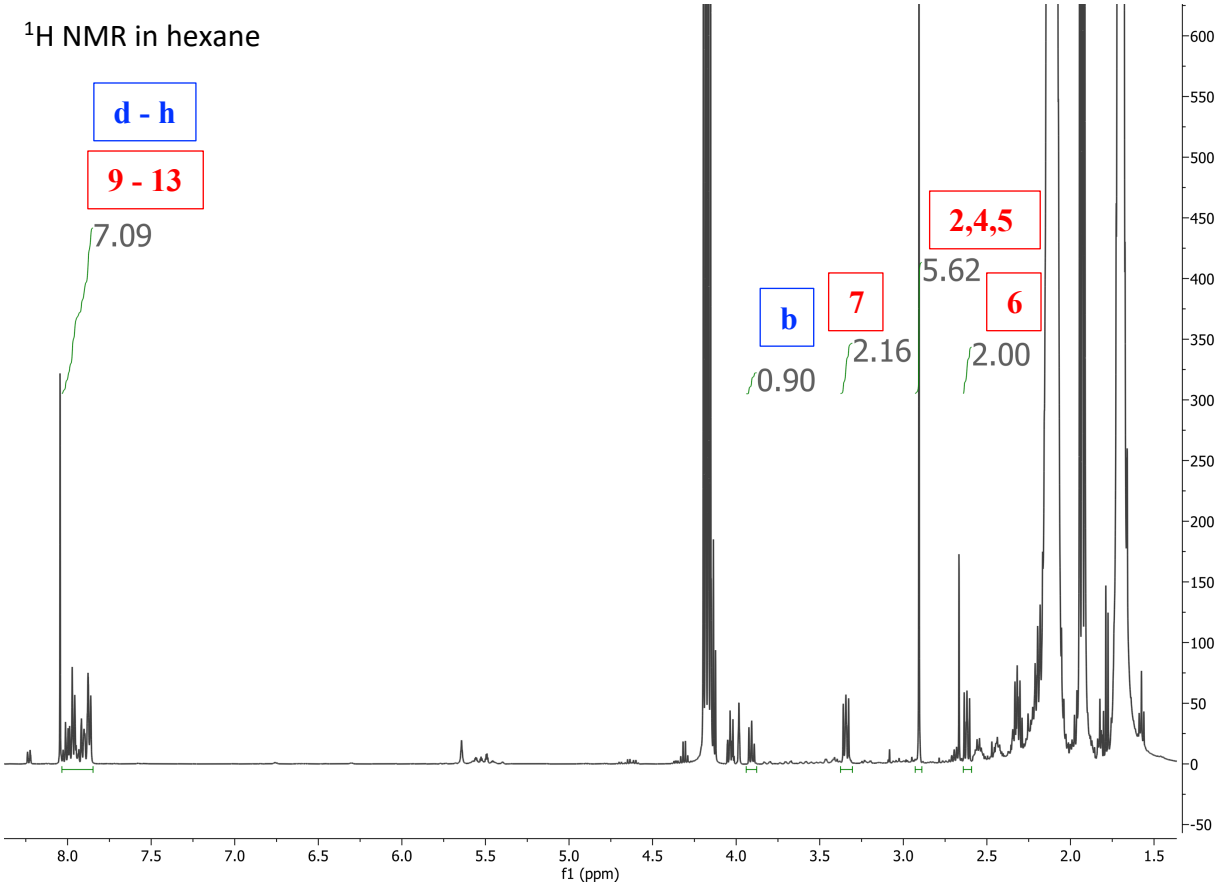

### 7.2.2. $Et_2BOOEt$ initiated ATRA of (2-iodoethyl)benzene to TCP

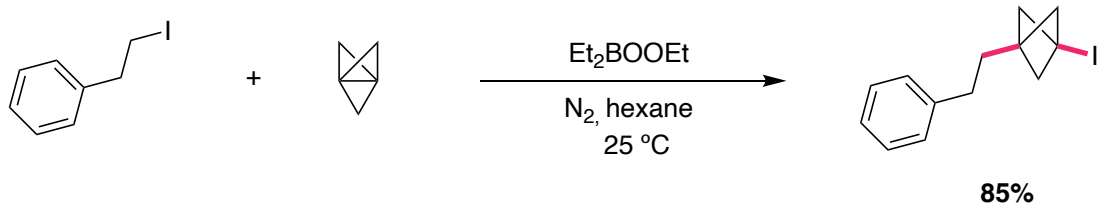


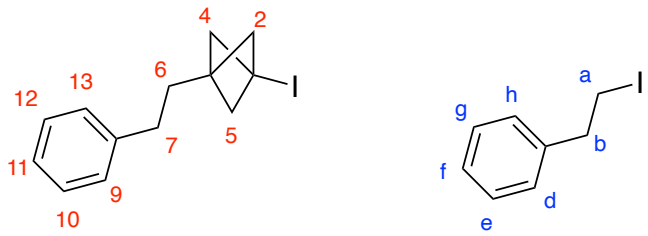


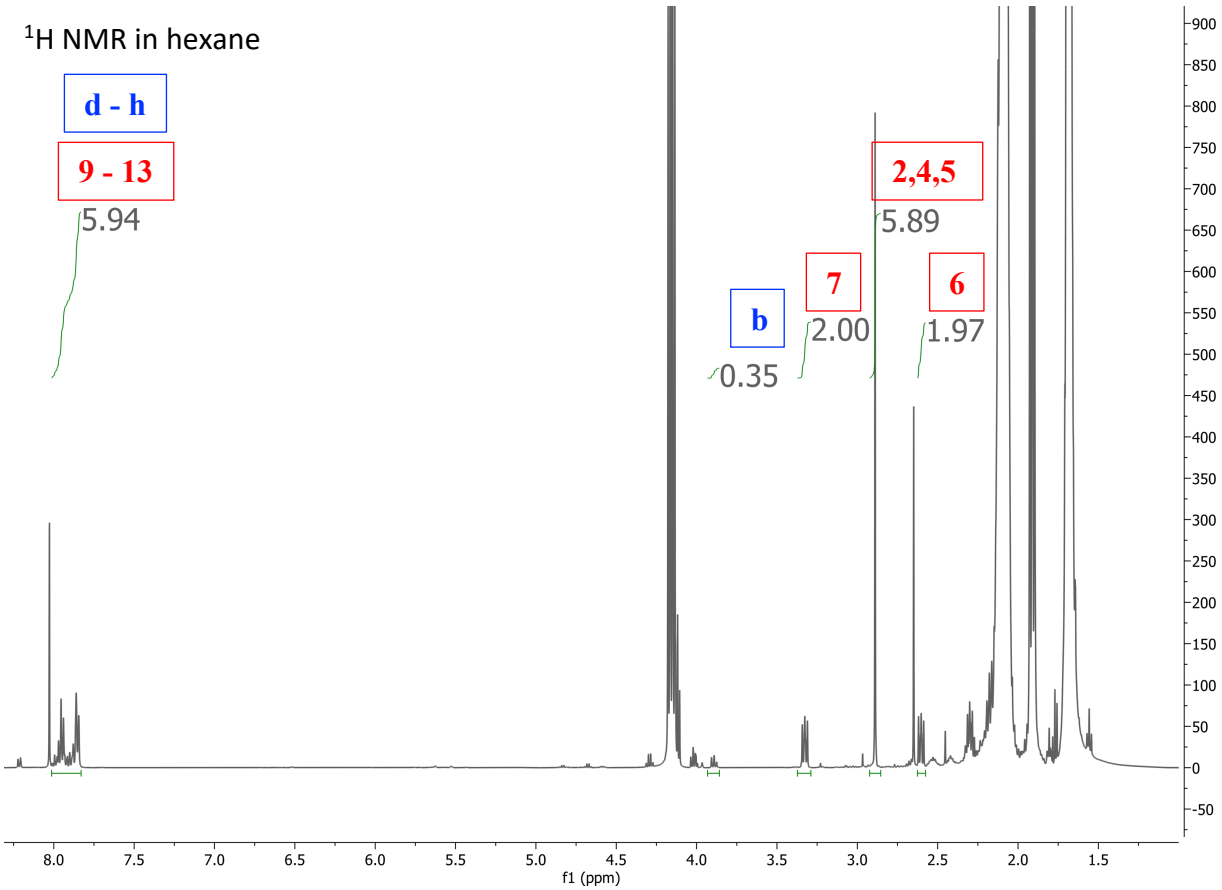

### 7.2.3. $Et_3B/Et_2BOOEt$ initiated ATRA of BnI to TCP

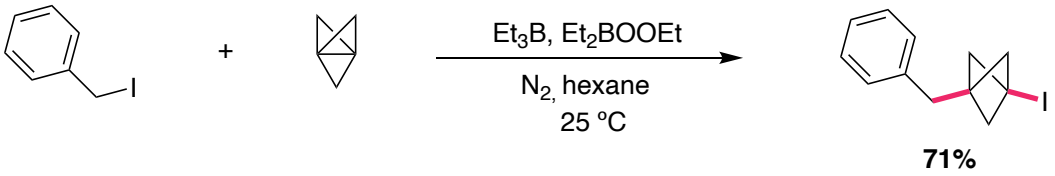


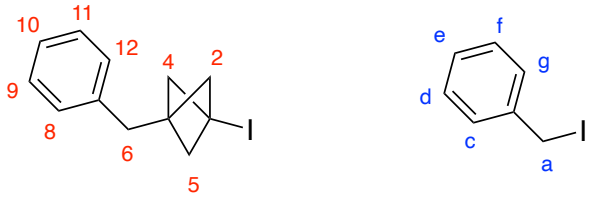


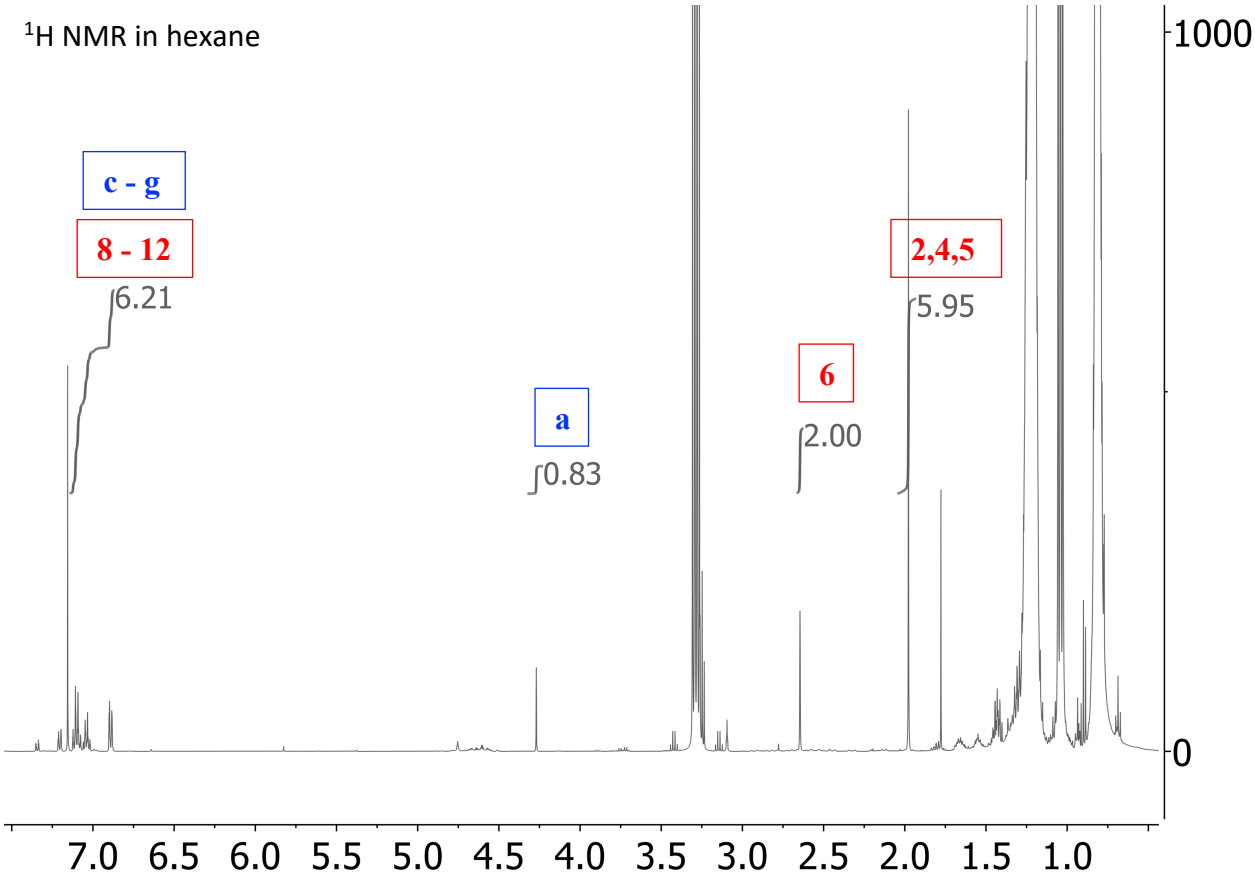

### 7.2.4. $Et_2BOOEt$ initiated ATRA of BnI to TCP

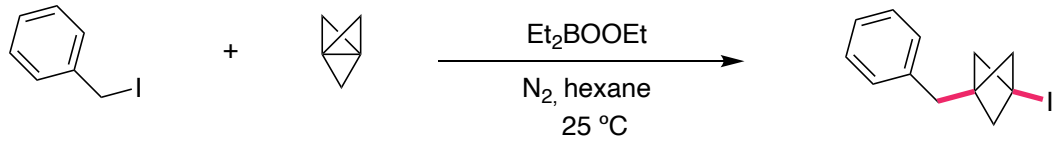


**90%**

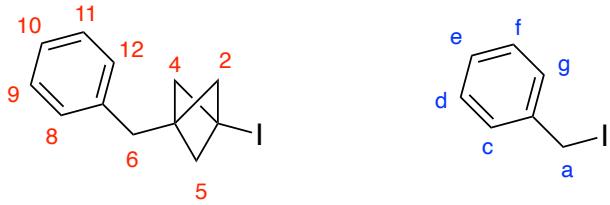


$^1$H NMR in hexane

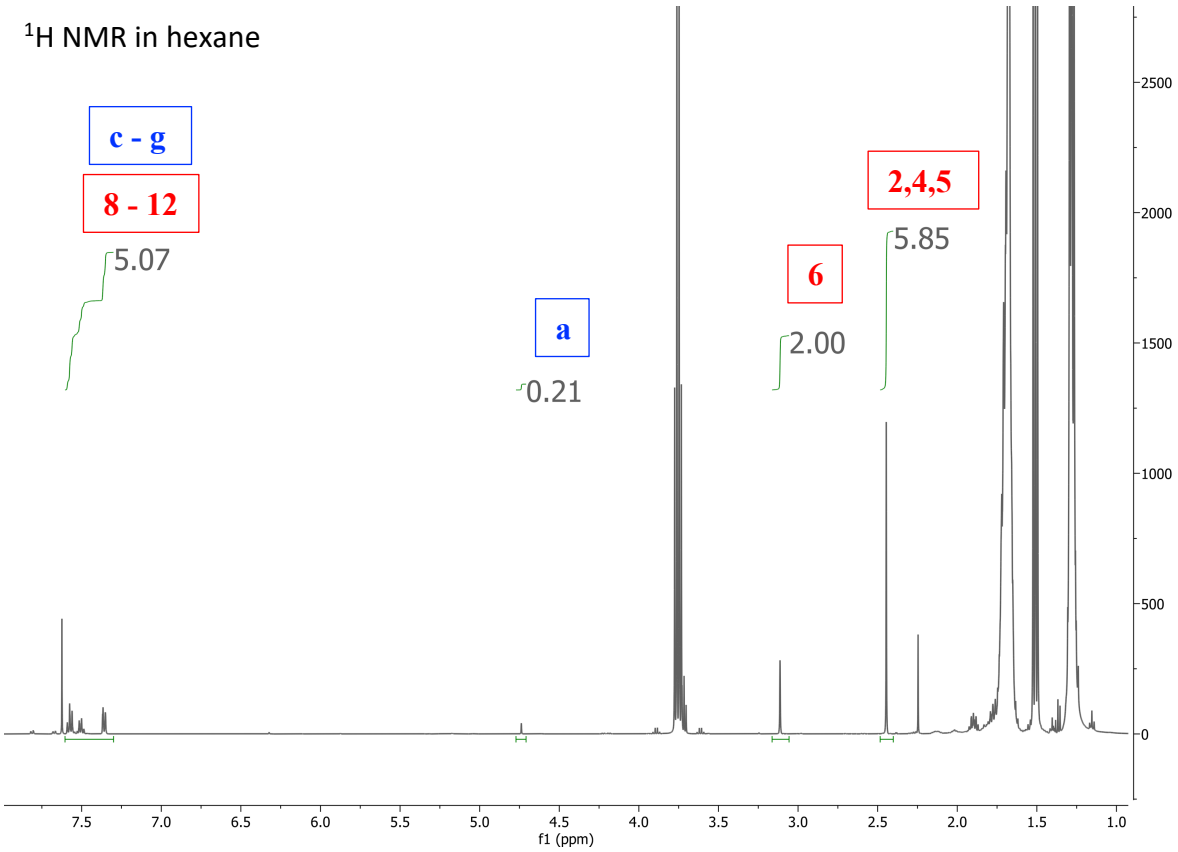

### 7.2.5. $Et_3B/Et_2BOOEt$ initiated ATRA of 2-iodopyridine to TCP

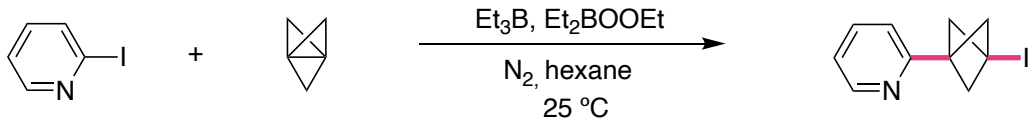


**29%**

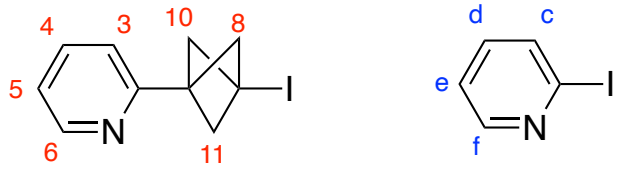


$^1$H NMR in hexane

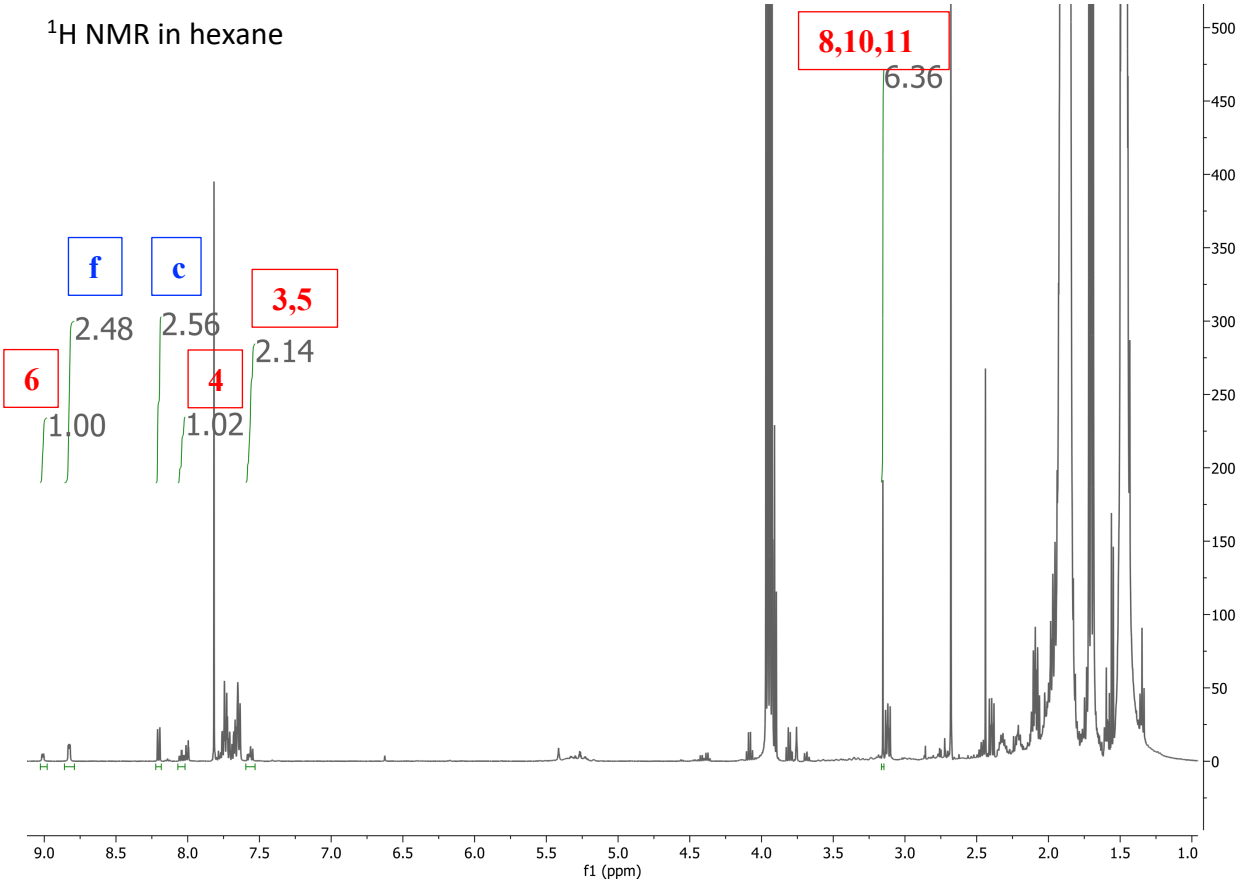

### 7.2.6. $Et_2BOOEt$ initiated ATRA of 2-iodopyridine to TCP

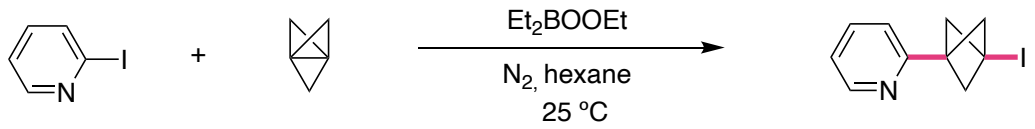


**40%**

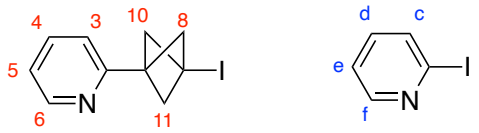

$^1$H NMR in hexane

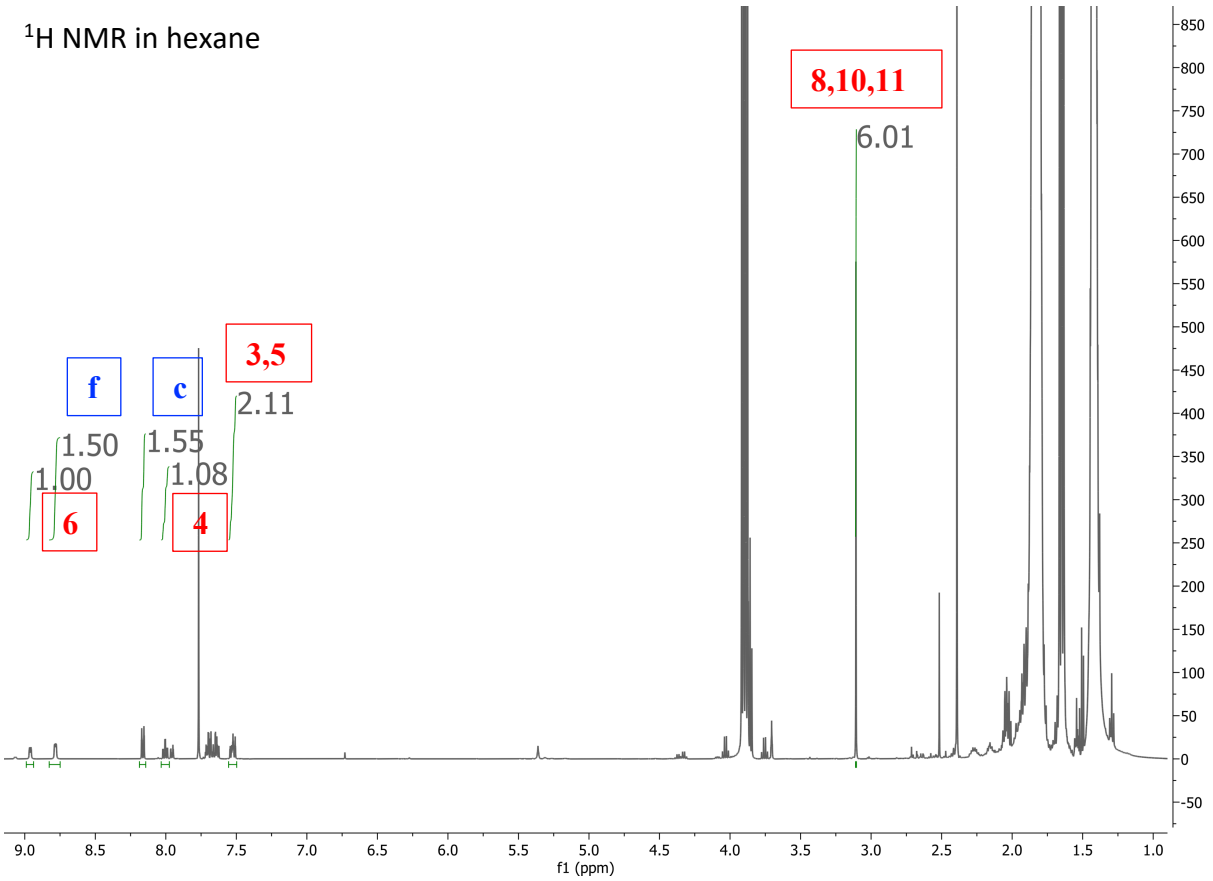

### 7.2.7. $Et_3B/Et_2BOOEt$ initiated ATRA of 4-iodotrifluorotoluene to TCP

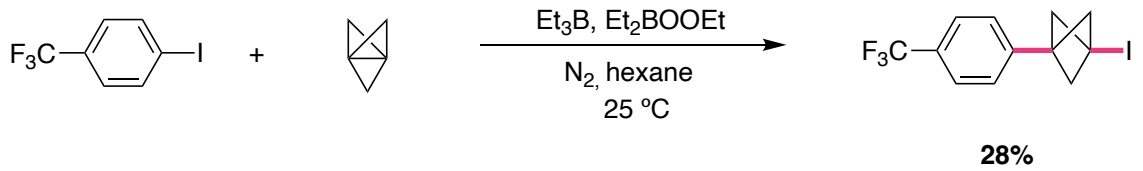


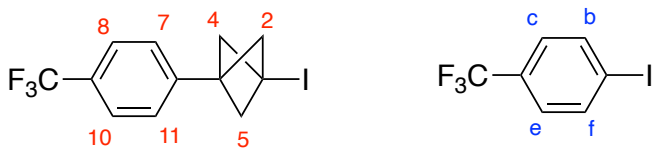


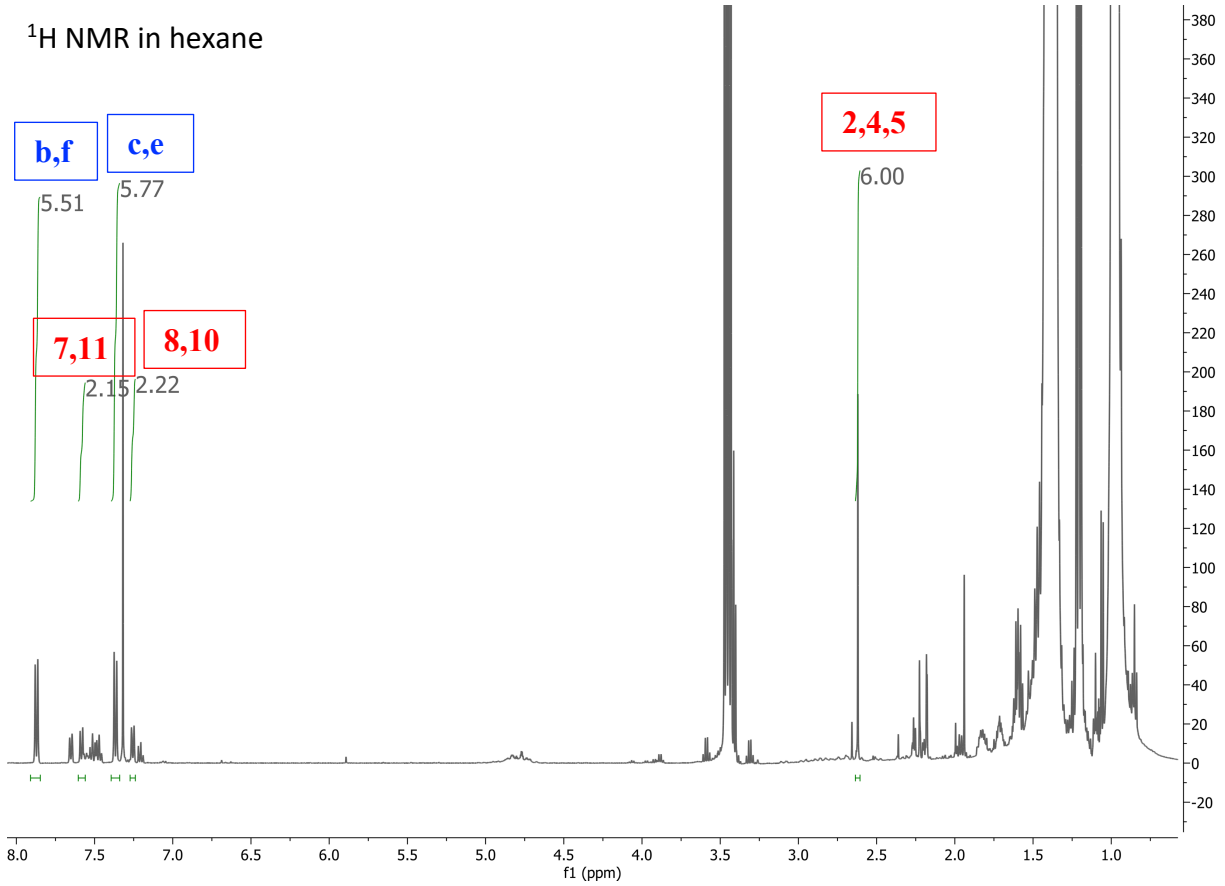

### 7.2.8. $Et_2BOOEt$ initiated ATRA of 4-iodotrifluorotoluene to TCP

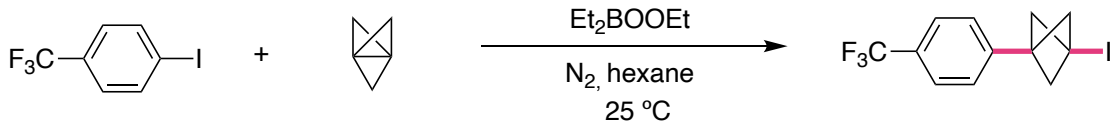


**33%**

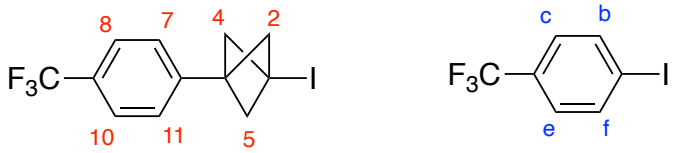


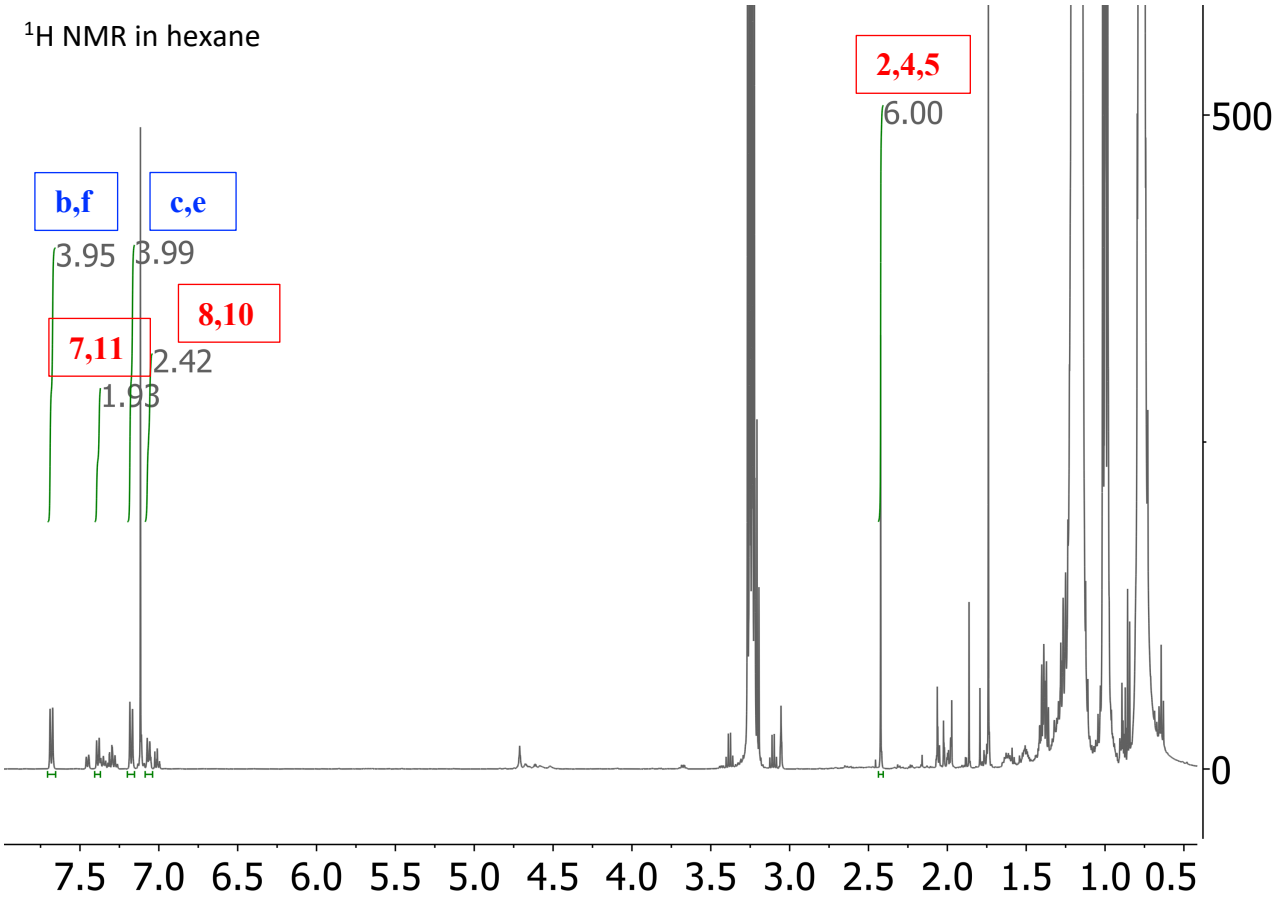

## 7.3. Synthesis NMR and MS data

### 7.3.1. 1.11M $Bu_3B$ in hexane

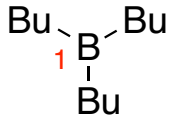


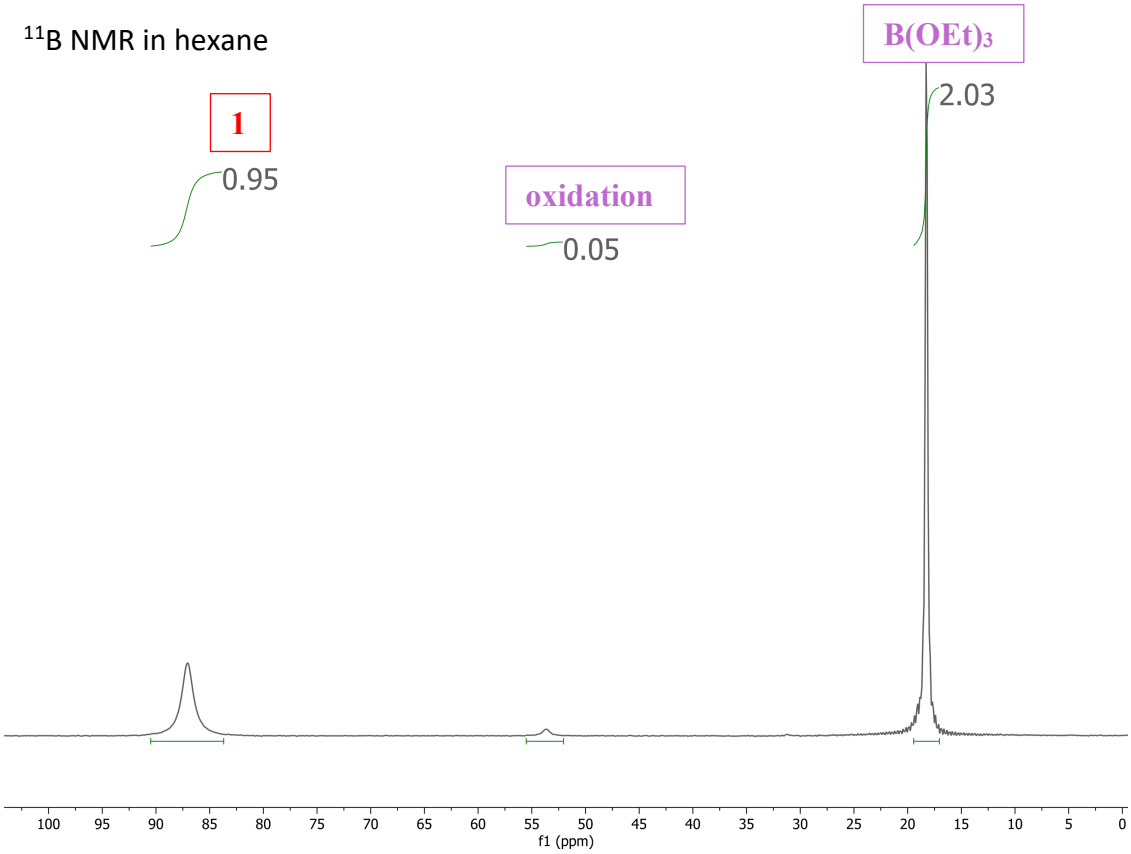

### 7.3.2. 50 mM $Et_2BOOEt$ in hexane

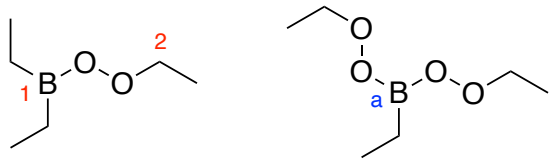


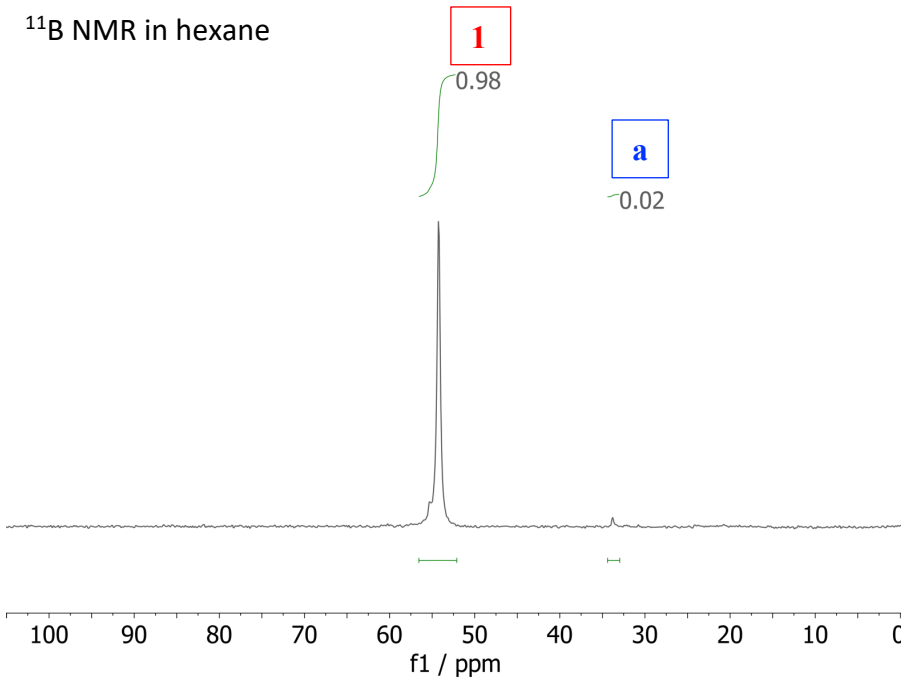


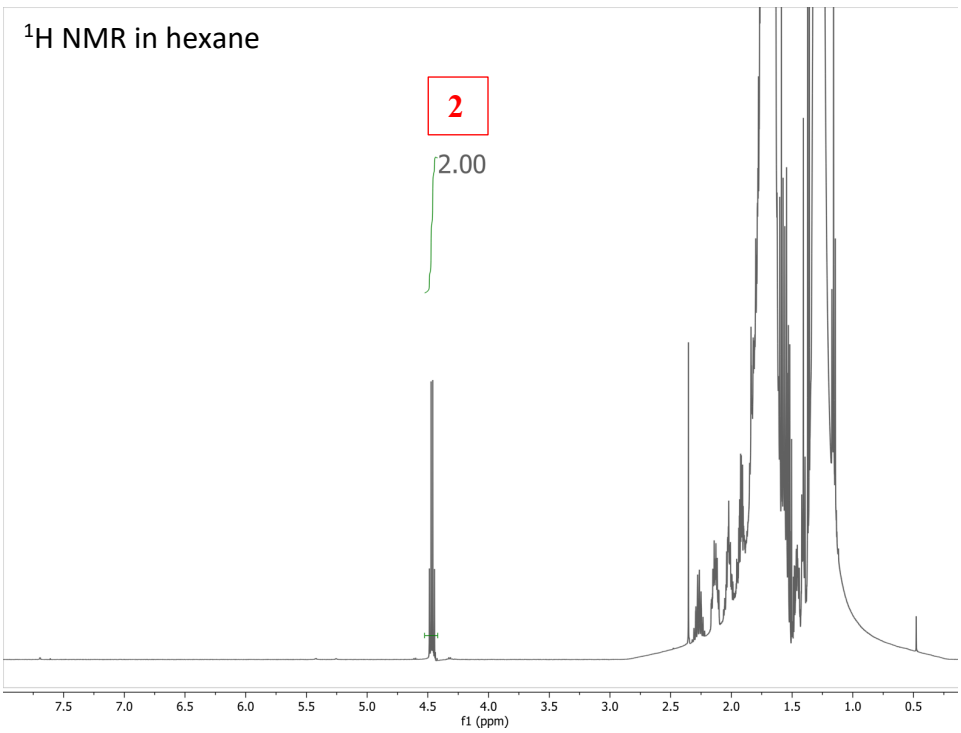

### 7.3.3. 50 mM $Bu_2BOOBu$ in hexane

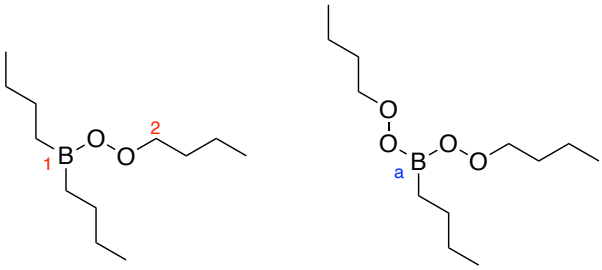


$^{11}B$ NMR in hexane

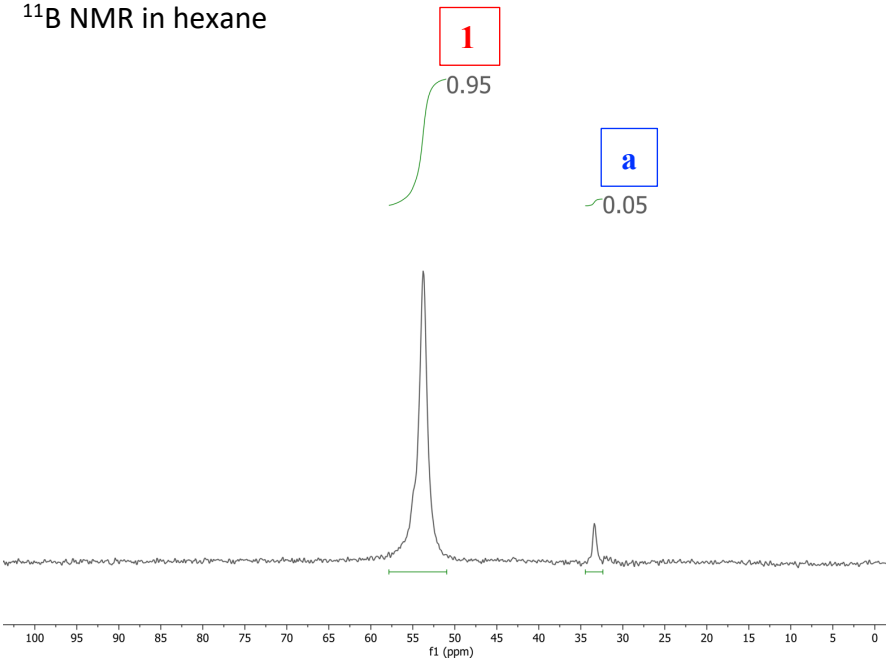


$^{1}H$ NMR in hexane

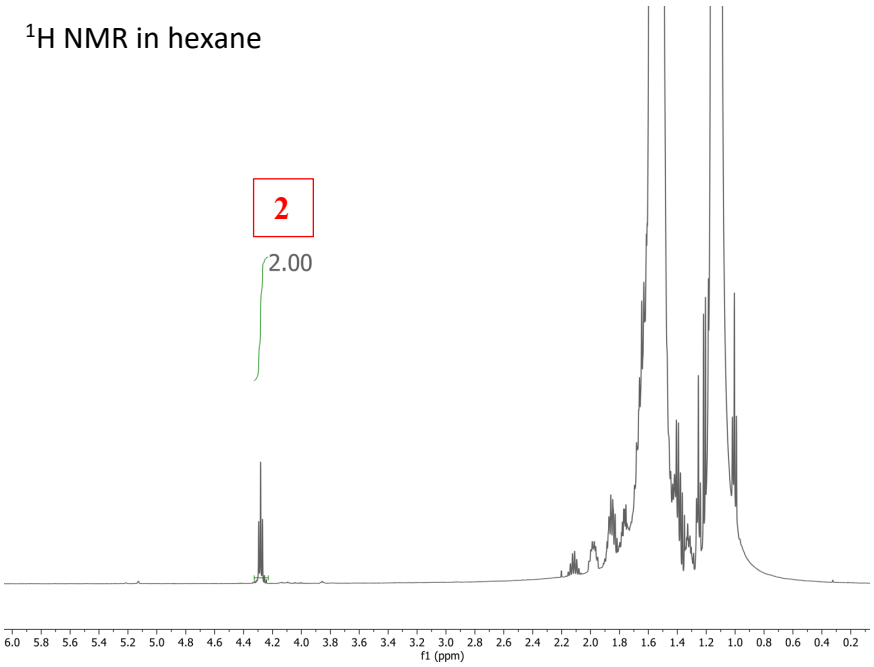

### 7.3.4. 1M TCP in $Et_2O$

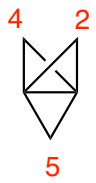


$^1H$ NMR in $Et_2O$

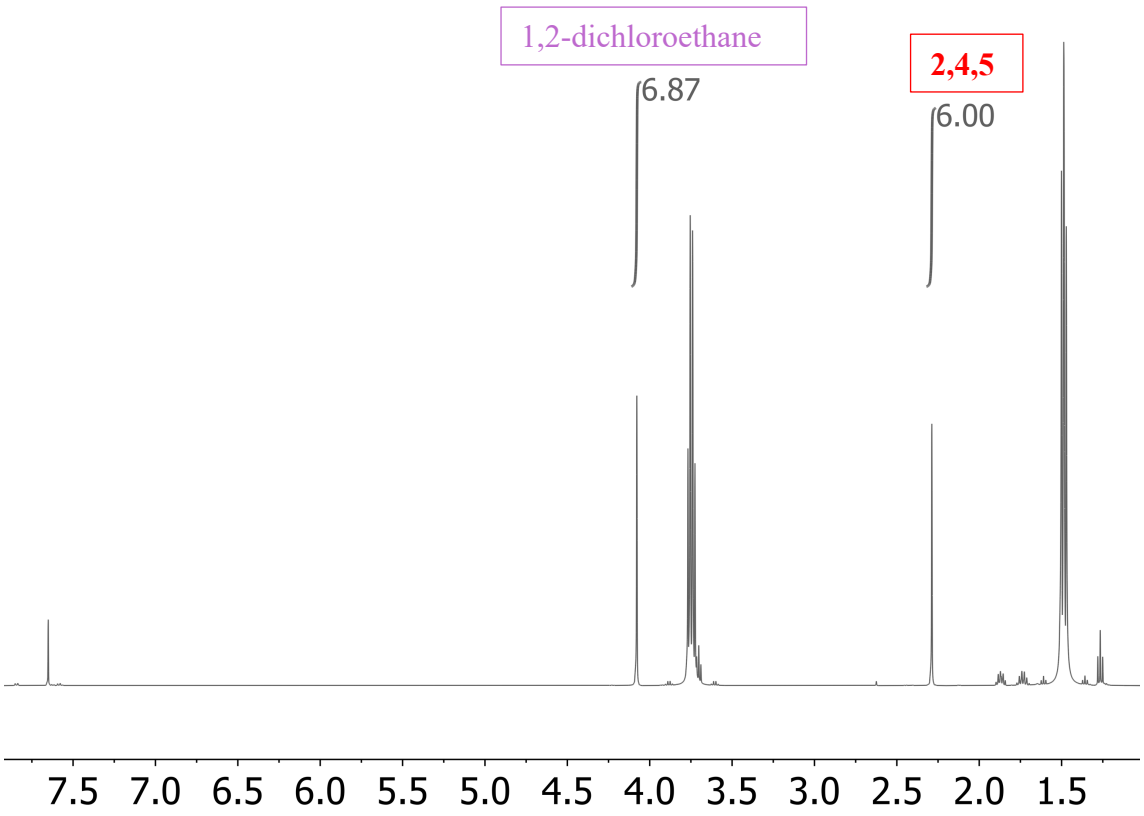

### 7.3.5. methyl 2-(((2,2,6,6-tetramethylpiperidin-1-yl)oxy)methyl)acrylate (first step in the synthesis of CHANT)

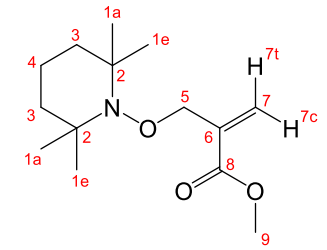


$^1$H NMR in $CDCl_3$

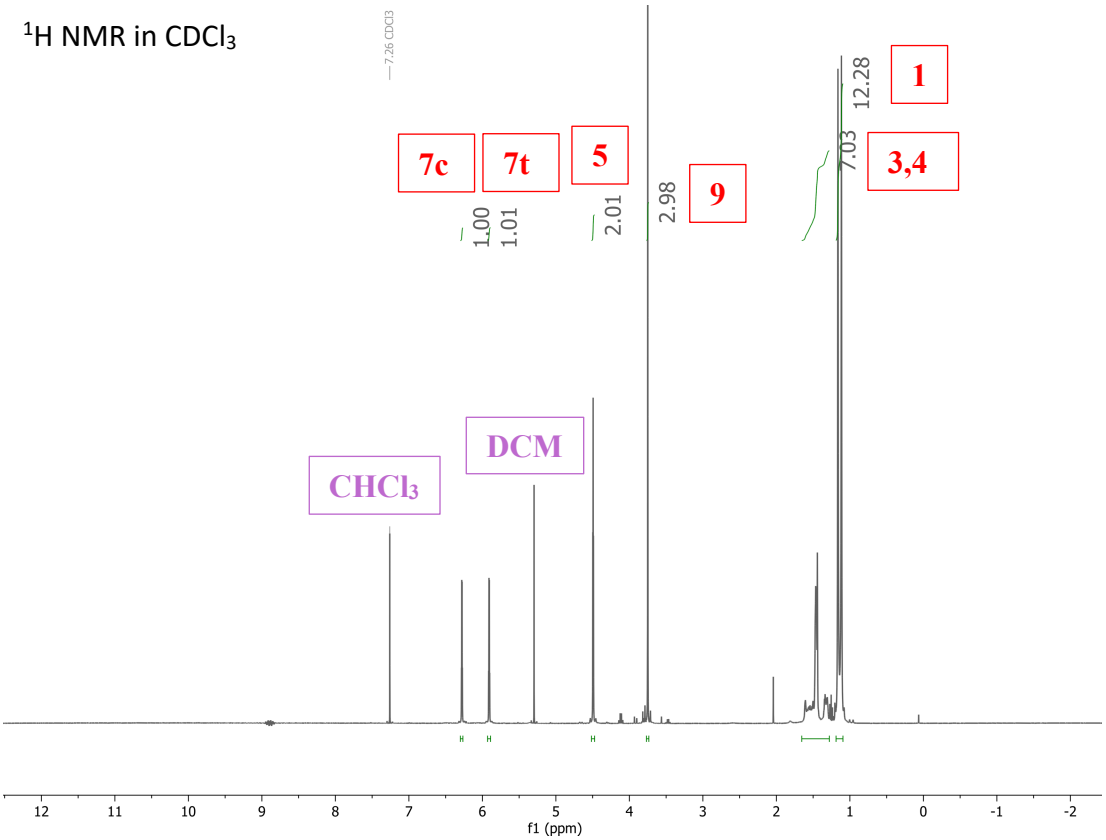


**Analysis Information**

| | | | |
|---|---|---|---|
| Analysis Filename | vc85711io_P1-F-6_01_21696.d | Acquisition Date | 15/10/2020 17:00:36 |
| Method | ESI_low mass_2c1s.m | Instrument | compact |
| Submission Name | vc85711io | ESI | Positive |

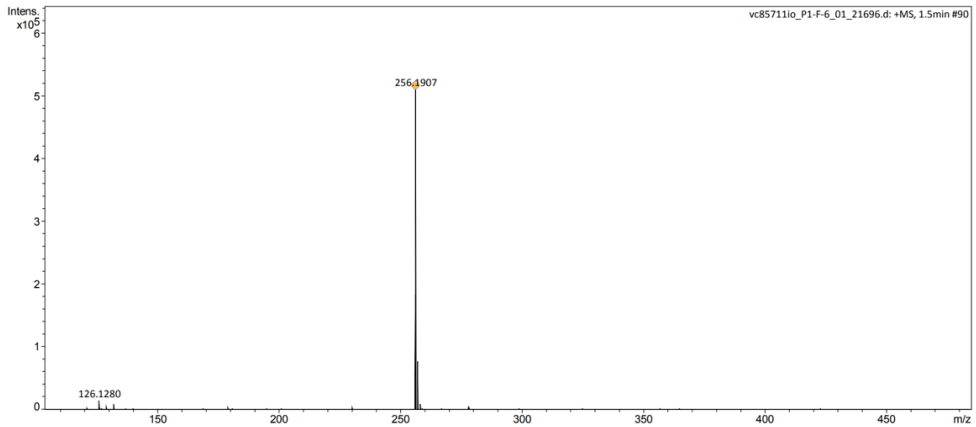


| Meas. m/z | # | Ion Formula | m/z | err [ppm] | err [mDa] | mSigma | Mean err [ppm] |
|---|---|---|---|---|---|---|---|
| 256.1907 | 1 | C14H26NO3 | 256.1907 | 0.2 | 0.1 | 4.2 | -0.6 |

### 7.3.6. 2-(((2,2,6,6-tetramethylpiperidin-1-yl)oxy)methyl)acrylic acid (second step in the synthesis of CHANT)

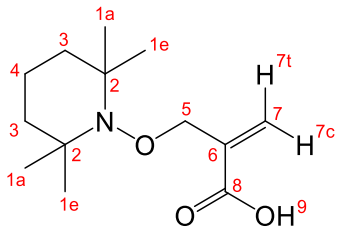


$^1$H NMR in $CDCl_3$

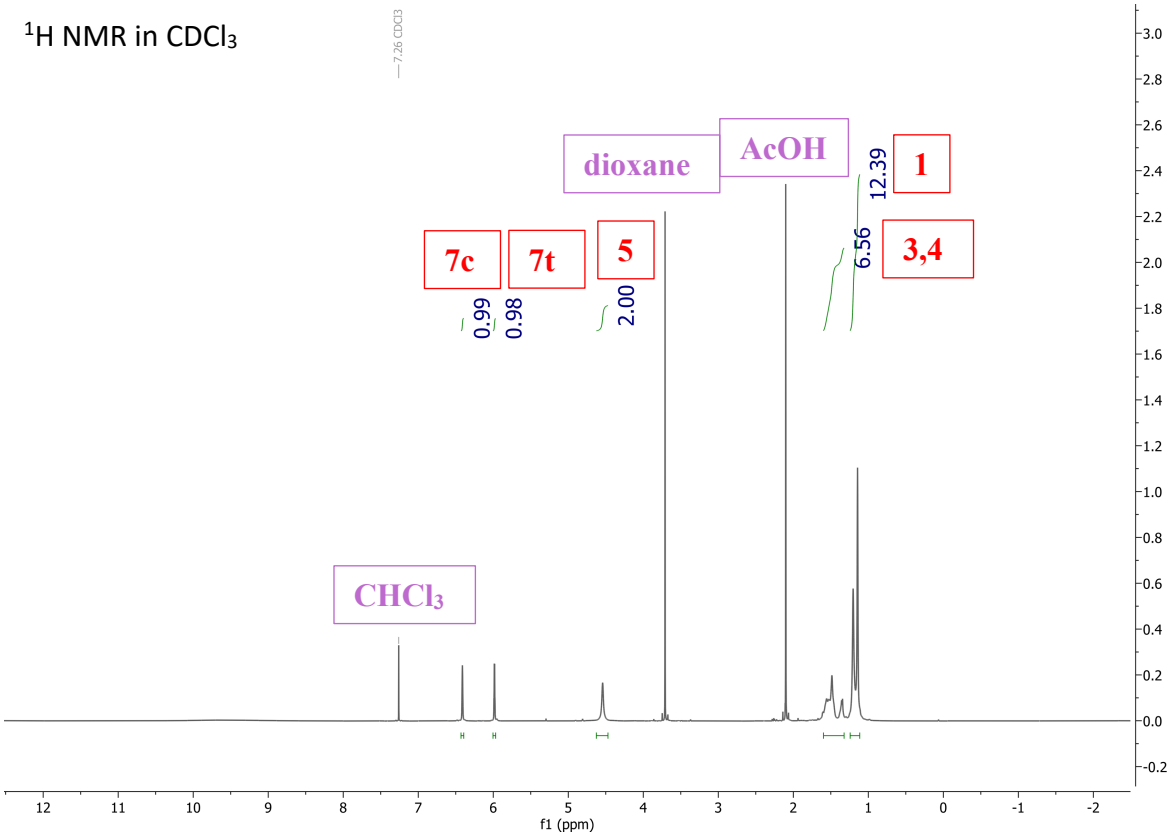


**Analysis Information**

| | | | |
|---|---|---|---|
| Analysis Filename | vc85799io_P1-C-1_01_21801.d | Acquisition Date | 20/10/2020 14:52:42 |
| Method | ESI_low mass_2c1s.m | Instrument | compact |
| Submission Name | vc85799io | ESI | Positive |

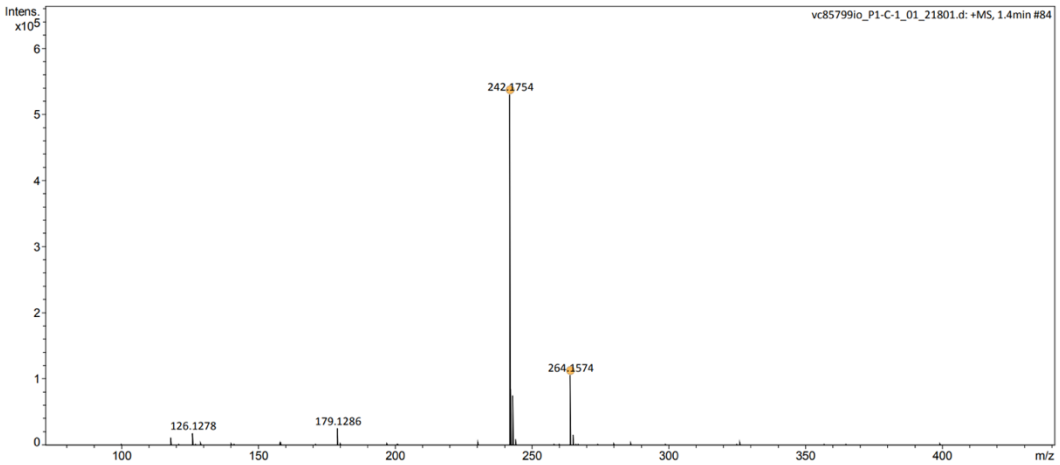


| Meas. m/z | # | Ion Formula | m/z | err [ppm] | err [mDa] | mSigma | Mean err [ppm] |
|---|---|---|---|---|---|---|---|
| 242.1754 | 1 | C13H24NO3 | 242.1751 | -1.3 | -0.3 | 3.8 | -1.1 |
| 264.1574 | 1 | C13H23NNaO3 | 264.1570 | -1.6 | -0.4 | 1.3 | -2.6 |

### 7.3.7. N-cyclohexyl-2-(((2,2,6,6-tetramethylpiperidin-1-yl)oxy)methyl)acrylamide (CHANT)

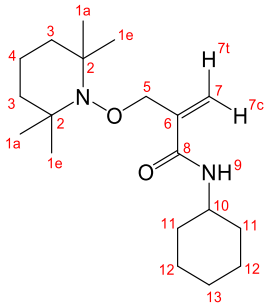


$^1$H NMR in $CDCl_3$

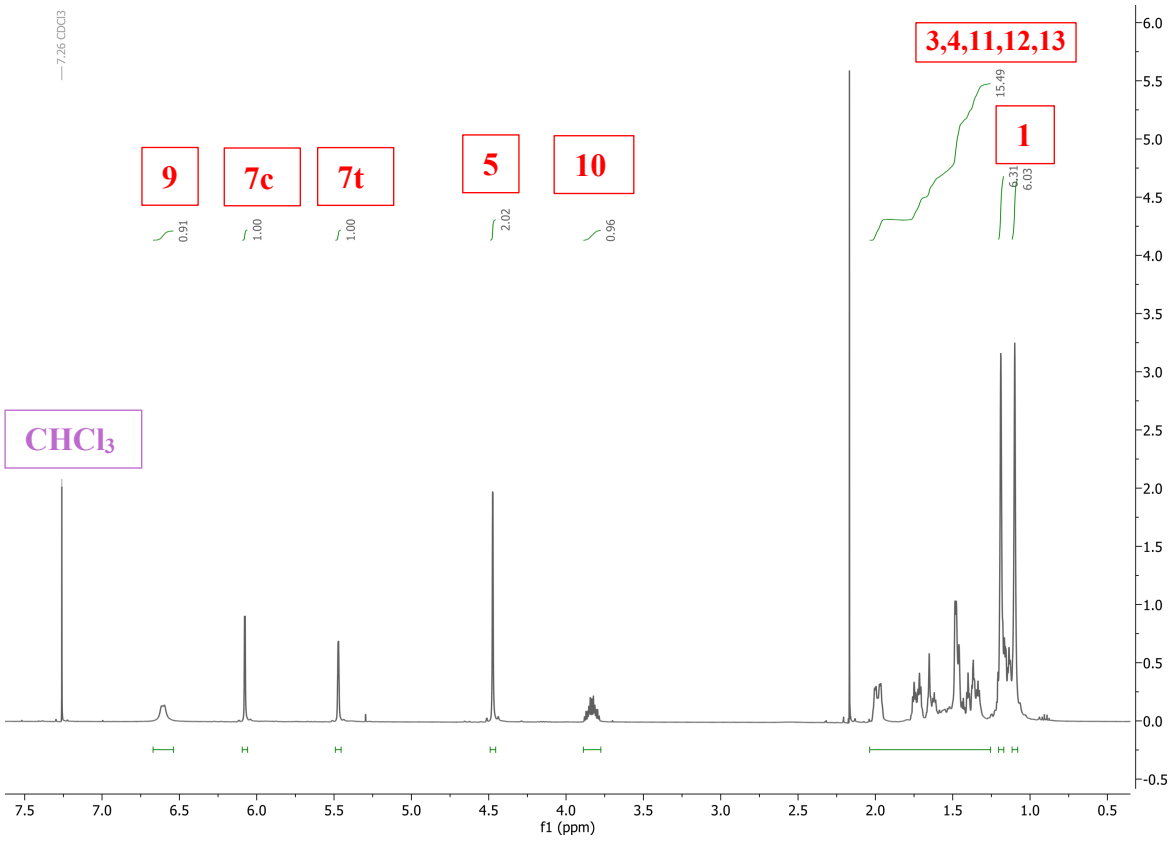


**Analysis Information**

| | | | |
|---|---|---|---|
| Analysis Filename | vc85979io_P1-E-9_01_22001.d | Acquisition Date | 26/10/2020 13:59:49 |
| Method | ESI_low mass_2c1s.m | Instrument | compact |
| Submission Name | vc85979io | ESI | Positive |

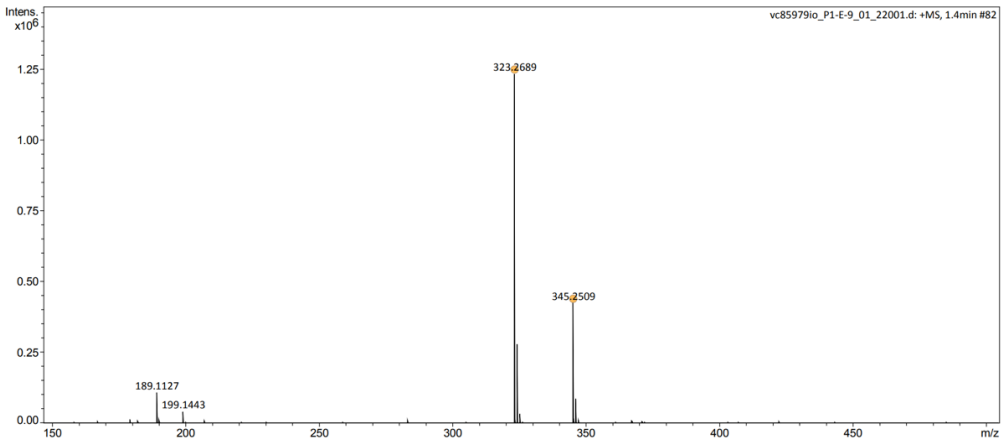


| Meas. m/z | # | Ion Formula | m/z | err [ppm] | err [mDa] | mSigma | Mean err [ppm] |
|---|---|---|---|---|---|---|---|
| 323.2689 | 1 | C19H35N2O2 | 323.2693 | 1.3 | 0.4 | 5.0 | 0.9 |
| 345.2509 | 1 | C19H34N2NaO2 | 345.2512 | 1.0 | 0.3 | 6.4 | -0.4 |

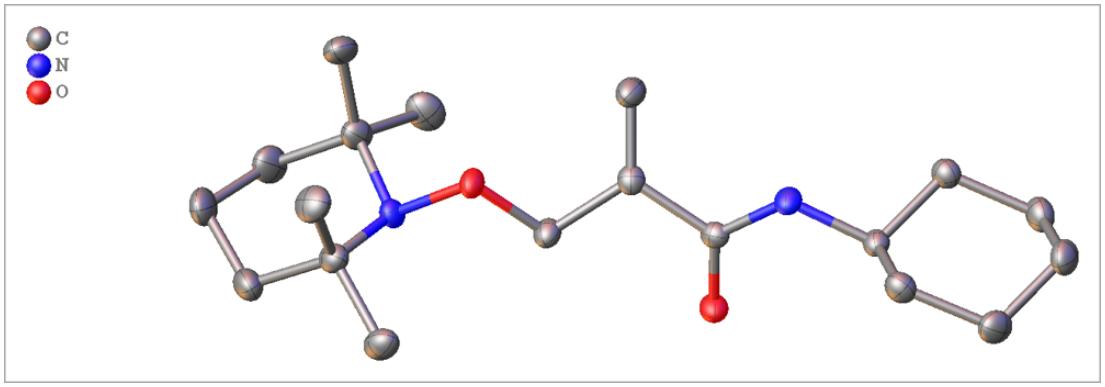


Data collected, solved and refined by Adrian C Whitwood

**Crystal data and structure refinement**

| | |
|---|---|
| Empirical formula | $C_{19}H_{34}N_2O_2$ |
| Formula weight | 322.48 |
| Temperature/K | 110.00(10) |
| Crystal system | orthorhombic |
| Space group | $P2_12_12_1$ |
| a/Å | 10.00003(12) |
| b/Å | 12.25581(15) |
| c/Å | 15.81509(18) |
| α/° | 90 |
| β/° | 90 |
| γ/° | 90 |
| Volume/Å$^3$ | 1938.27(4) |
| Z | 4 |
| $\rho_{calc}$g/cm$^3$ | 1.105 |
| μ/mm$^{-1}$ | 0.554 |
| F(000) | 712.0 |
| Crystal size/mm$^3$ | 0.22 × 0.193 × 0.145 |
| Radiation | Cu Kα (λ = 1.54184) |
| 2Θ range for data collection/° | 9.128 to 134.068 |

| | |
|---|---|
| Index ranges | $-11 \leq h \leq 11$, $-14 \leq k \leq 8$, $-18 \leq l \leq 18$ |
| Reflections collected | 11996 |
| Independent reflections | 3448 [$R_{int}$ = 0.0263, $R_{sigma}$ = 0.0240] |
| Data/restraints/parameters | 3448/0/345 |
| Goodness-of-fit on $F^2$ | 1.059 |
| Final R indexes [I>=2σ (I)] | $R_1$ = 0.0247, $wR_2$ = 0.0624 |
| Final R indexes [all data] | $R_1$ = 0.0254, $wR_2$ = 0.0628 |
| Largest diff. peak/hole / e $Å^{-3}$ | 0.16/-0.13 |
| Flack parameter | -0.07(6) |

**Fractional Atomic Coordinates (×$10^4$) and Equivalent Isotropic Displacement Parameters ($Å^2$×$10^3$). $U_{eq}$ is defined as 1/3 of the trace of the orthogonalised $U_{IJ}$ tensor.**

| Atom | *x* | *y* | *z* | U(eq) |
|---|---|---|---|---|
| C1 | 4007.0(16) | 4742.4(12) | 8513.0(10) | 25.6(3) |
| C2 | 3187(2) | 5044.7(15) | 9299.6(11) | 35.0(4) |
| C3 | 3288(2) | 4205.5(17) | 10002.5(10) | 37.3(4) |
| C4 | 2868.3(18) | 3099.8(15) | 9662.1(10) | 30.8(4) |
| C5 | 3682.8(15) | 2731.6(13) | 8891.6(9) | 22.8(3) |
| C6 | 3609(2) | 5503.7(14) | 7789.0(12) | 34.9(4) |
| C7 | 5511.8(19) | 4888.7(15) | 8681.8(11) | 32.9(4) |
| C8 | 2988.6(18) | 1733.6(14) | 8508.2(11) | 29.1(4) |
| C9 | 5102.5(17) | 2396.3(16) | 9143.7(11) | 31.9(4) |
| C10 | 3579.6(15) | 3119.3(13) | 6827.2(9) | 21.6(3) |
| C11 | 4403.1(15) | 3253.0(12) | 6034.0(9) | 19.0(3) |
| C12 | 3766.9(14) | 2752.4(11) | 5268.7(9) | 17.6(3) |
| C13 | 5534.9(16) | 3811.5(13) | 6011.4(10) | 26.1(3) |
| C14 | 4073.1(14) | 2161.8(12) | 3788.2(9) | 19.1(3) |
| C15 | 4421.5(17) | 960.1(12) | 3662.1(10) | 24.3(3) |

**Fractional Atomic Coordinates (×10$^4$) and Equivalent Isotropic Displacement Parameters (Å$^2$×10$^3$). $U_{eq}$ is defined as 1/3 of the trace of the orthogonalised $U_{IJ}$ tensor.**

| Atom | *x* | *y* | *z* | U(eq) |
|---|---|---|---|---|
| C16 | 3981.9(18) | 556.1(13) | 2791.0(10) | 29.2(4) |
| C17 | 4558.5(18) | 1256.4(14) | 2083.0(10) | 29.5(4) |
| C18 | 4183.7(16) | 2451.0(14) | 2209.3(9) | 27.5(3) |
| C19 | 4646.8(15) | 2858.8(12) | 3075.1(9) | 22.0(3) |
| N1 | 3582.1(12) | 3625.3(10) | 8260.2(7) | 19.4(3) |
| N2 | 4562.2(13) | 2560.1(10) | 4602.3(7) | 20.4(3) |
| O1 | 4408.8(10) | 3324.1(8) | 7541.0(6) | 20.1(2) |
| O2 | 2555.7(10) | 2546.8(9) | 5274.1(6) | 22.3(2) |

**Anisotropic Displacement Parameters (Å$^2$×10$^3$). The Anisotropic displacement factor exponent takes the form: $-2\pi^2[h^2a^{*2}U_{11}+2hka^*b^*U_{12}+\ldots]$.**

| Atom | $U_{11}$ | $U_{22}$ | $U_{33}$ | $U_{23}$ | $U_{13}$ | $U_{12}$ |
|---|---|---|---|---|---|---|
| C1 | 29.7(8) | 20.7(7) | 26.5(7) | -5.6(6) | 6.1(7) | -2.5(6) |
| C2 | 41.8(11) | 30.1(9) | 33.1(9) | -12.8(7) | 10.2(8) | -2.1(8) |
| C3 | 39.2(10) | 50.5(11) | 22.2(8) | -10.7(7) | 10.1(7) | -7.6(9) |
| C4 | 29.9(9) | 41.8(10) | 20.9(7) | 2.6(7) | 2.3(6) | -8.5(7) |
| C5 | 22.0(8) | 25.3(7) | 21.0(7) | 2.1(6) | -3.0(6) | -1.9(6) |
| C6 | 43.6(11) | 22.1(8) | 39.1(10) | 1.8(7) | 7.2(8) | 2.7(7) |
| C7 | 33.8(9) | 33.5(9) | 31.3(9) | -8.6(7) | 4.7(7) | -14.6(8) |
| C8 | 33.7(9) | 24.0(8) | 29.6(8) | 4.1(7) | -5.1(7) | -5.7(7) |
| C9 | 29.0(9) | 36.7(9) | 30.0(8) | 4.6(8) | -9.5(7) | 1.7(7) |
| C10 | 16.9(7) | 28.9(8) | 18.9(7) | -2.6(6) | -1.4(5) | -0.2(6) |
| C11 | 17.1(7) | 20.9(7) | 19.0(7) | 0.0(5) | -0.5(5) | 4.0(6) |
| C12 | 16.2(7) | 17.2(6) | 19.4(6) | 3.3(5) | -1.5(5) | 0.8(5) |
| C13 | 21.2(7) | 33.5(8) | 23.7(8) | -6.6(6) | 2.4(6) | -3.7(7) |

**Anisotropic Displacement Parameters ($Å^2 \times 10^3$). The Anisotropic displacement factor exponent takes the form: $-2\pi^2[h^2a^{*2}U_{11}+2hka^*b^*U_{12}+\ldots]$.**

| Atom | $U_{11}$ | $U_{22}$ | $U_{33}$ | $U_{23}$ | $U_{13}$ | $U_{12}$ |
|---|---|---|---|---|---|---|
| C14 | 14.9(7) | 25.2(7) | 17.3(7) | -0.7(5) | -0.6(5) | -1.1(6) |
| C15 | 25.4(8) | 22.9(7) | 24.6(8) | 2.6(6) | 2.6(6) | -0.2(6) |
| C16 | 31.7(9) | 25.5(8) | 30.4(8) | -8.4(6) | 4.8(7) | -2.6(7) |
| C17 | 28.5(9) | 38.6(9) | 21.2(7) | -7.7(7) | 4.6(7) | -0.8(7) |
| C18 | 27.9(8) | 35.0(8) | 19.7(7) | 3.4(6) | 0.0(6) | -0.1(7) |
| C19 | 22.2(8) | 22.9(7) | 21.0(7) | 1.9(6) | 0.0(6) | -0.3(6) |
| N1 | 19.6(6) | 21.6(6) | 16.9(6) | -2.7(5) | 4.3(5) | 0.3(5) |
| N2 | 13.1(6) | 28.7(7) | 19.2(6) | -2.5(5) | -0.9(5) | -0.5(5) |
| O1 | 16.3(5) | 27.7(5) | 16.3(5) | -5.1(4) | 1.0(4) | 1.4(4) |
| O2 | 15.3(5) | 31.4(6) | 20.1(5) | -0.5(4) | 0.1(4) | -1.5(4) |

**Bond Lengths**

| Atom | Atom | Length/Å | Atom | Atom | Length/Å |
|---|---|---|---|---|---|
| C1 | C2 | 1.536(2) | C11 | C12 | 1.4986(19) |
| C1 | C6 | 1.530(2) | C11 | C13 | 1.323(2) |
| C1 | C7 | 1.539(2) | C12 | N2 | 1.3412(19) |
| C1 | N1 | 1.4882(19) | C12 | O2 | 1.2372(18) |
| C2 | C3 | 1.518(3) | C14 | C15 | 1.526(2) |
| C3 | C4 | 1.517(3) | C14 | C19 | 1.527(2) |
| C4 | C5 | 1.534(2) | C14 | N2 | 1.4614(18) |
| C5 | C8 | 1.532(2) | C15 | C16 | 1.528(2) |
| C5 | C9 | 1.531(2) | C16 | C17 | 1.524(2) |
| C5 | N1 | 1.4854(19) | C17 | C18 | 1.524(2) |
| C10 | C11 | 1.5095(19) | C18 | C19 | 1.529(2) |
| C10 | O1 | 1.4230(17) | N1 | O1 | 1.4538(15) |

**Bond Angles**

| Atom | Atom | Atom | Angle/˚ | Atom | Atom | Atom | Angle/˚ |
|---|---|---|---|---|---|---|---|
| C2 | C1 | C7 | 110.72(14) | C13 | C11 | C12 | 123.58(13) |
| C6 | C1 | C2 | 108.67(14) | N2 | C12 | C11 | 117.05(12) |
| C6 | C1 | C7 | 108.26(14) | O2 | C12 | C11 | 119.57(13) |
| N1 | C1 | C2 | 106.68(13) | O2 | C12 | N2 | 123.38(13) |
| N1 | C1 | C6 | 106.60(13) | C15 | C14 | C19 | 110.95(12) |
| N1 | C1 | C7 | 115.66(13) | N2 | C14 | C15 | 111.16(12) |
| C3 | C2 | C1 | 113.20(15) | N2 | C14 | C19 | 109.76(12) |
| C4 | C3 | C2 | 109.07(14) | C14 | C15 | C16 | 111.39(13) |
| C3 | C4 | C5 | 113.42(14) | C17 | C16 | C15 | 111.77(13) |
| C8 | C5 | C4 | 107.99(13) | C16 | C17 | C18 | 110.58(13) |
| C9 | C5 | C4 | 111.38(13) | C17 | C18 | C19 | 110.90(13) |
| C9 | C5 | C8 | 108.00(14) | C14 | C19 | C18 | 111.39(12) |
| N1 | C5 | C4 | 106.33(12) | C5 | N1 | C1 | 118.58(11) |
| N1 | C5 | C8 | 106.98(11) | O1 | N1 | C1 | 106.34(10) |
| N1 | C5 | C9 | 115.84(13) | O1 | N1 | C5 | 107.47(10) |
| O1 | C10 | C11 | 108.80(11) | C12 | N2 | C14 | 123.54(12) |
| C12 | C11 | C10 | 113.28(12) | C10 | O1 | N1 | 109.52(9) |
| C13 | C11 | C10 | 123.04(13) | | | | |

**Hydrogen Bonds**

| D | H | A | d(D-H)/Å | d(H-A)/Å | d(D-A)/Å | D-H-A/° |
|---|---|---|---|---|---|---|
| N2 | H2 | O2[1] | 0.83(2) | 2.18(2) | 3.0027(16) | 167.7(19) |

[1]1/2+X,1/2-Y,1-Z

**Torsion Angles**

| A | B | C | D | Angle/˚ | A | B | C | D | Angle/˚ |
|---|---|---|---|---|---|---|---|---|---|
| C1 | C2 | C3 | C4 | -56.2(2) | C10 | C11 | C12 | N2 | -161.93(12) |
| C1 | N1 | O1 | C10 | -119.67(12) | C10 | C11 | C12 | O2 | 18.69(18) |
| C2 | C1 | N1 | C5 | -56.22(17) | C11 | C10 | O1 | N1 | 157.65(11) |
| C2 | C1 | N1 | O1 | -177.28(12) | C11 | C12 | N2 | C14 | -174.72(12) |
| C2 | C3 | C4 | C5 | 56.6(2) | C13 | C11 | C12 | N2 | 21.8(2) |
| C3 | C4 | C5 | C8 | -168.89(15) | C13 | C11 | C12 | O2 | -157.62(15) |
| C3 | C4 | C5 | C9 | 72.68(19) | C14 | C15 | C16 | C17 | 54.98(18) |
| C3 | C4 | C5 | N1 | -54.37(18) | C15 | C14 | C19 | C18 | 55.42(16) |
| C4 | C5 | N1 | C1 | 56.35(16) | C15 | C14 | N2 | C12 | -105.52(16) |
| C4 | C5 | N1 | O1 | 176.83(11) | C15 | C16 | C17 | C18 | -55.78(19) |
| C5 | N1 | O1 | C10 | 112.39(12) | C16 | C17 | C18 | C19 | 56.36(18) |
| C6 | C1 | C2 | C3 | 168.34(15) | C17 | C18 | C19 | C14 | -56.65(17) |
| C6 | C1 | N1 | C5 | -172.20(13) | C19 | C14 | C15 | C16 | -54.35(17) |
| C6 | C1 | N1 | O1 | 66.75(14) | C19 | C14 | N2 | C12 | 131.35(14) |
| C7 | C1 | C2 | C3 | -72.88(19) | N1 | C1 | C2 | C3 | 53.76(19) |
| C7 | C1 | N1 | C5 | 67.40(17) | N2 | C14 | C15 | C16 | -176.79(13) |
| C7 | C1 | N1 | O1 | -53.65(16) | N2 | C14 | C19 | C18 | 178.68(12) |
| C8 | C5 | N1 | C1 | 171.56(13) | O1 | C10 | C11 | C12 | 163.29(11) |
| C8 | C5 | N1 | O1 | -67.96(14) | O1 | C10 | C11 | C13 | -20.4(2) |
| C9 | C5 | N1 | C1 | -67.98(18) | O2 | C12 | N2 | C14 | 4.6(2) |
| C9 | C5 | N1 | O1 | 52.50(16) | | | | | |

**Hydrogen Atom Coordinates (Å×10$^4$) and Isotropic Displacement Parameters (Å$^2$×10$^3$).**

| Atom | *x* | *y* | *z* | U(eq) |
|---|---|---|---|---|
| H2A | 2210(20) | 5125(17) | 9114(14) | 39(5) |
| H2B | 3450(20) | 5750(20) | 9486(13) | 40(6) |

**Hydrogen Atom Coordinates (Å×10$^4$) and Isotropic Displacement Parameters (Å$^2$×10$^3$).**

| Atom | *x* | *y* | *z* | U(eq) |
|---|---|---|---|---|
| H3A | 4250(20) | 4194(17) | 10239(13) | 35(5) |
| H3B | 2710(20) | 4419(18) | 10462(14) | 43(6) |
| H4A | 1940(20) | 3117(15) | 9484(12) | 27(5) |
| H4B | 2960(20) | 2530(18) | 10085(13) | 31(5) |
| H6A | 2630(20) | 5402(18) | 7674(14) | 43(6) |
| H6B | 4150(20) | 5336(18) | 7261(14) | 39(5) |
| H6C | 3760(20) | 6267(19) | 7963(14) | 40(5) |
| H7A | 6060(20) | 4557(17) | 8249(13) | 33(5) |
| H7B | 5730(20) | 5660(20) | 8722(14) | 44(6) |
| H7C | 5750(20) | 4576(18) | 9255(14) | 37(5) |
| H8A | 3545(19) | 1434(16) | 8042(13) | 28(5) |
| H8B | 2090(20) | 1940(15) | 8281(12) | 30(5) |
| H8C | 2910(20) | 1199(18) | 8961(14) | 41(6) |
| H9A | 5530(20) | 2923(17) | 9526(13) | 34(5) |
| H9B | 5080(20) | 1660(20) | 9436(14) | 45(6) |
| H9C | 5670(20) | 2332(17) | 8659(13) | 32(5) |
| H10A | 2830(20) | 3633(16) | 6814(11) | 26(4) |
| H10B | 3220(17) | 2367(16) | 6837(11) | 23(4) |
| H13A | 6030(20) | 3928(15) | 5478(12) | 27(5) |
| H13B | 5950(20) | 4114(16) | 6514(13) | 31(5) |
| H14 | 3122(17) | 2222(13) | 3803(9) | 11(4) |
| H15A | 5380(20) | 860(15) | 3740(12) | 28(5) |
| H15B | 3980(20) | 533(16) | 4115(12) | 29(5) |
| H16A | 3000(20) | 599(16) | 2766(12) | 33(5) |
| H16B | 4200(20) | -201(17) | 2715(12) | 31(5) |
| H17A | 5560(20) | 1189(16) | 2080(13) | 34(5) |
| H17B | 4230(20) | 1002(16) | 1529(13) | 31(5) |

**Hydrogen Atom Coordinates (Å×10$^4$) and Isotropic Displacement Parameters (Å$^2$×10$^3$).**

| Atom | *x* | *y* | *z* | U(eq) |
|---|---|---|---|---|
| H18A | 3220(20) | 2527(16) | 2163(11) | 28(5) |
| H18B | 4540(20) | 2901(17) | 1759(13) | 35(5) |
| H19A | 4405(18) | 3607(16) | 3179(11) | 24(4) |
| H19B | 5640(20) | 2815(16) | 3084(12) | 32(5) |
| H2 | 5390(20) | 2634(16) | 4654(12) | 29(5) |

### 7.3.8. 2-methylenepentanoic acid (first step in the synthesis of trapped ethyl radical)

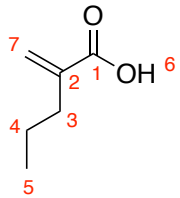


$^{1}$H NMR in $CDCl_3$

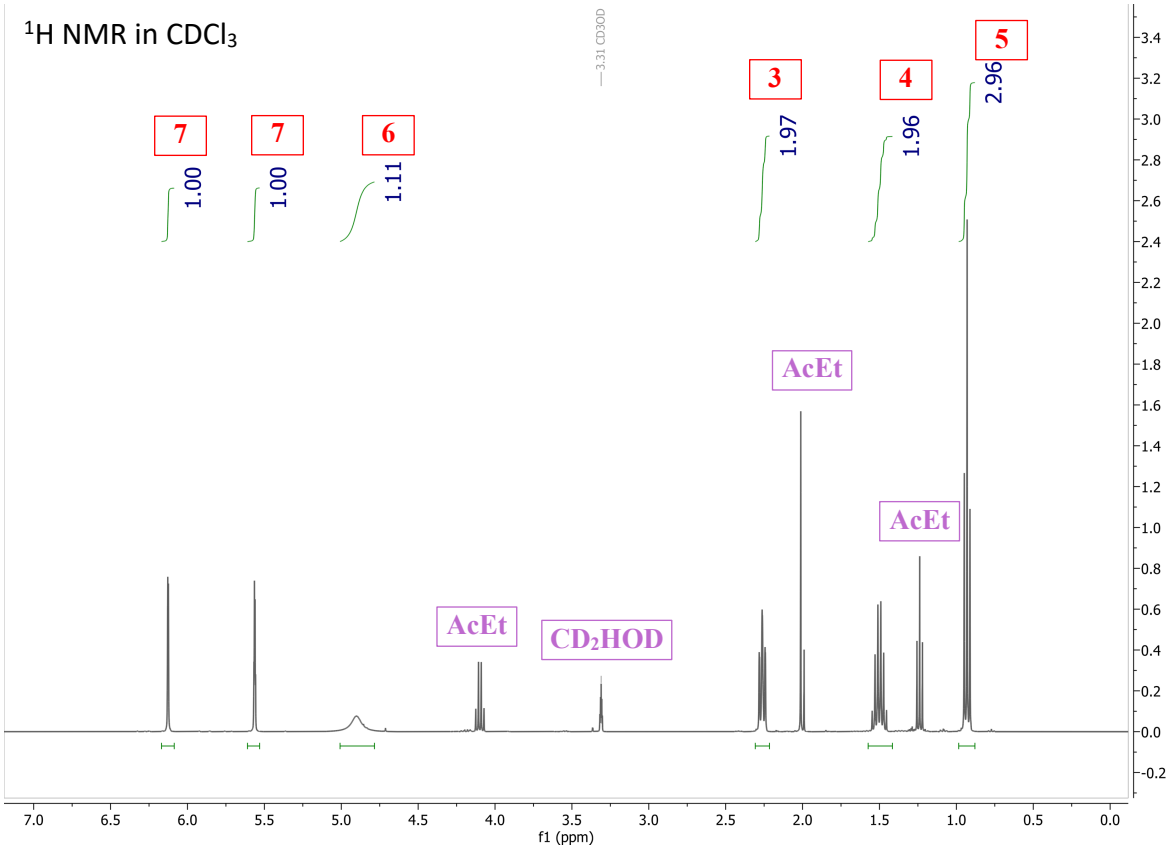


$^{13}$C NMR in $CDCl_3$

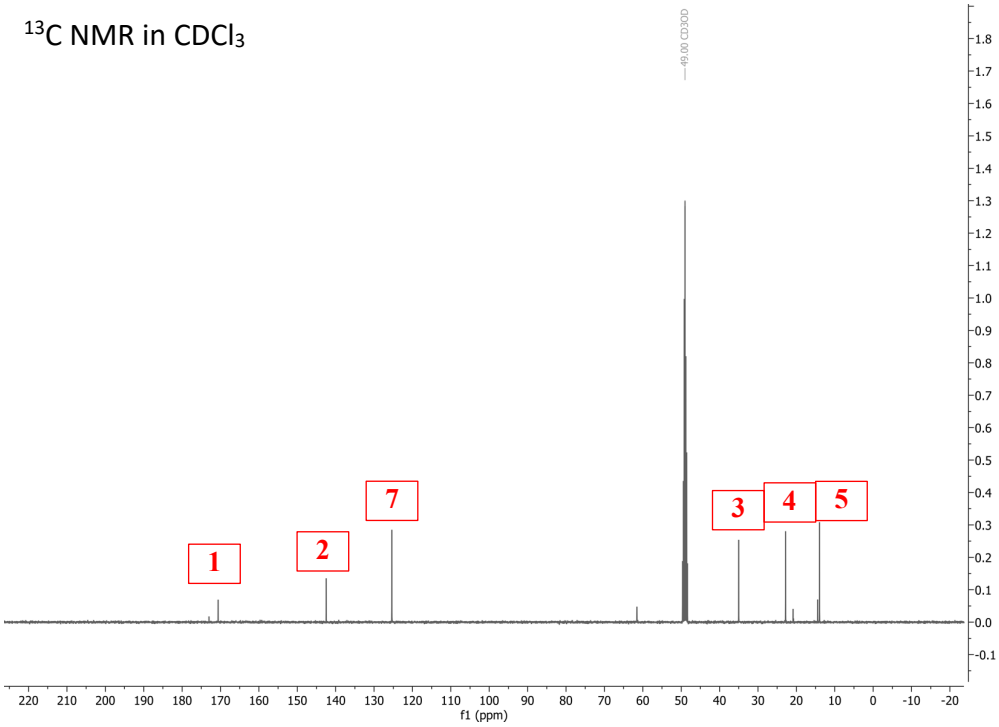

### 7.3.9. N-cyclohexyl-2-methylenepentanamide (trapped ethyl radical)

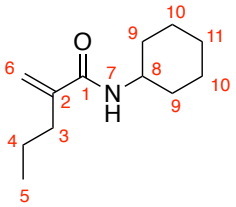

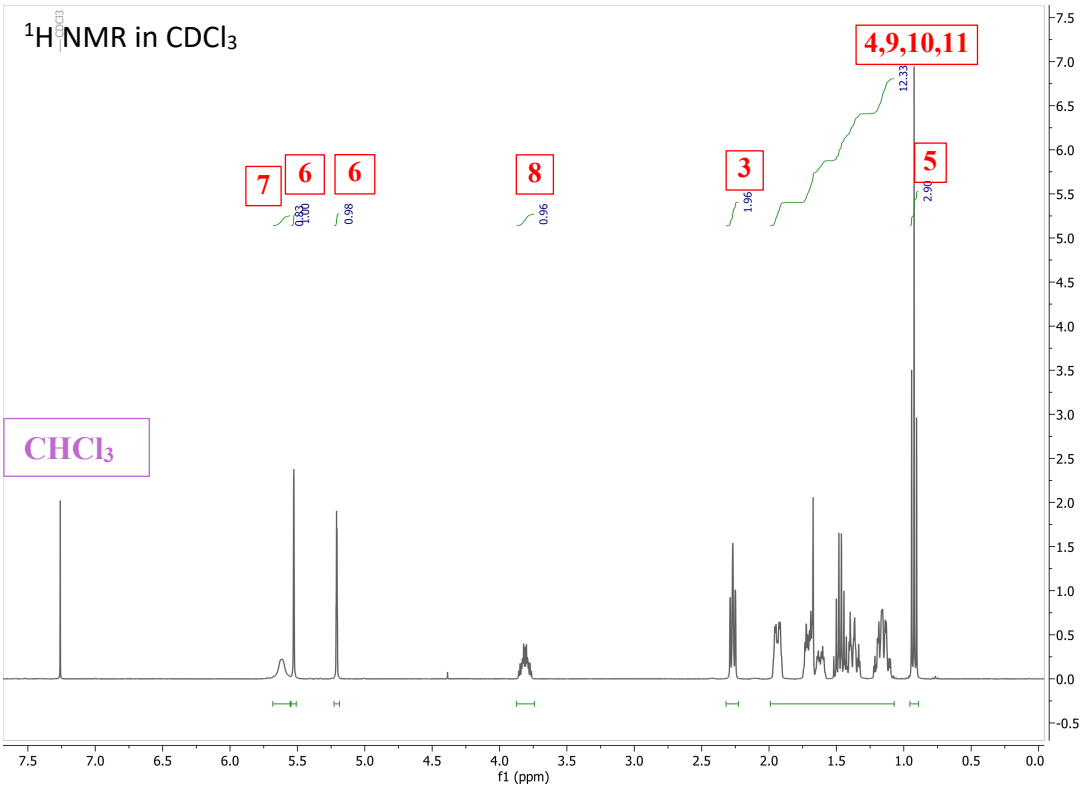


$^{13}$C NMR in CDCl$_3$

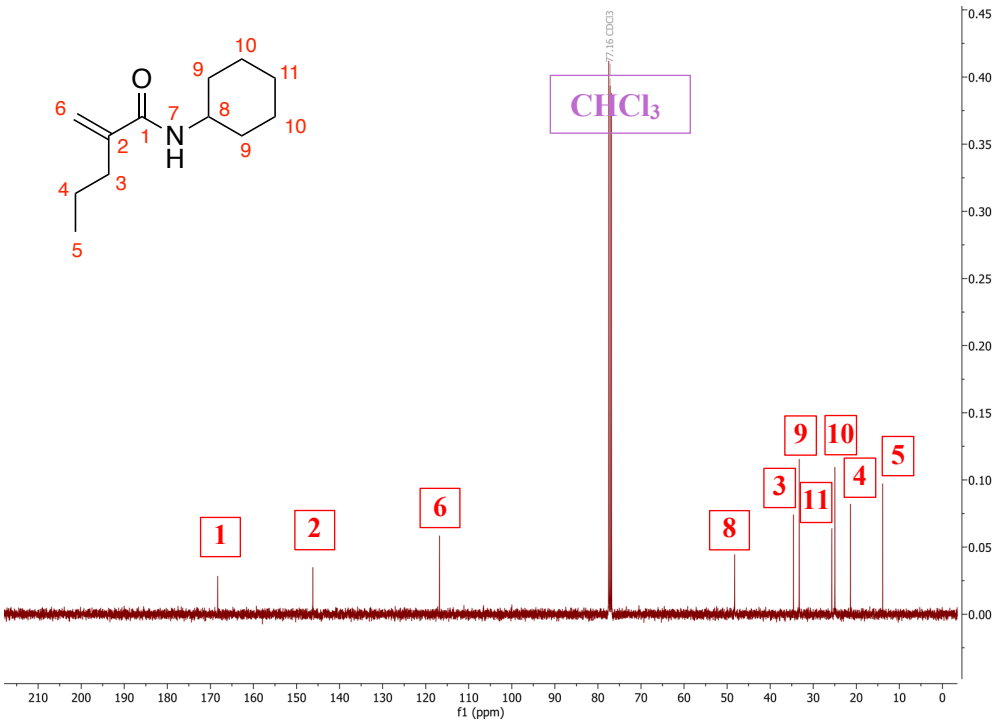

**Analysis Information**

| | | | |
|---|---|---|---|
| Analysis Filename | vc90922io_P1-E-1_01_27401.d | Acquisition Date | 16/06/2021 09:02:14 |
| Method | ESI_low mass_2c1s.m | Instrument | compact |
| Submission Name | vc90922io | ESI | Positive |

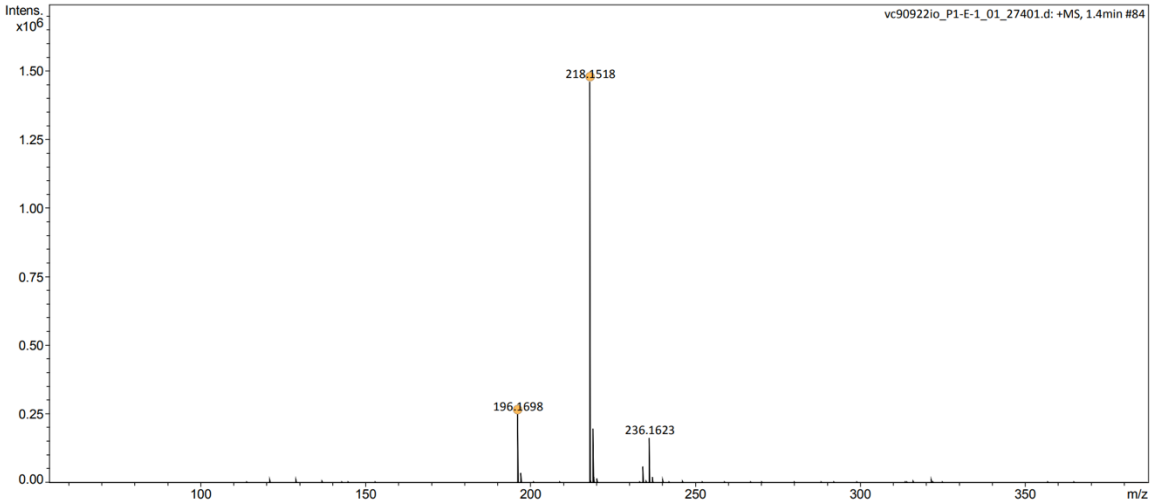


| Meas. m/z | # | Ion Formula | m/z | err [ppm] | err [mDa] | mSigma | Mean err [ppm] |
|---|---|---|---|---|---|---|---|
| 196.1698 | 1 | C12H22NO | 196.1696 | -1.3 | -0.3 | 3.9 | -1.3 |
| 218.1518 | 1 | C12H21NNaO | 218.1515 | -1.0 | -0.2 | 0.9 | -1.6 |

**Abbreviations**

| | |
|---|---|
| Ac | acetyl |
| AIBN | azobisisobutyronitrile |
| APCI | Atmospheric Pressure Ionisation |
| ATRA | Atom Transfer Radical Addition |
| BDE | Bond Dissociation Energy |
| Bn | benzyl |
| BPO | benzoyl peroxide |
| Bu | butyl |
| CHANT | N-cyclohexyl-2-(((2,2,6,6-tetramethylpiperidin-1-yl)oxy)methyl)acrylamide |
| CIDNP | Chemically Induced Dinamic Nuclear Polarisation |
| COSY | Correlated Spectroscopy |
| d | doublet |
| DEPT | Distortionless Enhancement by Polarisation Transfer |
| DIPEA | N,N-diisopropylethylamine |
| DMPO | 5,5-dimethyl-1-pyrroline N-oxide |
| EI | Electron Impact |
| EPR | Electron Paramagnetic Resonance |
| eq. | equivalents |
| ESI | Electron Spray Ionisation |
| ESR | Electron Spin Resonance |
| Et | ethyl |
| FPT | freeze-pump-thaw |
| GC | Gass Chromatography |
| HBTU | O-(benzotriazol-1-yl)-N,N,N',N'- |
| HMBC | Heteronuclear Multiple Bond Correlation |
| HMQC | Heteronuclear Multiple Quantum Coherence |
| iPr | isopropyl |
| LC-MS | Liquid Chromatography – Mass Spectrometry |
| m | multiplet |

| | |
|---|---|
| m/z | mass to charge ratio |
| MS | Mass Spectrometry |
| NMR | Nuclear Magnetic Resonance |
| Pr | propyl |
| q | quartet |
| rbf | round-bottomed flask |
| s | singlet |
| t | triplet |
| TCP | tricyclo[1.1.1.0]pentane |
| TEMPO | (2,2,6,6-tetramethylpiperidin-1-yl)oxyl |
| TMS | trimethylsilane |
| ToF | Time of Flight |

**References**


1. J. Fossey, D. Lefort and J. Sorba, *Free Radicals in Organic Chemistry*, Wiley, New York, 1995.
2. A. F. Parsons, *An Introduction to Free Radical Chemistry*, Blackwell Science, Oxford, 2000.
3. P. Renaud, *Radicals in Organic* Synthesis, Wiley, New York, 2008.
4. H. Togo, *Advanced Free Radical Reactions for Organic Synthesis*, Elsevier, Chiba, 2004.
5. D. L. Boger, *Israel Journal of Chemistry*, 1997, **37**, 119-129.
6. I. Ratera and J. Veciana, *Chemical Society Reviews*, 2012, **41**, 303-349.
7. C. Chatgilialoglu and A. Studer*, Biology and Materials*, Wiley, New York, 2012.
8. C. C. Winterbourn, *ChemTexts*, 2020, **6**, 7.
9. A. Phaniendra, D. B. Jestadi and L. Periyasamy, *Indian Journal of Clinical Biochemistry*, 2015, **30**, 11-26.
10. M. Gomberg, *Journal of the American Chemical Society*, 1900, **22**, 757-771.
11. F. Paneth and W. Lautsch, *Nature*, 1930, **125**, 564-564.
12. D. H. Hey and W. A. Waters, *Chemical Reviews*, 1937, **21**, 169-208.
13. J. Kochi, *Free Radicals*, Wiley, New York, 1973.
14. M. S. Kharasch, W. H. Urry and E. V. Jensen, *Journal of the American Chemical Society*, 1945, **67**, 1626-1626.
15. F. Minisci, R. Bernardi, F. Bertini, R. Galli and M. Perchinummo, *Tetrahedron*, 1971, **27**, 3575-3579.
16. A. G. Davies, *Journal of Chemical Research*, 2006, **3**, 141-148.
17. W. T. Borden, R. Hoffmann, T. Stuyver and B. Chen, *Journal of the American Chemical Society*, 2017, **139**, 9010-9018.
18. Z. X. Chen, Y. Li and F. Huang, *Chem*, 2021, **7**, 288-332.
19. A. Nilsen and R. Braslau, *Journal of Polymer Science Part A: Polymer Chemistry*, 2006, **44**, 697-717.
20. Y. Kita, K. Gotanda, A. Sano, M. Oka, K. Murata, M. Suemura and M. Matsugi, *Tetrahedron letters*, 1997, **38**, 8345-8348.
21. B. Giese, *Angewandte Chemie*, 1985, **24**, 553-565.

22. D. H. R. Barton and S. I. Parekh, *Half a Century of Free Radical Chemistry*, Cambridge University Press, Cambridge, 1993.
23. D. J. Hart, *Science*, 1984, **223**, 883-887.
24. G. E. Keck, E. J. Enholm, J. B. Yates and M. R. Wiley, *Tetrahedron*, 1985, **41**, 4079-4094.
25. G. Stork, *Bulletin of the Chemical Society of Japan*, 1988, **61**, 149-154.
26. N. A. Porter, D. R. Magnin and B. T. Wright, *Journal of the American Chemical Society*, 1986, **108**, 2787-2788.
27. D. P. Curranl and D. M. Rakiewicz, *Tetrahedron*, 1985, **41**, 3943-3958.
28. N. A. Romero and D. A. Nicewicz, *Chemical Reviews*, 2016, **116**, 10075-10166.
29. S. L. Tang, R. L. Smith and M. Poliakoff, *Green Chemistry*, 2005, **7**, 761-762.
30. M. M. Roessler and E. Salvadori, *Chemical Society Reviews*, 2018, **47**, 2534-2553.
31. E. Zavoisky, *J. Phys. USSR*, 1945, **9**, 211-245.
32. C. A. Rice-Evans, A. T. Diplock and M. C. R. Symons, *Techniques in Free Radical Research*, Elsevier Science Publishers B.V., Amsterdam, 1991.
33. V. Chechik, E. Carter and D. Murphy, *Electron Paramagnetic Resonance*, Oxford University Press, Oxford, 2016.
34. A. Yamada, M. Abe, Y. Nishimura, S. Ishizaka, M. Namba, T. Nakashima, K. Shimoji and N. Hattori, *Beilstein Journal of Organic Chemistry*, 2019, **15**, 863-873.
35. D. F. Church, *Analytical Chemistry*, 1994, **66**, 419A-427A.
36. C. Karunakaran, P. Santharaman and M. Balamurugan, in *Spin Resonance Spectroscopy*, ed. C. Karunakaran, Elsevier, 2018, pp. 49-110.
37. R. Kaptein and J. L. Oosterhoff, *Chemical Physics Letters*, 1969, **4**, 195-197.
38. M. Goez, in *Advances in Photochemistry*, 1997, pp. 63-163.
39. E. Schaffner and H. Fischer, *The Journal of Physical Chemistry*, 1995, **99**, 102-104.
40. O. A. Krumkacheva, V. R. Gorelik, E. G. Bagryanskaya, N. V. Lebedeva and M. D. Forbes, *Langmuir*, 2010, **26**, 8971-8980.
41. J. A. McCloskey, *Mass Spectrometry*, Academic Press, San Diego, 1990.
42. J. R. Chapman, *Practical Organic Mass Spectrometry: A Guide for Chemical and Biological Analysis*, John Wiley, Chichester, 1993.
43. E. de Hoffmann and V. Stroobant, *Mass Spectrometry: Principles and Applications*, John Wiley & Sons Ltd., Chichester, 2007.
44. G. L. Glish and R. W. Vachet, *Nature Reviews Drug Discovery*, 2003, **2**, 140-150.

45. F. W. McLafferty, *Annual Reviews of Analytical Chemistry,* 2011, **4**, 1-22.

46. H. Awad, M. M. Khamis and A. El-Aneed, *Applied Spectroscopy Reviews*, 2015, **50**, 158-175.

47. A. Gaudel-Siri, C. Marchal, V. Ledentu, D. Gigmes, D. Siri and L. Charles, *European Journal of Mass Spectrometry*, 2019, **25**, 229-238.

48. D. Hanson, J. Orlando, B. Noziere and E. Kosciuch, *International Journal of Mass Spectrometry*, 2004, **239**, 147-159.

49. B. Nozière and D. R. Hanson, *The Journal of Physical Chemistry A*, 2017, **121**, 8453-8464.

50. B. Nozière and L. Vereecken, *Angewandte Chemie International Edition*, 2019, **58**, 13976-13982.

51. H. Perkampus, *UV-Vis Spectroscopy and Its Applications*, Springer-Verlag, New York, 1992.

52. J. R. Lakowicz, *Principles of Fluorescence Spectroscopy*, Springer, New York, 2006.

53. A. Celebioglu and T. Uyar, *Journal of Agricultural Food Chemistry*, 2017, **65**, 5404-5412.

54. Y. Beldjoudi, M. A. Nascimento, Y. J. Cho, H. Yu, H. Aziz, D. Tonouchi, K. Eguchi, M. M. Matsushita, K. Awaga, I. Osorio-Roman, C. P. Constantinides and J. M. Rawson, *Journal of the American Chemical Society*, 2018, **140**, 6260-6270.

55. P. L. Zamora and F. A. Villamena, *The Journal of Physical Chemistry A*, 2012, **116**, 7210-7218.

56. M. Pelletier, V. Lavastre and D. Girard, *Toxicological Sciences*, 2002, **69**, 210–216.

57. M. A. Rudat and C. N. McEwen, *Journal of the American Chemical Society*, 1981, **103**, 4349-4354.

58. H. Iwahashi, C. E. Parker, R. P. Mason and K. B. Tomer, *Rapid Communications in Mass Spectrometry*, 1990, **4**, 352-354.

59. C. E. Parker, H. Iwahashi and K. B. Tomer, *Journal of the American Society for Mass Spectrometry*, 1991, **2**, 413-418.

60. Q. Guo, S. Y. Qian and R. P. Mason, *Journal of the American Society for Mass Spectrometry*, 2003, **14**, 862-871.

61. P. Domingues, C. Fonseca, A. Reis and M. R. M. Domingues, *Biomedical Chromatography*, 2012, **26**, 51-60.

62. C. Giorio, S. J. Campbell, M. Bruschi, F. Tampieri, A. Barbon, A. Toffoletti, A. Tapparo, C. Paijens, A. J. Wedlake, P. Grice, D. J. Howe and M. Kalberer, *Journal of the American Society*, 2017, **139**, 3999-4008.

63. A. Zaytsev, M. Breitenlechner, A. Novelli, H. Fuchs, D. A. Knopf, J. H. Kroll and F. N. Keutsch, *Atmospheric Measurement Techniques*, 2021, **14**, 2501-2513.

64. F. Leinisch, J. Jiang, E. F. DeRose, V. V. Khramtsov and R. P. Mason, *Free Radical Biology and Medicine*, 2013, **65**, 1497-1505.

65. S. Pou, D. J. Hassett, B. E. Britigan, M. S. Cohen and G. M. Rosen, *Analytical Biochemistry*, 1989, **177**, 1-6.

66. G. R. Buettner and L. W. Oberley, *Biochemical and Biophysical Research Communications*, 1978, **83**, 69-74.

67. N. Sankuratri, Y. Kotake and E. G. Janzen, *Free Radical Biology and Medicine*, 1996, **21**, 889-894.

68. N. Khan, C. M. Wilmot, G. M. Rosen, E. Demidenko, J. Sun, J. Joseph, J. O'Hara, B. Kalyanaraman and H. M. Swartz, *Free Radic Biol Med*, 2003, **34**, 1473-1481.

69. K. Stolze, N. Udilova, T. Rosenau, A. Hofinger and H. Nohl, *Biochemical Pharmacology*, 2003, **66**, 1717-1726.

70. T. Vogler and A. Studer, *Synthesis,* 2008, **13**, 1979-1993.

71. Y. Matsuoka, Y. Izumi, M. Takahashi, T. Bamba and K.-i. Yamada, *Analytical Chemistry*, 2020, **92**, 6993-7002.

72. X.-F. Xia, S.-L. Zhu, Y.-N. Niu, D. Zhang, X. Liu and H. Wang, *Tetrahedron*, 2016, **72**, 3068-3072.

73. P. J. Wright and A. M. English, *Journal of the American Chemical Society*, 2003, **125**, 8655-8665.

74. Y.-R. Luo, *Comprehensive handbook of chemical bond energies*, CRC press, 2007.

75. D. H. Barton, V. N. Le Gloahec and J. Smith, *Tetrahedron letters*, 1998, **39**, 7483-7486.

76. C. D. Cook and R. C. Woodworth, *Journal of the American Chemical Society*, 1953, **75**, 6242-6244.

77. V. Khizhnyi and G. Goloverda, *Theoretical and Experimental Chemistry*, 1988, **24**, 154-159.

78. A. Griva and E. Denisov, *International Journal of chemical kinetics*, 1973, **5**, 869-877.

79. P. J. H. Williams, G. A. Boustead, D. E. Heard, P. W. Seakins, A. R. Rickard and V. Chechik, *Journal of the American Chemical Society*, 2022, **144**, 15969-15976.

80. P. J. Williams, H. E. Ho, W. P. Unsworth, A. R. Rickard and V. Chechik, *Chemistry–A European Journal*, 2024, **30**, e202401500.

81. I. Ocaña, P. J. Williams, J. Donald, N. Griffin, G. Hodges, A. R. Rickard and V. Chechik, *Chimia*, 2024, **78**, 123-128.

82. K. Nozaki, K. Oshima and K. Uchimoto, *Journal of the American Chemical Society*, 1987, **109**, 2547-2549.

83. C. Ollivier and P. Renaud, *Chemical Reviews*, 2001, **101**, 3415-3434.

84. K. Nozaki, K. Oshima and K. Uchimoto, *Journal of the American Chemical Society*, 1987, **109**, 2547.

85. D. P. Curran and T. R. McFadden, *Journal of the American Chemical Society*, 2016, **138**, 7741-7752.

86. E. Frankland, *Journal of the Chemical Society,* 1862, **15**, 363-381.

87. J. Grotewold, J. Hernandez and E. A. Lissi, *Journal of the Chemical Society B*, 1971, 182.

88. A. G. Davies and B. P. Roberts, *Accounts of Chemical Research*, 1972, **5**, 387-392.

89. A. G. Davies, *Pure and Applied Chemistry*, 1974, **39**, 497-503.

90. A. G. Davies, K. U. Ingold, B. P. Roberts and R. Tudor, *Journal of the Chemical Society B*,, 1971, 698-712.

91. G. W. Kabalka, H. C. Brown, A. Suzuki, S. Honma, A. Arase and M. Itoh, *Journal of the American Chemical Society*, 1970, **92**, 710-712.

92. H. C. Brown and M. M. Midland, *Journal of the Chemical Society D: Chemical Communications*, **13**,1971, 699-700.

93. P. Renaud, A. Beauseigneur, A. Brecht-Forster, B. Becattini, V. Darmency, S. Kandhasamy, F. Montermini, C. Ollivier, P. Panchaud, D. Pozzi, E. M. Scanlan, A.-P. Schaffner and V. Weber, *Pure and Applied Chemistry*, 2007, **79**, 223-233.

94. P. Renaud, 2012.

95. K. Nozaki, K. Oshima and K. Utimoto, *Bulletin of the Chemical Society of Japan*, 2006, **60**, 3465-3467.

96. A. G. Davies, *Journal of Chemical Research*, **7**, 2008, 361-375.

97. R. Rensch and H. Friebolin, *Chemische Berichte,* 1977, **110**, 2189.

98. R. Huschens, R. Rensch and H. Friebolin, *Chemische Berichte,* 1981, **114**, 3581.

99. R. Uematsu, C. Saka, Y. Sumiya, T. Ichino, T. Taketsugu and S. Maeda, *Chemical Communications*, 2017, **53**, 7302-7305.
100. M. H. Abraham and A. G. Davies, *Journal of the Chemical Society,* 1959, 429.
101. O. Grummitt, *Journal of the American Chemical Society*, 1942, **64**, 1811-1814.
102. T. Parsons, M. Silverman and D. Ritter, *Journal of the American Chemical Society*, 1957, **79**, 5091-5098.
103. D. S. Matteson and R. A. Bowie, *Journal of the American Chemical Society*, 1965, **87**, 2587-2590.
104. A. G. Davies and B. P. Roberts, *Journal of the Chemical Society B*, 1967, 17-22.
105. A. G. Davies and B. P. Roberts, *Journal of the Chemical Society B*, 1969, 311.
106. J. Contreras, J. Grotewold, E. Lissi and R. Rozas, *Journal of Polymer Science Part A-1: Polymer Chemistry*, 1969, **7**, 2341-2349.
107. S. Korcek, G. Watts and K. Ingold, *Journal of the Chemical Society,* 1972, 242-248.
108. O. Grummitt, *J. Am. Chem. Soc.*, 1942, **64**, 1811.
109. J. Howard, *Canadian Journal of Chemistry*, 1972, **50**, 2298-2304.
110. J. A. Kerr, *Chemical Reviews*, 1966, **66**, 465-500.
111. J. A. Howard and K. U. Ingold, *Canadian Journal of Chemistry*, 1970, **48**, 873-880.
112. A. Mano Priya, B. Aazaad, V. P. Mythili and S. Lakshmipathi, *Computational and Theoretical Chemistry*, 2023, **1223**, 114082.
113. J. M. Backer, V. G. Budker, S. I. Eremenko and Y. N. Molin, *Biochimica et Biophysica Acta*, 1977, **460**, 152-156.
114. M. F. Sonnenschein, S. P. Webb, O. D. Redwine, B. L. Wendt and N. G. Rondan, *Macromolecules*, 2006, **39**, 2507-2513.
115. J. De Moor and G. Van der Kelen, *Journal of Organometallic Chemistry*, 1966, **6**, 235-241.
116. H. Friebolin and R. Rensch, *Organic magnetic resonance*, 1976, **8**, 576.
117. R. C. Petry and F. H. Verhoek, *Journal of the American Chemical Society*, 1956, **78**, 6416-6417.
118. M. H. Abraham and A. G. Davies, *Chemistry & Industry,* 1957, 1622.
119. H. C. Brown and M. M. Midland, *Tetrahedron*, 1987, **43**, 4059.
120. S. B. Mirviss, *Journal of the American Chemical Society*, 1961, **83**, 3051-3056.

121. P. Allies and P. Brindley, *Journal of the Chemical Society B: Physical Organic*, 1969, 1126-1131.
122. R. W. Law and J. L. Margrave, *The Journal of Chemical Physics*, 1956, **25**, 1086-1087.
123. H. Nöth and H. Vahrenkamp, *Chemische Berichte*, 1966, **99**, 1049-1067.
124. J. E. d. Moor and G. P. van der Kelen, *Journal of Organometallic Chemistry*, 1966, **6**, 235-241.
125. H. C. Brown, M. M. Midland and G. W. Kabalka, *Journal of the American Chemical Society*, 1971, **93**, 1024-1025.
126. J. W. Roddy and C. F. Coleman, *Talanta*, 1968, **15**, 1281-1286.
127. D. Michel, W. Böhlmann, J. Roland and S. Mulla-Osman, in *Molecules in Interaction with Surfaces and Interfaces*, eds. R. Haberlandt, D. Michel, A. Pöppl and R. Stannarius, Springer Berlin Heidelberg, Berlin, Heidelberg, 2004, pp. 217-274.
128. R. W. Fessenden and R. H. Schuler, *The Journal of Chemical Physics*, 1963, **39**, 2147-2195.
129. B. Maillard, K. U. Ingold and J. C. Scaiano, *Journal of the American Chemical Society*, 1983, **105**, 5095.
130. R. G. Gasanov, T. T. Vasilieva and S. I. Gapusenko, *Mendeleev Communications*, 1991, **1**, 70-71.
131. Y. Ichinose, S.-i. Matsunaga, K. Fugami, K. Oshima and K. Utimoto, *Tetrahedron Letters*, 1989, **30**, 3155-3158.
132. E. Lacôte and M. Malacria, *Comptes Rendus de l'Académie des Sciences - Series IIC - Chemistry*, 1998, **1**, 191-194.
133. S. Czernecki, E. Ayadi and J. Xie, *Tetrahedron letters*, 1996, **37**, 9193-9194.
134. K. Miura, Y. Ichinose, K. Nozaki, K. Fugami, K. Oshima and K. Utimoto, *Bulletin of the Chemical Society of Japan*, 1989, **62**, 143-147.
135. D. P. Curran, M. H. Chen, E. Spletzer, C. M. Seong and C. T. Chang, *Journal of the American Chemical Society*, 1989, **111**, 8872-8878.
136. Y. Kita and M. Matsugi, *Radicals in Organic Synthesis*, Wiley-VCH, Weinheim, 2001.
137. Y. Takeyama, Y. Ichinose, K. Oshima and K. Utimoto, *Tetrahedron letters*, 1989, **30**, 3159-3162.
138. E. Baciocchi and E. Muraglia, *Tetrahedron letters*, 1994, **35**, 2763-2766.

139. T. Nakamura, H. Yorimitsu, H. Shinokubo and K. Oshima, *Synlett*, 1998, **1998**, 1351-1352.

140. D. P. Curran and C. T. Chang, *The Journal of Organic Chemistry*, 1989, **54**, 3140-3157.

141. D. P. Curran, *Free Radicals in Synthesis and Biology*, Springer Netherlands, Dordrecht, 1989.

142. Z. Wang, F. Cui, Y. Sui and J. Yan, *Beilstein Journal of Organic Chemistry*, 2023, **19**, 1580-1603.

143. B. Kopping, C. Chatgilialoglu, M. Zehnder and B. Giese, *The Journal of Organic Chemistry*, 1992, **57**, 3994-4000.

144. T. L. Cottrell, *The Strenghts of Chemical Bonds*, Butterwoeth, London, 1958.

145. M. R. Medeiros, L. N. Schacherer, D. A. Spiegel and J. L. Wood, *Organic Letters*, 2007, **9**, 4427-4429.

146. G. Povie, M. Marzorati, P. Bigler and P. Renaud, *The Journal of Organic Chemistry*, 2013, **78**, 1553-1558.

147. J. Boivin and V. T. Nguyen, *Beilstein Journal of Organic Chemistry*, 2007, **3**, 45.

148. J. Boivin and V. T. Nguyen, *Beilstein Journal of Organic Chemistry*, 2007, **3**, 47.

149. J. Nugent, C. Arroniz, B. R. Shire, A. J. Sterling, H. D. Pickford, M. L. J. Wong, S. J. Mansfield, D. F. J. Caputo, B. Owen, J. J. Mousseau, F. Duarte and E. A. Anderson, *ACS Catalysis*, 2019, **9**, 9568-9574.

150. D. F. J. Caputo, C. Arroniz, A. B. Dürr, J. J. Mousseau, A. F. Stepan, S. J. Mansfield and E. A. Anderson, *Chemical Science*, 2018, **9**, 5295-5300.

151. P. Kaszynski, A. C. Friedli and J. Michl, *Journal of the American Chemical Society*, 1992, **114**, 601-620.

152. K. B. Wiberg and S. T. Waddell, *Journal of the American Chemical Society*, 1990, **112**, 2194-2216.

153. K. B. Wiberg and F. H. Walker, *Journal of the American Chemical Society*, 1982, **104**, 5239-5240.

154. W. Wu, J. Gu, J. Song, S. Shaik and P. C. Hiberty, *Angewandte Chemie International Edition*, 2009, **48**, 1407-1410.